2014-01-01

Enhanced Finite Element Modeling Of The Thermo-Mechanical Responses Of Jointed PCC Pavements Under Environmental And Traffic Loads

Mohammad Ali Zokaei Ashtiani
University of Texas at El Paso, mzokaeiashtiani@miners.utep.edu

ENHANCED FINITE ELEMENT MODELING OF THE THERMO-MECHANICAL RESPONSES OF JOINTED PCC PAVEMENTS UNDER ENVIRONMENTAL AND TRAFFIC LOADS

MOHAMMAD ALI ZOKAEI ASHTIANI

Department of Civil Engineering

APPROVED:

_____

Cesar J. Carrasco, Ph.D., Chair

_____

Soheil Nazarian, Ph.D.

_____

Carlos Martin Chang-Albitres, Ph.D.

_____

Pavana Prabhakar, Ph.D.

_____

Lev Khazanovich, Ph.D.

_____

Bess Sirmon-Taylor, Ph.D.
Interim Dean of the Graduate School

Dedication

To my love, Hoda

To my wonderful parents, Behnaz and Hedayat

ENHANCED FINITE ELEMENT MODELING OF THE THERMO-MECHANICAL RESPONSES OF JOINTED PCC PAVEMENTS UNDER ENVIRONMENTAL AND TRAFFIC LOADS

by

MOHAMMAD ALI ZOKAEI ASHTIANI, MSCE

DISSERTATION

Presented to the Faculty of the Graduate School of

The University of Texas at El Paso

in Partial Fulfillment

of the Requirements

for the Degree of

DOCTOR OF PHILOSOPHY

Department of Civil Engineering

THE UNIVERSITY OF TEXAS AT EL PASO

May 2014

Acknowledgements

I owe my deepest gratitude to the kind people that writing and completion of this doctoral dissertation would not have been possible without their help and support.

I would like to sincerely express my gratitude to my advisor, Dr. Cesar Carrasco, for his excellent guidance, support and encouragement. I would also like to thank Dr. Soheil Nazarian for his support and for giving me the opportunity to work on this research work at the Center for Transportation Infrastructure Systems (CTIS). I highly appreciate their great ideas in developing this research and providing me with invaluable feedbacks and comments.

My gratitude extends to my committee members, Dr. Carlos Chang, Dr. Pavana Prabhakar and Dr. Lev Khazanovich. Their feedback gave me a better insight into the quality of this work and future developing it.

I want to acknowledge the funders of my research project (NYPAS), Federal Highway Administration and New York Department of Transportation, especially Dr. Julian Bendaña.

I would like to thank all the staff at CTIS, especially Dr. Cesar Tirado who helped me in developing this project, and Dr. Imad Abdallah the coordinator of CTIS. I also would like to thank all of the graduate and undergraduate students who helped me in completion my research work.

I want to thank my father, Dr. Hedayat Zokaei Ashtiani, for his eternal encouragement and support through my life, my mother, Behnaz Gouya, for her continuous understanding and endless kindness and patience and my lovely brothers, Amin and Milad, for always having my back. I am especially thankful to my wonderful wife, Dr. Hoda Azari, for her love, encouragement, support and understanding.

Abstract

Jointed plain concrete pavements (JPCP) are the most commonly used type of rigid pavement systems and the accurate modeling of their thermo-mechanical responses is of primary importance in a mechanistic-empirical pavement design procedure. In JPCP, the temperature gradient and resulting slab shape play a crucial role in the magnitude of stresses and deflections caused by the superimposed traffic loads. Temperature gradients through the slab depth can produce thermal curling in slabs and can also produce slab expansion and contraction, which leads to the generation of frictional tractions between slabs and foundation. The prediction of these frictional tractions is complicated by the curling of the slabs that causes some portions of the slabs to lose contact with the foundation. From the initial development of pavement analysis software in the early 1970's, it was recognized that the finite element (FE) method was the most appropriate modeling tool, due to its potential ability to capture all the pavement response features. A series of software development efforts have culminated in the production of NYSLAB, a jointed pavement analysis tool that has the capability to predict the complete thermo-mechanical responses, due to the combined effect of environmental and vehicular loads. This dissertation presents a series of studies conducted toward developing an improved FE-based model to be used in the source code of NYSLAB. A complete review of characteristics and mechanistic behavior of components of JPCP is provided. Detailed mathematical models of pavement slabs, load transfer devices and foundation layers developed in NYSLAB are presented. In addition, the implementation of "interface elements" used to model the contact between pavement layers is included. These elements have the ability to capture the separation and sliding between pavement layers, due to thermal loads, and calculate the frictional traction at their interface. Finally, a series of parametric studies was carried out to determine that the governing equations that were used to idealize the behavior of JPCP in NYSLAB have been accurately selected and implemented in the FE model. The results presented in these studies highlight the capabilities of NYSLAB in modeling and considering the most important factors that affect the prediction of the stresses and strains produced in concrete slabs.

Table of Contents

List of Tables

List of Figures

Chapter 1: Introduction

1.1 Scope of Study

This study is mainly involved with the development of analytical and numerical procedures to evaluate rigid pavement responses subjected to vehicular loads and environmental conditions. The principle effort to be used for this analytical model development will focus on (1) the reliability of employed theories (2) feasibility of numerical methods and (3) applicability of the model consistent with the actual behavior of rigid pavements in the field.

The structural model of a rigid pavement system can be represented as a slab placed over an elastic foundation. An analysis of this type of structural system brings to light several applications of structural and geotechnical theories. The primary concern of pavement engineers is to detect and evaluate pavement behavior under different possible conditions. The goal of this evaluation is to explore and utilize the best possible options for simulating the pavement structure to predict their performances. This study is concerned with a comprehensive review of literature about the characteristics and mechanistic behavior of rigid pavements, the level and type of applied loads and analytical or experimental pavement analysis methods. The literature examines the identification and incorporation of structural theories (e.g. Theory of elasticity, plate theory), geotechnical theories (soil models) and soil-structure contact problems in the modeling of rigid pavements.

1.2 Problem Statement

Jointed plain concrete pavements (JPCP) are the most commonly used type of rigid pavement systems and the accurate prediction of their thermo-mechanical responses, due to the combined effect of environmental and traffic loads, are of primary importance for rigid pavement designers in a mechanistic-empirical pavement design procedure. Surface Portland cement concrete (PCC) slabs in JPCP often curl due to the effect of seasonal and daily temperature variations throughout the slab depth, which plays a critical role in the magnitude of stresses imposed by traffic loads. Field measurements reveal that the actual temperature gradient through the PCC slab depth is nonlinear (Ioannides *et al*., 1998; Choubane *et al*., 1992, Ashraf *et al*., 1996). This nonlinear thermal gradient can not only produce curling and expansion or contraction in slabs but actually leads to stresses that are higher than those

produced by a linear gradient with the same top to bottom temperature difference. While thermal curling tends to produce bending stresses in the slabs, because of slab-foundation interaction and slab self weight, the uniform thermal expansion or contraction tends to produce additional compressive or tensile stresses within the slabs, due to friction in slab-foundation interface. Therefore, in addition to the stiffness of PCC slabs and the level of applied loads, the stiffness of the underlying foundation layers and the contact conditions along the slab-foundation interface significantly impact the mechanical behavior of PCC pavements. Interface friction introduces nonlinearity and complicates the analysis of PCC pavements. A sophisticated modeling method, such as finite element (FE) modeling, is required to accurately idealize the slab-foundation contact conditions, which is impacted by temperature induced curling (separation) and expansion or contraction (sliding) in the PCC slabs (Zokaei Ashtiani *et al*., 2013).

Since the development of ILLI-SLAB in 1979, significant amount of research and development have been conducted to improve the capabilities of jointed pavement analysis tools. These accomplishments have culminated in some software packages such as JSLAB, ISLAB, and EverFE with the capability to analyze jointed pavements under self-weight, traffic and thermal loads. JSLAB and ISLAB incorporate two-dimensional (2D) FE models based on the plate-on-grade idealization. Even though the 2D tools have undergone several improvements, the underlying core of the software still maintains the formulation of the initial ILLI-SLAB source code, which was created when computer resources were limited. The limitations affected the maximum number of pavement layers and jointed PCC slabs that can be modeled, because their software developers had to implement algorithms with the minimum need of computer memory. The limitations also affected the number of elements that can be considered in the model generation and analysis. Even further restrictions appeared in the type of applied loads and the contact conditions, which in turn reduced the applicability of those tools in realistic analysis of rigid pavement systems. Modeling the contact between slab and foundation was limited to the vertical contact (separation), and modeling the horizontal or frictional contact (sliding) was not achievable in those tools. Moreover, thermal analysis of jointed slabs was unattainable in case of continuous foundation models. Three-dimensional (3D) FE analysis tools, such as EverFE, models

the slab more accurately and allows for the interpretation of detailed responses throughout the slab thickness. However, the number of elements, and consequently the number of degrees of freedom, which is needed to accurately model plates (slabs) in 3D analysis are substantially larger than those used in 2D plate analysis. For this reason modeling multi-slab pavement sections in EverFE is computationally intensive. A thorough review of existing rigid pavement analysis tools revealed that it would be beneficial to redesign these software completely by taking advantage of modern computer resources and the finite element modeling techniques available today. Identifying and understanding the potentials, limitations and applicability of current analysis tools, a new analysis tool is required to significantly enhance the efficiency and capabilities of FE-based jointed concrete pavement models.

1.3 Objectives of Research

The primary purpose of this research is to evaluate and improve existing rigid pavement analysis tools and develop a new tool that is able to analyze complete thermo-mechanical responses of jointed concrete pavements. The analytical tool must be able to realistically predict the stresses, strains, and displacements of the concrete slab and its supporting layers due to possible traffic and environmental loads, and make use of them in the design of the pavement system. For this reason, a new analysis tool, named NYSLAB, was developed at the University of Texas at El Paso. The NYSLAB source code was built up in MATLAB®, which has an interactive environment for numerical computation and programming. Matrix creation and calculation, which are necessary in the FE analysis, is quite feasible in MATLAB®. The specific objectives of this study and the corresponding approaches are described as follows:

1. *Finite element modeling of concrete slabs*. NYSLAB incorporates 2D FE modeling by considering the pavement section as a thin to medium-thick plate (slab) resting on an elastic foundation system. The first step in developing NYSLAB will be toward getting familiar with the plate and shell theories to model concrete slabs. To model multi-layer pavement slabs with different material property and thickness, which are bonded at their interface, the theory of laminated plates will be utilized. It is imperative that the finite element model accounts for all degrees of freedom needed to idealize the actual behavior of PCC slabs. The major variables that characterize the slab deformation

are the vertical deflection, the rotations about the slab longitudinal and transverse axes and the in-plane or horizontal displacements in the longitudinal and transverse directions. Appropriate slab modeling can be attained by employing such a structural theory that is able to estimate the responses that have significant impacts on rigid pavements performance. For instance, if the design of slab is intended to estimate the fatigue cracking, bending stresses are the main parameters. In this case, the incorporated plate or laminated plate theories should be able to calculate bending stresses and strains accurately throughout the slab thickness. An appropriate plate element with five degrees of freedom per node will be introduced to model the PCC slabs.

2. *Finite element modeling of load transfer devices*. The process of modeling the load transfer elements (dowels, ties, key and aggregate interlock) in NYSLAB, that are used to connect adjacent slabs in a JPCP system, will be examined. Moreover, the impact of horizontal interaction between the jointed slabs, due to thermal expansion and contraction, will be investigated. "Linkage elements" will be developed to capture this impact.
3. *Implementation of thermal and traffic loads in NYSLAB*. The major loads that rigid pavements are subjected to during their life are examined in this study. The procedure of implementation of nonlinear temperature gradient, built-in temperature gradient and tire loads to the FE model in NYSLAB will be explained.
4. *Finite element modeling of foundation*. The next step in modeling rigid pavements is the simulation of foundation or slab supports. In this manuscript all the existing foundation models (solid elastic, dense liquid and two or three parameter foundation) and their mathematical model will be reviewed. Moreover, a new procedure for determining the Vlasov foundation (Vlasov et al. 1966) parameters for one and two-layered foundation systems will be introduced and an iterative process for that purpose will be implemented in the source code of NYSLAB.
5. *Finite element modeling of contact between pavement layers*. One of the principal contributions of this research study is devoted to the modeling of contact between pavement layers (e.g. between concrete slabs and foundation or among unbonded concrete slabs). Separation and sliding of concrete slabs at the slab-foundation interface, due to thermal loads, are significant occurrences that

have great impacts on the slab responses in the analysis of rigid pavements. The first step in modeling contact is to identify the contact condition and frictional characterization of the interface and propose an appropriate constitutive friction law. The second step is to develop a finite element procedure and propose an interface element to simulate the contact at the pavement layer's interface.

6. *Parametric study*. A series of parametric studies will be carried out using NYSLAB to determine whether the governing equations that were used to idealize the behavior of jointed concrete pavements in NYSLAB have been accurately selected and implemented in the FE model. The parametric studies in this manuscript also attempts to provide better understanding of the interaction between the most relevant parameters that govern the performance of JPCP. The studies include the "Effect of nonlinear temperature gradient on responses of JPCP", "Effect of slab-foundation friction on responses of JPCP", "Impact of different approaches to modeling rigid pavement base layers on slab curling stresses", and "Effect of loss of support due to built-in curling on PCC slab stresses".

1.4 Significance of Study

The contribution of this research study to the field of pavement engineering is a thorough investigation of the potentials and limitations of rigid pavement analysis methods, in order to develop an improved finite element model for the analysis and design of jointed concrete pavements. Developing an advanced procedure to capture the separation and sliding of concrete slabs at their interface with the foundation (during daily temperature variations) and calculating the frictional stresses are the first known instances in modeling thermo-mechanical behavior of JPCP. Even though the mathematical model of foundations developed in NYSLAB is not the first attempt in this manner, the improved Vlasov foundation model in this tool allows for analyzing a pavement system with multiple jointed PCC slabs subjected to thermal loads, which was a missing link in other existing analysis tools. In addition, determining the Vlasov parameters is feasible through an iterative procedure in NYSLAB. Using laminated plate theory to model bonded slabs and developing interface elements between unbounded pavement layers, the developed model has the potential to analyze rigid pavement systems with any bonding or contact conditions. The parametric studies in this manuscript are the first known studies that employ finite element analysis and use real pavement properties (e.g., the dimensions and the stiffness

of pavement layers, slab-foundation friction and thermal and truck loads) to investigate the effect of friction between pavement layers, the effect of base layer rigidity, and the effect of loss of support due to built-in curling in estimating the PCC slab stresses. Accurate estimation of stresses produced in PCC slabs will be beneficial for pavement designers to predict the location and the time of generation of fatigue cracking. The completed analysis tool developed in this study will be a state-of-the-art tool that can be used by transportation agencies and engineers around the United States and the world to more realistically design and analyze pavements. Researchers can also use this tool to better understand the mechanistic behavior of rigid pavements to apply in the AASHTO Mechanistic-Empirical Pavement Design Guide.

1.5 Structure of the Dissertation

Chapter 2 provides a thorough review on the structures of rigid pavement systems and the available methods and tools for their design and analysis. The Laminated plate theories and their application in modeling pavement slabs are introduced. The functionalities of load transfer elements for connecting jointed slabs and the available modeling methods for simulating them are included. Different foundation models for idealizing the soil domain are reviewed. Lastly, an overview of the attempts on modeling contact between dissimilar bodies is presented. Chapter 3 explains the detail of the laminated plate theory and the plate element that used in NYSLAB to model the PCC slabs. The elements used for modeling the load transfer devices are introduced. Moreover, the procedure of applying the tire and thermal loads in the finite element model is presented. Chapter 4 provides the mathematical model of different foundation idealization used in NYSLAB. The process of calculation of foundation parameters is also included. Chapter 5 discusses the modeling of contact between pavement layers. A constitutive model and interface elements are introduced to demonstrate the frictional characteristics of pavement layers interface. The algorithm for the calculation of frictional stresses in the finite element analysis of rigid pavement systems in NYSLAB is described. Chapter 6 demonstrates a summary of the mathematical model of rigid pavement systems in NYSLAB. Chapter 7 presents the results of several parametric studies on the effect of different factors on the PCC slab stresses. Chapter 8 presents a

summary and conclusions of this research study. It also states the limitations of the developed tool and provides recommendations for future studies.

Chapter 2: Theoretical Background

This chapter contains the review on the structural elements of rigid pavement systems and an evaluation of the existing methods for modeling and analyzing jointed concrete pavements.

2.1 Rigid Pavement Analysis

This section is devoted to identifying the functionalities of rigid pavement systems and evaluating the available concepts for their design and analysis. Moreover, the applicability of available rigid pavement analysis tools will be examined and a new analysis tool, named NYSLAB, will be introduced.

2.1.1 Rigid Pavement System

Rigid pavement systems consist of a number of Portland cement concrete (PCC) slabs placed over one or more foundation layer(s) (base, sub-base, and subgrade). In a rigid pavement system, the PCC slab is the stiffest structural element that provides major bearing capacity against the applied loads. Pavement slabs can be composed of layers with different material property and thickness, with the interface between them considered either bonded or unbonded. The slab layers are usually placed over an unstabilized or stabilized base course. Unstabilized or unbound base courses may be composed of densely graded or open-graded granular materials. Stabilized bases are usually composed of granular materials bounded with Portland cement, asphalt, lime or fly ash blend, or other agents. Base layers can also contribute to the load resistance system. However, their main roles (as defined in some design guides) are to provide a uniform support for pavement slabs, contribute to the subgrade drainage and frost protection, improve the foundation strength, and prevent subgrade pumping (Hammons and Ioannides, 1997). One or more sub-base layer may also be used in the pavement foundation system. Sub-bases are usually made with lesser quality granular materials to replace soft and compressible soils. In addition, they can provide strength to the pavement system and offer frost and swelling protection. The last layer in a rigid pavement system is subgrade, which is either natural or compacted soil. The subgrade strength property is represented by resilient modulus, which is a function of soil classification, compaction and moisture content.

Jointed plain concrete pavements are the most commonly used type of rigid pavement systems, because of their reliability and proven performance. JPCP consists of jointed concrete slabs without structural reinforcements. Joints are often served to relief stresses and control cracking. In JPCP, load transfer devices are used, in both the longitudinal and transverse joints, to facilitate movements and transfer load caused by traffic and environmental effect from one slab to adjacent slab.

2.1.2 Rigid Pavement Analysis Methods

The initial and traditional pavement design procedures used an empirical approach based on observation and testing of pavement sections to detect the relevant characteristics affecting the pavement performance. Over the years, several mechanistic approaches have been proposed for the calculation of pavement responses (strains and stress) to complement empirically observed behavior of concrete pavements (Bordelon and Roesler, 2009). However, most of those mechanistic approaches, using closed form and approximate solutions for the calculation of concrete pavement stresses, are limited to simple slab geometry, particular tire load position and uniform boundary conditions.

Elastic Layer (EL) theories are the common method used for designing the pavements. The assumption of this method is to consider horizontally infinite slab and foundation, which in turn limits its applicability to only flexible pavements or pavements without discontinuities. The infinite nature of pavement layers in the EL theory also restricts the range of analysis to the case of interior loadings. PCC pavements with joint connections technically cannot be considered as an infinite slab; therefore, the concept of semi-elastic half space used in the EL theory is not applicable for jointed concrete pavements.

The first idealization of a rigid pavement system was introduced by Westergaard in the 1920's. He represented it as a case of slab-on-grade (Westergaard, 1926). In that case, the rigid pavement was modeled as a thin plate resting on an infinite number of independent springs. The stiffness of those independent springs, with constant value, characterized the subgrade rigidity in Westergaard's model. The magnitude of spring stiffness was represented as the modulus of subgrade reaction with the unit of force per area per unit deflection. Westergaard's initial analytical modeling had been adopted as a promising method for reliable design and was used as a design basis for new analysis tools (Hammons

and Metcalf, 1999). Westergaard extended his procedure to calculate stresses and deflections in rigid pavements due to interior, edge and corner loads. Although Westergaard's procedure had reached a certain level of maturity in idealization of rigid pavements, thereafter, several investigations were conducted to improve its model. The poor assumption regarding the modeling of thin slab layer and foundation and the restricted capabilities in considering tire loading position, thermal loads, and modeling load transfer devices were the main drawbacks of the Westergaard's method.

In JPCPs, the position of tires across the slab, the tire proximity to the edges and the stiffness of load transfer elements have a significant role in the mechanical performance of the pavement system. In addition, the contact conditions along the slab-foundation interface significantly impact the mechanical behavior of the pavement. The fact that temperature induced curling significantly impacts slab-base/subgrade contact conditions, and interface friction further complicates JPCP analysis because it introduces some nonlinearity to the problem. Finite element modeling is the most appropriate numerical method to consider this nonlinearity and take all the possible loads and environmental conditions into consideration (Carrasco et *al*., 2010). The use of numerical methods facilitates the solution of rigid pavement analysis for problems of practical importance. By taking advantages of the modern programming and finite element modeling tools and employing advanced computer resources, numerical modeling of different type of structures is now quite feasible.

2.1.3 Rigid Pavement Analysis Tools

A substantial amount of research and developments have been conducted for years to provide an analytical tool that would be able to model and analyze the behavior of rigid pavements. Several analytical software for modeling jointed concrete slabs on top of elastic foundations have been developed in the last five decades. In 1974, Huang and Wang used a finite element method for the analysis of jointed slabs on liquid foundations and further extended it for jointed slabs on solid foundations (Huang, 2004). Huang developed the WESLIQUID program, which was able to calculate stresses and deflections in concrete pavements and the subgrade with or without joints and cracks.

The first FE-based tool for the analysis of rigid pavements was developed in 1979 under the ILLI-SLAB software package (Ioannides, 1984). The original FE formulation of that software was based

on the classical plate theory on a Winkler foundation. A 2D thin plate element developed by Zienkiewicz (Zienkiewicz and Cheung, 1967) was used in that FE model. ILLI-SLAB used a rectangular four-node finite element with 12 degrees of freedom, first suggested by Melosh. Each node had three degrees of freedom: the vertical deflection in the z-direction, and two rotations about the *x*-axis and *y*-axis (Tabatabaie and Barenberg, 1980). In ILLI-SLAB, thermal loads could only be considered for one slab with fully bonded or completely unbonded slab-base interface conditions. Also, only a linear temperature distribution within the slab depth was allowed (Tabatabaie and Barenberg, 1980). In the case of a bonded stabilized base or overlay, full strain compatibility was assumed at the interface. For the unbonded layers, shear stresses at the interface were neglected (Heinrichs et *al*., 1989). Load transfer across the joints and cracks could be provided by aggregate interlock or dowels or by combinations of them (Ceylan et *al*., 1999). Since the first version, ILLI-SLAB has been under continuous revision and verification to improve its accuracy and capability. One of the improvements was the inclusion of elastic solid foundation. As such, ILLI-SLAB was the first program that had both types of ideal subgrades (liquid and solid elastic) in one package (Carrasco *et al*., 2010).

In 1986, Tayabji and Colley developed JSLAB based on ILLI-SLAB formulation. JSLAB had been revised to incorporate partial contact in slab/base interface, to consider non-uniformly spaced dowels in joints, and include the warping effect due to moister. JSLAB also calculated the thermal and principal stresses (Heinrichs *et al*., 1989). JSLAB was capable of considering a linear temperature and moisture distribution in a single layer pavement system of uniform thickness. For thermal analyses, JSLAB calculated thermal stresses after subtracting the stresses due to the slab weight. The next generation of this software, JSLAB2004, incorporated an axel configuration library and an "Express Mode" interface, while expanding the type of foundation models to six different subgrade types (Spring, Winkler, Boussinesq, Vlasov, Kerr, ZSS foundations). JSLAB2004 could analyze jointed concrete pavement responses under self-weight, traffic and thermal loads for a two-layer system of up to nine slabs. JSLAB2004 also provided the capability to calculate pavement responses and perform the time history analysis under moving loads at specified locations (Carrasco et *al*., 2010). In JSLAB2004, the FE model of the slab and the foundation was condensed to just one layer when thermal loads are

applied. For this reason continuous foundation models (e.g. Vlasov and solid elastic) could not be used in modeling multiple slabs (Carrasco et *al*., 2011). That program was able to model the separation between slabs and the foundation, as a consequence of positive and negative temperature gradient. However, modeling the horizontal interaction of slab-foundation is not possible.

ILSL2 was developed by Khazanovich and Ioannides to eliminate some of ILLI-SLAB's limitations. That finite element program used Totsky model (Khazanovich, 1994) to analyze interior loading cases more accurately by considering the effects of subgrade deformation under slab edges. ILSL2 offered a variety of subgrade options such as the Pasternak model, Kerr model and ZSS model. Only one single slab could be analyzed by using the Pasternak or Kerr foundation model. Khazanovich et *al*. developed ISLAB2000, at the ERES Division of Applied Research Associates, which had all the positive features of ILSL2 but was free of some unnecessary limitations (such as limitations on the number of nodes in the finite element model) (Carrasco et *al*., 2010). One of the improvements made during ISLAB2000 development was enabling curling analysis of slabs on the Pasternak and Kerr foundations. To do so, it was assumed that the slab and the subgrade was separated if there is a tensile stress between them. Rewriting of the code improved the software's ability to analyze mismatched joints and cracks, voids, mesh generation, load placement, and batch processing. ISLAB2000 could also solve pavement responses due to temperature, traffic, and construction loading. Moreover, it's Graphical User Interface for inputs and outputs made it more user-friendly (Buch et *al*., 2004).

EverFE is a rigid pavement three-dimensional FE analysis tool which was developed to overcome the limitation of 2D programs. 2D models are not capable of capturing detailed local responses and adequately model shear transfer at joints (Davids et *al*., 1998). EverFE was able to model up to nine jointed slab-shoulder system. Dowels, tie bars and linear or nonlinear aggregate interlock can be simulated at joints. Dowel looseness, dowel misalignment and mislocation can also be modeled in EverFE's 3D FE model (Davids, 2003). EverFE allowed for specifying up to three either bonded or unbonded elastic base layers. For unbonded slab-base interface, shear transfer can be captured via a bilinear elastic–plastic curve that defines the shear-stresses to relative-displacement constitutive relation. This relation can be obtained from an experimental push test for each type of base material to define the

relative displacement that slip occurs and to determine the frictional or shear stresses at the slip state. In this method the frictional or shear stresses are independent of the normal stresses. Linear or non-linear temperature gradient can be considered in that program. EverFE's finite element code employed 20-node quadratic brick elements to discretize the slab and the elastic base layers; 8-node planar quadratic elements for the dense liquid foundation; and 16-node quadratic interface elements to model both aggregate interlock joint shear transfer and shear transfer at the slab-base interface (Davids, 2003).

Recently, the National Cooperative Highway Research Program (NCHRP) developed a mechanistic-empirical method for rigid pavement design under project 1-37A, also called the Mechanistic-Empirical Pavement Design Guide (MEPDG) (AASHTO, 2004). This method employed a user-friendly procedure by incorporating several issues, such as actual traffic distribution by using axle load spectra, nonlinear temperature gradient, local environmental condition, local highway materials and damage (crack and faulting) prediction. Many highway agencies adopted the mechanistic-empirical design guide as a state-of-the-practice tool for the design of new and rehabilitated pavements.

2.1.4 Development of NYSLAB

To overcome the limitations of JSLAB2004, researchers at the University of Texas at El Paso completely redesigned this tool and developed a new JPCP analysis tool, named NYSLAB. The software was developed into a standalone executable program with a user friendly graphical interface. A new code, which was developed in MATLAB, significantly improved the capabilities of JSLAB2004. MATLAB's built-in capabilities allow for handling matrix and vector operations on which the FE method is based. The most significant improvements implemented in the first version of NYSLAB are:

a) Using an isoparametric finite element formulation that allows for the modeling of irregular geometries.
b) No limitation in the number of jointed slabs and foundation layers.
c) Using Mindlin plate theory (Reddy, 2004) to model PCC slabs to account for shear deformations that become significant for relatively thick plates.
d) Modeling contact between unbonded PCC layers and between PCC and foundation layer by using GAP elements to model separation between layers due to temperature gradient.

e) Extending foundation layer beyond the edge of the slabs to more accurately model the edge deflections and stresses.
f) Modeling of non-linear thermal gradient applied to any number of PCC layers.
g) Performing thermal analysis and calculating thermal stresses for any number of jointed slabs and for any type of foundation model.

Several comparison and parametric studies have verified the capability of the previous version of NYSLAB in calculating pavement responses for different geometric configurations, foundation models and parameters, and temperature gradient profiles (Carrasco et *al*., 2010 and 2011).

Although NYSLAB has increased the level of reliability in predicting the mechanical behavior of rigid pavements over other analytical tools, it still has some limitations. The major limitations of the initial NYSLAB are:

a) Slab elements in the mathematical model of NYSLAB have only three degrees of freedom per node: the vertical deflection and two rotations about the longitudinal and transverse axes. This means that only pure bending as a consequence of thermal curling; self weight and transverse loads can be captured in the PCC slabs while in-plane deformations, due to thermal expansion and contraction, cannot be considered.
b) NYSLAB employs Mindlin plate theory to model bonded slabs. Modeling bonded multi-layered system with different material property and thickness are not accurate using plate theories. Plate theories do not account for the inplane-bending coupling effect in an unsymmetric multi-layer composite system. For an unsymmetric composite lamiante, normal loads or bending moments may produce in-plane deformations in addition to bending in the laminate and in-plane forces may produce bending in addition to the in-plane deformations.
c) The Gap elements between unbonded layers can only model the separation (lifting) between layers due to thermal curling. Modeling the sliding between pavement layers and calculating the frictional stresses in their interface are not possible.

2.2 Laminated Plate Theory

Plates are flat structural elements, which their thickness is small compared to the in-plane dimensions. Applied loads to a plate may produce bending deformation and stretching. The plate bending properties may differ, based on its thickness-to-length ratio, and are determined with different assumptions and concepts. Thin plates are considered as two-dimensional structures with the plane strain state, where the plate normal deflection is small as compared to the plate thickness. The plane stress state is governed for thin plates with the thickness-to-length no greater than one-tenth. In thick plates, theories of thin plates become unreliable and thick-plate theory, which considers the plates as a three-dimensional problem of elasticity, should be applied to calculate their responses (Timoshenko and Woinowsky-Krieger, 1959; Reddy, 2007).

Two widely accepted plate theories are the Kirchhoff-Love theory (classical plate theory) and the Mindlin-Reissner theory (First-order shear deformation plate theory). The Classical plate theory adheres to Kirchhoff's hypothesis which states that straight lines perpendicular to the plate mid-surface before deformation remain straight, inextensible and normal after deformation. These assumptions lead to neglecting the normal strain and the transverse or out-of-plane shear strains. The "First-order shear deformation plate theory" assumes that the normal planes remain straight and inextensible but are not perpendicular to the plate mid-plane after deformation. This is equal to including transverse shear strains, which are considerable for relatively thick plates. In this case, the plate cross-section rotations (β_x and β_y) are not equal to the derivatives of the vertical displacement as in case of the classical plate theory (Reddy, 2004).

Composite laminates are formed by bonding layers with different thickness and material properties to achieve the desired stiffness. Laminates are used in applications that require bending and membrane strengths (Reddy, 2004). The mechanics of composite laminates have been investigated by several researchers (Jones, 1975, Daniel and Ishai, 2005). Two approaches have been proposed to analyze composite plates:

1- *Equivalent single-layer theory* (*ESL*), which considers laminated plates as a statically equivalent single layer having a complex constitutive behavior. ESL is based on reducing 3D continuum problem to a 2D problem by making certain assumptions. The "Classical laminated plate theory

(CLPT)" and the "First-order shear deformation laminated plate theory (FSDT)" are two promising theories based on the ESL.

2- *Three-dimensional elasticity theory,* which consists of traditional 3D elasticity formulations and "Layer-wise theory of Reddy". In those theories, each layer is modeled as a 3D solid element (Reddy, 2004).

In this study the ESL theory was employed for modeling the pavement slabs. The theory behind the ESL laminated plates will be discussed in chapter 3.

The classical laminated plate theory (CLPT) is the extension of the classical plate theory to composite laminates. The layers in the laminate are assumed to be perfectly bonded together and have uniform thickness. The zero out of plane shear stresses and strains in CLPT are equal to assuming infinity rigid plate in out of plane direction while it is certainly weaker in reality. This theory is acceptable for the analysis of thin plates, but for relatively thick plates, where the transverse deformations are not negligible and the failure is likely to occur in transverse directions, utilizing the classical theory is not accurate. The first-order shear deformation theory (FSDT) or Mindlin laminated plate theory is also an extension of Mindlin plate theory. This theory is an acceptable theory for the analysis of relatively thick laminates when the length-to-thickness ratio is larger than 20 (Bhatti, 2006). Transverse shear stresses can be calculated from the FSDT using the material law. However, the assumption of constant shear strains in thickness direction results in layerwise constant stresses (Rolfes and Rohwer, 1997). A number of studies have been conducted for analyzing the composite laminates for different applications using finite element models (Rolfes and Rohwer, 1997; Lee and Sin, 1994; Alfano et *al*., 2001; Goswami, 2006; Hu and Shi, 2009; Perez et *al*., 2005; Hughes and Tezduya, 1981; Bathe et *al*., 1989). These investigations dealt with various numerical problems in modeling composite laminates.

Most of the concrete pavement analysis tools such as ILLI-SLAB, JSLAB, WESLIQUID and WESLAYER utilize classical plate theory to model pavement slabs. In NYSLAB, the first-order shear deformation laminated plate theory will be employed to account for the shear deformation that becomes significant for relatively thick PCC slabs.

2.3 Loads in JPCP

Rigid pavements are subjected to traffic and environmental loads during their life. A design procedure that accurately considers the traffic and environmental conditions into analysis, results in better prediction of stresses and damages in the pavement, which in turn leads to a less maintenance and repair pavements that benefit the users through saving in money and time. Loads generated by trucks across the pavement slab and thermal gradients through the thickness of the slabs are the major loads used in the analysis and design of jointed concrete pavements since they are the most significant.

2.3.1 Traffic Loads

Traffic data and truck load distribution are two primary data in a life-time pavement design. In the 1993 AASHTO, the traffic flow of different axle loads and axle configurations is converted into an equivalent number of 18-kips single-axle loads, known as equivalent single-axle loads (ESALs). The total ESALs for the design are calculated by multiplying ESAL per vehicle to the average annual daily traffic (AADT), growth factor, lane distribution, and directional distribution. ESAL has been widely used as the traffic load data by most pavement design methods. However, it has been observed that using the ESAL value for any given axle load and axle configuration, which is to be an indication of its relative impacts on the pavement performance, is not capable of involving all factors that cause pavement damages. In addition to the factors such as pavement type and the present serviceability index that are used to determine the number of ESAL, a distress type, failure mode and other pavement conditions are important in applying the load distribution (Li et *al*., 2009; Haider and Harichandran, 2007). A more realistic approach to estimate the effects of actual traffic on pavement responses and distresses is the method proposed by the Guide for Mechanistic-Empirical Design of New and Rehabilitated Pavement Structures (2004). Instead of using ESALs, the new approach uses a load spectrum to account for variety of magnitudes and repetitions of each single load on the pavement. The predicted truck traffic in this procedure is classified by axle type (single, tandem, tridem or quad) and their axle load and axle repetition. This accurate characterization of truck load allows for more accurate prediction of pavement responses and for detailed damage analysis. The MEPDG requires specific type of traffic data for the design of pavement structures. Axle load distribution factors (ALDF), monthly

adjustment factors (MAF), hourly distribution factors (HDF), and vehicle class distributions (VCD) are some of the required data. Axle configuration and truck tire spacing are other required data used in a pavement design procedure.

2.3.2 Thermal Loads

Changing in temperature through the thickness of PCC slabs causes the pavement slabs to curl and may exert additional stresses in them. The resulting shape and stresses of curled slab depend on the sign and magnitude of the temperature gradient. During sunny days thermal expansion occurs throughout the PCC slab depth while the increase in temperature at the top is greater than that at its bottom; in this case the slab curls downward (concave down). During nights when temperature drops, the PCC slabs contract while the decrease at the top is greater than that at the bottom; in this case the slab curls upward (Corners lifted). The amount of curling depends on the temperature gradient and the slab length (Yu et *al*., 1998).

A mathematical solution to address the effect of temperature curling on concrete slabs was first introduced by Westergaard (1927) and then continued with Bradbury (1938) with graphical solution for curling stress. It was concluded that the curling stress due to temperature might be as high as the stress due to traffic loads. Westergaards's solution assumed full contact between the slab and a Winkler foundation and the calculated curling stresses in this method were not a function of the slab size. Westergaards's solution was limited to linear temperature gradients. The objections against Westergaard's linear temperature gradient raised since the study by Teller and Sutherland (1935), where they reported that the actual temperature gradient through the slab thickness were highly nonlinear.

Nonlinear thermal gradient can produce stresses in slabs due to their external and internal restraints (Ioannides and Khazanovich, 1998). Subgrade reaction, edge contact between adjacent slabs and slab-foundation friction are the external restraints that can produce stresses in slabs, due to thermal curling and thermal expansion or contraction. Also, the restraining interaction of surrounding layers across the slab depth, which resists against the distortion of the slab as a consequence of nonlinear thermal gradient, can produce additional internal stresses in the slab. This internal stress can be attributed to self-equilibrating stress (Zokaei Ashtiani et *al*., 2013).

The effect of nonlinear temperature gradient on pavement responses can be addressed by subdividing the stress due to the nonlinear temperature profile into three parts: a) the axial strain component caused by uniform temperature changes within the slab thickness (expansion or contraction) b) the equivalent linear bending strain, and c) the nonlinear self-equilibrating internal strains (Thomlinson, 1940). The uniform component of the total nonlinear temperature gradient produces expansion or contraction in concrete slabs, which results in their in-plane deformations. This uniform thermal component tends to produce uniform tensile or compressive stresses in the concrete slabs due to their external restrains, such as slab-foundation friction and edge contact between adjacent slabs. The linear part of the total temperature gradient produces curling due to the difference in temperature between the top and bottom surface of the slab. The linear temperature gradient tends to produce bending stresses in concrete slabs due to their external restraints, such as subgrade or foundation reaction, slab weight, and joint connection between adjacent slabs.

Based on the measured temperature data from six constructed concrete slabs, Richardson and Armaghani (1987) concluded that a quadratic profile is more likely to fit the actual temperature profile through the slab depth. Having the temperature value at the top (T_t), bottom (T_b) and mid-plane (T_m) of the concrete slab, the quadratic function will be determined as,

$$T(z) = A + Bz + Cz^2 \tag{2-1}$$

where z is the vertical distance from the bottom of the slab, and coefficients A, B, and C are expressed as:

$$A = T_b, \qquad B = \frac{4T_m - 3T_b - T_t}{h}, \qquad C = \frac{2(T_b + T_t - 2T_m)}{h^2} \tag{2-2}$$

Choubane and Tia (1992) used the same quadratic temperature distribution to propose a step-by-step solution to calculate stresses induced by nonlinear temperature gradient. Ioannides and Khazanovich (1998) noted that the linear bending strains only depend on the temperature difference between the top and bottom surface of the slab if the actual temperature gradient is expressed with quadratic function. In this case, only the second order component (C) contributes to the slab distortion or

self-equilibrating internal strains. The temperature at any discrete point through the slab depth can be used to characterize the quadratic equation. Since the greatest change in temperature profile throughout the slab depth occurs within the top portion of the slab, due to the impact of solar radiation, a quadratic equation that includes the temperature at a point close to the top surface, in addition to the temperature at the top and bottom surface, will better predict the nonlinearity of the actual temperature gradient (Bordelon and Roesler, 2009).

Mohammad and Hansen (1996) proposed a closed form solution for analyzing the residual or internal stresses in concrete pavements subjected to nonlinear temperature gradient. The total thermal stress in their method is calculated by superposing the internal stress to the stresses due to external restrains. They used a third-order polynomial to represent actual temperature profile in concrete slabs. In order to validate the closed form solution proposed by Mohammad and Hansen, Pane et *al.* (1998) developed a 3D finite element model to accurately model the in-plane and distortion behavior of the concrete slab due to nonlinear temperature gradient. The proposed 3D element (20-node brick element) allowed for specifying more than two temperature values across the slab thickness. The results showed that the assumptions of plane sections remaining plane for the slab subjected to nonlinear temperature gradient is valid for the entire section except for the 5 percent area close to the free edges. Also the predicted stresses profile obtained from 3D FE analysis were in well agreement with the closed form solution. Shokry et *al.* (2003) also examined the effect of nonlinearity in temperature gradient on dowel jointed concrete slabs by developing a 3D FE model. They concluded that the temperature gradient profile should not be modified by any breakdown into uniform and gradient components, i.e., the assumptions of superposition in slab stress calculation should be avoided. They highlighted the effect of dowel bars resistance to the thermal expansion and contraction of slabs.

An alternative process to calculate the slab stresses, subjected to nonlinear temperature gradient, is to use a piecewise integration approximation by assuming a linear temperature change between discrete temperature points throughout the slab depth. This method may be more accurate than the polynomial approximation of temperature-change (quadratic or cubic temperature profile), because many temperature data cannot be accurately matched with single polynomial equation. The separation of

the total temperature gradient into three axial, linear and self-equilibrating components can also be involved in this method. Janssen and Snyder (2000) proposed the temperature-moment concept for the estimation of linear temperature gradient by finding a linear gradient that produces equivalent bending moment from any given nonlinear temperature profile (Bordelon and Roesler, 2009).

In 2D FE-based analysis tools such as ILLI-SLAB and JSLAB2004, determining thermal load effects was limited to linear thermal gradient. Harik et *al*. (1996) proposed a method to superimpose the stresses induced by the nonlinear temperature change to the stresses caused by linear temperature gradient, obtained from the 2D analysis tool through the finite element analysis. The 3D FE rigid pavement analysis tool, EverFE, and 2D FE tool ISLAB2000 can consider linear or nonlinear temperature gradient in the analysis.

2.3.3 Built-in Curling

In addition to the temperature gradient due to daily temperature change through the slab depth, the combination of these four nonlinear components can also influence the curling in concrete slabs (Lederle et *al*., 2001; Rao and Roesler, 2005):

1. Built-in temperature gradient - PCC slabs are flat and the temperature gradient is always zero during initial curing of the concrete. However, before the concrete hardens, the concrete slabs may be exposed to high temperature in sunny days, which results in high positive temperature gradient. This temperature gradient refers to "zero-stress temperature gradient" that is developed in the PCC slabs. When that gradient in the slabs is removed and the temperature gradient reduces, the slab tends to curl upward. This can translate to an effective temperature gradient, with the opposite sign but the same magnitude as the positive "zero-stress temperature gradient", which is built into the PCC slabs (Beckemeyer et al., 2002; Rao and Roesler, 2005). It can be concluded that a zero temperature gradient does not necessarily correspond to the flat slab condition and the slab curls upward when the temperature gradient is zero.

2. Moisture gradient - The curling can also occur because of the difference in shrinkage strains, due to different relative humidity between the top and bottom of the concrete slab. The amount of curling in the slab in this case is influenced by the environmental condition and drainage (Janssen, 1987; Lim et *al*., 2009).

3. Drying shrinkage - Drying shrinkage occurs in concrete slabs after hardening and is affected by early-age curing condition. The amount of drying shrinkage is higher at the top of the slab than at the bottom because of the high relative humidity at the bottom. This difference in drying shrinkage results in permanent shrinkage within the concrete slab, which causes the slab to curl upward.

4. Creep - Creep can cause stresses in curled slab during the early ages of concrete drying, due to external restrains such as slab self-weight and edge contact between adjacent slabs. Different creep strains between the top and bottom of the slab tend to counteract the effect of fixed curling in the slab, due to shrinkage and built-in temperature gradient. Studies indicate that creep can have a significant impact on the stresses and strains in concrete pavement slabs due to curling and warping in both the early ages of the slab and the long-term life of the slab (Lederle et *al*., 2001; Jeong et *al*., 2004).

The combination effect of these components (built-in temperature gradient, moisture gradient, drying shrinkage and creep) was defined as an effective built-in temperature difference (EBITD) (Jeong et *al*., 2004). This has also been reported by other researchers as "locked-in curvature" and "zero-stress temperature". In the 2002 AASHTO Design Guide, except for the moisture gradient that is modeled using monthly/seasonal fluctuations in ambient relative humidity, the other three components of the effective built-in temperature were grouped together as the "permanent" curl and obtained through calibration as –5.6ºC (Yu et *al*., 2004).

The built-in curling components are influenced by concrete material properties such as coefficient of thermal expansion, thermal conductivity, permeability, and mix design parameters (Rao and Roesler, 2005). The paving season and time of day are found to directly affect the magnitude of built-in temperature gradient. It has been observed that pavements that are constructed during the late fall or late in the day or during nights develop a small amount of built-in curling (Hansen et *al*., 2006). A study by Hansen et *al*. (2006) concluded that the slab stress, due to the combined effect of built-in and daily temperature changes and multi-axle loading at joints, are below the stress necessary to initiate fatigue failure (below 45% of the flexure strength). They indicated that the additional slab uplift due to moisture warping is a factor for inducing top-down cracking.

Determining the amount of built-in curling, which can be defined as an equivalent temperature gradient causing the deformed slab, is an important concern in a pavement design procedure. One of the traditional methods to quantify the built-in curling in a concrete slab is to use a surface profiler to measure the deflection along the length of the slab. The surface profiles are then compared and fitted to the deflection of the same slab, estimated by a FE program subjected to a range of temperature gradients. The temperature gradient that produces the same deformed slab as the measured surface profile is considered as built-in temperature gradient. The drawbacks of using surface profiles are their limited resolution and disregarding the situation in which the slab comes in contact with the base or subgrade. Other studies have used measurement instruments along with thermocouples embedded in the slab to find the temperature gradient in which the slab comes in contact with the base layer. One of the drawbacks of this method is the difficulty in determining when the slab comes in contact and when the flat slab condition is reached (Yu et *al*., 1998; Fang, 2001). Another method is to backcalculate the built-in curling by employing an artificial neural network and using the results of falling weight deflectometer (Lederle et *al*., 2001).

An FHWA-sponsored study (Yu et *al*., 1998) showed that the magnitude of built-in curling is about 1 °F/in. on average for pavements in a wet-freeze climate (Beckemeyer et *al*., 2002). The 2008 AASHTO design guide established a value of -10 °F as optimum built-in temperature gradient to minimize cracking during the national calibration. In case of available local calibration, the local value can be used.

2.4 Load Transfer Devices in JPCP

Four types of joints with different functionalities are usually used in concrete pavements: transverse joints, longitudinal joints, construction joints and expansion joints. In jointed concrete pavements, load transfer devices are used in both the longitudinal and transverse joints to facilitate transferring load, caused by traffic and environment, from one slab to the adjacent slab. Load transfer is a design parameter that characterizes the reduction in load resistance capacity of the loaded slab due to presence of load transfer devices at the joint. The main purposes of using load transfer systems in transverse joints are to prevent faulting, reduce slab deflections, control mid-slab cracking, reduce

pumping and bending stresses in slabs due to loss of base support and finally provide a smooth, safe and comfortable ride (Byrum et *al.* 2001; Snyder, 2001; Hammons et *al*., 1995). Two principal methods that are commonly used to provide load transfer across the transverse joints are "Aggregate and key interlock" and "Dowel bars". Figure 2.1 and 2.2 show the application of these load transfer devises in jointed concrete pavements.

Aggregate and key interlock transfer the loads through friction across irregular cracks and joints. This mechanism is effective only for low volume traffic and small join opening (Ioannides and Korovesis, 1990). Dowel bars are used to transfer the loads caused by thermal curling and high traffic across the joints. Elastic properties and size of dowels and concrete slabs as well as the dowel spacing affect the performance of load transfer mechanism. The dowel bars are often constructed to allow for the horizontal movement of slabs, caused by thermal and moisture expansion and contraction. Dowels are anticipated to move freely along their length, thus the dowel axial force is considered negligible. In order to fulfill this functional purpose, the dowel-concrete interaction should be minimized by using bond-breaking agents. Also, substantial effort should be performed to ensure appropriate dowel alignment (Buczkowski and Torbacki, 2001).

Figure 2.1 : Aggregate interlocks (Hoffman, 2009).

(a) Tie Bars (b) Dowels

Figure 2.2: Application of dowels and tie bars (Hoffman, 2009).

The performance of load transfer in dowel bars depends on the interaction between the bars and the supporting concrete matrix (known as modulus of dowel support), which can be obtained by loading test. The contact between dowel bars and concrete in the area close to joints eventually lose, due to repeated traffic loads and poor constructions. Consequently, voids formed around the dowels will cause dowel looseness (Maitra et *al*., 2009). Some studies show that dowel looseness intensely affects the load transfer efficiency, which in turn results in larger deflections and stresses in concrete pavements (Davids, 2000).

Evaluation and design of dowel bars have been examined by several researchers since 1930. The finite element procedure for analyzing the behavior of dowel bars was first developed by Tabatabaie et *al*. (1979) during the process of development of ILLI-SLAB. They suggested 1.0 ℓ instead of 1.8 ℓ (ℓ is the radius of relative stiffness of the slab-subgrade system) for the effective distance of dowel's effective action. They used a constant value for modulus of dowel support in their 2D model. A number of numerical studies showed that only dowel diameter, modulus of subgrade reaction and modulus of dowel support have significant impact on pavement responses (Ioannides and Korovesis, 1992). Maintaining the dowel diameter constant, these researchers adopted joint load-transfer efficiency which is the ratio of the deflection of the unloaded side to the loaded side.

The ILLI-SLAB model considers dowel bars as thick-beam element. In this small span beam element, the main load transfer mechanism is shear since the effect of bending is negligible. The shear

stiffness of supported dowels consists of two parts, which are combined as springs in series: the shear stiffness of thick beam and the stiffness provided by the concrete matrix, which manifested as dowel-concrete interaction. In the calculation of the second part of the spring stiffness, the embedded segment of dowels was considered as infinity long beam resting on a Winkler foundation. Nishizawa et *al*. (1989) developed a three dimensional finite element model to improve the embedded segments by considering it as a bending beam element with finite length. Dowel looseness was not addressed in their models.

Gue et *al.* (1993) proposed a model to consider looseness by assuming the uniform looseness for all dowels to predict the pavement responses for various degrees of dowel bar looseness. They found out that longitudinal flexural stresses are sensitive to the degree of dowel bar support. Channakeshava et *al*. (1993) simulated the small gap caused by dowel looseness by implementing interface spring elements, connecting the nodes in beam element and concrete elements. The stiffness of these elements can be obtained similar to the experimental and analytical analysis for computing the subgrade reaction spring. They performed separate localized analysis to predict the effect of local stress caused by dowel looseness. The spring load versus vertical displacement curve obtained from applying shear force to the dowels caused bending in the concrete matrix. This demonstrated the nonlinear treatment and a gradual loss of stiffness in dowels with increase in load.

Davids (2000) developed a three dimensional finite element model based on the embedded beam finite element formulation to model the dowel looseness and inclusion of bond-slip law between dowel and slab. Results indicated that small gaps between dowels and slabs (<0.2 mm) increase vertical stress at base layer and tensile stress in the concrete slab, subjected to traffic and temperature loads. Motamarri (2003) performed a comprehensive experimental study to examine the behavior of dowel-concrete interface. The attempts were involved testing on the performance of bond-breaking materials, finding strain profile in concrete around dowel bars, measuring pulling and pushing forces of dowels and predicting coefficient of friction at the dowel-concrete interface.

Load transfer systems in longitudinal joints are commonly needed for slabs with widths larger than 15 feet and are achieved through aggregate interlock, tie bars or the combination of both mechanisms. Tie bars are usually used to hold the adjacent slabs together. In the design process, the

proper tie bar is chosen to hold the slabs over base layer without yielding or pulling out the steel bars. Tie bars spacing depends on the thickness of slab, the friction between the slab and the base layer and the distance to free edge. Tie bars are constrained to move along their length. Consequently, the bond between steel tie bars and concrete produces shear stiffness in their interface (Choi and Won, 2009). The pull-out test is required to obtain the bond behavior. Concrete strength, steel bar yield strength, bar size and surface condition were found to have significant impact on the bond actions (Mallela et *al*., 2009). Many researches proposed bi-linear or tri-linear relationship to define the bond stress - slip relationship in the tie bars - slab interaction.

2.5 Foundation Models

In a rigid pavement system all traffic and environmental loads are transferred from the concrete slab to the foundation layers. Foundation domain which may consist of stabilized base, unbound granular base, granular subbase and compacted or natural subgrade layers provide support to the concrete slabs. The following is a detailed description of the foundation models currently used in the analysis of rigid pavements.

2.5.1 Winkler Foundation

Winkler model is the simplest idealization of foundation behavior in a problem of rigid slabs on foundations. The Winkler foundation model considers the slab supporting layers as an infinite set of independent linear elastic vertical springs with a constant axial stiffness (Ioannides et *al*., 1985; Huang, 2004; Ioannides, 2006). The stiffness is referred as the modulus of subgrade reaction. There is no shear interaction is assumed between springs in this model. The Winkler foundation is also referred as dense liquid foundation, where the displacement at each spring is proportional to the load applied to it and completely independent of the pressure or displacements produced at the neighboring points. The vertical pressure produced at any point on the foundation surface in the Winkler model is assumed to be proportional to the vertical deflection *w*(x,y) at that point as,

$$q_{(x,y)} = Kw_{(x,y)} \tag{2-3}$$

where K is the spring axial stiffness defined as $K = Ak$, with k is equal to the Winkler parameter (modulus of subgrade reaction) and A is the associated surface area.

The main drawback of using the Winkler model is that the plate (slab) experiences a rigid body deflection without any bending moment or shear force when subjected to uniformly distributed loads (Dutta and Roy, 2002; Ioannides et *al*., 1985). This may lead to an extremely unrealistic response prediction in the analysis of slab on grade. Also, this foundation model is unable to predict the soil domain displacement at the slab edges. There are discontinuities in the soil responses inside and outside the slab, and the soil displacement outside the loaded plate is assumed to be zero. Another issue with the Winkler model involves difficulties in determining the modulus of subgrade reaction or *k*-value. The value of *k* is not unique for a specific type of soil and it depends on the geometry and elastic properties of soil, the plate dimension and the level of applied load (Vallabhan and Daloglu, 1999). Because the *k*-value is the only parameter in the Winkler model that characterizes the subgrade stiffness, care must be taken for its accurate determination for practical pavement design.

Several researchers such as Terzaghi (1955), Cheung and Zienkiewicz (1965) and Vesic (1961) studied to develop techniques to calculate the Winkler parameter. The methods for estimating the subgrade *k*-value in a pavement design procedure were categorized in NCHRP 1-30 to three general approaches: correlation methods, backcalculation methods, and plate testing methods (Hall et *al*., 1997).

Correlation Methods

The accuracy of correlation methods for the calculation of *k*-value for new/reconstruction designs depends not only upon the soil properties, such as soil classification, moisture level, density, California bearing ration (CBR), or Hveem stabilometer (R-value) data, but also upon the slab size and stiffness. One of the first correlations for k-value was proposed by Vesic (1961). He found a correlation for the Winkler parameter, which is a function of both the soil stiffness and the slab stiffness:

$$k = \frac{0.65E_s}{(1-\nu_s{}^2)} \sqrt[12]{\frac{E_s B^4}{EI}} \tag{2-4}$$

where E_s and v_s are the modulus of elasticity and Poisson's ratio of the soil, B is the footing width and E and I are the modulus of elasticity and moment of inertia of the square footing. Vesic reported the lack of assurance of the correlated Winkler parameter since he found that the footing length-to-width ratio, the load distribution, the depth of the soil continuum and the layering effect yield non-unique *k*-value (Straughan, 1990).

According to the 1986 ASHTTO, the estimation of *k* is through the correlations with the subgrade resilient modulus, as well as various adjustments for the base layer stiffness and thickness, presence of shallow rock, potential loss of slab support due to erosion, and seasonal variations. In the 1993 AASHTO and NCHRP 1-37A design guide, the value of subgrade, base, and subbase resilient modulus are the direct inputs that are adjusted with environmental effects and then converted into an average monthly effective *k*-value (Christopher et *al*., 2006). Another correction to the seasonally adjusted k-value in the correlation method is applied when the fill material is placed above the natural subgrade, or a rigid layer is present at a depth of 10 ft or less beneath the existing subgrade surface.

Back-calculation methods

Back-calculation methods are appropriate for rehabilitation purposes. Nondestructive methods, such as the falling-weight deflectometer (FWD) testing method, are applicable for estimating the *k*-value in case of overlay or reconstructed pavements design. Two of the back-calculation algorithms are the AREA method and Best-fit method, which are currently included in the AASHTO design guide:

1. *AREA algorithm*. In the AREA method, the area of the concrete slab deflection basin obtained from the numerical analysis is matched with the area of the slab deflection from FWD testing. The AREA method proposed in the AASHTO assumes the concept of infinite slab (Westergaard model) and employs the radius of relative stiffness as a function of the area of the slab deflection to calculate the subgrade k-value. In this method, different sensor configurations in FWD analysis may be employed to investigate their effect on the back-calculated results (Hall et al., 1997). For any given number and configuration of sensor deflection, the AREA parameter is computed from the trapezoidal rule. In the calculation of the area of deflection basin, the slab deflection at different sensor location is normalized

to the deflection of either the point of applied load or the third sensor, 12 inches away from the point of applied load.

The advantage of the AREA method proposed in the AASHTO is in its ease of use without the need for using backcalculation software. The disadvantages of this algorithm involve the assumption of horizontally infinite slab and foundation, and the idealization of the entire pavement structure above the subgrade as a single slab. To compensate the first limitation, a correction factor for finite slab size for correcting the back-calculated results was proposed in the AASHTO design guide. Alternatively, to avoid the inaccurate results from the analysis of infinite slab, the deflection basin obtained from finite element analysis can be used to calculate the area. To address the second limitation, a method for dividing the composite elastic modulus of the pavement into two modules for the slab and the base has been proposed (Hall et *al*., 1997).

2. *Best Fit algorithm*. The best fit algorithm is another back-calculation method that aims to find a combination of concrete elastic modulus and subgrade *k*-value for which the calculated deflection basin closely matches the measured profile from FWD tests. The problem can be represented as the minimization of the error function, defined as follows:

$$F(E,k) = \sum_{i=0}^{n} \alpha_i (w(r_i) - W_i)^2 \tag{2-5}$$

where α_i is the weighting factor, $w(r_i)$ is the calculated deflection, and W_i is the measured deflection. The detailed equations for the minimization of the error function with respect to k and ℓ can be found in Hall (1992), Khazanovich (2001), and Ioannides (1990).

2.5.2 Elastic Solid Foundation

It has been investigated by several researchers (Cheung and Zienkiewicz, 1965; Pickett and Ray, 1952) that the actual behavior of soil is more like elastic solid rather than dense liquid. Unlike the Winkler model that assumes no interaction between adjacent springs, the solid elastic foundation considers full shear interaction in the soil stratum. Therefore, the surface deflection is continuous, meaning that the deflection at any surface point is influenced by the loads acting on other points. The

solid elastic model is often called as "Boussinesq" model. Pickett et *al*. (1952) developed theoretical solutions for concrete slabs on an elastic half-space. Their research resulted in design charts for concrete pavements. In the Boussinesq equation, the deflection of any point *j* due to a point load at *i* (P_i) on an isotropic elastic half-space is given as:

$$w_{ij} = \frac{P_i(1-\nu_s^2)}{\pi E_s r_{i,j}} \tag{2-6}$$

Where r_{ij} is the distance between points *i* and *j*, and E_s, ν_s are modulus of elasticity and Poisson's ratio of the soil. That equation was developed by Giroud (1968) and used in ILLI-SLAB to calculate deflection over an elastic foundation. The deflection at the center of the uniformly loaded rectangular area can be calculated as follow (Figure 2.3):

$$w_{ii} = 4\int_{\xi=0}^{\xi=\frac{a}{2}}\int_{\eta=0}^{\eta=\frac{a}{2}} \frac{P_i(1-\nu_s^2)}{ab\pi E_s}\frac{1}{\sqrt{(\xi^2+\eta^2)}}d\xi d\eta \tag{2-7}$$

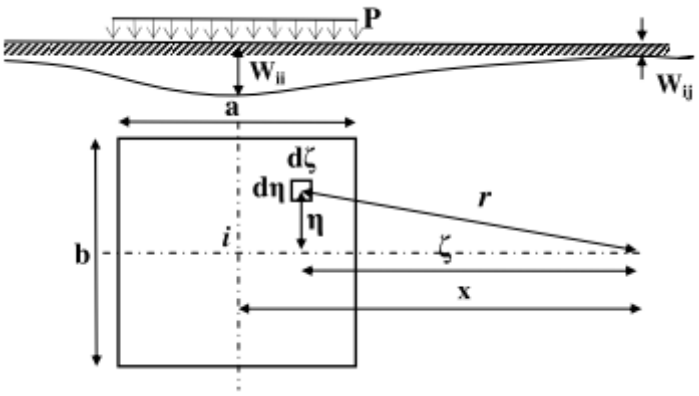

Figure 2.3: Soil deflection due to uniform rectangular load in Boussinesq model (Cheung et *al*, 1965).

where, *a* and *b* are the dimensions of the rectangular element formed by connecting the center points of the four elements connected to each node in the FE mesh of the foundation. For edge and corner nodes this equation is adjusted to account for the fact that there could only be two or one element connected to a node. It should be noted that this formulation is only valid for rectangular elements. For the point

outside the rectangular loaded area, the deflection can be calculated using Eq. 2-7 by replacing the rectangular load with the resultant force *P*.

Cheung and Zienkiewicz (1965) proposed a method for incorporating the elastic solid subgrade in a two-dimensional plate bending finite element model. Their solution for this problem was as complete as the Westergaard solution. To introduce soil nonlinearity, Ioannidas et *al.* (1985) proposed a resilient modulus characterization for the elastic solid foundation (Limouee, 2009).

The shear interaction described by the Boussinesq model is stronger than usually observed in the field. Since Boussinesq is a continuum model, it is not well suited for implementation on previous analysis software that directly adds the foundation stiffness to the slab stiffness (Khazanovich, 2003).

2.5.3 Two Parameter Foundation

As discussed before, the discontinuous nature of spring elements in the Winkler model implies no interaction among the soil medium. This may lead to an inaccurate idealization of subgrade behavior, especially in the case of extreme external applied load. In this case, the subgrade response is limited only to the point of applied load while the neighboring points remain unaffected. The completely continuous model in elastic solid theories has also been found to be not absolutely accurate, because the responses of subgrade decade faster than predicted by Boussinesq theory (Ioannides et *al*., 1984). The high shear interaction for soil medium in elastic solid models results in generation of infinite stresses under the edges and corners of the resting plate (AASHTO, Appendix QQ, 2003).

The inherent problems with the Winkler model and the mathematical complexity of the elastic solid model have encouraged researchers to improve the idealization of subgrade with more realistic models. Two-parameter models have been proposed with the intension of adding another parameter to the axial stiffness in the Winkler model to better represent the behavior of surrounding soil domain.

Filonenko-Borodich foundation

Filonenko-Borodich (1940) improved the Winkler model by connecting the top ends of the individual Winkler springs with an elastic membrane, stretched to a constant tension T (Dutta and Roy, 2002). Figure 2.4 shows the mathematical idealization of this model. The mathematical formulation of this model can be expressed as:

$$P = kw - T\nabla^2 w \tag{2-8}$$

where P and w are the surface subgrade pressure and deflection, respectively. k is the axial stiffness of the vertical springs similar to the Winkler model and T is the tensile force. No method is offered for the determination of k and T in that model.

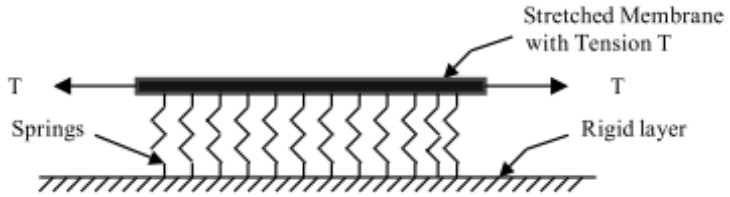

Figure 2.4: Filonenko-Borodich foundation model (Dutta and Roy, 2002).

Hetenyi's foundation

In this model, the interaction amongst the discrete springs is achieved by incorporating a thin elastic plate with flexural rigidity D, as shown in Figure 2.5. The subgrade pressure in this model determined as:

$$P = kw + D\nabla^4 w \tag{2-9}$$

where all the terms have been previously defined. In this model no method is suggested for the computation of D.

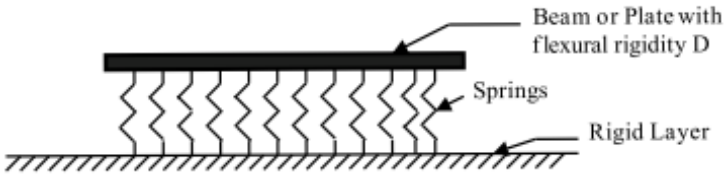

Figure 2.5: Hetenyi's foundation model (Dutta and Roy, 2002).

Pasternak foundation

Pasternak improved the Winkler model by connecting the top of the springs with an incompressible plate that can only carry shear stresses (Figure 2.6). The subgrade pressure in this model can be represented as:

$$P = kw - G\nabla^2 w \tag{2-10}$$

where, G is the shear modulus of the shear layer. The detailed formulation of the model can be found in the literature (Pasternak, 1954).

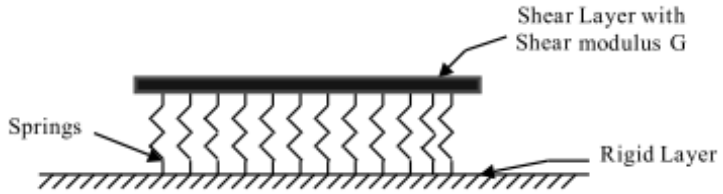

Figure 2.6: Pasternak foundation model (Dutta and Roy, 2002).

A primary problem with the presented two-parameter foundation models is that the second parameter, used to connect the vertical springs, has no physical meaning and obtaining them is not feasible. Recognizing the impracticalities involved in the implementation of the proposed foundation model, Vlasov and Leont'ev started with the modification of elastic solid model to introduce a new foundation model.

Vlasov foundation

Vlasov's theory (Vlasov and Leont'ev, 1966) for the analysis of structures on elastic foundations was developed on the basis of Vlasov's general variational method. This theory considers the elastic foundation as a single or two-layer model, which is characterized by normal stiffness and shear stiffness obtained from general soil elastic properties and the layer dimensions. The Vlasov model, which considers shear interactions between spring elements in each foundation layer, is more realistic than the simple idealization in the Winkler theory and is simpler than the theory of the elastic solid semi-infinite space. In addition, another parameter was introduced in Vlasov model, identified as γ, to characterize the

vertical deformation profile within the soil continuum. However, no procedure was developed by Vlasov to calculate the value of γ.

Vallabhan and Das (1989) developed an iterative procedure to estimate the γ for a problem of beams on elastic foundations. They found that for a uniformly loaded beam on an elastic foundation, the γ parameter is dependent upon the ratio of the depth of the soil stratum to the length of the beam (Straughan, 1990). Vallabhan and Das (1989) concluded that if the loads are fairly evenly distributed on the beam, the results from the Vlasov model are sufficiency accurate for practical designs. Jones and Xenophontos (1977) used variational principles to obtain parameter γ by experimental examination instead of an iterative procedure.

2.5.4 Kerr Foundation

The Kerr foundation model is a three-parameter model developed to extend the two parameter models (Pasternak) in an attempt to make them more realistic. The Kerr model consists of two spring layers, interconnected by a shear layer (Kerr, 1964). This model considers a two-layer foundation, assuming that the upper layer is very thin so that its shear stiffness is negligible (Figure 2.7). The main advantage of the top spring layer is to enable the two parameter foundation model to take into account the level of continuity of the vertical displacements of soil at the boundary of slab edges.

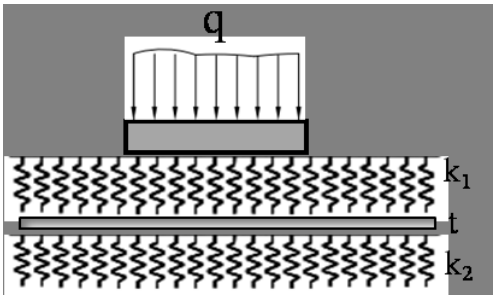

Figure 2.7: Description of a loaded plate placed over Kerr foundation.

The response of the foundation surface subjected to a uniformly distributed load q(x,y) is governed by:

$$\left(1+\frac{k_2}{k_1}\right)q-\frac{t}{k_1}\nabla^2 q = k_2 w - G\nabla^2 w \tag{2-11}$$

where k_1 is the stiffness of upper spring layer, k_2 is the stiffness of lower spring layer, and t is the stiffness of shear layer. According to the Kerr conclusion, the advantage of this model is that "because of the upper spring layer, no concentrated reactions or infinite reaction pressure can appear, not even along the edge of a rigid stamp". Another advantage of this model over two parameter foundation models is the additional boundary condition that may restraint the foundation, which may affect the behavior of the top structure. A detailed study on the equilibrium equation of Kerr foundation and the process of obtaining the Kerr Foundation parameters were developed by Jones and Xenophontos (1976). One of the weaknesses of the Kerr model is in its requirement of three parameters that are difficult to determine experimentally.

2.5.5 Zhemochkin, Sinitsyn and Shtaerman (ZSS) Foundation

The Zhemochkin-Sinitsyn-Shtaerman (ZSS) model is a two-parameter foundation model based on plasticity concepts that consists of a series of independent springs on an elastic half-space (Khazanovich, 1994). The ZSS model is a combination of the Winkler and the Boussinesq model. Non-recoverable spring deformations simulate the plastic component and the resilient parts of soil deflections are modeled through the elastic half-space. For high k-values (Winkler parameter), ZSS produces results similar to the conventional Boussinesq model. Shtaerman and Hemtenyi suggested a simpler linear model by ignoring the plastic deformations and assuming both deflection components as elastic, which is the predicted behavior in the JSLAB implementation (Khazanovich, 1994). The ZSS model allows deflection profile discontinuities at a loaded slab edge, which is equivalent to the Winkler model assumptions (Limouee, 2009).

2.6 Contact between Pavement Layers

In JPCP, the contact conditions along the slab-foundation interface significantly impact the mechanical behavior of pavements. The contact between pavement layers can be considered either bonded or unbonded in their design process or in their construction. In bonded slabs, shear stresses can be transferred completely in their interface, and theoretically no sliding or separation can occur between them. On the other hand, unbonded slabs can move with respect to each other and shear stresses can be produced in their interface when they are subjected to external loads. Analyzing the contact condition in

this dissertation is focused on the contact between slab layers that are unbonded in their interface, and between the bottom slab layer and the foundation surface. The influence of contact condition is more pronounced when the pavement is subjected to thermal loads. Even though several researchers have attempted to identify and model the contact between pavement layers, there are still many gaps that need to be explored in order to accurately account for the separation and slipping of pavement slabs under thermal loads in a pavement analysis process. What is fundamentally missing from most efforts is an attempt to model the horizontal interaction between slab and foundation and calculate the frictional stresses.

2.6.1 Characteristics of Contact between Dissimilar Bodies

Most of the finite element analyses of structural systems involve analyzing the contact between dissimilar sections. The nature of contact between two surfaces may depend on the magnitude and direction of applied loads and the characteristics of contacting surfaces. For most of the contact problems, the impenetrability condition may be applied which implies that no boundary point of the first body in contact can penetrate the other. Based on that restriction, the contact constraints for each pair of associated nodes in contact can be defined in their normal direction. The normal contact constraint states that the contact normal traction is compressive if two boundary nodes are in contact. On the other hand, the normal traction is zero if the boundary nodes are separated.

The contact may also be frictional or frictionless. The presence of friction can produce tangential or shear traction, as well as normal traction, along the contact region. The frictional constraints can be defined as tangential tractions that take action opposite to the direction of slippage. The tangential tractions cannot go beyond the specific limit of frictional stresses. Depending on the state of the contacting surface and the level of applied loads on the interface, contact condition in the tangential direction can be in the completely stick or completely slip mode. In the stick mode, the magnitude of tangential traction is lower that the limit value of frictional resistance. In this zone both normal and tangential displacements are continues along the contact area (Urzua et *al*., 1977). When the applied tangential tractions exceeds the frictional or bond resistance limit, the relative body movement increases and slip occurs.

Of particular interest in a rigid pavement system is pavement layer connections. Pavement slab layers are not bonded together unless a proper interlayer bond material is employed. The contact between the bottom slab layer and the foundation surface is generally unbonded. In JPCP, the contact conditions along the slab-foundation interface significantly impact the mechanical behavior of pavements. As described in the previous sections, under thermal curling the pavement slabs may lose their contact from the foundation (uplifting). Also, the horizontal displacements, due to thermal expansion and contraction in concrete slabs, can produce frictional contact between slabs and foundation.

In the next section, the finite element procedures that have been proposed to model the contact between pavement layers will be reviewed.

2.6.2 Solutions to Contact Problems

Several finite element techniques and mathematical solutions have been proposed to analyze contact problems for different structural systems. In such problems, non-linearity arises both from changing the state of contact and presence of friction. Thus, even for a structural system with linear materials and solution schemes, solving the problem involving contact requires nonlinear or iterative process.

In one of the solution strategies, contact problems are considered as a case of minimization of a functional, e.g. potential energy or virtual work, subjected to particular constraints. Variational principles can be applied to the equilibrium equations and constraints model to create the weak formulation. Contact constrains in this case can be formulated as variational inequalities in the weak formulation to be used in the optimization of variational equations (Petersson, 1977; Tornstenfelt, 1983; Fredriksson et *al*., 1977; Oden and Kikuchi, 1982; Shyu et *al*., 1989). The Lagrangian multiplier, the Penalty method and the mixed or hybrid method are three generally used methods applied in the finite element solution procedure involving contact to use in optimization of variational equalities.

The Lagrange multiplier method imposes the contact constraint by applying an exact value as the Lagrange multiplier to the variational equations. In this method, nodal displacements and Lagrange multipliers are considered as independent variables. In the penalty methods, the displacement constraints

are imposed as constant penalty parameters to the weak form of equilibrium equations. This is accomplished by assuming that the normal and tangential tractions at each contacting point are proportional to the relative displacement (in the normal or tangential directions) of its associated adjacent nodes in contact (Chandrasekaran et *al*., 1987; Pantano and Averill, 2002; Shyu et *al*., 1989). The penalty parameters in this method are the approximate value of Lagrange parameters. The solving process in this method offers approximate solutions. However, many studies showed acceptable results for different contact problems using the penalty method. A complete study and application of the penalty method can be found in the works of Fiacco (2007), Peric and Owen (1992) and Pantano (2002). The mixed method considers displacements and tractions as independent variables. Several studies have been conducted to make use of this method (Heyliger and reddy, 1987, Simo et *al*., 1985) that consider element displacements or contact tractions as nodal values in the global equilibrium equations.

In another class of solution, contact conditions are applied directly by imposing the geometric compatibility of the contacting surface during the incremental loading process (Chandrasekaran et *al*., 1987). The main advantage of this method is that the various frictional conditions at the interface can be easily imposed and the algorithms are generally independent of the material constitutions. Francavilla and Zienkiewicz (1975) proposed a procedure to obtain flexibility matrices in terms of contact pressure for frictionless contact problems, and Sachdeva and Ramakrishnan (1981) extended this method for two-dimensional contact problems with friction. In that model, compatibility of displacements is applied to the nodes in contact depending on their contact condition. The number of iterations needed to solve the problem in these methods is quite small. Okamoto and Nakazawa (1979) formulated the incremental equilibrium equations by using the principle of virtual work. The geometrical and the kinematic boundary conditions on contact surfaces are considered as additional conditions, independent of the stiffness equations. The advantage of their model is that in each solution step only part of the simultaneous equations, referred as the contact surface, is required to be solved instead of overall equations. Chandrasekaran et *al*. (1987) presented a finite element procedure to predict the contact surface tractions and the area of contact. In that procedure, at the end of each equilibrium iteration, additional load increment is applied to comply the geometric compatibility. That method leads to a good

result after little iteration. Shyu *et al*. (1989) proposed a mixed finite element method for contact problems with friction. In that method, the finite element formulations are obtained from a perturbed Lagrangian variational principle, where both the displacements and the contact pressure in each element are predicted.

2.6.3 Contact Constitutive Relationship

In addition to finding a solution method for the contact problem, an appropriate constitutive relationship for the frictional behavior of the bodies in contact needs to be defined. Classical and non-classical friction laws are two commonly used constitutive relations in contact problems. Several studies solving the contact problem with classical (Chandrasekaran et *al*., 1987; Campos et *al*., 1982) and non-classical (Oden and Pires, 1983; Oden and Pires, 1984) friction laws have been reported in the literature. For the contact problems involving soils, a constitutive model representing the elasto-plastic behavior of the contact condition of rock joints that allows for dilation, roughness, and hardening and softening responses of joints, can be applied (Carol and Alonso, 1983; Desai et *al*., 1984; Ghaboussi et *al*., 1973; Gens et *al*., 1990). For the application of soil-structure interaction, a simple linear elastic Mohr-Coulomb strength principle can be used to define the maximum allowable shear stresses (Day and Potts, 1994; Beer, 1985).

For an ideal contact system between two rigid surfaces with no adhesion, a linear relationship between the normal force (weight) and the amount of frictional force can be assumed by applying coefficient of friction. However, in reality, the adhesion between layers and deformability of two bodies in contact are not linear behaviors. Therefore, assuming a linear relationship between the normal force and the frictional resistance is not an accurate method for determining the frictional resistance. Wesevich et *al*. (1987) conducted a comprehensive study and experimental work on the frictional behavior of several stabilized bases in concrete pavements. They concluded that for loose bases, the failure plane at sliding is at the slab-base interface and thus, the magnitude of frictional resistance is directly dependent on the slab weight. In stabilized bases, the adhesion component is high and the failure plane in sliding is not at the slab-base interface. In this case, the use of coefficient of friction is not realistic for determining the frictional resistance. Alternatively, push-off tests are required to obtain the

frictional force - movement profiles. The elastic properties of the base material that defines the slope of the curve and the condition of sliding plane and roughness of the materials that defines the peak of the frictional resistance and the behavior of movements after sliding are the main parameters that may result in different types of frictional force - movement curves. Figures 2.8 and 2.9 show the effect of stiffness and texture of the base materials on the frictional force - movement curves.

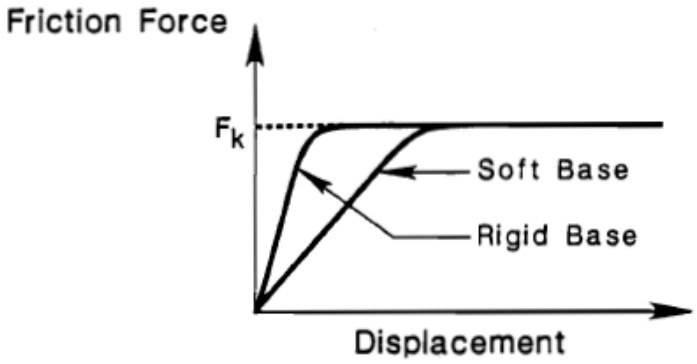

Figure 2.8: Effect of the stiffness of base material on the constitutive curve (Wesevich et *al*., 1987).

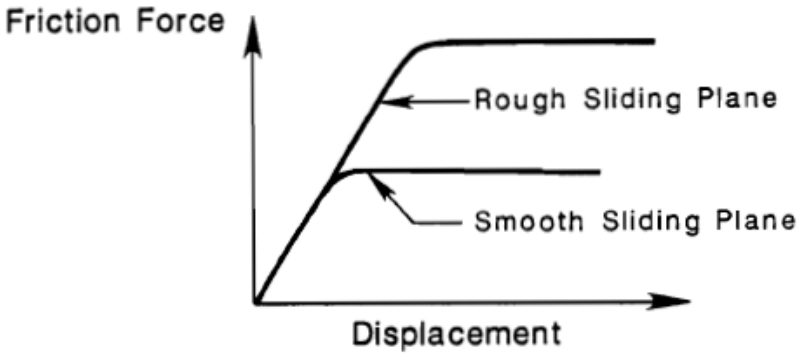

Figure 2.9: Effect of the roughness of the sliding plane on the constitutive curve (Wesevich et *al*., 1987).

2.6.4 Review of Interface Elements for Contact Problems

Once the contact constitutive relationship for the problem involved friction is defined, an appropriate contact finite element can be introduced. Several contact elements with special solution schemes have been proposed to model the discontinuities at the soil-structure interface. Uruz et *al*. (1977) developed a finite element procedure by using the variational principal with the Lagrangian

multiplier to obtain a numerical solution to the contact problems. Nine-node interface elements were developed in their study that incorporates inter-body traction as primary variables. Simons and Bergan (1986) developed a contact element for three dimensional analysis of contact problems with slip and friction. The contact formulation in that model was based on the concept of a spring-supported moving disk that transfers the normal contact forces and the Coulomb friction forces. The stiffness of the element was calculated from incremental equilibrium equations, depending on whether the element was free to move or not. The frictional force was then calculated from the equilibrium equations of springs. Ghaboussi *et al*. (1973) proposed a formulation for the problem involved with the soil-structure interaction. Relative motions between surrounding solid elements were considered as independent degrees-of-freedom in their model.

One of the methods for modeling the interface between soils and structures is the use of zero thickness or thin elements proposed by several researchers. Ill-conditioning of the stiffness matrix, convergence of the nonlinear solution algorithm and high stress gradients were found to be the cause of numerical instability in these types of elements. Goodman et *al*. (1968) proposed a zero thickness element to model jointed rocks. Day et *al*. (1994) modified the Goodman elements to four and six node isoparametric formulation to make the interface element compatible with quadrilateral 2D elements. A linear elastic perfectly plastic model using a Mohr-Coulomb failure criterion was used to model the contact condition in their model. Day et *al*. (1994) reported that the effect of ill-conditioning can be reduced by reducing the size of the adjacent 2D elements. Also, in order to increase the convergence time they recommended using the tangent elasto-plastic stiffness matrix calculated at the beginning of each increment instead of using the elastic global stiffness matrix. Gens et *al*. (1990) developed a zero thickness element to be used in 2D and 3D problems involving contact and employed an elasto-plastic constitutive law. For 2D contact problems, the analysis of pull-out test of reinforcement elements extracting from the surrounding materials was considered as a solution method in their study. Also, they concluded that in the case of partial sliding, if the Newton-Cotes integration scheme is adopted, the obtaining results become quite satisfactory than those obtained from Gauss integration scheme. In this

case, the element can be regarded as a linkage element in which the relationship between each pair of adjacent nodes is independent of the rest of the element.

Desai et *al*. (1984) developed a thin solid element to simulate the interface behavior. They reported some computational advantages of this type of element compared to other elements, such as zero thickness elements, in many two and three dimensional problems. The choice of element thickness is important in this method. While considering the large thickness leads the thin-layer element to behave as a solid element, the small thickness causes computational difficulties. Pande and Sharma (1979) proposed an 8-node parabolic thin isoparametric joint element based on the relative displacements as independent variables. They studied the aspect of ill-conditioning in the computation of thin element characteristics.

For the problem of plates resting on elastic half-space foundations, Feng and Owen (1996) proposed the coupled "Finite Element" / "Boundary Element" alternative solution approach, in which the boundary element equations were not explicitly assembled into the finite element equations. Instead, an iterative scheme was used to obtain the final solution. The reason for using the boundary element method was that in the finite element method, the discretization of the foundation led to a very large system of algebraic equation.

Barbero et *al*. (1995) proposed a contact element to analyze the connection between laminated composite plates in the case of the three-dimensional layer-wise constant shear theory. The proposed element can be used to capture the friction by using an orthotropic Coulomb friction law with two different coefficients of friction in the orthogonal directions. A special integration method was used to account for the partial contact and slip.

The interface element proposed in this study (will explain in chapter 5) was based on the isoparametric formulation of the 3D interface element proposed by Barbero et *al*. (1995), but was modified to be consistent with the 2D plate elements used in the modeling of the pavement slab layers.

Chapter 3: Finite Element Model of Concrete Slabs

The objective of this chapter is to propose an FE model to idealize the behavior of pavement slabs. Bonded pavement slabs are modeled as composite laminated plates in NYSLAB. This allows for modeling slab layers with different material properties and thickness with one single composite laminate. The "first order shear deformation laminated plate theory" is used in NYSLAB to model the composite slabs. This model is capable of capturing shear deformations, which are important in the modeling of thick slabs. The detailed formulation of this theory and its applicability in characterizing the pavement slab behavior are discussed here. The FE model of pavement slabs developed in NYSLAB and the procedure for including truck loads and thermal loads into the load vector are also included in this chapter. Lastly, the load transfer elements used to model the connection between jointed slabs are introduced.

3.1 The First-Order Shear Deformation Laminated Plate Theory

The first-order shear deformation theory (FSDT) or Mindlin laminated plate theory is an extension of the Mindlin plate theory to composite laminates. The layers in the laminate are assumed to be perfectly bonded together and have uniform thickness. The plane stress state is governed in this theory. Consider a laminated plate with total thickness of h composed of N orthotropic layer which are completely bonded together. The coordinate system is chosen such that the x-y plane coincides with the middle plane of the laminate and the z-axis is perpendicular to that mid-plane (Figure 3.1).

Figure 3.1: Geometry of the laminated plates.

The position (u,v,w) of each arbitrary point in the laminate after deformation can be expressed as (see Figure 3.2):

$$\begin{aligned} u(x,y,z) &= u_0(x,y) + z\phi_x(x,y) \\ v(x,y,z) &= v_0(x,y) + z\phi_y(x,y) \\ w(x,y,z) &= w_0(x,y) \end{aligned} \tag{3-1}$$

Figure 3.2 - Undeformed and deformed state of plate under the assumptions of FSDT (Reddy, 2007).

where u_0, v_0, w_0 are the displacements of that arbitrary point in the laminate mid-plane ($z = 0$), and ϕ_x, ϕ_y are the rotations about the y and x axes, respectively. In the FSDT, the third part of Kirchhoff hypothesis is not valid; i.e., the transverse normal do not remain perpendicular to the mid-plane after deformation. It denotes that ϕ_x, ϕ_y are not equal to the derivatives of transverse deflection as the case in the CLPT. It is worth mentioning that ϕ_x, ϕ_y do not follow the right-hand rule. It means that the real rotations according to the right-hand rule about the x and y axes will be $-\phi_y$ and ϕ_x, respectively. The transverse (vertical) deflection is constant through the laminate thickness and normal strain is zero in the FSDT. The inextensibility of vertical deflection requires that w not be a function of the thickness coordinate, z (Reddy, 2004). The strain tensor, shown in Eq. 3-2 and 3-3, consists of membrane strains and flexural strains. The nonlinear components are eliminated in the strain tensor.

$$\begin{bmatrix}\epsilon_{xx}\\ \epsilon_{yy}\\ \gamma_{xy}\end{bmatrix}=\begin{bmatrix}\epsilon^0{}_{xx}\\ \epsilon^0{}_{yy}\\ \gamma^0{}_{xy}\end{bmatrix}+\begin{bmatrix}\epsilon^1{}_{xx}\\ \epsilon^1{}_{yy}\\ \gamma^1{}_{xy}\end{bmatrix}=\begin{bmatrix}\frac{\partial u_0}{\partial x}\\ \frac{\partial v_0}{\partial y}\\ \frac{\partial u_0}{\partial y}+\frac{\partial v_0}{\partial x}\end{bmatrix}+z\begin{bmatrix}\frac{\partial \emptyset_x}{\partial x}\\ \frac{\partial \emptyset_y}{\partial y}\\ \frac{\partial \emptyset_x}{\partial y}+\frac{\partial \emptyset_y}{\partial x}\end{bmatrix} \tag{3-2}$$

$$\begin{bmatrix}\gamma_{yz}\\ \gamma_{xz}\end{bmatrix}=\begin{bmatrix}\frac{\partial w_0}{\partial y}+\emptyset_y\\ \frac{\partial w_0}{\partial x}+\emptyset_x\end{bmatrix} \tag{3-3}$$

where ε_{xx} , ε_{yy} , γ_{xy} are the in-plane strains which are linear through the laminate thickness, and γ_{yz}, γ_{xz} are out of plane shear strains which are constant through the thickness.

3.1.1 Equilibrium Equation in FSDT

The static governing equations of the FSDT will be derived by applying the principle of virtual displacement as:

$$\int_\Omega (\delta U+\delta W)d\Omega \tag{3-4}$$

where the virtual strain energy, δU, and the virtual work, δW, are given as:

$$\begin{aligned}\delta U &= \int_\Omega \{\int_{-\frac{h}{2}}^{\frac{h}{2}}\left[\sigma_{xx}\delta\epsilon_{xx}+\sigma_{yy}\delta\epsilon_{yy}+\sigma_{xy}\delta\gamma_{xy}+\sigma_{xz}\delta\gamma_{xz}+\sigma_{yz}\delta\gamma_{yz}\right]dz\}\,dxdy\\ &= \int_\Omega \left\{\int_{-\frac{h}{2}}^{\frac{h}{2}}\left[\sigma_{xx}(\delta\varepsilon^0_{xx}+z\delta\varepsilon^1_{xx})+\sigma_{yy}\left(\delta\varepsilon^0_{yy}+z\delta\varepsilon^1_{yy}\right)+\sigma_{xy}\left(\delta\gamma^0_{xy}+z\delta\gamma^1_{xy}\right)+\sigma_{xz}\delta\gamma_{xz}+\ \sigma_{yz}\delta\gamma_{yz}\right]dz\right\}dxdy\end{aligned} \tag{3-5}$$

$$\begin{aligned}\delta W &= -\int_\Omega (q_{zz}\delta w)dxdy-\int_{\Gamma_y}\int_{-\frac{h}{2}}^{\frac{h}{2}}[(q_{xx}\delta u+q_{xy}\delta v+q_{xz}\delta w)dzdy-\int_{\Gamma_x}\int_{-\frac{h}{2}}^{\frac{h}{2}}[(q_{yx}\delta u+q_{yy}\delta v+q_{yz}\delta w)dzdx\\ &= -\int_\Omega (q_{zz}\delta w_0)dxdy-\int_{\Gamma_y}\int_{-\frac{h}{2}}^{\frac{h}{2}}\left[q_{xx}(\delta u_0+z\delta\phi_x)+q_{xy}\left(\delta v_0+z\delta\phi_y\right)+q_{xz}\delta w_0\right]dzdy\\ &\quad -\int_{\Gamma_x}\int_{-\frac{h}{2}}^{\frac{h}{2}}\left[q_{yx}(\delta u_0+z\delta\phi_x)+q_{yy}(\delta v_0+z\delta\phi_y)+q_{yz}\delta w_0\right]dzdx\end{aligned} \tag{3-6}$$

where $q_{zz}, q_{xx}, q_{yy}, q_{xy}, q_{xz}, q_{yz}$ are the distributed loads applied to the laminate.

By substituting δU and δW from Eq. 3-5 and 3-6 into the virtual work equation (Eq. 3-4) and integrating through the laminate thickness, we obtain,

$$\begin{aligned}\int_{\Omega} [N_{xx}\delta\varepsilon^0_{xx} + M_{xx}\delta\varepsilon^1_{xx} + N_{yy}\delta\varepsilon^0_{yy} + M_{yy}\delta\varepsilon^1_{yy} + N_{xy}\delta\gamma^0_{xy} + M_{xy}\delta\gamma^1_{xy} + V_x\delta\gamma_{xz} + V_y - q_{zz}\delta w_0]\, dxdy \\ - \int_{\Gamma_y} \left[\hat{N}_{xx}\delta u_0 + \hat{M}_{xx}\delta\phi_x + \hat{N}_{xy}\delta v_0 + \hat{M}_{xy}\delta\phi_y + \hat{V}_x\delta w_0\right] dy \\ - \int_{\Gamma_x} \left[\hat{N}_{yy}\delta v_0 + \hat{M}_{yy}\delta\phi_y + \hat{N}_{xy}\delta u_0 + \hat{M}_{xy}\delta\phi_x + \hat{V}_y\delta w_0\right] dx = 0 \end{aligned} \tag{3-7}$$

with,

$$\begin{bmatrix} N_{xx} \\ N_{yy} \\ N_{xy} \end{bmatrix} = \int_{-\frac{h}{2}}^{\frac{h}{2}} \begin{Bmatrix} q_{xx} \\ q_{yy} \\ q_{xy} \end{Bmatrix} dz \quad \begin{bmatrix} M_{xx} \\ M_{yy} \\ M_{xy} \end{bmatrix} = \int_{-\frac{h}{2}}^{\frac{h}{2}} \begin{Bmatrix} q_{xx} \\ q_{yy} \\ q_{xy} \end{Bmatrix} z\, dz \quad \begin{bmatrix} V_x \\ V_y \end{bmatrix} = \int_{-\frac{h}{2}}^{\frac{h}{2}} \begin{Bmatrix} q_{xz} \\ q_{yz} \end{Bmatrix} dz$$

$$\begin{bmatrix} \hat{N}_{xx} \\ \hat{N}_{yy} \\ \hat{N}_{xy} \end{bmatrix} = \int_{-\frac{h}{2}}^{\frac{h}{2}} \begin{Bmatrix} q_{xx} \\ q_{yy} \\ q_{xy} \end{Bmatrix} dz \quad \begin{bmatrix} \hat{M}_{xx} \\ \hat{M}_{yy} \\ \hat{M}_{xy} \end{bmatrix} = \int_{-\frac{h}{2}}^{\frac{h}{2}} \begin{Bmatrix} q_{xx} \\ q_{yy} \\ q_{xy} \end{Bmatrix} z\, dz \quad \begin{bmatrix} \hat{V}_x \\ \hat{V}_y \end{bmatrix} = \int_{-\frac{h}{2}}^{\frac{h}{2}} \begin{Bmatrix} q_{xz} \\ q_{yz} \end{Bmatrix} dz \tag{3-8}$$

where, N_{xx}, N_{yy}, N_{xy} denote in-plane force resultants, M_{xx}, M_{yy}, *and* M_{xy} denote Moment resultants, and V_x, V_y are out of plane shear force resultants in the laminate.

As shown in Eq. 3-2 and 3-3, the out-of-plane shear strains are constant throughout the laminate thickness. The constant out-of-plane shear stress, resulting from the constant out-of-plane shear strain, contradicts the quadratic shear stress variation obtained from the theory of elasticity, which considers zero shear stresses at the top and bottom of the laminate. This inconsistency can be adjusted by applying *shear correction coefficient* (*K*) in the computation of out-of-plane shear forces. The value of *K* is computed in a manner that when multiplies to the strain energy, due to transverse shear stress, gives the same strain energy as a result of exact transverse stresses determined by the three-dimensional elasticity theory (Reddy, 2004). Shear forces can be rewritten as follow:

$$\begin{bmatrix} V_x \\ V_y \end{bmatrix} = K \int_{-\frac{h}{2}}^{\frac{h}{2}} \begin{Bmatrix} \sigma_{xz} \\ \sigma_{yz} \end{Bmatrix} dz \tag{3-9}$$

For the rectangular laminate using in this study, the shear correction factor is given as *K*=5/6.

The equilibrium equations are obtained by setting the coefficients $(\delta u_0, \delta v_0, \delta w_0, \delta \phi_x, \delta \phi_y)$ of equation 3-7 to zero independently:

$$\frac{\partial N_{xx}}{\partial x} + \frac{\partial N_{xy}}{\partial y} = 0 \tag{3-10}$$

$$\frac{\partial N_{xy}}{\partial x} + \frac{\partial N_{yy}}{\partial y} = 0 \tag{3-11}$$

$$\frac{\partial V_x}{\partial x} + \frac{\partial V_y}{\partial y} + q = 0 \tag{3-12}$$

$$-V_x + \frac{\partial M_{xx}}{\partial x} + \frac{\partial M_{xy}}{\partial y} = 0 \tag{3-13}$$

$$-V_y + \frac{\partial M_{xy}}{\partial x} + \frac{\partial M_{yy}}{\partial y} = 0 \tag{3-14}$$

3.1.2 Laminate Constitutive Equations

Using laminate constitutive equation for *N*-layer of lamina with orthotropic material and using Hooke's law, the resultant forces and moments in a matrix form can be expressed as follows:

$$\begin{bmatrix} N_{xx} \\ N_{yy} \\ N_{xy} \end{bmatrix} = \begin{bmatrix} A_{11} & A_{12} & A_{13} \\ A_{12} & A_{22} & A_{23} \\ A_{13} & A_{23} & A_{33} \end{bmatrix} \begin{bmatrix} \varepsilon^0{}_{xx} \\ \varepsilon^0{}_{yy} \\ \gamma^0{}_{xy} \end{bmatrix} + \begin{bmatrix} B_{11} & B_{12} & B_{13} \\ B_{12} & B_{22} & B_{23} \\ B_{13} & B_{23} & B_{33} \end{bmatrix} \begin{bmatrix} \varepsilon^1{}_{xx} \\ \varepsilon^1{}_{yy} \\ \gamma^1{}_{xy} \end{bmatrix} \tag{3-15}$$

$$\begin{bmatrix} M_{xx} \\ M_{yy} \\ M_{xy} \end{bmatrix} = \begin{bmatrix} B_{11} & B_{12} & B_{13} \\ B_{12} & B_{22} & B_{23} \\ B_{13} & B_{23} & B_{33} \end{bmatrix} \begin{bmatrix} \varepsilon^0{}_{xx} \\ \varepsilon^0{}_{yy} \\ \gamma^0{}_{xy} \end{bmatrix} + \begin{bmatrix} D_{11} & D_{12} & D_{13} \\ D_{12} & D_{22} & D_{23} \\ D_{13} & D_{23} & D_{33} \end{bmatrix} \begin{bmatrix} \varepsilon^1{}_{xx} \\ \varepsilon^1{}_{yy} \\ \gamma^1{}_{xy} \end{bmatrix} \tag{3-16}$$

$$\begin{bmatrix} V_x \\ V_y \end{bmatrix} = k \begin{bmatrix} As_{11} & As_{12} \\ As_{21} & As_{22} \end{bmatrix} \begin{bmatrix} \gamma_{xz} \\ \gamma_{yz} \end{bmatrix} \tag{3-17}$$

where, A_{ij} are called extensional stiffness, D_{ij} are bending stiffness, B_{ij} are bending-extensional coupling stiffness, and As_{ij} are shear stiffness, which are defined in terms of stiffness and thickness of each layer.

$$A_{ij} = \sum_{k=1}^{N} Q_{ij}^{(k)} (z_{k+1} - z_k) \tag{3-18}$$

$$B_{ij} = \frac{1}{2} \sum_{k=1}^{N} Q_{ij}^{(k)} (z^2{}_{k+1} - z^2{}_k) \tag{3-19}$$

$$D_{ij} = \frac{1}{3} \sum_{k=1}^{N} Q_{ij}^{(k)} (z^3{}_{k+1} - z^3{}_k) \tag{3-20}$$

$$As_{ij} = \sum_{k=1}^{N} G_{ij}^{(k)} (z_{k+1} - z_k) \tag{3-21}$$

For the k^{th} layer with isotropic material, Q_{ij} and G_{ij} are given as:

$$Q_{ij}^{k} = \frac{E^{(k)}}{1 - \nu^{(k)2}} \begin{bmatrix} 1 & \nu^{(k)} & 0 \\ \nu^{(k)} & 1 & 0 \\ 0 & 0 & \dfrac{1 - \nu^{(k)}}{2} \end{bmatrix} \tag{3-22}$$

$$G_{ij}^{k} = \begin{bmatrix} G^{(k)} & 0 \\ 0 & G^{(k)} \end{bmatrix} \qquad G^{(k)} = \frac{E^{(k)}}{2(1+\nu^{(k)})} \tag{3-23}$$

3.2 Finite Element Modeling of FSDT in NYSLAB

In the finite element method, the domain of the problem is discretized into a set of finite elements. Over each finite element, the governing equations are approximated by polynomial "interpolation" functions. The responses inside each element can be expressed as interpolated values from the element nodal points by using an appropriate interpolation function.

The differential equations of the governing equations of a structural problem can be represented in the weighted-integral or weak form. The weak form requires less differentiability of the dependent variables than the original differential equations. The dependent variables are approximated by an appropriate interpolation function and substituted into the weak form of the equations (Reddy, 2004).

Three major finite element methods developed for the analysis of plates are:

a) *Displacement methods***,** which are based on the principles of virtual variational displacement. All the governing finite element equations in this method are expressed in terms of nodal displacements.

b) *Mixed or Hybrid methods***,** which are based on the mixed variational of displacements and stresses, concurrently and independently.

c) *Equilibrium models***,** which are based on the principle of virtual force.

Displacement methods are the most commonly used methods in the finite element analysis of CLPT and FSDT. In this study, displacement methods are utilized for the finite element modeling of plates.

3.2.1 Weak Forms of Equilibrium Equations

In the First-order shear deformation theory, the weak form of the equilibrium equations are derived by applying the principle of virtual displacement. In this procedure, each equation governing the FSDT (Eq. 3-10 to 3-14) is multiplied by a weight function, which expressed as virtual variation in terms of displacement($\delta u_0, \delta v_0, \delta w_0, \delta \phi_x, \delta \phi_y$), and then integrated in the element domain. For example, the first equilibrium equation (Eq. 3-10) multiples by δu_0 and integrates over the element domain:

$$\int_{\Omega} \delta u_0 \left[\frac{\partial N_{xx}}{\partial x} + \frac{\partial N_{xy}}{\partial y}\right] dxdy = 0 \tag{3-24}$$

By using integration by parts:

$$\int_{\mathbf{\Omega^e}} \left(\frac{\partial \delta u_0}{\partial x} N_{xx} + \frac{\partial \delta u_0}{\partial y} N_{xy}\right) dxdy - \oint_{\Gamma^e} (P_x)\delta u_0 ds \tag{3-25}$$

By following the same procedure for other equilibrium equations (Eq. 3-11 to 3-14), the linear weak form of the equilibrium equations are obtained as:

$$\int_{\Omega^e} \left(\frac{\partial \delta v_0}{\partial x} N_{xy} + \frac{\partial \delta v_0}{\partial y} N_{yy} \right) dxdy - \oint_{\Gamma^e} (P_y) \delta v_0 ds \tag{3-26}$$

$$\int_{\Omega^e} \left(\frac{\partial \delta w_0}{\partial x} V_x + \frac{\partial \delta w_0}{\partial y} V_y - \delta w_0 q \right) dxdy - \oint_{\Gamma^e} Q \delta w_0 ds \tag{3-27}$$

$$\int_{\Omega^e} \left(\frac{\partial \delta \phi_x}{\partial x} M_{xx} + \frac{\partial \delta \phi_x}{\partial y} M_{xy} + \delta \phi_x V_x \right) dxdy - \oint_{\Gamma^e} T_x \delta \phi_x ds \tag{3-28}$$

$$\int_{\Omega^e} \left(\frac{\partial \delta \phi_y}{\partial x} M_{xy} + \frac{\partial \delta \phi_y}{\partial y} M_{yy} + \delta \phi_y V_y \right) dxdy - \oint_{\Gamma^e} T_y \delta \phi_x ds \tag{3-29}$$

where,

$$P_x = N_{xx} n_x + N_{xy} n_y \qquad P_y = N_{xy} n_x + N_{yy} n_y \qquad Q = V_x n_x + V_y n_y$$

$$T_x = M_{xx} n_x + M_{xy} n_y \qquad T_y = M_{xy} n_x + M_{yy} n_y \tag{3-30}$$

n_x *and* n_y are the direction cosines of the unit normal on the boundary Γ^e of the element domain Ω^e.

3.2.2 Interpolation Function and Numerical Integration

Two types of interpolation functions that have been proposed to be used in the finite element analysis of laminated plates will be examined in this section (Ochoa and Reddy, 1992): The *Lagrange* interpolation, which is the one where only the function is interpolated (C^0 element), and the *Hermit* interpolation, in which the function and its derivatives are interpolated (C^1 element). In the weak forms of the FSDT (3-25 to 3-29), only the first derivatives of dependent variables $(u_0, v_0, w_0, \phi_x, \phi_y)$ are appear. Therefore, all of them can be approximated using Lagrange interpolation functions. All five

quantities are approximated in terms of the element nodal in-plane displacements (*u, v*), transverse displacements (*w*) and rotations (ϕ_x, ϕ_y) as follows:

$$u = \sum_{j=1}^{m} N_j^T u_j \ , v = \sum_{j=1}^{m} N_j^T v_j \ , w = \sum_{j=1}^{m} N_j^T w_j \ , \emptyset_x = \sum_{j=1}^{m} N_j^T \emptyset_{x\,j} \ , \emptyset_y = \sum_{j=1}^{m} N_j^T \emptyset_{y\,j} \tag{3-31}$$

where N_j are the Lagrange interpolation functions and *m* is the number of nodes in the element.

In this study, a nine-node isoparametric quadrilateral element was used to discretize the laminate (pavement slabs) domain (Figure 3.3). Each element has five degrees of freedom per node (totaling 45 degrees of freedom). To interpolate the strains inside each element in terms of the nodal values, the Lagrange quadratic interpolation functions in terms of natural coordinates are given in Eq. 3-32.

Figure 3.3: A nine-node quadrilateral element with five degrees of freedom per node.

$$\begin{pmatrix} N_1 \\ N_2 \\ N_3 \\ N_4 \\ N_5 \\ N_6 \\ N_7 \\ N_8 \\ N_9 \end{pmatrix} = \begin{pmatrix} \frac{1}{4}(\xi^2-\xi)(\eta^2-\eta) \\ \frac{1}{4}(\xi^2+\xi)(\eta^2-\eta) \\ \frac{1}{4}(\xi^2+\xi)(\eta^2+\eta) \\ \frac{1}{4}(\xi^2-\xi)(\eta^2+\eta) \\ \frac{1}{2}(1-\xi^2)(\eta^2-\eta) \\ \frac{1}{2}(\xi^2+\xi)(1-\eta^2) \\ \frac{1}{2}(1-\xi^2)(\eta^2+\eta) \\ \frac{1}{2}(\xi^2-\xi)(1-\eta^2) \\ (1-\xi^2)(1-\eta^2) \end{pmatrix} \tag{3-32}$$

For isoparametric elements the same interpolation functions are used to transform the coordinates of element in global coordinate system into the element local coordinate as follow:

$$x = \sum_{j=1}^{m} N_j^T(\xi,\eta)x_j^e \qquad y = \sum_{j=1}^{m} N_j^T(\xi,\eta)y_j^e \tag{3-33}$$

The strain tensor in each element contains the derivatives of interpolation function (N_j) with respect to the global coordinates (x, y). The relationship between the derivatives of N_j with respect to the global and local coordinates ($\frac{\partial N_j}{\partial x}$ and $\frac{\partial N_j}{\partial y}$ to $\frac{\partial N_j}{\partial \xi}$ and $\frac{\partial N_j}{\partial \eta}$) can be obtained by using chain rule of partial differentiation as,

$$\begin{Bmatrix} \frac{\partial N_j}{\partial \xi} \\ \frac{\partial N_j}{\partial \eta} \end{Bmatrix} = \begin{bmatrix} \frac{\partial x}{\partial \xi} & \frac{\partial y}{\partial \xi} \\ \frac{\partial x}{\partial \eta} & \frac{\partial y}{\partial \eta} \end{bmatrix}^e \begin{Bmatrix} \frac{\partial N_j}{\partial x} \\ \frac{\partial N_j}{\partial y} \end{Bmatrix} \tag{3-34}$$

The transformation matrix in Eq. 3-34 is called the *Jacobian* matrix and its determinant is called the *jacobian*. *Jacobian* must be positive in order to have nonsingular *Jacobian* matrix. The *Jacobian* matrix can be expressed in terms of the global coordinates as:

$$J = \begin{bmatrix} \frac{\partial x}{\partial \xi} & \frac{\partial y}{\partial \xi} \\ \frac{\partial x}{\partial \eta} & \frac{\partial y}{\partial \eta} \end{bmatrix} = \begin{bmatrix} \frac{\partial N_1}{\partial \xi} & \frac{\partial N_2}{\partial \xi} & \cdots & \frac{\partial N_m}{\partial \xi} \\ \frac{\partial N_1}{\partial \eta} & \frac{\partial N_2}{\partial \eta} & \cdots & \frac{\partial N_m}{\partial \eta} \end{bmatrix} \begin{bmatrix} x_1 & y_1 \\ x_2 & y_2 \\ \vdots & \vdots \\ x_m & y_m \end{bmatrix} \tag{3-35}$$

The derivatives of interpolation functions with respect to the global coordinates are defined as B_c matrix:

$$B_c = \begin{bmatrix} \frac{\partial N_1}{\partial x} & \frac{\partial N_1}{\partial y} \\ \frac{\partial N_2}{\partial x} & \frac{\partial N_2}{\partial y} \\ \vdots & \vdots \\ \frac{\partial N_9}{\partial x} & \frac{\partial N_9}{\partial y} \end{bmatrix} = \begin{bmatrix} \frac{\partial N_1}{\partial \xi} & \frac{\partial N_1}{\partial \eta} \\ \frac{\partial N_2}{\partial \xi} & \frac{\partial N_2}{\partial \eta} \\ \vdots & \vdots \\ \frac{\partial N_9}{\partial \xi} & \frac{\partial N_9}{\partial \eta} \end{bmatrix} \frac{[J]}{\det[J]} \tag{3-36}$$

Gauss-Legendre quadrature method is used for numerical integration over a two dimensional element domain. The location selected for the nine Gauss points over each element are shown in Figure 3.4.

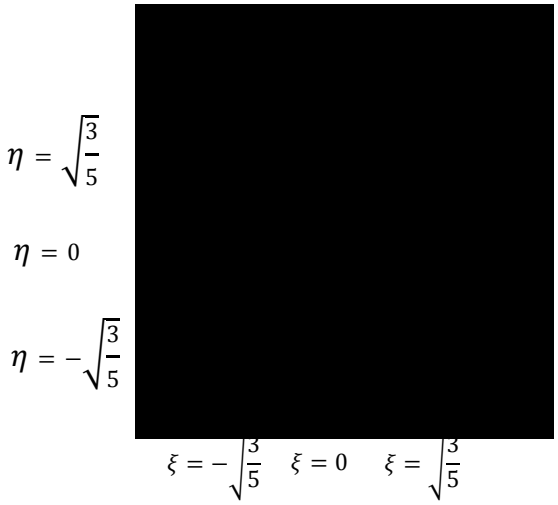

Figure 3.4: Location of the nine Gauss points.

3.2.3 Shear Locking

A common problem in using such C^0 plate elements in the FSDT is that they suffer from shear locking. As the plate thickness becomes small in relation to the plate in-plane dimensions, the transverse shear strains are expected to disappear due to pure bending subjected to the plate, but they cannot disappear at all the element points and the plate element become extremely stiff. Thus, it yields small

incorrect deformations compared to the real solution in the bending analysis of plates (Ochoa and Reddy, 1992; Bathe and Dvorkine, 1985). To solve the shear locking problem, various solution schemes have been proposed. Reduced numerical integration order for the shear stiffness matrix is one of these methods and even though it eliminates the shear locking problem, it produces the problem of rank deficiency which can lead to oscillatory behavior. Bathe and Dvorkin (1985) introduced an effective 4-node element based on the mixed integration scheme (MITC) which does not lock in thin plate/shell analysis and does not have any spurious zero energy modes.

In this study, four quadrature points are used for the integration of the shear stiffness matrix while the bending stiffness matrix is integrated using nine quadrature points. Our experience in modeling concrete slabs by using nine node elements and such integration scheme demonstrated no numerical deficiency or locking. Therefore using an MITC plate element has not been necessary in this study.

3.2.4 Stiffness Matrix of Laminated Plate Element

The weak form of the laminate equilibrium equations yields upon substitution of all variables (degrees of freedom) from Eq. 3.31 into Eq. 3.25 to 3.29.

$$\int_{\Omega} \left(\frac{\partial N_i}{\partial x} N_{xx} + \frac{\partial N_i}{\partial y} N_{xy}\right) dxdy - \oint_{\Gamma} P_x N_i ds \tag{3-37}$$

$$\int_{\Omega} \left(\frac{\partial N_i}{\partial x} N_{xy} + \frac{\partial N_i}{\partial y} N_{yy}\right) dxdy - \oint_{\Gamma} P_y N_i ds \tag{3-38}$$

$$\int_{\Omega} \left(\frac{\partial N_i}{\partial x} V_x + \frac{\partial N_i}{\partial y} V_y + N_i q\right) dxdy - \oint_{\Gamma} Q N_i ds \tag{3-39}$$

$$\int_{\Omega} \left(\frac{\partial N_i}{\partial x} M_{xx} + \frac{\partial N_i}{\partial y} M_{xy} + N_i V_x\right) dxdy - \oint_{\Gamma} T_x N_i ds \tag{3-40}$$

$$\int_{\Omega} \left(\frac{\partial N_i}{\partial x} M_{xy} + \frac{\partial N_i}{\partial y} M_{yy} + N_i V_y\right) dxdy - \oint_{\Gamma} T_y N_i ds \tag{3-41}$$

By expanding Eq. 3-37 to 3-41, the finite element model of the first-order shear deformation theory for linear and static case will be obtained as:

$$[K^e]\{U^e\} = \{F^e\}$$

$$\begin{bmatrix} [K^{11}] & [K^{12}] & [K^{13}] & [K^{14}] & [K^{15}] \\ [K^{12}]^T & [K^{22}] & [K^{23}] & [K^{24}] & [K^{25}] \\ [K^{13}]^T & [K^{23}]^T & [K^{33}] & [K^{34}] & [K^{35}] \\ [K^{14}]^T & [K^{24}]^T & [K^{11}]^T & [K^{44}] & [K^{45}] \\ [K^{15}]^T & [K^{25}]^T & [K^{35}]^T & [K^{45}]^T & [K^{55}] \end{bmatrix} \begin{Bmatrix} u^e \\ v^e \\ w^e \\ {\phi_x}^e \\ {\phi_x}^e \end{Bmatrix} = \begin{Bmatrix} F^1 - {F_T}^1 \\ F^2 - {F_T}^2 \\ F^3 \\ F^4 - {F_T}^4 \\ F^5 - {F_T}^5 \end{Bmatrix} \tag{3-42}$$

where the elements of the sub-matrices $[K^{\alpha\beta}]$ for $\alpha = 1, 2, \dots, 5$ and their numerical integral expressions using the Gauss quadrature method are defined as:

- If full integration (9 Gauss points) is used for all bending, stretching, and shear stiffness matrices:

$$K_{ij}^{1\alpha} = \int_{-1}^{1}\int_{-1}^{1} B_c C^{1\alpha} B_c^T \det J d\xi d\eta = \sum_{i=1}^{9}\sum_{j=1}^{9} w_i w_j B_c(\xi_i,\eta_j) C^{1\alpha} B_c^T(\xi_i,\eta_j) \det J(\xi_i,\eta_j) \tag{3-43}$$

$$K_{ij}^{2\alpha} = \int_{-1}^{1}\int_{-1}^{1} B_c C^{2\alpha} B_c^T \det J d\xi d\eta = \sum_{i=1}^{9}\sum_{j=1}^{9} w_i w_j B_c(\xi_i,\eta_j) C^{2\alpha} B_c^T(\xi_i,\eta_j) \det J(\xi_i,\eta_j) \tag{3-44}$$

$$K_{ij}^{33} = \kappa\int_{-1}^{1}\int_{-1}^{1} B_c C^{33} B_c^T \det J d\xi d\eta = \kappa\sum_{i=1}^{9}\sum_{j=1}^{9} w_i w_j B_c(\xi_i,\eta_j) C^{33} B_c^T(\xi_i,\eta_j) \det J(\xi_i,\eta_j) \tag{3-45}$$

$$K_{ij}^{34} = \kappa\int_{-1}^{1}\int_{-1}^{1} B_c C^{34} {N_r}^T \det J d\xi d\eta = \kappa\sum_{i=1}^{9}\sum_{j=1}^{9} w_i w_j B_c(\xi_i,\eta_j) C^{34} {N_r}^T(\xi_i,\eta_j) \det J(\xi_i,\eta_j) \tag{3-46}$$

$$K_{ij}^{35} = \kappa\int_{-1}^{1}\int_{-1}^{1} B_c C^{35} {N_r}^T \det J d\xi d\eta = \kappa\sum_{i=1}^{9}\sum_{j=1}^{9} w_i w_j B_c(\xi_i,\eta_j) C^{35} {N_r}^T(\xi_i,\eta_j) \det J(\xi_i,\eta_j) \tag{3-47}$$

$$K_{bij}^{4\alpha} = \int_{-1}^{1}\int_{-1}^{1} B_c C^{4\alpha} B_c^T \det J d\xi d\eta = \sum_{i=1}^{9}\sum_{j=1}^{9} w_i w_j B_c(\xi_i,\eta_j) C^{4\alpha} B_c^T(\xi_i,\eta_j) \det J(\xi_i,\eta_j) \tag{3-48}$$

$$K_{sij}^{44} = \kappa Gh \int_{-1}^{1}\int_{-1}^{1} N_r N_r^T \det J d\xi d\eta = \kappa Gh \sum_{i=1}^{9}\sum_{j=1}^{9} w_i w_j N_r(\xi_i,\eta_j) N_r^T(\xi_i,\eta_j) \det J(\xi_i,\eta_j) \quad (3\text{-}49)$$

$$K_{bij}^{55} = \int_{-1}^{1}\int_{-1}^{1} B_c C^{55} B_c^T \det J d\xi d\eta = \sum_{i=1}^{9}\sum_{j=1}^{9} w_i w_j B_c(\xi_i,\eta_j) C^{55} B_c^T(\xi_i,\eta_j) \det J(\xi_i,\eta_j) \quad (3\text{-}50)$$

$$K_{sij}^{55} = \kappa Gh \int_{-1}^{1}\int_{-1}^{1} N_r N_r^T \det J d\xi d\eta = \kappa Gh \sum_{i=1}^{9}\sum_{j=1}^{9} w_i w_j N_r(\xi_i,\eta_j) N_r^T(\xi_i,\eta_j) \det J(\xi_i,\eta_j) \quad (3\text{-}51)$$

where,

$$C^{11} = \begin{bmatrix} A_{11} & A_{13} \\ A_{13} & A_{33} \end{bmatrix} \quad C^{12} = \begin{bmatrix} A_{13} & A_{12} \\ A_{33} & A_{23} \end{bmatrix} \quad C^{14} = \begin{bmatrix} B_{11} & B_{13} \\ B_{13} & B_{33} \end{bmatrix} \quad C^{15} = \begin{bmatrix} B_{13} & B_{12} \\ B_{33} & B_{23} \end{bmatrix}$$

$$C^{22} = \begin{bmatrix} A_{33} & A_{23} \\ A_{23} & A_{22} \end{bmatrix} \quad C^{24} = \begin{bmatrix} B_{13} & B_{33} \\ B_{12} & B_{23} \end{bmatrix} \quad C^{25} = \begin{bmatrix} B_{33} & B_{23} \\ B_{23} & B_{22} \end{bmatrix}$$

$$C^{33} = \begin{bmatrix} As_{22} & As_{12} \\ As_{12} & As_{11} \end{bmatrix} \quad C^{34} = \begin{bmatrix} As_{22} \\ As_{12} \end{bmatrix} \quad C^{35} = \begin{bmatrix} As_{12} \\ As_{11} \end{bmatrix}$$

$$C^{44} = \begin{bmatrix} D_{11} & D_{13} \\ D_{13} & D_{33} \end{bmatrix} \quad C^{45} = \begin{bmatrix} D_{13} & D_{12} \\ D_{33} & D_{23} \end{bmatrix} \quad C^{55} = \begin{bmatrix} D_{33} & D_{23} \\ D_{23} & D_{22} \end{bmatrix} \quad (3\text{-}52)$$

*B*c is the matrix of derivatives of interpolation functions which defined in Eq. 3-36.

K = $5/6$ is the shear correction factor which is used for the terms containing shear stresses.

K_b^{44} and K_s^{44} are the bending stiffness and the shear stiffness matrices of submatix K^{44}. With the same definition for K_b^{55} and K_s^{55}, the total stiffness matrix for K^{44}, K^{45}, K^{55} will be derived as,

$$K_{jj}^{44} = K_{b}{}_{jj}^{44} + K_{s}{}_{jj}^{44}$$

$$K_{jj}^{45} = K_{b}{}_{jj}^{45}$$

$$K_{jj}^{55} = K_{b}{}_{jj}^{55} + K_{s}{}_{jj}^{55}$$

Also, $K^{13} = K^{23} = 0$, which indicates that in-plane displacements is independent of vertical loads.

- If the reduced integration for the shear stiffness matrices is necessary, all sub-matrices $[K^{\alpha\beta}]$ that contain $As_{11}, As_{22}, As_{12}$ are integrated using four Gauss quadrature points as,

$$K_{ij}^{33} = \kappa \int_{-1}^{1}\int_{-1}^{1} B_c C^{33} B_c^T \det J d\xi d\eta = \kappa \sum_{i=1}^{4}\sum_{j=1}^{4} w_i w_j B_c(\xi_i,\eta_j) C^{33} B_c^T(\xi_i,\eta_j) \det J(\xi_i,\eta_j) \tag{3-53}$$

$$K_{ij}^{34} = \kappa \int_{-1}^{1}\int_{-1}^{1} B_c C^{34} N_r^{\ T} \det J d\xi d\eta = \kappa \sum_{i=1}^{4}\sum_{j=1}^{4} w_i w_j B_c(\xi_i,\eta_j) C^{34} N_r^{\ T}(\xi_i,\eta_j) \det J(\xi_i,\eta_j) \tag{3-54}$$

$$K_{ij}^{35} = \kappa \int_{-1}^{1}\int_{-1}^{1} B_c C^{35} N_r^{\ T} \det J d\xi d\eta = \kappa \sum_{i=1}^{4}\sum_{j=1}^{4} w_i w_j B_c(\xi_i,\eta_j) C^{35} N_r^{\ T}(\xi_i,\eta_j) \det J(\xi_i,\eta_j) \tag{3-55}$$

$$K_{sij}^{44} = \kappa G h \int_{-1}^{1}\int_{-1}^{1} N_r N_r^{\ T} \det J d\xi d\eta = \kappa G h \sum_{i=1}^{4}\sum_{j=1}^{4} w_i w_j N_r(\xi_i,\eta_j) N_r^{\ T}(\xi_i,\eta_j) \det J(\xi_i,\eta_j) \tag{3-56}$$

$$K_{sij}^{55} = \kappa G h \int_{-1}^{1}\int_{-1}^{1} N_r N_r^{\ T} \det J d\xi d\eta = \kappa G h \sum_{i=1}^{4}\sum_{j=1}^{4} w_i w_j N_r(\xi_i,\eta_j) N_r^{\ T}(\xi_i,\eta_j) \det J(\xi_i,\eta_j) \tag{3-57}$$

The components of force vector, F and F_T in Eq. 3-42 represent the external applied loads and the thermal loads. In the next chapter the process of inclusion of applied loads to the equilibrium equation of the pavement system will be examined.

3.3 Load Vectors

The implementation of truck loads and thermal loads in FE analysis of rigid pavements in NYSLAB are discussed in this section.

3.3.1 Truck Loads in NYSLAB

In NYSLAB, a generous truck library is implemented that enables users to analyze pavements with various truck types, from the standard truck to any case truck. In the mathematical model, truck loads are transferred through the contact "patch" between the tires and the pavement slabs (Byrum et *al*, 2011). The contact patch is assumed to be rectangular and the load is considered to be uniform across the patch. Because the rectangular patch will not necessarily have the same dimensions as the slab elements, and more than likely the patch will span more than one slab element, the tire loads are

simulated as an equivalent series of point loads. This eliminates the need to calculate the nodal loads associated with a distributed load that does not cover the entire element. The rectangular tire contact patch is treated as a nine node rectangular element (see Figure 3.5).

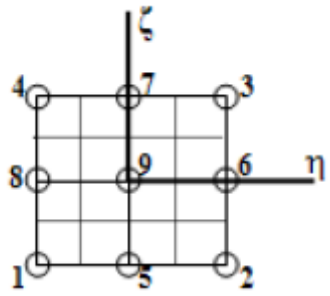

Figure 3.5: Nide node rectangular tire load patch

Each tire load can be divided into nine concentrated loads that coincide with the nine nodal points. The intensity of these loads is calculated as:

$$F_{tr} = \iint_A N^T p dA \tag{3-58}$$

Where N is the interpolation function similar to the interpolation function used for isoparametric nine-node plate elements (Eq. 3-32) and p is the tire contact pressure.

3.3.2 Thermal Loads in NYSLAB

In NYSLAB, the temperature profile through the thickness of the concrete slab is represented as a cubic function that can be fitted by considering the temperature at four different points through the slab depth. This order of polynomial was selected because it is common for temperature to be measured at four points across the thickness of the slabs at pavement test sites (Yu *et al*., 1998). Assuming the origin at the mid-plane of the slab, the temperature gradient is defined as:

$$\Delta T = a_0 + a_1 z + a_2 z^2 + a_3 z^3 \tag{3-59}$$

where the a_i can be fitted from the field data measured at a specific pavement site. The constant term a_0 produces expansion and contraction in the PCC slab. The linear term a_1 produces pure bending in the

PCC slab, due to the temperature difference between its top and bottom. The higher-order terms of temperature profile in Eq. 3-59 (a_2 and a_3) produce internal stress in the PCC slab, regardless of its external constraints.

The resultant thermal forces and thermal moments for each laminated plate (bonded pavement slabs) can be expressed as:

$$N_T = \sum_{k=1}^{N} \int_{Z_k}^{Z_{k+1}} Q^{(k)} \alpha^{(k)} \Delta T \, dz \tag{3-60}$$

$$M_T = \sum_{k=1}^{N} \int_{Z_k}^{Z_{k+1}} Q^{(k)} \alpha^{(k)} \Delta T \, z \, dz \tag{3-61}$$

where Q is the stiffness components which is the function of modulus of elasticity and Poisson's ratio and α is the coefficient of thermal expansion for each layer in the N-layer laminate,

$$Q_{ij}^{k} = \frac{E^{(k)}}{1 - \nu^{(k)2}} \begin{bmatrix} 1 & \nu^{(k)} & 0 \\ \nu^{(k)} & 1 & 0 \\ 0 & 0 & \dfrac{1 - \nu^{(k)}}{2} \end{bmatrix} \tag{3-62}$$

$$\alpha^{(k)} = \begin{bmatrix} \alpha \\ \alpha \\ 0 \end{bmatrix} \tag{3-63}$$

The total laminate constitutive equations become,

$$\begin{Bmatrix} \{N\} \\ \{M\} \end{Bmatrix} = \begin{bmatrix} [A] & [B] \\ [B] & [D] \end{bmatrix} \begin{Bmatrix} \{\varepsilon^0\} \\ \{\varepsilon^1\} \end{Bmatrix} - \begin{Bmatrix} \{N_T\} \\ \{M_T\} \end{Bmatrix} \tag{3-64}$$

where, the matrices N and M are the total resultant force and moment in the laminate. Matrices A, B, and D were defined in Eq. 3-18 to 3-20.

In the finite element model of the laminate, the contribution of thermal loads are added to the force vector (Eq 3-42) as,

$$F_T^1 = \int_s \frac{\partial N_i}{\partial x} N_T dxdy \tag{3-65}$$

$$F_T^2 = \int_s \frac{\partial N_i}{\partial y} N_T dxdy \tag{3-66}$$

$$F_T^4 = \int_s \frac{\partial N_i}{\partial x} M_T dxdy \tag{3-67}$$

$$F_T^5 = \int_s \frac{\partial N_i}{\partial y} M_T dxdy \tag{3-68}$$

where, N_i is the interpolation function defined in Eq. 3-32.

3.4 Load Transfer Elements

Adjacent slabs in a jointed concrete pavement system in NYSLAB can be connected with dowels, tie bars and aggregate or key interlock, or a combination of those load transfer devices through their joints. Dowels and tie bars are used in the transverse and longitudinal joints, respectively, and can be placed in uniform or non-uniform intervals (Figure 3.6).

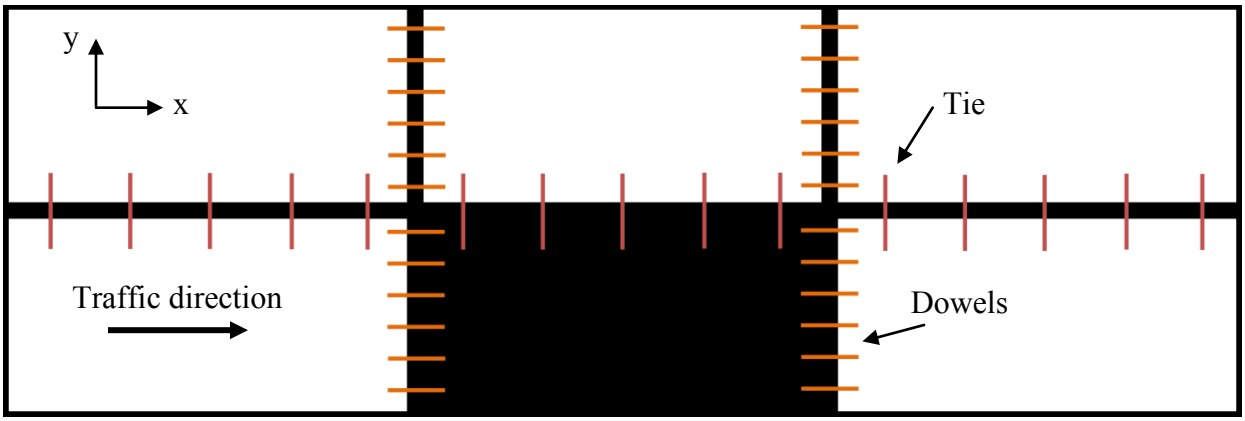

Figure 3.6: Placement of dowels and tie bars in transverse and longitudinal joints

Dowels and tie bars are modeled as beam elements in NYSLAB, similar to the load transfer elements used in ILLI-SLAB and JSLAB2004. The beam elements have two degrees of freedom per node, including a vertical displacement (w) and a rotation about the axis perpendicular to the beam longitudinal axis (Figure 3.7 and 3.8). Because of the small unconstrained length of dowels and tie bars,

over the small separation between the slabs (usually a fraction of an inch), the major load-transfer mechanism in those elements is shear. For this reason, a Timoshenko beam is used for the modeling of short-beam (thick- beam) elements. The stiffness matrix for the Timoshenko beam, shown below, is given as:

Figure 3.7: dowel bar degrees of freedom

Figure 3.8: Tie bar degrees of freedom

$$k_b = C\begin{bmatrix} 12 & 6L & -12 & 6L \\ 6L & (4+\emptyset)L^2 & -6L & (2-\emptyset)L^2 \\ -12 & -6L & 12 & -6L \\ 6L & (2-\emptyset)L^2 & -6L & (4+\emptyset)L^2 \end{bmatrix} \quad (3\text{-}69)$$

where,

$$C = \frac{EI}{L^3(1+\emptyset)} \tag{3-70}$$

$$\emptyset = \frac{24I_d(1+\nu)}{A_{sh}L^2} \tag{3-71}$$

$I_d = Moment\ of\ inertia\ of\ dowel\ cross\ section$

$E_d, \nu_d = Modulus\ of\ elasticity\ and\ Poisson's\ ratio\ of\ dowel$

$A_{sh} = Effective\ cross\ section\ of\ dowel\ (shear\ area)$

$L = Joint\ spacing$

In addition to the stiffness of the portion of dowels over the joint opening, the support provided by the concrete matrix also contributes to the load-transfer mechanism (Ioannides and Korovesis, 1992). This support from the concrete slab is called dowel-concrete interaction (DCI) parameter. Therefore, the total load-transfer mechanism in dowels, which resist the deformation in the vertical direction, can be obtained by combining two springs in series associated with the stiffness components of the vertical deflection from the Timoshenko beam and the DCI parameter as:

$$D = \frac{1}{\frac{1}{DCI} + \frac{1}{12C}} \tag{3-72}$$

For the practical purposes, a value of 1.5×10^6 psi/in. has been used for dowel-concrete interaction (Ioannides and Korovesis, 1992; Tabatabaie et *al*., 1979). The stiffness matrix of dowels aligned with the *x* axis according to the degrees of freedom *w* and rotation $\emptyset_x$ is derived as:

$$k_d = \begin{bmatrix} D & 6LC & -D & 6LC \\ 6LC & (4+\emptyset)CL^2 & -6LC & (2-\emptyset)CL^2 \\ -D & -6CL & D & -6LC \\ 6LC & (2-\emptyset)CL^2 & -6LC & (4+\emptyset)CL^2 \end{bmatrix} \tag{3-73}$$

The stiffness matrix of tie bars aligned with the y axis with the degrees of freedom w and $\emptyset_y$ is derived as:

$$k_t = \begin{bmatrix} D & -6LC & -D & -6LC \\ -6LC & (4+\emptyset)CL^2 & 6LC & (2-\emptyset)CL^2 \\ -D & 6CL & D & 6LC \\ -6LC & (2-\emptyset)CL^2 & 6LC & (4+\emptyset)CL^2 \end{bmatrix} \tag{3-74}$$

The above stiffness matrices only account for two degrees of freedom in dowels or tie bars. The total stiffness matrix of those elements should include the components corresponding to all the degrees of freedom considered in the modeling of pavement slabs. Because dowels are free from movement along their length, the stiffness components associated with their axial direction (u) is zero. Tie bars are constrained to move along their length, therefore an axial stiffness (corresponding to v) equal to $k_a = A_t E_t / L$ needs to be considered (A_t and E_t are the cross section area and the modulus of elasticity of tie bars). Another stiffness that is needed to be considered for dowels and tie bars are their stiffness in the direction perpendicular to their length. For dowels, stiffness equal to D is needed in the y direction to account for the shear transfer between adjacent slabs in cases of thermal expansion and contraction. For tie bars similar stiffness is required in the x direction associated with the degrees of freedom u. The total stiffness matrix for dowels and tie bars considering five degrees of freedom per node of a beam element are derived as:

$$[K_{dowel}] = \begin{bmatrix} 0 & 0 & 0 & 0 & 0 & 0 & 0 & 0 & 0 & 0 \\ 0 & D & 0 & 0 & 0 & 0 & -D & 0 & 0 & 0 \\ 0 & 0 & D & 6LC & 0 & 0 & 0 & -D & 6LC & 0 \\ 0 & 0 & 6LC & (4+\emptyset)CL^2 & 0 & 0 & 0 & -6LC & (2-\emptyset)CL^2 & 0 \\ 0 & 0 & 0 & 0 & 0 & 0 & 0 & 0 & 0 & 0 \\ 0 & 0 & 0 & 0 & 0 & 0 & 0 & 0 & 0 & 0 \\ 0 & -D & 0 & 0 & 0 & 0 & D & 0 & 0 & 0 \\ 0 & 0 & -D & -6LC & 0 & 0 & 0 & D & -6LC & 0 \\ 0 & 0 & 6LC & (2-\emptyset)CL^2 & 0 & 0 & 0 & -6LC & (4+\emptyset)CL^2 & 0 \\ 0 & 0 & 0 & 0 & 0 & 0 & 0 & 0 & 0 & 0 \end{bmatrix} \begin{matrix} (u)_L \\ (v)_L \\ (w)_L \\ (\emptyset_x)_L \\ (\emptyset_y)_L \\ (u)_R \\ (v)_R \\ (w)_R \\ (\emptyset_x)_R \\ (\emptyset_y)_R \end{matrix} \tag{3-75}$$

$$[K_{tie}] = \begin{bmatrix} D & 0 & 0 & 0 & 0 & -D & 0 & 0 & 0 & 0 \\ 0 & A_tE_t/L & 0 & 0 & 0 & 0 & -A_tE_t/L & 0 & 0 & 0 \\ 0 & 0 & D & -6LC & 0 & 0 & 0 & -D & -6LC & 0 \\ 0 & 0 & -6LC & (4+\emptyset)CL^2 & 0 & 0 & 0 & 6LC & (2-\emptyset)CL^2 & 0 \\ 0 & 0 & 0 & 0 & 0 & 0 & 0 & 0 & 0 & 0 \\ -D & 0 & 0 & 0 & 0 & D & 0 & 0 & 0 & 0 \\ 0 & -A_tE_t/L & 0 & 0 & 0 & 0 & A_tE_t/L & 0 & 0 & 0 \\ 0 & 0 & -D & 6LC & 0 & 0 & 0 & D & 6LC & 0 \\ 0 & 0 & -6LC & (2-\emptyset)CL^2 & 0 & 0 & 0 & 6LC & (4+\emptyset)CL^2 & 0 \\ 0 & 0 & 0 & 0 & 0 & 0 & 0 & 0 & 0 & 0 \end{bmatrix} \begin{matrix} (u)_L \\ (v)_L \\ (w)_L \\ (\emptyset_x)_L \\ (\emptyset_y)_L \\ (u)_R \\ (v)_R \\ (w)_R \\ (\emptyset_x)_R \\ (\emptyset_y)_R \end{matrix}$$

(3-76)

For the aggregate interlock and keyed connection, a bar element with one degree of freedom per node, associated with the vertical displacement *w*, is used. These bars connect corresponding nodes across the jointed slabs. The stiffness of this bar element is calculated from the stiffness per unit length of the interlock or key. The stiffness of this bar element is given by:

$$[K_{key}] = \frac{EA}{L}\begin{bmatrix} 1 & -1 \\ -1 & 1 \end{bmatrix} \tag{3-77}$$

3.5 Horizontal Interaction between Adjacent Slabs

Uniform temperature-change, within the depth of pavement slabs during daily temperature variation, can cause thermal expansion and contraction in concrete slabs. Slab buckling or blow up may occur in slab joints as a result of excessive expansion of concrete slabs in hot weathers (Figure 3.9). This is because the joint spacing is not enough to allow for expansion relief in slab joints.

Figure 3.9: Rigid pavement blowup

The impact of horizontal interaction between adjacent jointed slabs, due to thermal expansion in producing additional compressive stress, is considered in the mathematical model of NYSLAB (Figure 3.10). For this purpose linkage elements are used between the jointed slabs in both the transverse and longitudinal joints to capture the horizontal interaction between them (Figure 3.11).

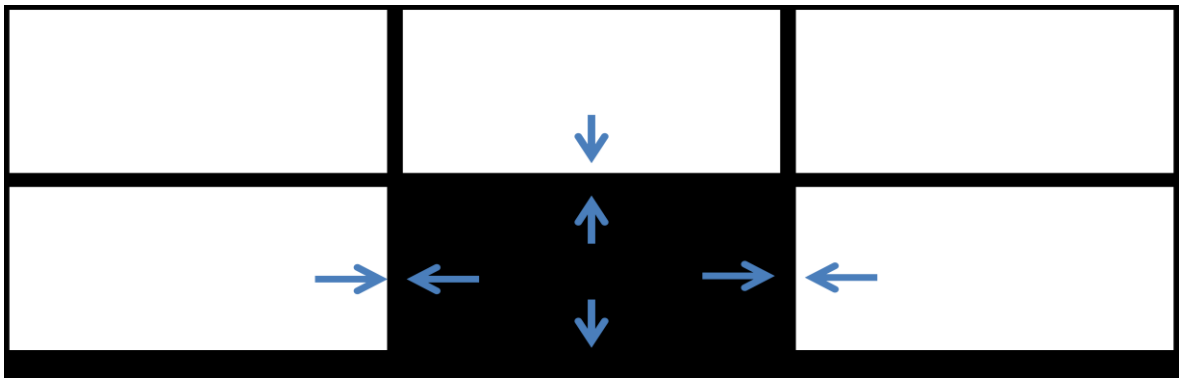

Figure 3.10: Horizontal interaction between jointed slabs due to thermal expansion

Linkage elements are modeled as 6-node one dimensional elements with one degree of freedom per node (Figure 3.12). The first three nodes of each linkage element are associated with the slab nodes across the transverse or longitudinal joint and the other three nodes are associated with the adjacent slab on that joint.

The linkage elements have the capability of being activated when two adjacent nodes, associated with two neighboring slabs, come in contact during thermal expansion (gap closes). These nodes are deactivated when the relative displacement of the nodes opens the initial gap. When each node of a linkage element is activated, the stiffness is equal to 1000 times the maximum of diagonal of the global stiffness matrix, which is assigned to that node based on its area of contact. On the other hand, when a node of linkage element is deactivated, its stiffness is given as 10^{-9} times the minimum of the diagonal of the global stiffness matrix. Using linkage elements allows us to model the horizontal interaction between adjacent jointed slabs and calculates the compressive stresses within the slabs, due to additional constrains provided by the adjacent slabs.

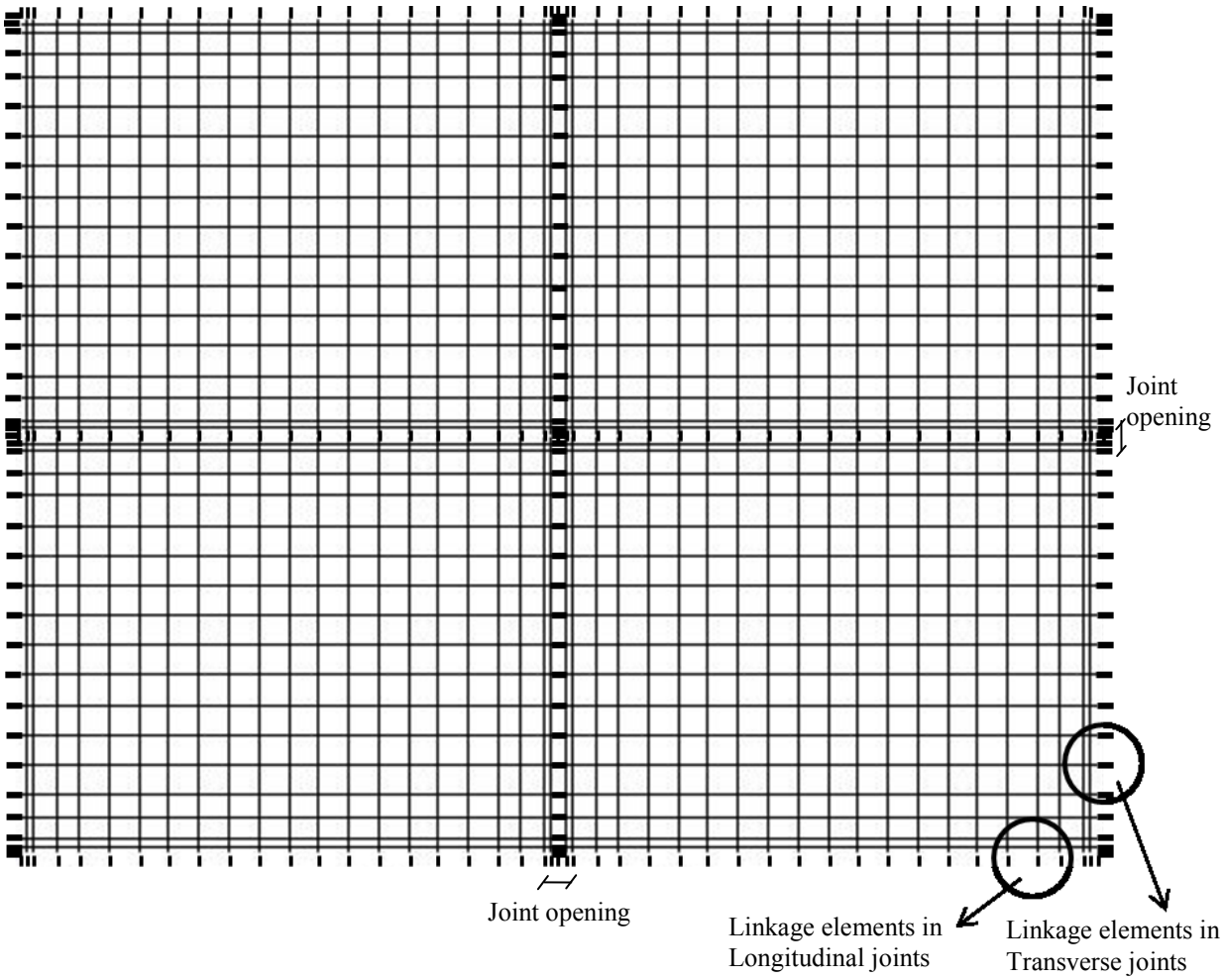

Figure 3.11: Location of linkage elements across the joints

a) Across the transverse joints b) Across the longitudinal joints

Figure 3.12: Linkage elements

Chapter 4: Finite Element Model of Foundation

The structural behavior of concrete slabs is generally more predictable than their supporting foundation layers. There have been numerous studies and attempts to find the best idealization of foundation layers. These studies involved finding an accurate though simple model with the ability to reflect the actual behavior of the foundation in a rigid pavement system. These proposed methods have some limitations in sense of theory and application. Different foundation types that have been widely used in rigid pavement analysis tools were described in chapter 2 of this manuscript. In this chapter the finite element models of foundation types used in NYSLAB are described.

4.1 Finite Element Model of Winkler Foundation

The simplest approach to idealize the Winkler foundation in the finite element analysis of a rigid pavement system is to model the foundation layers with springs attached to the bottom of the finite element plate (slab) nodes. Chilton and Wekezer (1990) developed a finite element method to model such slab-foundation systems. Their model assumed that the elastic foundation will deflect consistently with the surrounding structural elements. Thurhan (1992) concluded that the coefficient of the Winkler foundation stiffness matrix in the Chilton model would not provide a rigid body displacement when the plate is uniformly loaded. Thurhan developed a modified Winkler stiffness matrix that gives exactly a constant q/k displacement in the plate when subjected to uniformly distributed loads.

In NYSLAB, foundation elements do no share nodes with slab elements. If the foundation is to be modeled as a Winkler model, all the foundation layers (base, subbase and subgrade) are converted to one layer and idealize as a bed of independent springs (Figure 4.1). The stiffness of each spring is represented as a single modulus of subgrade reaction or k-value. The value of k is estimated using back-calculation methods (e.g. AREA method or Best-fit method) described in chapter 2. Figure 4.2 demonstrates an 18-node element used to discretize the Winkler foundation domain. Each node has one degree of freedom associated with the vertical deflection (w). The top nodes of each foundation element coincide with the top surface of the entire foundation system (top of the base course) and the bottom nods coincide with the bottom surface of the foundation system (top of the bedrock).

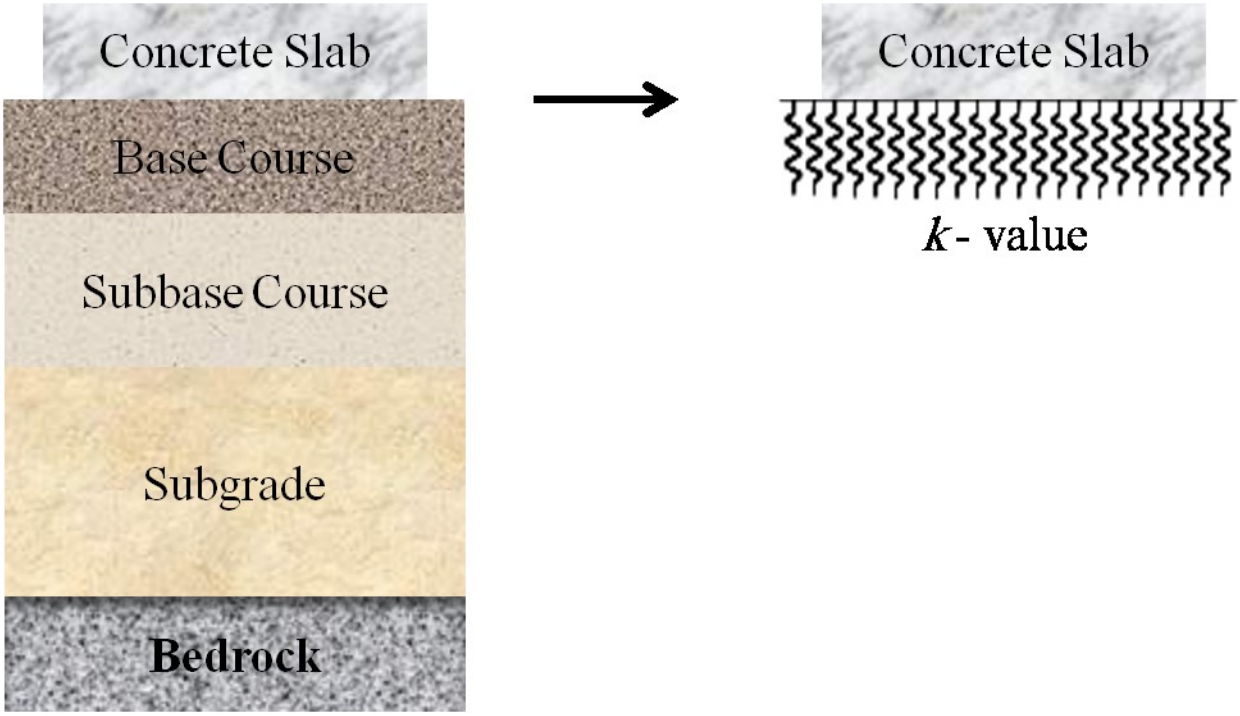

Figure 4.1: Idealizing of foundation system as a Winkler model in NYSLAB

Figure 4.2: 18-node foundation element in Winkler model

4.2 Finite Element Model of Elastic Solid (Boussinesq) Foundation

In chapter 2, the formulation for calculating the deflection of the top surface of a boussinesq foundation, which uniformly loaded in a rectangular area, was represented in Eq. 2-6 and Eq. 2-7. In those equations, the deflection at a given point is related to the forces acting on the foundation domain. Therefore, the solid elastic foundation model is not based on a FE model formulation but rather uses a flexibility matrix that then is inverted to obtain a stiffness matrix. The stiffness matrix is then calculated as:

$$K_b = S^{-1} \tag{4-1}$$

This matrix is then added, through a degree of freedom mapping scheme, to the global stiffness matrix. It is important to note that the flexibility and stiffness matrices of the Boussinesq model are full matrices and thus memory intensive. This not only affects memory requirements but also increases the computation time for the manipulation of the global stiffness matrix and the solution for the displacement vector.

To reduce the memory and CPU time overhead, the stiffness matrix is made sparse by zeroing all off-diagonal elements associated with nodes separated by more than a specified distance. This distance is an input parameter, but 10 ft was found to produce good results since at that distance the flexibility has decayed significantly. The use of smaller distances tends to significantly affect the stresses in the slabs (Carrasco et *al*, 2010).

4.3 Finite Element Model of Vlasov Foundation

As discussed in chapter 2, the Vlasov theory considers each layer of foundation as a two-parameter foundation model. This mathematical foundation model cannot be reduced to an equivalent single layer, as is the case in the Winkler model (Figure 4.3). Two parameters of Vlasov foundation are represented as layer normal stiffness (κ) and layer shear stiffness (τ), which are the function of general soil elastic properties and the layer dimensions. An important concern in the application of the Vlasov model is the determination of these parameters. In NYSLAB, an iterative procedure, based on the formulation proposed by Vlasov and leontev, was developed to internally determine the Vlasov

parameters. This process is limited in NYSLAB to up to two layer of Vlasov foundation, and will be explained in the following sections.

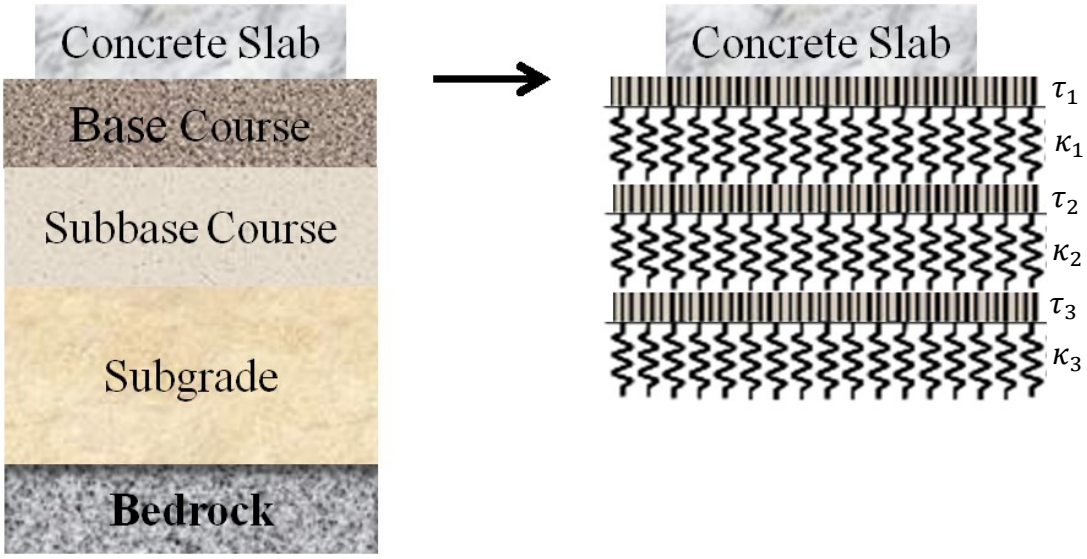

Figure 4.3: Idealizing of foundation system as Vlasov model in NYSLAB

4.3.1 Vlasov Parameters for One-layer Foundation

Consider an elastic foundation of thickness H, modulus of elasticity of E_s and Poisson's ratio of ν_s, with a plate on top of it subjected to a uniform load (Figure 4.4). The horizontal displacements of the foundation domain are assumed to be negligible compared to its vertical displacement. The vertical displacement of a point in the foundation stratum can be represented as the vertical displacement of the foundation surface ($\overline{w}(x,y)$), due to applied loads to the plate, multiplies by a proper mode shape function $\emptyset(z)$. The horizontal and vertical displacements of the foundation will be:

$$u(x,y,z) = 0$$

$$v(x,y,z) = 0$$

$$w(x,y,z) = \overline{w}(x,y,0)\emptyset(z) \tag{4-2}$$

The value of $\emptyset(z)$ which determines the variation of the surface displacement in z direction should satisfy these boundary conditions:

$$\emptyset(z) = 1 \quad for\ z = 0$$

$$\emptyset(z) = 0 \quad for\ z = H \tag{4-3}$$

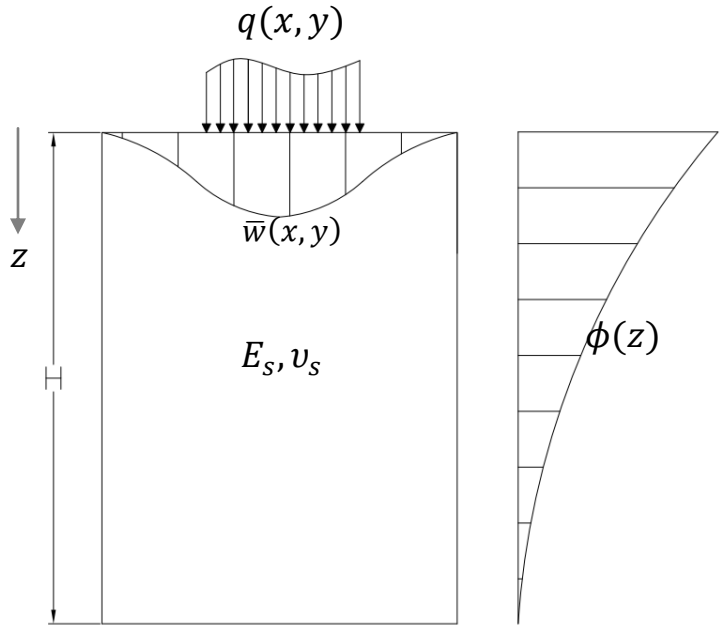

Figure 4.4: Description of a loaded plate placed over an elastic foundation

Since the thickness of the plate is small compared to the other plate dimensions, the vertical deflection at the plate mid-plane can be assumed to be equal to the foundation surface displacement. The strains and stresses in the foundation medium can be determined by using the strain- displacement equation of elasticity proposed by Timoshenko (Thuhan, 1990):

$$\varepsilon_{xx} = \frac{\partial u}{\partial x} = 0 \qquad \gamma_{xy} = \frac{\partial u}{\partial y} + \frac{\partial v}{\partial x} = 0$$

$$\varepsilon_{yy} = \frac{\partial v}{\partial x} = 0 \qquad \gamma_{xz} = \frac{\partial u}{\partial z} + \frac{\partial w}{\partial x} = \frac{\partial \bar{w}}{\partial x}\emptyset(z) \tag{4-4}$$

$$\varepsilon_{zz} = \frac{\partial w}{\partial z} = \bar{w}(x,y)\frac{\partial \emptyset}{\partial z} \qquad \gamma_{yz} = \frac{\partial v}{\partial z} + \frac{\partial w}{\partial y} = \frac{\partial \bar{w}}{\partial y}\emptyset(z)$$

The stress-strain relationship for a linearly elastic homogenous soil medium can be expressed as,

$$\sigma_{xx} = \bar{E}\left[\varepsilon_{xx} + \frac{\upsilon_s}{1-\upsilon_s}(\varepsilon_{yy} + \varepsilon_{zz})\right] \qquad \tau_{xy} = G\varepsilon_{xy}$$

$$\sigma_{yy} = \bar{E}\left[\varepsilon_{yy} + \frac{\upsilon_s}{1-\upsilon_s}(\varepsilon_{xx} + \varepsilon_{zz})\right] \qquad \tau_{xz} = G\varepsilon_{\mathrm{xz}} \tag{4-5}$$

$$\sigma_{zz} = \bar{E}\left[\varepsilon_{zz} + \frac{\upsilon_s}{1-\upsilon_s}(\varepsilon_{xx} + \varepsilon_{yy})\right] \qquad \tau_{yz} = G\varepsilon_{yz}$$

where,

$$\bar{E} = \frac{E_s(1-\upsilon_s)}{(1+\upsilon_s)(1-2\upsilon_s)} \tag{4-6}$$

$$G = \frac{E_s}{2(1+\upsilon_s)} \tag{4-7}$$

The total strain in the soil-structure system can be written as,

$$\Pi = \Pi_p + \Pi_s + Q \tag{4-8}$$

where

$\Pi_p =$ the strain energy stored in the plate

$\Pi_s =$ the strain energy stored in the soil

$Q =$ work by external loads

The strain energies of the plate and soil can be determined as,

$$\pi_p = \int \left(\frac{\partial^2 w}{\partial x^2}, \frac{\partial^2 w}{\partial y^2}, 2\frac{\partial^2 w}{\partial x \partial y}\right)[D]\left(\frac{\partial^2 w}{\partial x^2}, \frac{\partial^2 w}{\partial y^2}, 2\frac{\partial^2 w}{\partial x \partial y}\right)^T dxdy \tag{4-9}$$

where $[D]$ is the plate flexural rigidity.

$$\Pi_s = \frac{1}{2}\int_0^H \int_{-\infty}^{\infty}\int_{-\infty}^{\infty} (\sigma_{xx}\epsilon_{xx} + \sigma_{yy}\epsilon_{yy} + \sigma_{zz}\epsilon_{zz} + \tau_{xy}\gamma_{xy} + \tau_{yz}\gamma_{yz} + \tau_{xz}\gamma_{xz})dxdydz$$

$$\Pi_s = \frac{1}{2}\int_0^H \int_{-\infty}^{\infty}\int_{-\infty}^{\infty} (\bar{E}\bar{w}^2(\frac{\partial \emptyset}{\partial z})^2 + G(\nabla\bar{w})^2\phi^2)dxdydz \tag{4-10}$$

The work by external loads is determined as:

$$Q = -\int_{\Omega} \bar{q}\bar{w}dxdy \tag{4-11}$$

By minimizing the total potential energy, and using variational principles, under the variation of two dependent variables $\bar{w}$ and $\emptyset$, the equilibrium equation of the entire structural system in the plate domain will be obtained as,

$$\frac{\partial \Pi}{\partial \bar{w}} = 0 \tag{4-12}$$

$$\frac{\partial \Pi}{\partial \phi} = 0 \tag{4-13}$$

$$\begin{aligned} \Longrightarrow \ \delta\Pi = &\int_0^H \int_{-\infty}^{\infty} \int_{-\infty}^{\infty} (D\nabla^4 \bar{w} + \bar{E}\bar{w}\left(\frac{\partial \emptyset}{\partial z}\right)^2 - G\nabla^2 \bar{w}\phi^2 - \bar{q})\delta\bar{w}dxdydz \\ &+ \int_0^H \int_{-\infty}^{\infty} \int_{-\infty}^{\infty} (-\bar{E}\bar{w}^2\left(\frac{\partial^2 \emptyset}{\partial z^2}\right) + G(\nabla\bar{w})^2\phi)\delta\phi dxdydz = 0 \end{aligned} \tag{4-14}$$

By defining κ and 2τ as the following (Eq. 4-16 and 4-17), and by taking the first term of Eq. 4-14 (multiplied by $\delta\bar{w}$) to zero, the equilibrium equations inside and outside the plate domain will be determined as,

$$D\nabla^4 \bar{w} - 2\tau\nabla^2 \bar{w} + k\bar{w} = q \tag{4-15}$$

with,

$$k = \int_0^H \bar{E}\left(\frac{\partial \emptyset}{\partial z}\right)^2 dz \tag{4-16}$$

$$2\tau = \int_0^H G\phi^2 dz \tag{4-17}$$

By taking the second expression (multiplied by $\delta\emptyset$) to zero in Eq. 4-14, the differential equation for the vertical deformation shape function of the soil layer will be expressed as,

$$-m\frac{\partial^2\emptyset}{\partial z^2}+n\emptyset=0 \tag{4-18}$$

where *m* and *n* are defined as:

$$m=\int_{-\infty}^{+\infty}\int_{-\infty}^{+\infty}\bar{E}\bar{w}^2dxdy \tag{4-19}$$

$$n=\int_{-\infty}^{+\infty}\int_{-\infty}^{+\infty}G(\nabla\bar{w})^2dxdy \tag{4-20}$$

With the boundary conditions defined in Eq. 4-3, the differential equation (Eq. 4-18) can be solved as,

$$\emptyset(z)=\frac{sinh\gamma(1-\frac{z}{H})}{sinh\gamma} \tag{4-21}$$

where γ is the coefficient that determines the mode shape for the vertical deflection of the soil domain and can be expressed as:

$$\gamma=H\sqrt{\frac{n}{m}} \tag{4-22}$$

As it appears from Eq. 4-16 and Eq. 4-17, the Vlasov parameters *k* and 2τ depend on the elastic properties of the soil material, the thickness of the soil layer, and the vertical deflection mode shape $\emptyset$. Mode shape $\emptyset$ is a function of coefficient γ, which is determined based upon the area of the vertical deflection basin and the area of the gradient of vertical deflection basin of a plate subjected to external load *q*. An iterative process is needed to evaluate the Vlasov foundation parameters (Buczkowski and Torbacki, 2001; Vallabhan and Daloglu, 1999; Straughan, 1990; Vlasov and Leont'ev, 1966; Turhan, 1990). In that process, the coefficient γ is initially set, for an instance equal to 0.5, and then used to determine initial *k* and 2τ. With the obtained initial soil parameters and solving the equilibrium equation

of pavement structure (Eq. 4-15) by running NYSLAB, the vertical deflection and the gradient of the vertical deflection can be calculated. Then, the updated value of γ is calculated using Eq. 4-22 by applying new values for *m* and *n* from Eq. 4-19 and 4-20. The process is repeated until the difference between γ in two consequence iteration will be less than a small acceptable error.

4.3.2 Vlasov Parameters for Two-layer Foundation

Consider an elastic foundation consists of two layers of thickness h_1 and h_2 (Figure 4.5), with different modulus of elasticity and Poisson's ratio (with the total thickness of $H = h_1 + h_2$). The horizontal and vertical displacement of a point in the elastic foundation are given as,

$u(x,y) = 0$

$v(x,y) = 0$

$$w(x,y) = \bar{w}_1(x,y)\emptyset_1(z) + \bar{w}_2(x,y)\emptyset_2(z) \tag{4-23}$$

where $\bar{w}_1(x,y)$ and $\bar{w}_2(x,y)$ represent the vertical displacement of the top of the first and second foundation layers, respectively. $\emptyset_1(z)$ and $\emptyset_2(z)$ are the mode shape functions, which define the variation of the surface displacement of the first and second foundation layer in *z* direction. The functions $\emptyset_1(\mathrm{z})$ and $\emptyset_2(\mathrm{z})$ can be chosen based on the nature of the problem. For a (base+subgrade) foundation system, where the base layer is thin compared to the thick subgrade, it is assumed that the vertical deflection varies linearly through the layer thickness. The variation of the vertical displacement in the lower layer can be expressed with a nonlinear function. Functions $\emptyset_1(\mathrm{z})$ and $\emptyset_2(\mathrm{z})$ for each foundation layer can be expressed as (Vlasov and Leont'ev, 1966):

$$\emptyset_1 = 1 - \emptyset_2, \quad \emptyset_2 = \frac{z}{h_1} \qquad 0 \le z \le h_1 \tag{4-24}$$

$$\emptyset_1 = 0, \qquad \emptyset_2 = \emptyset_z \qquad h_1 < z \le h_2 \tag{4-25}$$

where $\emptyset_z$ is a nonlinear mode shape for the lower layer that will be determined later.

The horizontal strains in the foundation stratum are assumed to be zero. The vertical strain as well as shear strains will be expressed as:

$$(\varepsilon_z)_1 = \frac{\partial w}{\partial z} = \bar{w}_1\left(\frac{\partial \emptyset_1}{\partial z}\right) + \bar{w}_2\left(\frac{\partial \emptyset_2}{\partial z}\right) \qquad (\varepsilon_z)_2 = \frac{\partial w}{\partial z} = \bar{w}_2\left(\frac{\partial \emptyset_2}{\partial z}\right)$$

$$(\gamma_{xz})_1 = \left(\frac{\partial \bar{w}_1}{\partial x}\right)\phi_1 + \left(\frac{\partial \bar{w}_2}{\partial x}\right)\phi_2 \qquad (\gamma_{xz})_2 = \left(\frac{\partial \bar{w}_2}{\partial x}\right)\phi_2 \qquad (4\text{-}26)$$

$$(\gamma_{yz})_1 = \left(\frac{\partial \bar{w}_1}{\partial y}\right)\phi_1 + \left(\frac{\partial \bar{w}_2}{\partial y}\right)\phi_2 \qquad (\gamma_{yz})_2 = \left(\frac{\partial \bar{w}_2}{\partial y}\right)\phi_2$$

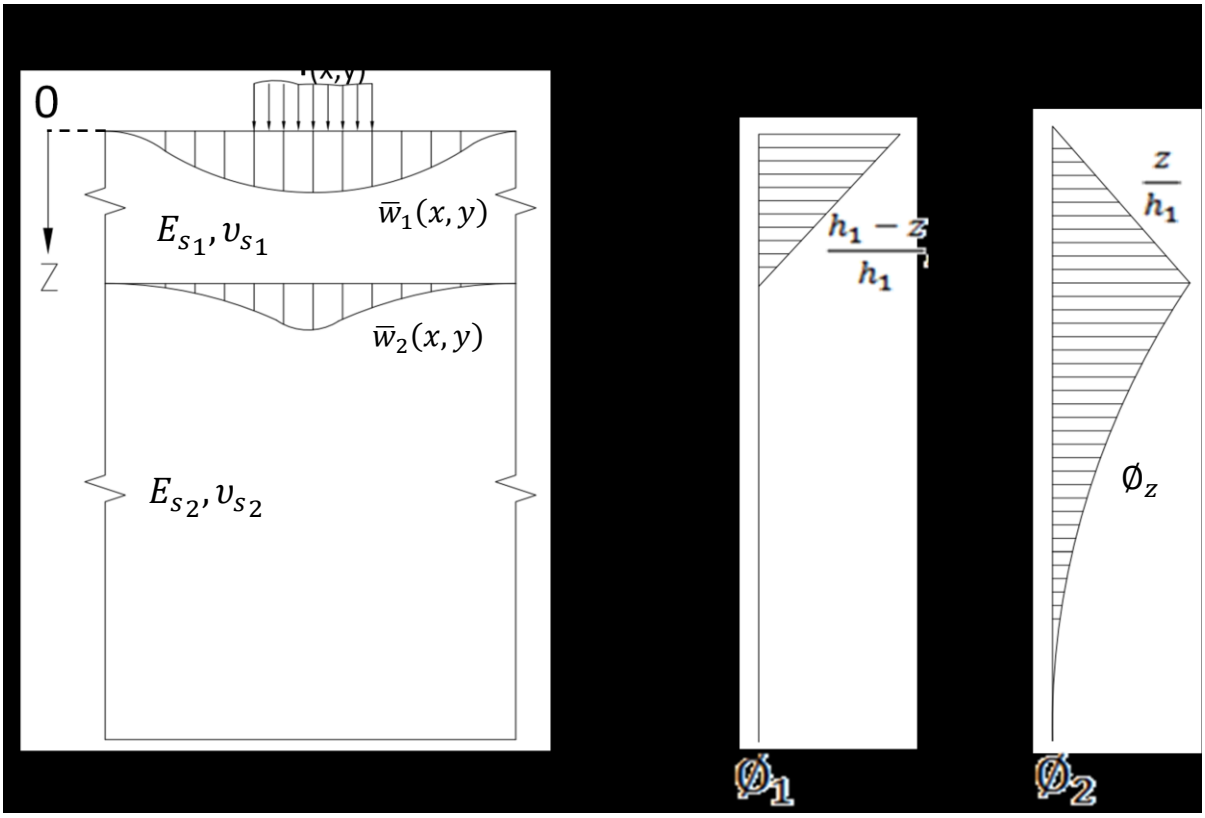

Figure 4.5: Description of a loaded plate placed over a two-layered elastic foundation

The stress-strain relationship for two-layered linearly elastic homogenous soil medium can be expressed as,

$$(\sigma_{zz})_1 = \bar{E}_1(\varepsilon_{zz})_1 \qquad (\sigma_{zz})_2 = \bar{E}_2(\varepsilon_{zz})_2$$

$$(\tau_{xz})_1 = G_1(\gamma_{xz})_1 \qquad (\tau_{xz})_2 = G_2(\gamma_{xz})_2 \tag{4-27}$$

$$(\tau_{yz})_1 = G_1(\gamma_{yz})_1 \qquad (\tau_{yz})_2 = G_2(\gamma_{yz})_2$$

where,

$$\bar{E}_1 = \frac{E_{s_1}(1-\upsilon_{s_1})}{(1+\upsilon_{s_1})(1-2\upsilon_{s_1})} \qquad G_1 = \frac{E_{s_1}}{2(1+\upsilon_{s_1})} \tag{4-28}$$

$$\bar{E}_2 = \frac{E_{s_2}(1-\upsilon_{s_2})}{(1+\upsilon_{s_2})(1-2\upsilon_{s_2})} \qquad G_2 = \frac{E_{s_2}}{2(1+\upsilon_{s_2})} \tag{4-29}$$

The potential energy, stored in the foundation stratum Π_s, can be expressed as:

$$\Pi_s = \frac{1}{2}\int_0^{h_1}\int_{-\infty}^{\infty}\int_{-\infty}^{\infty}\left((\sigma_{zz})_1(\varepsilon_z)_1 + (\tau_{xz})_1(\gamma_{xz})_1 + (\tau_{yz})_1(\gamma_{yz})_1\right)dxdydz$$

$$+\frac{1}{2}\int_{h_1}^{H}\int_{-\infty}^{\infty}\int_{-\infty}^{\infty}\left((\sigma_{zz})_2(\varepsilon_z)_2 + (\tau_{xz})_2(\gamma_{xz})_2 + (\tau_{yz})_2(\gamma_{yz})_2\right)dxdydz \tag{4-30}$$

By substituting strains and stresses from Eq. 4-28 into 4-31:

$$\begin{aligned}\Pi_s = \frac{1}{2}\int_0^{h_1}\int_{-\infty}^{\infty}\int_{-\infty}^{\infty}\Bigg[&\bar{E}_1\left(\bar{w}_1^2\left(\frac{\partial\emptyset_1}{\partial z}\right)^2 + \bar{w}_2^2\left(\frac{\partial\emptyset_2}{\partial z}\right)^2 + 2\bar{w}_1\bar{w}_2\left(\frac{\partial\emptyset_1}{\partial z}\right)\left(\frac{\partial\emptyset_2}{\partial z}\right)\right)\\ &+ G_1\left(\left(\frac{\partial\bar{w}_1}{\partial x}\right)^2\phi_1^2 + \left(\frac{\partial\bar{w}_2}{\partial x}\right)^2\phi_2^2 + 2\left(\frac{\partial\bar{w}_1}{\partial x}\frac{\partial\bar{w}_2}{\partial x}\right)\phi_1\phi_2\right)\\ &+ G_1\left(\left(\frac{\partial\bar{w}_1}{\partial y}\right)^2\phi_1^2 + \left(\frac{\partial\bar{w}_2}{\partial y}\right)^2\phi_2^2 + 2\left(\frac{\partial\bar{w}_1}{\partial y}\frac{\partial\bar{w}_2}{\partial y}\right)\phi_1\phi_2\right)\Bigg]dxdydz\\ &+\frac{1}{2}\int_{h_1}^{H}\int_{-\infty}^{\infty}\int_{-\infty}^{\infty}\left[\bar{E}_2\left(\bar{w}_2^2\left(\frac{\partial\emptyset_2}{\partial z}\right)^2\right) + G_2((\nabla\bar{w}_2)^2\phi_2^2)\right]dxdydz\end{aligned} \tag{4-31}$$

The potential energy stored in the plate is given as:

$$\Pi_p = \int_{\Omega} \left(\frac{\partial^2 \bar{w}_1}{\partial x^2}, \frac{\partial^2 \bar{w}_1}{\partial y^2}, 2\frac{\partial^2 \bar{w}_1}{\partial x \partial y}\right)[D]\left(\frac{\partial^2 \bar{w}_1}{\partial x^2}, \frac{\partial^2 \bar{w}_1}{\partial y^2}, 2\frac{\partial^2 \bar{w}_1}{\partial x \partial y}\right)^T dxdy \tag{4-32}$$

The work by external load q is given as:

$$Q = -\int_{\Omega} q\bar{w}_1 dxdy \tag{4-33}$$

By minimizing the total potential energy ($\pi = \pi_s + \pi_p + Q$), and using variational principles under the variation of $\bar{w}_1, \emptyset_1, \bar{w}_2$ and $\emptyset_2$, the equilibrium equation of the entire structural system in the plate domain will be obtained as,

$\frac{\partial \Pi}{\partial \bar{w}_1} = 0$ and by taking variation to $\bar{w}_1$:

$$\int_0^{h_1}\int_{-\infty}^{\infty}\int_{-\infty}^{\infty}\left(D\nabla^4\bar{w}_1 + \bar{E}_1\left(\bar{w}_1\left(\frac{\partial \emptyset_1}{\partial z}\right)^2 + \bar{w}_2\left(\frac{\partial \emptyset_1}{\partial z}\right)\left(\frac{\partial \emptyset_2}{\partial z}\right)\right) - G_1\left(\nabla^2\bar{w}_1{\emptyset_1}^2 + \nabla^2\bar{w}_2\emptyset_1\emptyset_2\right) - \bar{q}\right)\delta\bar{w}_1 dxdydz = 0 \tag{4-34}$$

$\frac{\partial \Pi}{\partial \bar{w}_2} = 0$ and by taking variation to $\bar{w}_2$:

$$\int_0^{h_1}\int_{-\infty}^{\infty}\int_{-\infty}^{\infty}\left(\bar{E}_1\left(\bar{w}_2\left(\frac{\partial \emptyset_2}{\partial z}\right)^2 + \bar{w}_1\left(\frac{\partial \emptyset_1}{\partial z}\right)\left(\frac{\partial \emptyset_2}{\partial z}\right)\right) - G_1\left(\nabla^2\bar{w}_2{\emptyset_2}^2 + \nabla^2\bar{w}_1\emptyset_1\emptyset_2\right)\right)\delta\bar{w}_2 dxdydz + \int_{h_1}^{H}\int_{-\infty}^{\infty}\int_{-\infty}^{\infty}\left(\bar{E}_2\left(\bar{w}_2\left(\frac{\partial \emptyset_2}{\partial z}\right)^2\right) - G_2\left(\nabla^2\bar{w}_2{\emptyset_2}^2\right)\right)\delta\bar{w}_2 dxdydz = 0 \tag{4-35}$$

$\frac{\partial \Pi}{\partial \emptyset_1} = 0$ and by taking variation to $\emptyset_1$:

$$\int_0^{h_1}\int_{-\infty}^{\infty}\int_{-\infty}^{\infty}\left(\bar{E}_1\left(-\bar{w}_1^2\left(\frac{\partial^2\emptyset_1}{\partial z^2}\right)+\bar{w}_1\bar{w}_2\left(\frac{\partial^2\emptyset_2}{\partial z^2}\right)\right)\right.$$
$$\left.+G_1\left((\nabla\bar{w}_1)^2\emptyset_1+\left(\left(\frac{\partial\bar{w}_1}{\partial x}\right)\left(\frac{\partial\bar{w}_2}{\partial x}\right)+\left(\frac{\partial\bar{w}_1}{\partial y}\right)\left(\frac{\partial\bar{w}_2}{\partial y}\right)\right)\emptyset_2\right)\right)\delta\emptyset_1 dxdydz = 0 \qquad (4\text{-}36)$$

$\frac{\partial \Pi}{\partial \emptyset_2} = 0$ and by taking variation to $\emptyset_2$:

$$\int_0^{h_1}\int_{-\infty}^{\infty}\int_{-\infty}^{\infty}\left(\bar{E}_1\left(-\bar{w}_2^2\left(\frac{\partial^2\emptyset_2}{\partial z^2}\right)+\bar{w}_1\bar{w}_2\left(\frac{\partial^2\emptyset_1}{\partial z^2}\right)\right)\right.$$
$$\left.+G_1\left((\nabla\bar{w}_2)^2\emptyset_2+\left(\left(\frac{\partial\bar{w}_1}{\partial x}\right)\left(\frac{\partial\bar{w}_2}{\partial x}\right)+\left(\frac{\partial\bar{w}_1}{\partial y}\right)\left(\frac{\partial\bar{w}_2}{\partial y}\right)\right)\emptyset_1\right)\right)\delta\emptyset_2 dxdydz$$
$$+\int_{h_1}^{H}\int_{-\infty}^{\infty}\int_{-\infty}^{\infty}\left(-\bar{E}_2\bar{w}_2^2\left(\frac{\partial^2\emptyset_2}{\partial z^2}\right)+G_2(\nabla\bar{w}_2)^2\emptyset_2\right)\delta\emptyset_2 dxdydz = 0 \qquad (4\text{-}37)$$

where,

$$\int_0^{h_1}{\emptyset_1}^2\,dz = \frac{h_1}{3} \qquad \int_0^{h_1}\left(\frac{\partial\emptyset_1}{\partial z}\right)^2 dz = \frac{1}{h_1}$$

$$\int_0^{h_1}{\emptyset_2}^2\,dz = \frac{h_1}{3} \qquad \int_0^{h_1}\left(\frac{\partial\emptyset_2}{\partial z}\right)^2 dz = \frac{1}{h_1} \qquad (4\text{-}38)$$

$$\int_0^{h_1}\emptyset_1\emptyset_2\,dz = \frac{h_1}{6} \qquad \int_0^{h_1}\left(\frac{\partial\emptyset_1}{\partial z}\right)\left(\frac{\partial\emptyset_2}{\partial z}\right)dz = -\frac{1}{h_1}$$

By substituting Eq. 4-38 into Equation 4-34 to 4-37:

Eq. 4-35 $\implies D\nabla^4\bar{w}_1 + k_1\bar{w}_1 - k_1\bar{w}_2 - 2\tau_1\nabla^2\bar{w}_1 - \tau_1\nabla^2\bar{w}_2 = \bar{q}$ (4-39)

Eq. 4-36: $\implies k_1\bar{w}_2 - k_1\bar{w}_1 + k_2\bar{w}_2 - 2\tau_1\nabla^2\bar{w}_2 - \tau_1\nabla^2\bar{w}_1 - 2\tau_2\nabla^2\bar{w}_2 = 0$ (4-40)

Eq. 4-38: $\Longrightarrow -m\frac{\partial^2 \emptyset_2}{\partial z^2} + n\emptyset_2 = 0$ (4-41)

where,

$$k_1 = \frac{\bar{E}_1}{h_1} \qquad k_2 = \bar{E}_2 \int_{h_1}^{H} {\phi_2'}^2 \, dz \tag{4-42}$$

$$2\tau_1 = \frac{G_1 h_1}{3} \qquad 2\tau_2 = G_2 \int_{h_1}^{H} {\phi_2}^2 dz$$

$$m = \int_{-\infty}^{+\infty} \int_{-\infty}^{+\infty} \bar{E}_2 {\bar{w}_2}^2 dxdy \tag{4-43}$$

$$n = \int_{-\infty}^{+\infty} \int_{-\infty}^{+\infty} G_2 (\nabla \bar{w}_2)^2 dxdy \tag{4-44}$$

With the boundary conditions $\emptyset_2(h_1) = 1$ and $\emptyset_2(H) = 0$, the differential equation 4-43 can be solved as,

$$\emptyset_2(z) = \frac{\sinh \gamma(H - z)}{\sinh \gamma h_2} \tag{4-45}$$

where γ is the coefficient denoting the mode shape for the vertical deflection of the second soil layer and can be expressed as:

$$\gamma = \sqrt{\frac{n}{m}} \tag{4-46}$$

Eq. 4-39 and Eq. 4-40 are the equilibrium equations of a plate on a two-layer foundation, which can be rewritten as:

$$D\nabla^4 \bar{w}_1 + k_1(\bar{w}_1 - \bar{w}_2) - 2\tau_1 \nabla^2 \bar{w}_1 - \tau_1 \nabla^2 \bar{w}_2 = \bar{q} \tag{4-47}$$

$$-k_1 \bar{w}_1 - \tau_1 \nabla^2 \bar{w}_1 + (k_1 + k_2)\bar{w}_2 - (2\tau_1 + 2\tau_2)\nabla^2 \bar{w}_2 = 0 \tag{4-48}$$

As it appears from the above equations, Vlasov parameters k_1 and τ_1 depend only on the elastic properties and the thickness of the top soil layer. Soil parameters k_2 and τ_2 depend on the elastic properties and the thickness of the bottom soil layer and the vertical deflection mode shape $\emptyset_2$. The mode shape $\emptyset_2$ for the second layer is a function of coefficient γ, which is determined based on the area of the vertical deflection basin ($\bar{w}_2$) and the area of the gradient of vertical deflection basin ($\nabla\bar{w}_2$) of the top surface of the bottom foundation layer. An iterative process, similar to the one used for the one-layer foundation, is needed to estimate the Vlasov foundation parameters k_2 and τ_2.

4.3.3 Applicability of Vlasov Model

The procedure for estimating the Vlasov foundation parameters presented above was based on the theoretical idealization of foundation layer with vertical springs connected with a shear layer. Utilizing the Vlasov method has been limited to the research purposes and has not been popular for regular pavement designs. The 2004 AASHTO MEPDG does not recommend using this model for the performance prediction of concrete pavements. One of the reasons that MEPDG does not tend to apply the Vlasov model could be because of the limitations of existing analysis tools in modeling the Vlasov foundation. These limitations affected the analysis of jointed concrete pavements due to thermal loads. The application of the Vlasov foundation in the existing analysis tools was limited to the analysis of only a single slab subjected to wheel loads. The other reason is that no test method has been established to verify the estimated Vlasov parameters. The mathematical model presented in the next section attempts to provide a reliable idealization of the Vlasov foundation that can be incorporated for the thermal analysis of jointed concrete pavements.

4.3.4 Review on the Finite Element Models of Vlasov Foundation

Modeling a rigid pavement system, consisting of a plate resting on a two parameter foundation, has been investigated by several researchers. The main purpose of these efforts involved finding a solution to estimate vertical displacement at the foundation surface and then obtaining the coefficient γ to compute soil (Vlasov) parameters. To solve the equilibrium equation 4-15, Vlasov and Leontev (1996) proposed an approximate closed form solution for the displacement function $\bar{w}(x, y)$ for the case of concentrated load and distributed load applied to the plate. Straughan (1990) expanded the Vlasov

solution to determine the vertical displacement of the foundation surface beyond the slab edge, and at the plate corner, by dividing the domain outside the plate into eight regions. In that model, by solving Eq. 4-15 in the domain outside the plate and at $z = 0$, for a rectangular plate with dimensions of $2a$ in the x direction and $2b$ in the y direction, the assumed displacement functions can be expressed as:

For a $< x < \infty$ and – b $< y < b$,

$$\bar{w}(x,y) = W_a e^{-\lambda(x-a)} \tag{4-49}$$

For b $< y < \infty$ and– a $< x < a$,

$$\bar{w}(x,y) = W_b e^{-\lambda(y-b)} \tag{4-50}$$

For a $< x < \infty \; and \; b < y < \infty$,

$$\bar{w}(x,y) = W_c e^{-\lambda(x-a)} e^{-\lambda(y-b)} \tag{4-51}$$

where,

$$\lambda = \sqrt{\frac{k}{2\tau}}$$

W_a : vertical displacement at the plate edge (x=a)

W_b : vertical displacement at the plate edge (y=b)

W_c: vertical displacement of the plate corner

By having the displacement function of the foundation surface inside and outside the plate domain, integrals m, n and coefficient γ will be calculated.

Straughan used the principle of virtual displacement to compute equivalent boundary force from the soil continuum, acting on the edge of the plate, for each of those regions. The virtual work done by the edge shear force on the plate should be equal to the virtual strain energy in the soil continuum in that region (7). The shear force along the plate edges will be obtained as:

$$\bar{V}_x = -\left(\sqrt{2k\tau}\bar{w} + 2\tau\frac{\partial\bar{w}}{\partial x} - \frac{\tau}{\lambda}\frac{\partial^2\bar{w}}{\partial y^2}\right) \qquad @\ x = a \qquad (4\text{-}52)$$

$$\bar{V}_y = -\left(\sqrt{2k\tau}\bar{w} + 2\tau\frac{\partial\bar{w}}{\partial y} - \frac{\tau}{\lambda}\frac{\partial^2\bar{w}}{\partial x^2}\right) \qquad @\ y = b \qquad (4\text{-}53)$$

$$R_c = \frac{3}{2}\tau W_c \qquad @\ \text{plate corner} \qquad (4\text{-}54)$$

In order to solve the mathematical model for rectangular plates on an elastic foundation, Straughan developed a finite difference method. The euilibrium equation ($D\nabla^4\bar{w} - 2t\nabla^2\bar{w} + k\bar{w} = q$) was solved for the associated boundary conditions defined as follows:

at $x = \pm a$: $M_x = 0\ and\ V_x = \bar{V}_x$

at $y = \pm b$: $M_y = 0\ and\ V_y = \bar{V}_y$

where M_x and M_y are moments in the *x* and *y* directions, respectively, and V_x and V_x are the shear force in the *x* and *y* direction, which defined in Eq. 4-52 and Eq. 4-53.

Kolar and Nemec (1989) developed a simplified three-dimensional finite element model that allowed for modeling of soil medium outside the plate domain. In their model, the boundary conditions based on arbitrary Vlasov parameters (*k*, τ, and γ) were used to impose the reaction of the foundation outside the plate as elastic springs distributed along the plate.

Turhan (1992) developed a finite element procedure for the analysis of rectangular plates on two parameter foundations. In that procedure the axial stiffness matrix and the shear stiffness matrix of the two parameter foundation were computed. The global stiffness matrix in Turhan formulation was derived by superimposing the stiffness matrix of plate to the axial and shear stiffness matrix of foundation. The axial and shear stiffness matrices of foundation in the natural coordinates ξ and η were expressed as:

$$[k_k]^e = kab\int_{-1}^{+1}\int_{-1}^{+1}[N]^T[N]d\xi d\eta \qquad (4\text{-}55)$$

$$[k_t]^e = 2\tau ab \int_{-1}^{+1} \int_{-1}^{+1} \left(\frac{1}{a^2} \left[\frac{\partial N}{\partial \xi}\right]^T \left[\frac{\partial N}{\partial \xi}\right] + \frac{1}{b^2} \left[\frac{\partial N}{\partial \eta}\right]^T \left[\frac{\partial N}{\partial \eta}\right] \right) d\xi d\eta \quad (4\text{-}56)$$

Turhan (1992) presented the explicit form of the above stiffness matrices. In the Turhan model, the finite element model of entire plate-foundation system is limited to the region inside the plate domain. The effects of the infinite soil domain outside the plate are reflected by applying equivalent stiffness parameters on the plate boundaries by incorporating special elastic spring forces. The purpose of reducing the infinite domain outside the plate was to solve the equilibrium equation in a smaller plate domain, instead of modeling the entire foundation. Two types of stiffness were considered to reflect the effect of the soil outside the plate at the plate edges: the axial stiffness corresponding to the vertical displacement and rotational stiffness corresponding to the rotation of the plate at its edges. Minimizing the potential energy, they calculated the reactive forces per unit length of the plate boundaries and the rotational restraint per unit length of the boundary along the x direction as (Vallabhan et *al*., 1999):

$$V = \sqrt{2\tau k} W_a \quad (4\text{-}57)$$

$$M_x = \frac{1}{2} 2\tau \sqrt{\frac{2\tau}{k}} \theta_x \quad (4\text{-}58)$$

where W_a and θ_x are the vertical displacement and rotation at the edge of the plate. Vallabhan and Daloglu (1999) examined the finite element solution proposed by Turhan by comparing the results from that method to those from 3D finite element method and the classical Vlasov model with an arbitrary γ parameter.

Celik and Saygun (1999) presented a new finite element model by combining the stiffness of the plate element into the stiffness of the foundation element. In their model, the effect of the surrounding soil was considered by modeling the limited soil region outside the plate edges. The foundation element in that model was a four node rectangular element with one degree of freedom (vertical displacement) per node. The stiffness matrices corresponding to the axial and shear deformation of the soil were compute as:

$$k_{ij} = k \iint w_i w_j dA \tag{4-59}$$

$$\tau_{ij} = 2\tau \iint \left(\frac{\partial w_i}{\partial x} \frac{\partial w_j}{\partial x} + \frac{\partial w_i}{\partial y} \frac{\partial w_j}{\partial y} \right) dA \tag{4-60}$$

Buczkowski and Torbacki (2001) developed a finite element model for the analysis of Mindlin plates resting on a two parameter foundation. The foundation domain was modeled with 18-node quadratic zero thickness elements. To express the displacement of a point on the foundation in terms of the nodal foundation point, the same Lagrange interpolation function used for the plate element was used for the foundation. In their model the explicit stiffness matrix corresponding to the first and second foundation parameters were obtained.

Ozgan and Daloglu (2008) extracted the explicit forms of the axial and the shear stiffness matrix of foundation (Eq. 4-60 and 4-61) for two cases of four-node and eight-node quadrilateral elements. The effect of the surrounding soil domain on the plate behavior was applied similar to the Straughan model by considering them as boundary forces.

A finite element model for the analysis of a slab placed on the Pasternak foundation was first developed by Ioannides et *al*. (1985) and implemented into the finite element program ILLI-SLAB. In ILLI-SLAB, 4-node elements with three degrees of freedom per node were used to model foundation domain. The foundation element shared nodes with those used to discretize the plate (slab). That model failed to properly model the effect of foundation beyond the slab edge and therefore it was limited to the case with interior loads (Khazanovich, 2003). To overcome this limitation, Khazanovich and Ioannides (1993) modeled the extended foundation in horizontal directions by introducing semi-infinite elements. The new modification was implemented into the finite element program ILSL2. That model assumed the approximation of the Straughan model, where the deflections beyond the slab can be represented as a function of the deflection of the slab edge and the foundation parameters.

The finite element program ILISL2 can also analyze slabs on Kerr foundations. Kerr foundation in ILISL2 are modeled as 8-node elements with 3 degrees of freedom per node with four nodes on top of the upper spring layer and four nodes at the top of lower layer. ILSL2 has two major limitations in analysis of a slab on Pasternak and Kerr foundation: 1) only wheel loads can be considered (thermal

analysis is impossible) and 2) only a single slab can be modeled. Modeling multiple jointed slabs is impossible.

The finite element program ISLAB2000 (Khazanovich et *al*., 2000) made some improvements to ILSL2 by enabling thermal analysis of slabs on Pasternak and Kerr foundations. In ISLAB2000, the separation of slabs due to thermal curling was considered for the Kerr foundation, where the contact pressure was estimated equal to the stress in the upper spring layer (Khazanovich, 2003). In the finite element model of ISLAB2000, the nodes on top of the Pasternak foundation share the same nodes with the slab. Thus, modeling the slab separation due to thermal curling is impossible in the case of using a Pasternak foundation. To overcome this limitation, Khazanovich and Ioannides (1993) proposed that for the thermal analysis of a slab on the Pasternak foundations, the foundation may be converted into a Kerr foundation with a very stiff upper spring layer. However, a very high stiffness for upper springs caused numerical instability and non-convergence of the finite element solution. Carrasco et *al*. (2011) studied the effect of the foundation model on the PCC slab deflection employing NYSLAB. They concluded that the deflections with the Vlasov model close to the edges are significantly lower than those with the Winkler model. This difference was attributed as a result of added foundation stiffness because of the extension of the foundation in the Vlasov model.

4.3.5 Modeling One-Layer Vlasov Foundation in NYSLAB

In NYSLAB, each layer of the Vlasov foundation is modeled with 18 node elements with one vertical displacement degree of freedom per node (Figure 4.6). The assumption is that each layer has constant thickness and the foundation cross section is constant through the layer thickness. Foundation layer is extended beyond the slab edges to take into account the stiffness of the surrounding soil. Depending on the geometry of the pavement system, the width of the extended region outside the plate domain, necessary for modeling the effect of the surrounding soil, is estimated in NYSLAB (usually between 6 ft to 10 ft). Foundation elements and slab elements do not share nodes.

The axial stiffness of the foundation can be determined by minimizing the axial terms of the potential energy of the total foundation system (Eq. 4-59):

$$\Pi_{\mathrm{k}} = \frac{1}{2}\int_{\Omega_e} [\overline{w}(x,y)]^T k\, [\overline{w}(x,y)] dA \tag{4-61}$$

$$[K_k]^{(e)} = \frac{\partial^2(\Pi_{\mathrm{k}})}{\partial \overline{w}_i \partial \overline{w}_j} \tag{4-62}$$

Figure 4.6: An 18-node Vlasov foundation element.

By expressing the vertical displacement *w* at each point of the foundation domain with the interpolated element nodal value we have:

$$\overline{w} = \sum_{i=1}^{9} N_i \overline{w}_i \tag{4-63}$$

$$[K_k]^{(e)} = k \iint_A B_k^T B_k dA \tag{4-64}$$

where *N* is the interpolation function similar to the one used for the plate element (Eq. 3-32) and B_k is derived as:

$$B_k = [0 \;\; 0 \;\; N_1 \;\; 0 \;\; 0 \;\; 0 \;\; 0 \;\; N_2 \;\; 0 \;\; 0 \;\; \ldots] \tag{4-65}$$

Using nine Gauss integral points, the axial stiffness matrix of the foundation in the local coordinate system will be derived as:

$$[K_k]_{ij}^{(e)} = k\int_{-1}^{+1}\int_{-1}^{+1} B_k^T B_k detJ d\xi d\eta = \sum_{i=1}^{9}\sum_{j=1}^{9} W_i W_j B_k^T(\xi_i,\eta_j) k B_k(\xi_i,\eta_j) detJ(\xi_i,\eta_j) \tag{4-66}$$

where W_i and W_j are the weight factors of nine quadrature Gauss points.

By minimizing the terms of the total potential energy corresponding to the foundation shear stiffness, the shear stiffness of Vlasov foundation will be derived as:

$$\Pi_\tau = \frac{1}{2}\int_{\Omega_e}\left[\frac{\partial\bar{w}}{\partial x},\frac{\partial\bar{w}}{\partial x}\right]^T 2\tau\left[\frac{\partial\bar{w}}{\partial x},\frac{\partial\bar{w}}{\partial x}\right] dA \tag{4-67}$$

$$[K_\tau]^{(e)} = \frac{\partial^2(\Pi_\tau)}{\partial\bar{w}_i\partial\bar{w}_j} \tag{4-68}$$

$$[K_\tau]^{(e)} = 2\tau\iint_A B_\tau^T B_\tau dA \tag{4-69}$$

where,

$$B_\tau^T = \begin{bmatrix} 0 & 0 & \dfrac{\partial N_1}{\partial x} & 0 & 0 & 0 & 0 & \dfrac{\partial N_2}{\partial x} & \cdots \\ 0 & 0 & \dfrac{\partial N_1}{\partial y} & 0 & 0 & 0 & 0 & \dfrac{\partial N_2}{\partial y} & \cdots \end{bmatrix} \tag{4-70}$$

Using nine Gauss integral points, the shear stiffness matrix of the foundation in the local coordinate system will be derived as:

$$[K_\tau]_{ij}^{(e)} = 2\tau\int_{-1}^{+1}\int_{-1}^{+1} B_\tau^T B_\tau detJ d\xi d\eta = \sum_{i=1}^{9}\sum_{j=1}^{9} W_i W_j B_\tau^T\left(\xi_i,\eta_j\right)(2\tau) B_\tau(\xi_i,\eta_j) detJ(\xi_i,\eta_j) \tag{4-71}$$

Eq. 4-66 and Eq. 4-71 represent the integration over the horizontal cross section of the element. The total foundation element stiffness matrix for one-layer foundation is then calculated as:

$$\left[K_f\right]^{(e)} = \begin{bmatrix} K_k + K_\tau & -K_k \\ -K_k & K_k \end{bmatrix}_{90\times 90} \tag{4-72}$$

4.3.6 Modeling Two-Layer Vlasov Foundation in NYSLAB

In a two-layer Vlasov foundation, the system of equilibrium equation represented in Eq. 4-47 and Eq. 4-48 should be solved.18-node quadrilateral elements similar to the foundation element in Figure 4.5 are used to discretize the two-layer foundation system (Figure 4.7). In this case, the foundation layers are extended beyond the slab edges to consider the stiffness of the surrounding soil.

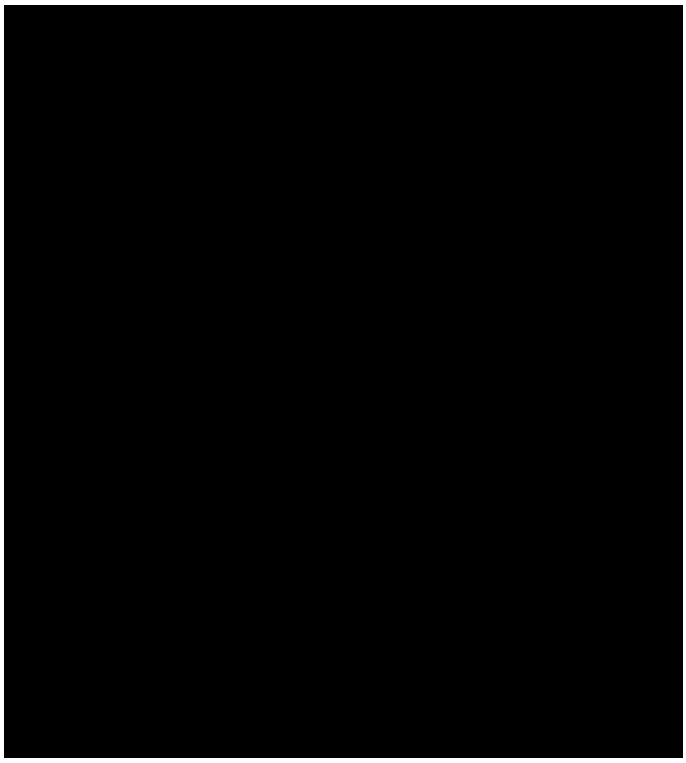

Figure 4.7: 18-node foundation element to model two-layer Vlasov foundation systems.

The axial and shear stiffness matrix for each layer of foundation will be derived according to Eq. 4-66 and Eq. 4-71:

Foundation layer 1:

$$[(K_k)_1]_{ij}^{(e)} = k_1 \int_{-1}^{+1} \int_{-1}^{+1} B_k^T B_k detJ d\xi d\eta = \sum_{i=1}^{9} \sum_{j=1}^{9} W_i W_j B_k^T(\xi_i, \eta_j)(k_1) B_k(\xi_i, \eta_j) detJ(\xi_i, \eta_j) \quad (4\text{-}75)$$

$$[(K_\tau)_1]_{ij}^{(e)} = 2\tau_1 \int_{-1}^{+1} \int_{-1}^{+1} B_\tau^T B_\tau detJ d\xi d\eta = \sum_{i=1}^{9} \sum_{j=1}^{9} W_i W_j B_\tau^T(\xi_i, \eta_j)(2\tau_1) B_\tau(\xi_i, \eta_j) detJ(\xi_i, \eta_j) \quad (4\text{-}76)$$

Foundation layer 2:

$$[(K_k)_2]_{ij}^{(e)} = k_1 \int_{-1}^{+1} \int_{-1}^{+1} B_k^T B_k detJ d\xi d\eta = \sum_{i=1}^{9} \sum_{j=1}^{9} W_i W_j B_k^T(\xi_i, \eta_j)(k_2) B_k(\xi_i, \eta_j) detJ(\xi_i, \eta_j) \quad (4\text{-}77)$$

$$[(K_\tau)_2]_{ij}^{(e)} = 2\tau_2 \int_{-1}^{+1} \int_{-1}^{+1} B_\tau^T B_\tau detJ d\xi d\eta = \sum_{i=1}^{9} \sum_{j=1}^{9} W_i W_j B_\tau^T(\xi_i, \eta_j)(2\tau_2) B_\tau(\xi_i, \eta_j) detJ(\xi_i, \eta_j) \quad (4\text{-}78)$$

The total stiffness matrix for the first and second layer of a two-layer Vlasov foundation can be expressed as:

$$\left[(K_f)_1\right]^{(e)} = \begin{bmatrix} (K_k)_1 + (K_t)_1 & -(K_k)_1 + \frac{1}{2}(K_t)_1 \\ -(K_k)_1 + \frac{1}{2}(K_t)_1 & (K_k)_1 + (K_t)_1 \end{bmatrix}_{90\times 90} \quad (4\text{-}79)$$

$$\left[(K_f)_2\right]^{(e)} = \begin{bmatrix} (K_k)_2 + (K_t)_2 & -(K_k)_2 + \frac{1}{2}(K_t)_2 \\ -(K_k)_2 + \frac{1}{2}(K_t)_2 & (K_k)_2 + (K_t)_2 \end{bmatrix}_{90\times 90} \quad (4\text{-}80)$$

4.4 Soil Continuity Elements

For modeling the Winkler foundation in NYSLAB, the foundation layer below each slab is modeled as disconnected segments to allow for the independence of Winkler springs across the joints and beyond the edge of the slabs. For continuous foundation models, such as Vlasov and Boussinesq, the foundation layers are extended beyond the edge of the slabs. This facilitates capturing the responses

of the slab edges. The foundation layers in these cases are connected across the joints with stiff springs which are called “soil continuity elements”. The stiffness matrix of these elements is derived as:

$$[K_{scont}] = \begin{bmatrix} 0 & 0 & 0 & 0 & 0 & 0 & 0 & 0 & 0 & 0 \\ 0 & 0 & 0 & 0 & 0 & 0 & 0 & 0 & 0 & 0 \\ 0 & 0 & jointK & 0 & 0 & 0 & 0 & -jointK & 0 & 0 \\ 0 & 0 & 0 & 0 & 0 & 0 & 0 & 0 & 0 & 0 \\ 0 & 0 & 0 & 0 & 0 & 0 & 0 & 0 & 0 & 0 \\ 0 & 0 & 0 & 0 & 0 & 0 & 0 & 0 & 0 & 0 \\ 0 & 0 & 0 & 0 & 0 & 0 & D & 0 & 0 & 0 \\ 0 & 0 & -jointK & 0 & 0 & 0 & 0 & jointK & 0 & 0 \\ 0 & 0 & 0 & 0 & 0 & 0 & 0 & 0 & 0 & 0 \\ 0 & 0 & 0 & 0 & 0 & 0 & 0 & 0 & 0 & 0 \end{bmatrix}$$

where *jointK* is given as 1000 times the maximum of the diagonal of the global stiffness matrix and is associated with the vertical deflection (*w*) degrees of freedom.

Chapter 5: Modeling the Contact between Pavement Layers

In the mathematical model of NYSLAB, the unbonded slab Layers are modeled independently from one another and from the foundation layer. Modeling the contact between these layers is of great importance, since the contact conditions along their interface significantly impacts the mechanical behavior of pavement. Pavement slabs may partially lose their contact with other layers, and they may slip along each other due to thermal loads. A thorough review of the different alternatives for modeling contact condition and different contact elements was presented in chapter 2. The characteristics of contact conditions between pavement layers were also explained in chapter 2. In this chapter "interface elements" are proposed to connect unbonded pavement slabs and to connect the bottom slab and the surface of top foundation layer in order to capture the loss of contact (separation) and slipping between them. A contact constitutive model is also presented to provide insight into the frictional characteristic of pavement layers interface. Moreover, an iterative procedure to solve the finite element model of jointed concrete pavements involved with contact between layers is included.

5.1 Contact-Friction Constitutive Law

Consider two surfaces (e.g. a plate and soil surface) in contact with the initial gap *G* between them (Fig 5.1). The relative displacement between each point at the top surface and its associated point at the bottom surface is defined as,

$$\Delta V = V^{(t)} - V^{(b)} \tag{5-1}$$

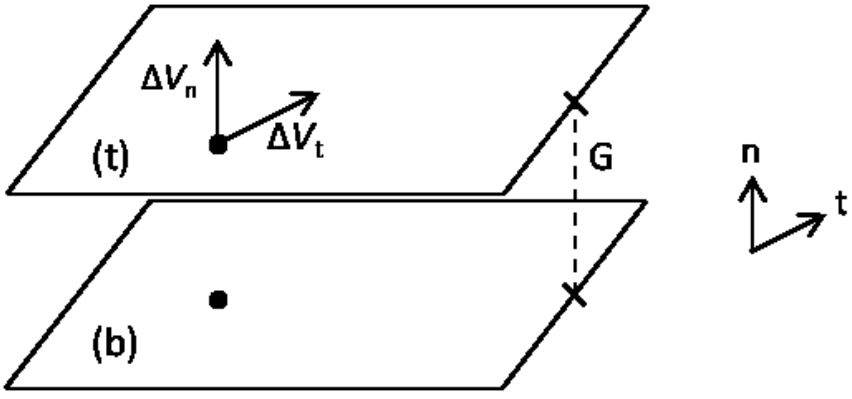

Figure 5.1: Position of surfaces in contact.

The normal and tangential components (normal and tangent to the contact surface) of the relative displacement of each point of contact are defined as ΔV_n *and* ΔV_t , respectively. Also, the normal and tangential components of the contact traction at each point of contact are defined as F_n *and* F_t, respectively. Depending on the magnitude and direction of applied loads, the normal traction at each point of contact can be calculated based on two possible contact conditions:

1. Gap opening. In this state, separation between the two surfaces at the point of contact occurs, and the normal traction is in tension.

$$F_n = k_1 \Delta V_n \qquad \textit{if} \quad \Delta V_n > -G \tag{5-2}$$

2. Gap closing. In this state, the two surfaces come in contact at the point of contact, and the normal traction is in compression.

$$F_n = -k_1 G + k_2(\Delta V_n + G) = k_2 \Delta V_n + (k_2 - k_1)G \qquad \textit{if} \quad \Delta V_n \leq -G \tag{5-3}$$

where k_1 and k_2 are constant penalty parameters, defining the stiffness in the constitutive equation for the normal traction (Figure 5.2). Theoretically, the normal traction is zero when a separation occurs. Assuming zero traction (k_1 equal to zero), may result in an ill-conditioned secant stiffness matrix with zero diagonal components. Numerical problems caused by this type of stiffness matrix can be avoided by selecting a very small value for the stiffness component in the gap opening state.

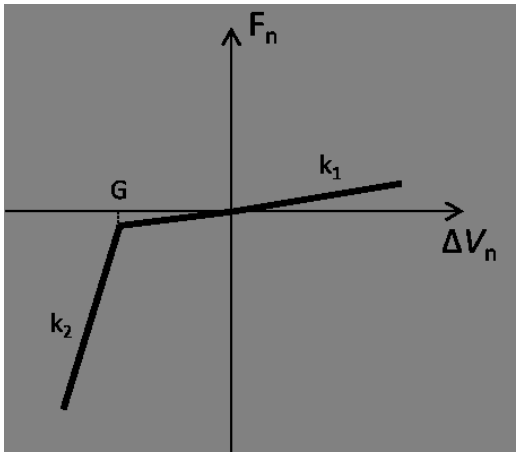

Figure 5.2: Plot of the constitutive relation for the normal traction.

The characterization of the frictional constitutive relation for each point of contact depends on the relative tangential displacement of its corresponding nodes in two contacting surfaces. The relative tangential displacement identifies the state of contact at each point, whether in slip mode or in stick mode. The frictional constitutive equation in the tangential direction, which correlates the frictional or tangential tractions to the tangential relative displacements, is represented as a multi-linear relation (see Figure 5.3). In this relation, $\Delta\bar{V}_s$ refers to the relative tangential displacement when slip occurs, and $\bar{F}_t$ is the frictional traction at that state. The coefficients k_3 and k_4 are also the penalty parameters, corresponding to the tangential stiffness at the interface of contacting surfaces before and after slip. Assuming zero tangential stiffness (k_4 equal to zero) when slip occurs, may cause numerical instability. Frictional tractions can be computed by using a specific slip rule, which in our model is the linear Mohr-Coulomb friction law. This friction law correlates the tangential (frictional) traction to the normal traction at each point of contact by incorporating a coefficient of friction.

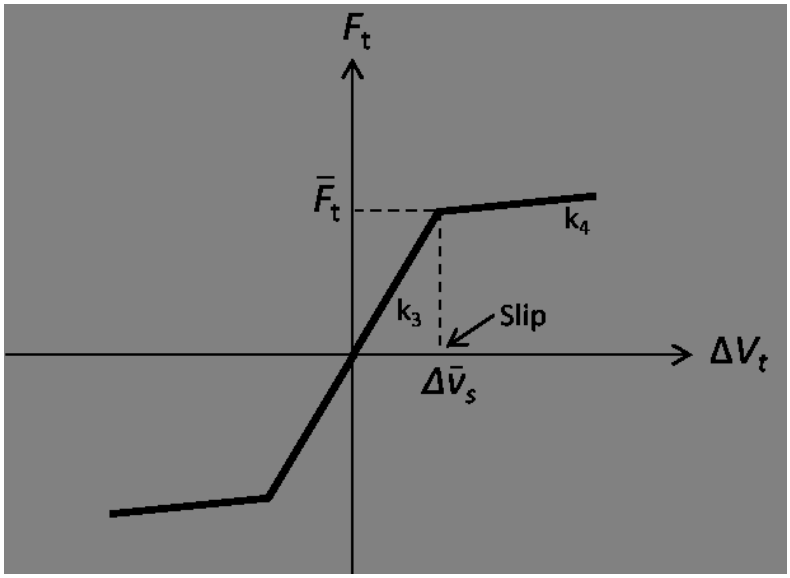

Figure 5.3: Plot of the constitutive relation for the tangential traction.

When two contacting points are in separation mode (gap opening), the frictional traction is zero,

$$\bar{F}_t = 0 \qquad if \quad \Delta V_n > -G \tag{5-4}$$

For points that maintain their contact, the maximum tangential or frictional traction at the condition where slip occurs is derived according to the Mohr-Coulomb friction law:

$$\overline{F}_{\mathrm{t}} = -\mu\, F_{\mathrm{n}} \qquad if \quad \Delta \mathrm{V_n} \leq \text{-G} \tag{5-5}$$

where μ is the coefficient of friction in the interface, and F_n is the normal traction. The negative sign in Eq. 5-5 indicates that the tangential tractions act in the opposite direction of slippage. The tangential displacement that defines the limit at which slip occurs can be derived as:

$$\Delta\overline{V}_s = \frac{\overline{F}_t}{k_3} = -\mu \frac{k_2 \Delta V_n + (k_2 - k_1)G}{k_3} \tag{5-6}$$

Let ΔV_x be the x component of the relative tangential displacement (ΔV_t) of a point in contact, as shown in Figure 5.4. Parameter γ_x is defined as,

$$\gamma_{\mathrm{x}} = \frac{\Delta V_{\mathrm{x}}}{\Delta \overline{V}_s} \tag{5-7}$$

If $\gamma_x \leq 1$ slip does not occur in x direction (stick mode) and the constitutive equation for the tangential traction in that direction is derived as (see Figure 5.3):

$$F_{\mathrm{tx}} = k_3\, \Delta V_{\mathrm{x}} \tag{5-8}$$

On the other hand, if $\gamma_{\mathrm{x}} > 1$ slip occurs and the constitutive equation in x direction is derived as:

$$F_{\mathrm{tx}} = k_4\, \Delta V_{\mathrm{x}} + (k_3 - k_4)\Delta \overline{V}_s \tag{5-9}$$

Similar constitutive relations are applied in the y direction. The states of contact (slip or stick) in the x and y directions are considered independently, in contrast to the assumption of Barbero et *al*. (1995) that indicates if slip occurs in one direction, no slip occurs in its orthogonal direction.

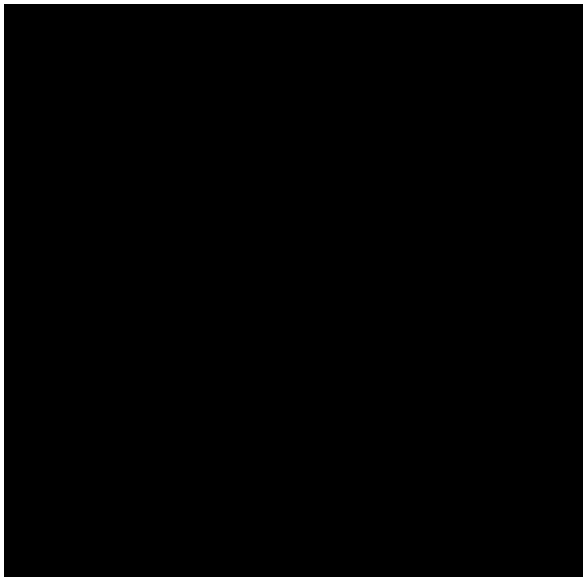

Figure 5.4: Components of tangential displacement.

Finally, depending on the state of contact (whether the two surfaces maintain contact and whether slip occurs in each direction), the normal and tangential components of the constitutive relations for each point of contact can be written by incorporating Eq. 5-2 and 5-3, and Eq. 5-8 and 5-9 as:

$$F = (D_s + D_{ns})\Delta V + (\mathrm{H} + I)G \tag{5-10-a}$$

where, F is the traction matrix defined as:

$$F = \begin{bmatrix} F_{\mathrm{tx}} \\ F_{\mathrm{ty}} \\ F_{\mathrm{n}} \end{bmatrix} \tag{5-10-b}$$

ΔU represents the vector of relative displacements:

$$\Delta U = \begin{bmatrix} \Delta V_{\mathrm{x}} \\ \Delta V_{\mathrm{y}} \\ \Delta U_{\mathrm{n}} \end{bmatrix} \tag{5-10-c}$$

D_s and D_{ns} represent the contact stiffness matrices:

$$D_s = \begin{bmatrix} s_1 & 0 & 0 \\ 0 & s_2 & 0 \\ 0 & 0 & s_3 \end{bmatrix} \quad \text{(5-10-d)}$$

$$D_{ns} = \left(\frac{k_2}{k_3}\right) \begin{bmatrix} 0 & 0 & f_1 \\ 0 & 0 & f_2 \\ 0 & 0 & 0 \end{bmatrix} \quad \text{(5-10-e)}$$

H and *I* represent the gap vector:

$$H = \left(\frac{k_2 - k_1}{k_3}\right) \begin{bmatrix} f_1 \\ f_2 \\ 0 \end{bmatrix} \qquad I = \begin{bmatrix} 0 \\ 0 \\ f_3 \end{bmatrix} \quad \text{(5-10-f)}$$

Parameters s_1, s_2, s_3 ,f_1 and f_2 are defined for each node based on the state of contact:

a) If there is no contact ($\Delta V_n > -G$),

$$s_1 = s_2 = f_1 = f_2 = f_3 = 0, \quad s_3 = k_1 \quad \text{(5-10-g)}$$

b) If two surfaces are in contact ($\Delta V_n \leq -G$) and if no slip occurs in the *x* direction ($\gamma_x \leq 1$) and the *y* direction ($\gamma_y \leq 1$),

$$s_1 = s_2 = k_3,\ s_3 = k_2,\ f_1 = f_2 = 0,\ f_3 = k_2 - k_1 \quad \text{(5-10-h)}$$

c) If slip occurs in both x and y directions ($\gamma_x > 1$) and ($\gamma_y > 1$)

$$s_1 = s_2 = k_4,\ s_3 = k_2,$$

$$f_1 = R_1(k_4 - k_3)\mu \qquad f_2 = R_2(k_4 - k_3)\mu \qquad f_3 = k_2 - k_1$$

$$R_1 = \frac{\Delta V_x}{\sqrt{\Delta V_x{}^2 + \Delta V_y{}^2}} \quad R_2 = \frac{\Delta V_y}{\sqrt{\Delta V_x{}^2 + \Delta V_y{}^2}} \quad \text{(5-10-i)}$$

5.2 The Interface Finite Element

An isoparametric 18-node interface element (Figure 5.5) is used here to model the frictional contact between the slab layers and between the bottom slab and the foundation (soil). This element is compatible with the plate element and the foundation element used in NYSLAB to model the composite slabs and the foundation layers. In case of contact between two unbonded slabs (see Figure 5.6), the top and the bottom surfaces of the interface elements are coincident with the mid-plane of the connected laminated plates. For the slab-foundation contact (see Figure 5.7), the top and the bottom surfaces of the interface elements are coincident with the mid-plane of the laminate and the top layer of the foundation elements, respectively. The initial gap between the two surfaces, *G*, which is used in the constitutive equations, is not the actual thickness of the interface element since the analysis here is 2D and the interface element is a 2D element. The advantage of using this interface element over commonly used 1D spring connections between contacting nodes is the proper distribution of the normal and tangential stiffness for non-uniform meshes.

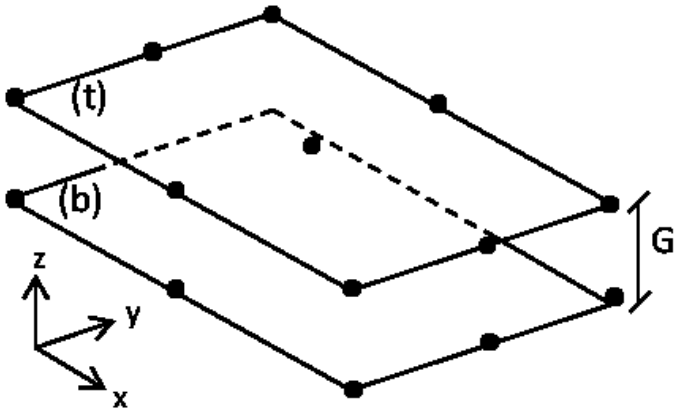

Figure 5.5: Interface Element.

5.2.1 Plate – Plate Contact

For two plates (in the composite slabs) in contact (Figure 5.6), ΔV represents the relative tangential displacement between the bottom surface of the top plate and the top surface of the bottom plate. In finite element modeling of laminated plates, the nodal points in each element are defined at the mid-plane of the laminate. The interface element nodal points coincide with those laminate element

nodes. The components of ΔV in the x and y directions with respect to the plate mid-plane displacements and the plate rotations can be derived as:

$$\Delta V_x = V_x^{(t)} - V_x^{(b)} = \left(U_x^{(t)} - \emptyset_x^{(t)} h^{(t)}\right) - \left(U_x^{(b)} - \emptyset_x^{(b)} h^{(b)}\right) \tag{5-11}$$

$$\Delta V_y = V_y^{(t)} - V_y^{(b)} = \left(U_y^{(t)} - \emptyset_y^{(t)} h^{(t)}\right) - \left(U_y^{(b)} - \emptyset_y^{(b)} h^{(b)}\right) \tag{5-12}$$

where $U_x^{(t)}$ and $U_y^{(t)}$ are the top plate mid-plane displacements in x and y directions; $U_x^{(b)}$ and $U_y^{(b)}$ are the bottom plate mid-plane displacements in x and y directions; $\emptyset_x^{(t)}$ and $\emptyset_y^{(t)}$ are the top plate rotations about y and x axes, respectively, and $\emptyset_x^{(b)}$ and $\emptyset_y^{(b)}$ are the bottom plate rotations about y and x axes, respectively. $h^{(t)}$ and $h^{(b)}$ are the distance between the mid-plane of the top and the bottom plate to the contact surface.

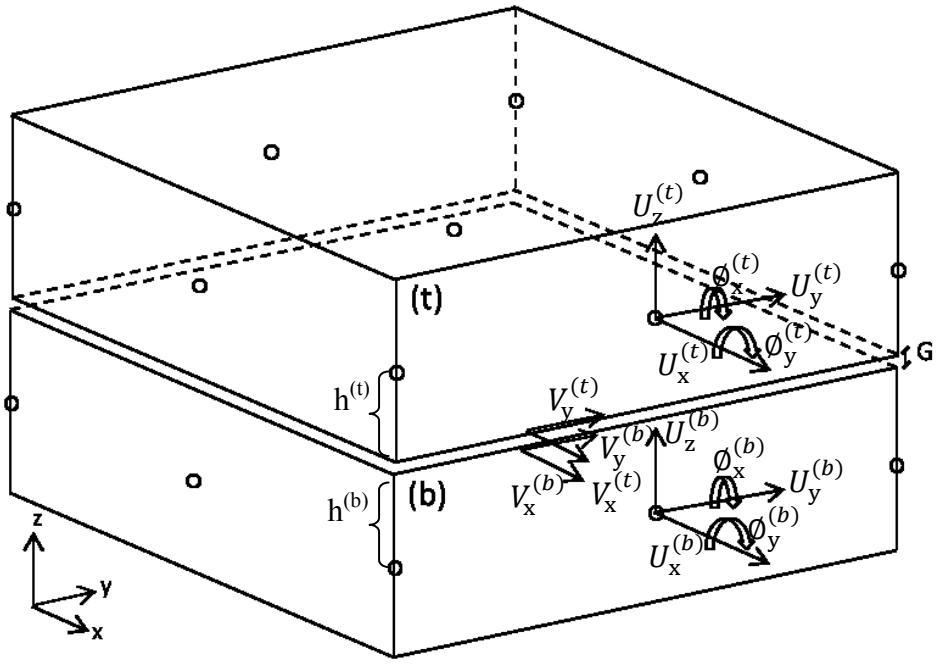

Figure 5.6: Geometry of two plates in contact.

The frictional tractions are generated at the contacting surfaces of the plates, where there are no nodal points in the plate element since the finite element is 2D based. For this reason, the effect of

frictional traction must be applied to the mid-plane of the plates, where the interface element and the plate element nodes are located. For this purpose, additional frictional moments, equal to the multiplication of the frictional traction to the half thickness of each plate ($h^{(t)}$ or $h^{(b)}$), should be applied to the interface element nodes (Figure 5.7). For example, the frictional traction in the x direction, generated at the top surface of the interface element ($F_x^{(t)}$), can be derived according to Eq. 5-8 and 5-9, depending on the state of slip. The frictional moment is then determined as:

$$M_x^{(t)} = -F_x^{(t)} h^{(t)} \tag{5-13}$$

The frictional traction and the frictional moment at the bottom surface of the interface element are equal to:

$$F_x^{(b)} = -F_x^{(t)} \tag{5-14}$$

$$M_x^{(b)} = F_x^{(b)} h^{(b)} \tag{5-15}$$

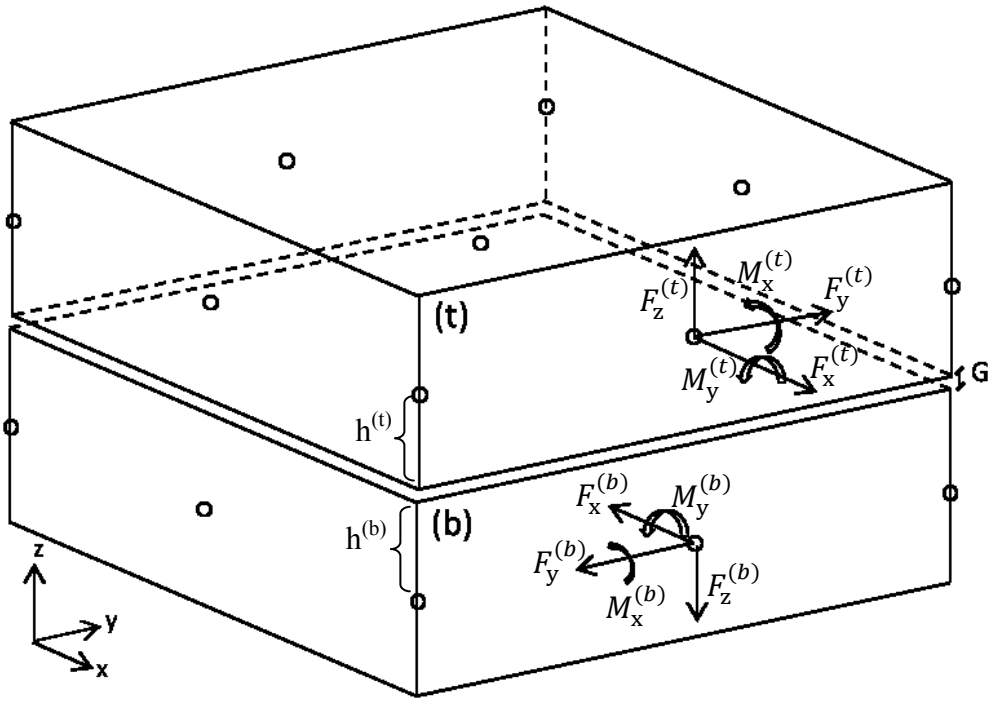

Figure 5.7: Kinematics of two plates in contact.

In the above equations, superscripts (*t*) and (*b*) represent the top and the bottom surface of the interface elements, respectively. The frictional tractions and the frictional moments in the *y* direction can be obtained similarly.

The total constitutive relation (consisting of the normal and tangential components) of the interface element for the contact of two plates, with respect to the plate's degrees of freedom, is derived as:

$$F = (D_s + D_{ns})\Delta U + (H + I)G \tag{5-16-a}$$

where,

$$\Delta U = U^{(t)} - U^{(b)} \qquad \left(U^{(t)} = \left\{U_x^{(t)}, U_y^{(t)}, U_z^{(t)}, \emptyset_x^{(t)}, \emptyset_y^{(t)}\right\}^T, \quad U^{(b)} = \left\{U_x^{(b)}, U_y^{(b)}, U_z^{(b)}, \emptyset_x^{(b)}, \emptyset_y^{(b)}\right\}^T\right)$$

$$F = \begin{Bmatrix} F^{(t)} \\ F^{(b)} \end{Bmatrix} \qquad \left(F^{(t)} = \left\{F_x^{(t)}, F_y^{(t)}, F_z^{(t)}, M_x^{(t)}, M_y^{(t)}\right\}^T, \quad F^{(b)} = \left\{F_x^{(b)}, F_y^{(b)}, F_z^{(b)}, M_x^{(b)}, M_y^{(b)}\right\}^T\right)$$

$$\{F^{(t)}\} = \left(\begin{bmatrix} D_s^{(tt)} & -D_s^{(tb)} \end{bmatrix} + \begin{bmatrix} D_{ns}^{(t)} & -D_{ns}^{(t)} \end{bmatrix}\right) \begin{Bmatrix} U^{(t)} \\ U^{(b)} \end{Bmatrix} + (\{H^{(t)}\} + \{I^{(t)}\})G$$

$$\{F^{(b)}\} = \left(\begin{bmatrix} -D_s^{(bt)} & D_s^{(bb)} \end{bmatrix} + \begin{bmatrix} -D_{ns}^{(b)} & D_{ns}^{(b)} \end{bmatrix}\right) \begin{Bmatrix} U^{(t)} \\ U^{(b)} \end{Bmatrix} + (\{-H^{(b)}\} + \{-I^{(b)}\})G$$

$$\begin{Bmatrix} F^{(t)} \\ F^{(b)} \end{Bmatrix} = \left(\begin{bmatrix} D_s^{(tt)} & -D_s^{(tb)} \\ -D_s^{(bt)} & D_s^{(bb)} \end{bmatrix} + \begin{bmatrix} D_{ns}^{(t)} & -D_{ns}^{(t)} \\ -D_{ns}^{(b)} & D_{ns}^{(b)} \end{bmatrix}\right) \begin{Bmatrix} U^{(t)} \\ U^{(b)} \end{Bmatrix} + \left(\begin{Bmatrix} H^{(t)} \\ -H^{(b)} \end{Bmatrix} + \begin{Bmatrix} I^{(t)} \\ -I^{(b)} \end{Bmatrix}\right) G \tag{5-16-b}$$

with,

$$D_s^{(tt)} = \begin{bmatrix} s_1 & 0 & 0 & -s_1 h^{(t)} & 0 \\ 0 & s_2 & 0 & 0 & -s_2 h^{(t)} \\ 0 & 0 & s_3 & 0 & 0 \\ -s_1 h^{(t)} & 0 & 0 & s_1 (h^{(t)})^2 & 0 \\ 0 & -s_2 h^{(t)} & 0 & 0 & s_2 (h^{(t)})^2 \end{bmatrix} \tag{5-16-c}$$

$$D_s^{(tb)} = \begin{bmatrix} s_1 & 0 & 0 & s_1 h^{(b)} & 0 \\ 0 & s_2 & 0 & 0 & s_2 h^{(b)} \\ 0 & 0 & s_3 & 0 & 0 \\ -s_1 h^{(t)} & 0 & 0 & -s_1 h^{(t)} h^{(b)} & 0 \\ 0 & -s_2 h^{(t)} & 0 & 0 & -s_2 h^{(t)} h^{(b)} \end{bmatrix} \quad \text{(5-16-d)}$$

$$D_s^{(bt)} = \begin{bmatrix} s_1 & 0 & 0 & -s_1 h^{(t)} & 0 \\ 0 & s_2 & 0 & 0 & -s_2 h^{(t)} \\ 0 & 0 & s_3 & 0 & 0 \\ s_1 h^{(b)} & 0 & 0 & -s_1 h^{(t)} h^{(b)} & 0 \\ 0 & s_2 h^{(b)} & 0 & 0 & -s_2 h^{(t)} h^{(b)} \end{bmatrix} \quad \text{(5-16-e)}$$

$$D_s^{(bb)} = \begin{bmatrix} s_1 & 0 & 0 & s_1 h^{(b)} & 0 \\ 0 & s_2 & 0 & 0 & s_2 h^{(b)} \\ 0 & 0 & s_3 & 0 & 0 \\ s_1 h^{(b)} & 0 & 0 & s_1 (h^{(b)})^2 & 0 \\ 0 & s_2 h^{(b)} & 0 & 0 & s_2 (h^{(b)})^2 \end{bmatrix} \quad \text{(5-16-f)}$$

$$D_{ns}^{(t)} = \left(\frac{k_2}{k_3}\right) \begin{bmatrix} 0 & 0 & f1 & 0 & 0 \\ 0 & 0 & f2 & 0 & 0 \\ 0 & 0 & 0 & 0 & 0 \\ 0 & 0 & -f_1 h^{(t)} & 0 & 0 \\ 0 & 0 & -f_2 h^{(t)} & 0 & 0 \end{bmatrix} \quad \text{(5-16-g)}$$

$$D_{ns}^{(b)} = \left(\frac{k_2}{k_3}\right) \begin{bmatrix} 0 & 0 & f1 & 0 & 0 \\ 0 & 0 & f2 & 0 & 0 \\ 0 & 0 & 0 & 0 & 0 \\ 0 & 0 & f_1 h^{(b)} & 0 & 0 \\ 0 & 0 & f_2 h^{(b)} & 0 & 0 \end{bmatrix} \quad \text{(5-16-h)}$$

$$H^{(t)} = \left(\frac{k_2 - k_1}{k_3}\right) \begin{bmatrix} f1 \\ f2 \\ 0 \\ -f_1 h^{(t)} \\ -f_2 h^{(t)} \end{bmatrix} \qquad H^{(b)} = \left(\frac{k_2 - k_1}{k_3}\right) \begin{bmatrix} f1 \\ f2 \\ 0 \\ f_1 h^{(b)} \\ f_2 h^{(b)} \end{bmatrix} \quad \text{(5-16-i)}$$

$$I^{(t)} = \begin{bmatrix} 0 \\ 0 \\ f3 \\ 0 \\ 0 \end{bmatrix} \qquad I^{(b)} = \begin{bmatrix} 0 \\ 0 \\ f3 \\ 0 \\ 0 \end{bmatrix} \quad \text{(5-16-j)}$$

Parameters s_1, s_2, s_3 ,f_1 and f_2 are defined for each node based on the state of contact (same as Eq.5-10). It should be noted that when slip occurs, the elements of matrix D_{ns} are not zero and the constitutive matrix in Eq. 5-16-a is not symmetric.

5.2.1 Plate – Foundation Contact

The contact between a plate element and a Winkler foundation element is shown in Figure 5.8. The same procedure as the plate-plate contact can be applied to determine the contact constitutive equation. $h^{(b)}$ in this case is set to zero.

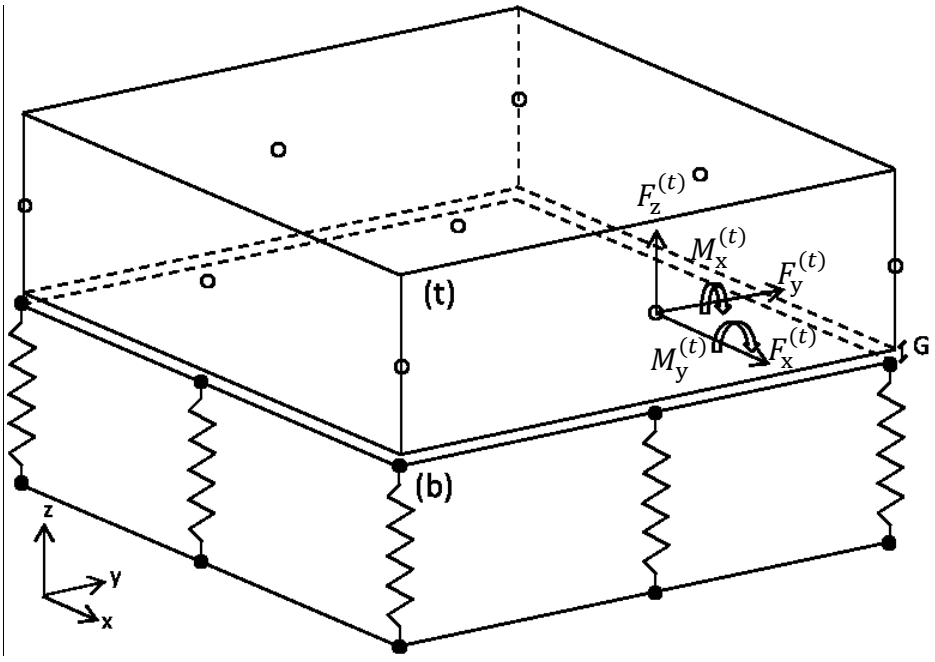

Figure 5.8: Geometry of plate – foundation in contact.

5.3 Finite Element Modeling of Interface

The first step in developing the finite element formulation of the interface is to obtain the weak forms of equilibrium equations, by applying the principle of virtual displacement to the contact constitutive equations. The internal virtual work is derived by applying the virtual displacement $\delta\Delta U$ to the constitutive equation (Eq.5-16),

$$W_i = \int \{[(D_s + D_{ns})\Delta U + (H + I)G]\delta(\Delta U)\}dxdy \tag{5-17}$$

The external virtual work is given as,

$$W_e = \int_\Omega \left\{F^{(t)}\delta U^{(t)} + F^{(b)}\delta U^{(b)}\right\} dx\, dy \tag{5-18}$$

Finally, according to the virtual work principle W_i is equal to W_e. By employing the same Lagrange interpolation function used for the 9-node plate elements, the displacement vector of the interface element in terms of nodal values are:

$$U^{(t)} = N_i u_i^{(t)}, \quad U^{(b)} = N_i u_i^{(b)} \tag{5-19}$$

where $u_i^{(t)}$and $u_i^{(b)}$ (*i=1,2,....,9*) are the nodal displacements of the top and the bottom surface of the interface element. The following equation yields upon substitution from Eq. 5-19 into 5-17 and 5-18:

$$\begin{aligned}\int_\Omega \Big\{&\Big(D_s^{(tt)}N_iN_ju^{(t)}\delta u^{(t)} - D_s^{(tb)}N_iN_ju^{(b)}\delta u^{(t)} - D_s^{(bt)}N_iN_ju^{(t)}\delta u^{(b)} + D_s^{(bb)}N_iN_ju^{(b)}\delta u^{(b)}\Big)\\ &+\Big(D_{ns}^{(t)}N_iN_ju^{(t)}\delta u^{(t)} - D_{ns}^{(t)}N_iN_ju^{(b)}\delta u^{(t)} - D_{ns}^{(b)}N_iN_ju^{(t)}\delta u^{(b)} + D_{ns}^{(b)}N_iN_ju^{(b)}\delta u^{(b)}\Big)\\ &+G\big(H^{(t)} + I^{(t)}\big)N_i\delta u^{(t)} - G\big(H^{(b)} + I^{(b)}\big)N_i\delta u^{(b)}\Big\}\, dxdy\\ &= \int_\Omega \left\{F^{(t)}N_i\delta u^{(t)} - F^{(b)}N_i\delta u^{(b)}\right\}dxdy\end{aligned} \tag{5-20}$$

By rearranging the above matrices and vectors, the following equations can be defined,

$$K_s^{(tt)} = \int_\Omega B^T D_s^{(tt)} B dxdy \qquad K_s^{(tb)} = \int_\Omega B^T D_s^{(tb)} B dxdy \tag{5-21}$$

$$K_s^{(bt)} = \int_\Omega B^T D_s^{(bt)} B dxdy \qquad K_s^{(bb)} = \int_\Omega B^T D_s^{(bb)} B dxdy \tag{5-22}$$

$$K_{ns}^{(t)} = \int_{\Omega} B^T D_{ns}^{(t)} B dxdy \qquad K_{ns}^{(b)} = \int_{\Omega} B^T D_{ns}^{(b)} B dxdy \tag{5-23}$$

$$Q^{(t)} = \int_{\Omega} B^T (H^{(t)} + I^{(t)}) G dxdy \qquad Q^{(b)} = \int_{\Omega} B^T \left(H^{(b)} + I^{(b)}\right) G dxdy \tag{5-24}$$

With,

$$B = \begin{bmatrix} N_1 & 0 & 0 & 0 & 0 & N_2 & 0 & \dots & N_9 & 0 & 0 & 0 & 0 \\ 0 & N_1 & 0 & 0 & 0 & 0 & N_2 & \dots & 0 & N_9 & 0 & 0 & 0 \\ 0 & 0 & N_1 & 0 & 0 & 0 & 0 & \dots & 0 & 0 & N_9 & 0 & 0 \\ 0 & 0 & 0 & N_1 & 0 & 0 & 0 & \dots & 0 & 0 & 0 & N_9 & 0 \\ 0 & 0 & 0 & 0 & N_1 & 0 & 0 & \dots & 0 & 0 & 0 & 0 & N_9 \end{bmatrix} \tag{5-25}$$

where $(K_s^{(tt)}, K_s^{(tb)}, K_s^{(bt)}, K_s^{(bb)})$ and $(K_{ns}^{(t)}, K_{ns}^{(b)})$ are defined as the components of symmetric and unsymmetric stiffness matrices of the interface elements, respectively, and $Q^{(t)}, Q^{(b)}$ are the elements of the interface gap force vector at the top and the bottom surface.

The numerical integration scheme for determining the interface element stiffness matrices and force vectors is of great importance and may differ from those applied in regular plate elements. For each interface element, it is possible for the nodes to have different states of contact during the analysis procedure (e.g., contact/separation mode or slip/stick mode), which in turn results in different constitutive equations. In this case, the Gauss integration method gives inaccurate approximation of the integrals because the value of the function (constitutive equation) in this method should be determined at 9 Gauss points (located between the element nodal points), in which the constitutive equation and the state of contact are not defined. Alternatively, the Newton-Cotes or Simpson's numerical method, as proposed by several researchers (Desai and Zaman, 1984; Barbero et *al*., 1995), can be used to overcome this integration problem. Three integration points in each direction coincide with the nodal points. In the case of a fine mesh, this integration scheme will give acceptable approximation for the integration of the interface stiffness matrix and force vector. For example, the integral of $K_s^{(tt)}$ (Eq. 5-21), using Newton-Cotes method, in the element local coordinate is determined as,

$$K_s^{(tt)} = \int_{-1}^{1}\int_{-1}^{1} \mathrm{B}^{\mathrm{T}} D_s^{(tt)} B detJ \, d\xi d\eta = \sum_{i=1}^{9}\sum_{j=1}^{9} w_i w_j B^T(\xi_i,\eta_j) D_s^{(tt)} B(\xi_i,\eta_j) detJ(\xi_i,\eta_j) \tag{5-26}$$

where $D_s^{(tt)}$ is the constitutive matrix for each element node, and J is the *Jacobian*. w_i and w_j are the weight factors as shown in Figure 5.9.

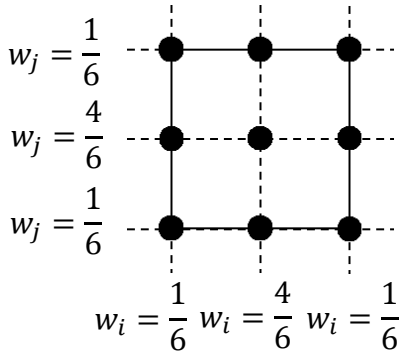

Figure 5.9: Integration points in interface elements.

Finally, the equilibrium equation of the interface element is derived as,

$$F^{(e)} = K_s^{(e)} U^{(e)} + K_{ns}^{(e)} U^{(e)} + Q^{(e)} \tag{5-27}$$

where $K_s^{(e)}$ and $K_{ns}^{(e)}$ are the symmetric and unsymmetric parts of the interface element stiffness matrix, which are the function of the nodal displacements and the state of contact at each node, and $Q^{(e)}$ is the interface gap force vector, which is a function of the nodal displacements, the state of contact and the initial gap:

$$K_s^{(e)} = \begin{bmatrix} K_s^{(tt)} & -K_s^{(tb)} \\ -K_s^{(bt)} & K_s^{(bb)} \end{bmatrix}^{(e)} \tag{5-28}$$

$$K_{ns}^{(e)} = \begin{bmatrix} K_{ns}^{(t)} & -K_{ns}^{(t)} \\ -K_{ns}^{(b)} & K_{ns}^{(b)} \end{bmatrix}^{(e)} \tag{5-29}$$

$$Q^{(e)} = \begin{bmatrix} Q^{(t)} \\ -Q^{(b)} \end{bmatrix}^{(e)} \tag{5-30}$$

5.4 Solving the System of Algebraic Equation

The global algebraic system of equations of the pavement system is obtained by assembling the discrete constitutive equations for all the interface elements, and adding to the governing equilibrium equations of the plates and foundation elements. The symmetric stiffness matrix of the interface elements (K_s) can be assembled to the global stiffness matrix of the entire structure. However, assembling the non-symmetric stiffness matrix of the interface elements (K_{ns}) produces asymmetricity in the global stiffness matrix. To avoid creating an unsymmetric global stiffness matrix, K_{ns}can be added to the global force vector (right-hand-side) as:

$$(K_G + K_s)U = F_G - K_{ns}U - Q \tag{5-31}$$

where K_G and F_G are the global stiffness matrix and global force vector of the entire structure (plates and foundations). The stiffness matrices K_G and K_s are created sparse in the source code. For the sparse matrix in the left-hand-side of Eq. 5-31, the MATLAB® software uses modified Cholesky factorization (CHOLMOD) to compute U. The obtained algebraic system of equations is nonlinear. An iterative procedure was implemented to find the solutions. The solution at each step (i) is calculated in terms of the results obtained at the previous step (i-1) as:

$$U^{(i)} = \left[K_G + K_s(U^{(i-1)})\right] \backslash \left\{F_G - K_{ns}\, U^{(i-1)} - Q(U^{(i-1)})\right\} \tag{5-32}$$

At the first step, all of the interface elements are in contact, due to the slab self-weight. Moreover, all of the nodes of the interface elements are assumed to be initially in stick mode. Convergence is attained when in two consecutive iterations there is no change produced in the state of contact or slip, and the difference in the tangential displacements is less than acceptable error ($\frac{|U^i - U^{i-1}|}{|U^i|} \ll \varepsilon$). For the nodes that lose their contact, the convergence test will not be conducted. In the flow chart presented in Fig. 5.10, the procedure for solving the problem including contact between pavement layers is demonstrated.

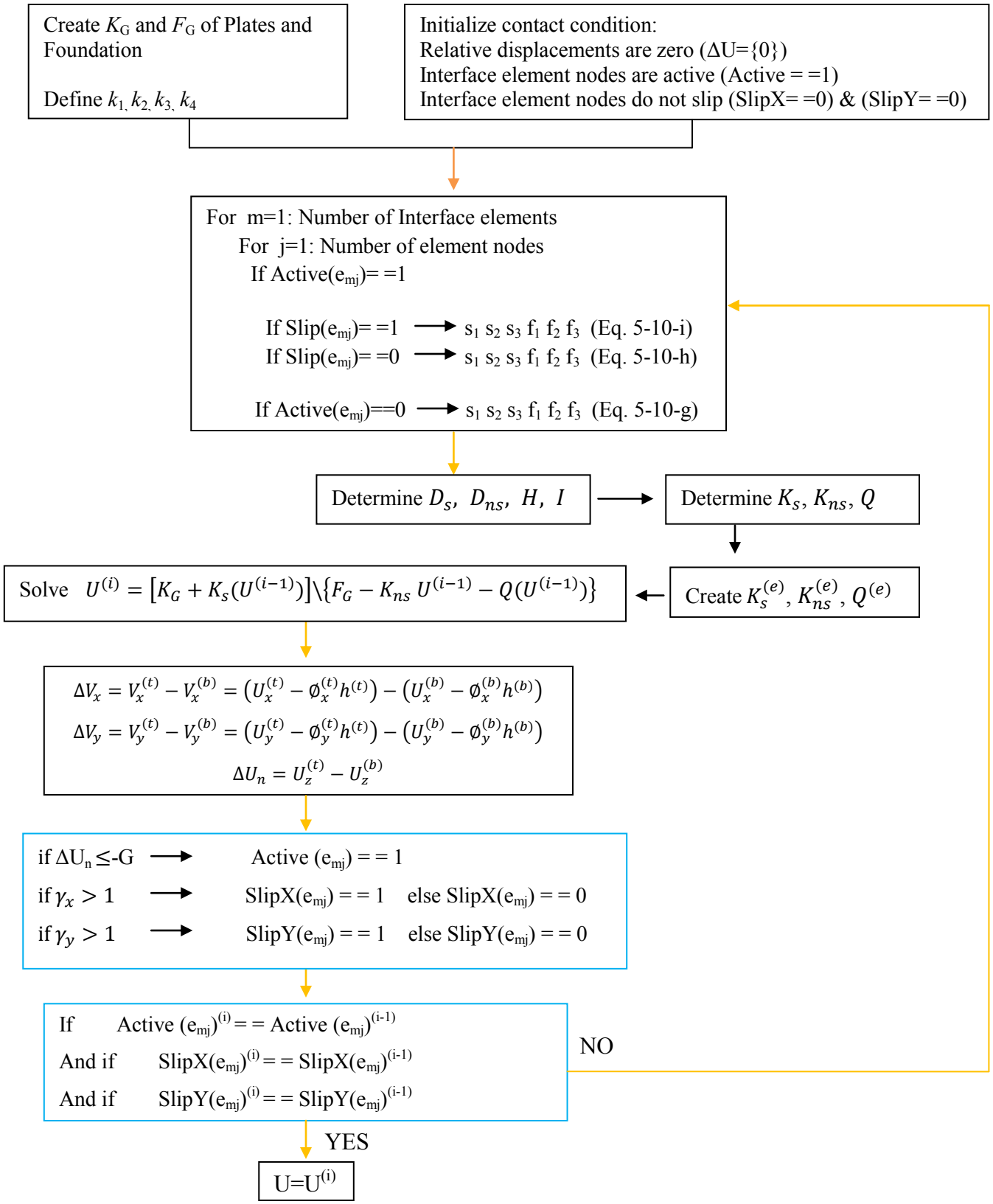

Figure 5.10: Flowchart for solving the contact problem.

5.5 Modeling PCC slab / Base Contact by Using Push-Off Test

As explained in chapter 2, assuming a linear frictional law may not be accurate for some types of base courses (with high levels of adhesion). Shear transfer at the slab – base interface can be captured via a bilinear elastic – plastic curve that defines the shear stresses to relative displacement constitutive relation. This relation can be obtained from an experimental push-off test of the PCC slab for each type of base material to define the relative displacement for which slip occurs, and determine the frictional or shear stresses at the slip state. Figure 5-11 shows a typical frictional stress – movement curve. In this method the frictional or shear stresses are independent of the normal stresses.

Figure 5.11: Contact constitutive relation obtained from push-off test.

The same nine-node interface element is used in this method to model the interface domain. The constitutive relation in normal direction of the contact surface is obtained similar to Eq. 5-2 and 5-3. The tangential constitutive relation in this method is achieved directly from the obtained frictional stress – movement curve. The state of contact in each node of the interface element is defined based on whether or not the tangential displacement at that node is higher than the limit of "slip" determined from the tangential constitutive curve. The process of developing contact equilibrium equations and the finite element model are similar to the contact model using a linear frictional law described in the previous sections.

Chapter 6: Summary of Mathematical Model of JPCP in NYSLAB

The finite element model of each component of jointed concrete pavements was introduced in the previous chapters. The layers that constitute the pavement section (PCC slabs and foundation) were modeled independently. Figure 6.1 illustrates the mathematical model of a typical pavement section in the formulation of NYSLAB.

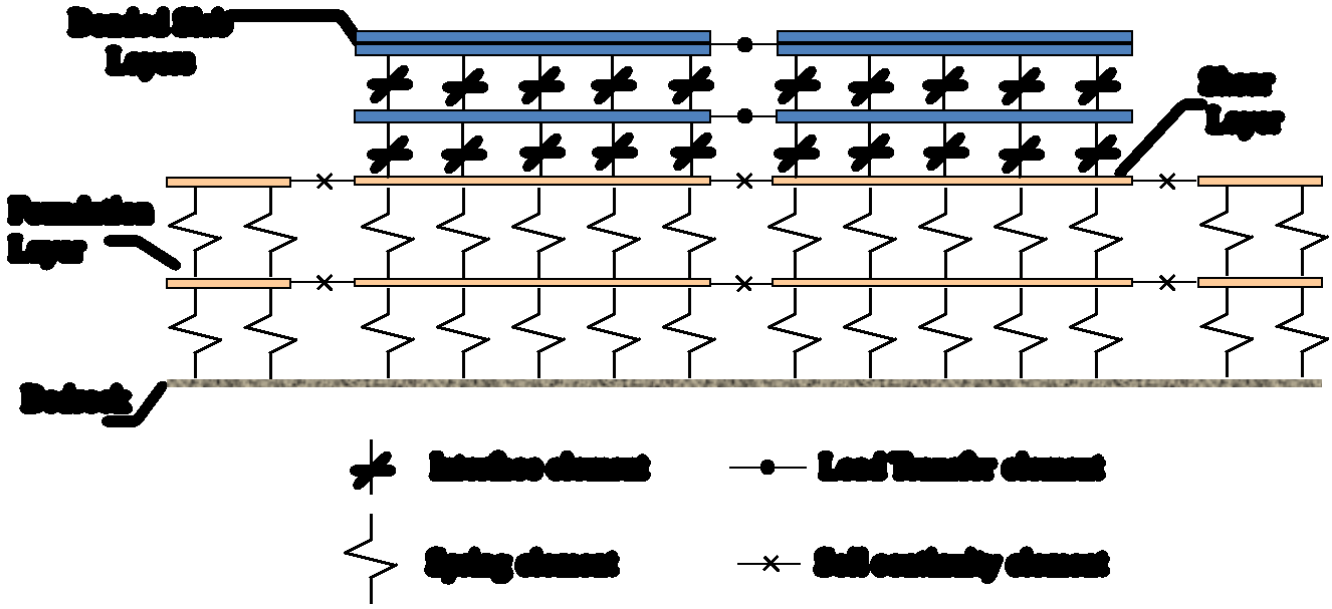

Figure 6.1: Jointed pavement section as modeled in NYSLAB.

6.1 Pavement slabs

Pavement slab layers were modeled as plate elements, with their interface considered either bonded or unbonded. Bonded pavement slab layers (e.g. bonded concrete overlays or bonded PCC slab/base course) were modeled as a single composite laminate. Debonded slab layers were connected to one another through interface elements. A nine-node isoparametric quadrilateral element was used to discretize the laminate domain. Each element has five degrees of freedom per node as shown in Figure 3.3 in chapter 3. The element nodes were defined at the middle plane of each laminate.

6.2 Foundation Layers

Five foundation models were included in NYSLAB to idealize the behavior of foundation system: Winkler, Vlasov, Kerr, ZSS and Boussinesq. All the foundation models, except for the Boussinesq (elastic solid) can be modeled as a single or a combination of two Vlasov layers in a series. In the Winkler model, all the foundation layers (base, subbase and subgrade) were represented as one layer of disconnected spring elements (one Vlasov layer with a zero shear parameter). In this model, the contribution of all foundation layers was manifested as a single modulus of subrade reaction or *k*-value (see Figure 4.1), which is the stiffness of each "spring element". In the Winkler model, the spring elements of the foundation layer below each slab were not connected to the spring elements corresponding to the foundation layer of the adjacent slab, to allow for the independent action of Winkler springs across the joints. Figure 6.2 shows the pavement system in Figure 6.1 with its foundation modeled as a Winkler layer.

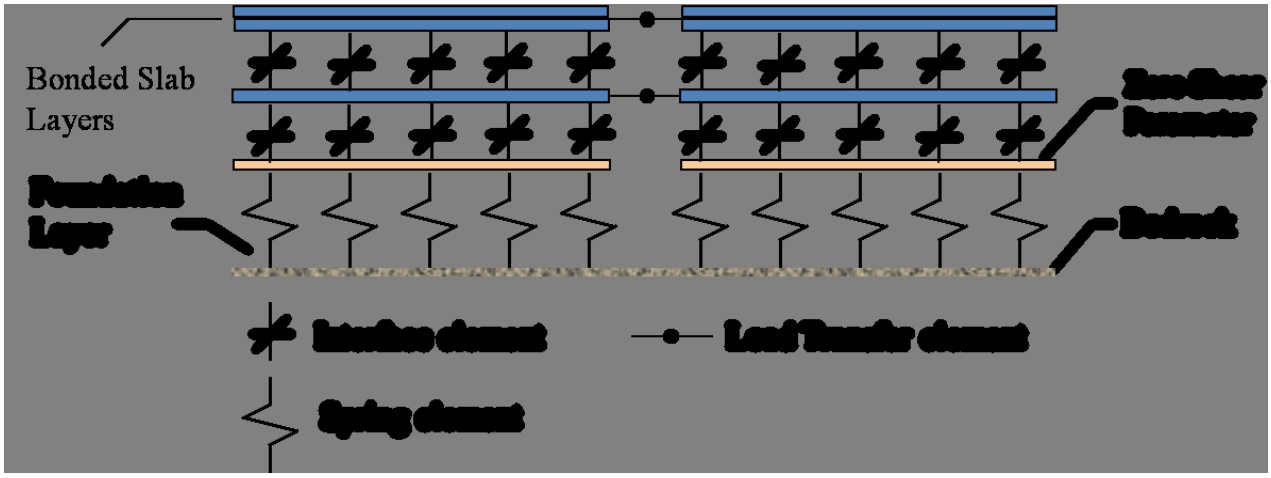

Figure 6.2: Jointed pavement section with a Winkler foundation.

The Kerr foundation can be modeled as two Vlasov layers when the shear parameter on the top layer is set to zero. The ZSS foundation was modeled as a Vlasov layer with zero shear coefficient on the top of a Boussinesq foundation. To model foundations with shear layer or the Boussinesq foundation, the foundation layers were extended beyond the edge of the slabs and the soil elements were connected across the joints with soil continuity elements. The width of the foundation extension is

calculated so that the foundation deformation decays to less than 10% of the maximum edge deflection (Carrasco et *al*., 2011).

In NYSLAB, there are two options to assign the foundation parameters. In the first option, the foundation parameters are assigned by the user as an input based on the type of foundation. For example, in the Winkler model, a single equivalent *k*-value is the only input. For the Vlasov model, the layer normal stiffness (κ) and the layer shear stiffness (τ) of each foundation layer are two parameters that can be assigned for any number of foundation layers. In the second option, users assign the general elastic properties of the soil (modulus of elasticity, Poisson's ration) and the layer thickness. NYSLAB then computes internally the equivalent *k*-value when the Winkler model is used, and calculates the layer normal stiffness (κ) and the layer shear stiffness (τ) for each layer when the Vlasov model is used.

6.3 Base Layers

The base layer can be modeled either as a plate element or as part of a Winkler or a Vlasov foundation system in NYSLAB. Therefore, the user has the option to assign different structural contributions for the base layer based on the type of base course (stabilized or unbounded) and their expected performance/role in the pavement system.

6.4 Interface Elements

Unbonded layers within the composite slab were connected to one another through interface elements. The same type of interface element was used to model the interface between the bottom slab layer and the top foundation layer. Interface elements have the characteristic of being active in each node when in compression and inactive when in tension to model the interface separation produced during curling. Each node of the interface elements has the ability to define the state of contact during sliding as a consequence of thermal expansion and contraction—whether in slip mode or stick mode. The active/inactive and slip/stick states are determined through an iterative process. The use of interface elements facilitates the modeling of the loss of contact between layers when thermal curling occurs and when voids between the PCC slabs and the foundation are present. Also, calculating the frictional or shear stress at the interface between layers and determining the state of contact is possible by using these

elements and by applying an appropriate constitutive friction law. For each node in contact, normal and shear stresses are related through the following isotropic Mohr-Coulomb friction law,

$$F_t = \mu \, \mathrm{F_n} \tag{6-1}$$

where, F_t is the tangential or shear stress, F_n is the normal stress, and μ is the coefficient of friction. Shear stress at each node of interface element is calculated based on the normal stress at that point, which can be influenced by temperature curling and vehicular loads.

Nine-node interface elements, consistent with the elements used to discretize the slabs and foundation layers, are used in the interface (see Figure 5.5). These elements have the capability to capture relative displacements between two surfaces in contact in two orthogonal tangential (horizontal) directions and normal (vertical) direction. The only parameter that is needed to account for the effect of friction in the analysis procedure in NYSLAB is the coefficient of friction in the slab-slab or slab-foundation interfaces.

6.5 Load Transfer Elements

Load transfer elements such as dowels, tie bars, aggregate interlock and key connection were used in the longitudinal and transverse joints to connect the jointed slabs. Those elements facilitate transferring loads applied by traffic or environment from one slab to the adjacent slab. Dowels and tie bars were modeled as beam elements and aggregate interlock and key connections were modeled as a bar element. Linkage elements were also implemented to capture the horizontal interaction between adjacent jointed slabs.

6.6 Degrees of Freedom and Boundary Conditions

Plate elements used to discretize the pavement slabs have five degrees of freedom (DOF) per node: Two in-plane displacements in the *x* direction (or longitudinal direction) and in the *y* direction (or transverse) direction (*u* and *v*), vertical displacement in the *z* direction (*w*), and two rotations about the *x* and *y* axes (ϕ_y, ϕ_x). The plate elements are free to move in all their degrees of freedom (as shown in Figure 6.3).

In each node of foundation elements, vertical displacement (w) is the only DOF that was contributed into the calculation of the foundation stiffness matrix (Figure 6.4). The foundation domain was assumed as an infinite continuum in the horizontal directions, which results in infinite stiffness in those directions. In order for foundation elements to be consistent with the plate elements and to apply the horizontally infinite nature of the foundation in the mathematical model, the foundation elements were constrained to move in the x and y directions. Also, the rotational DOF (ϕ_y, ϕ_x) were constrained in those elements.

Figure 6.3: Nine-node plate element with five degrees of freedom per node.

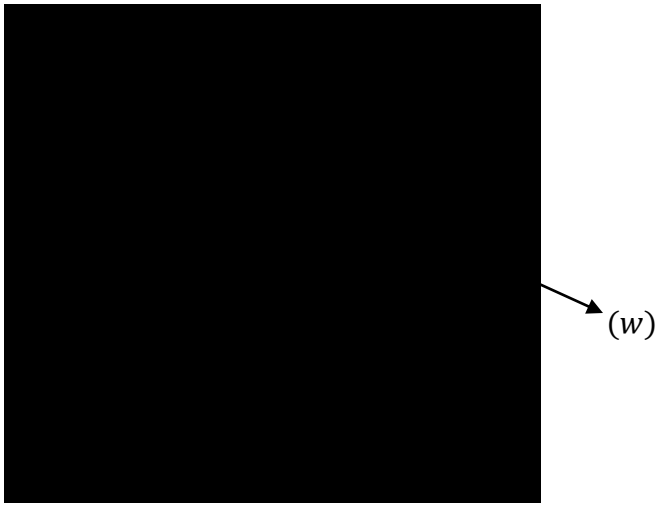

Figure 6.4: 18-node foundation element with one degree of freedom per node.

The bottoms of the subgrade layer (the last layer of foundation system on top of the bedrock), coincide with the bottom of the last spring elements, were constrained in all DOF. In case of continuous foundations (Vlasov, Boussinesq), where the foundation elements are extended beyond the slab edges, the nodes in the outer edges of those extended foundation elements will be constrained in all five DOF.

In dowel bars, only three DOF (w, ϕx, and v) contribute to the manipulation of stiffness matrix. The components corresponding to the other two DOF (u and ϕ_y) are zero in the stiffness matrix. In tie bars, four DOF (w, ϕy, and u, v) contribute to the generation of stiffness matrix.

6.7 Modeling Anomalies in Foundation

NYSLAB has the capability to model irregularities in the foundation. Anomalies and voids are two irregularities that can be considered by user in a particular region (as shown in Figure 6.5). In case of anomalies, different foundation parameter (e.g. k-value), corresponding to the anomaly area, can be designated. In case of presence of void, the amount of initial gap between the PCC slab and the foundation, due to loss of support, can be defined.

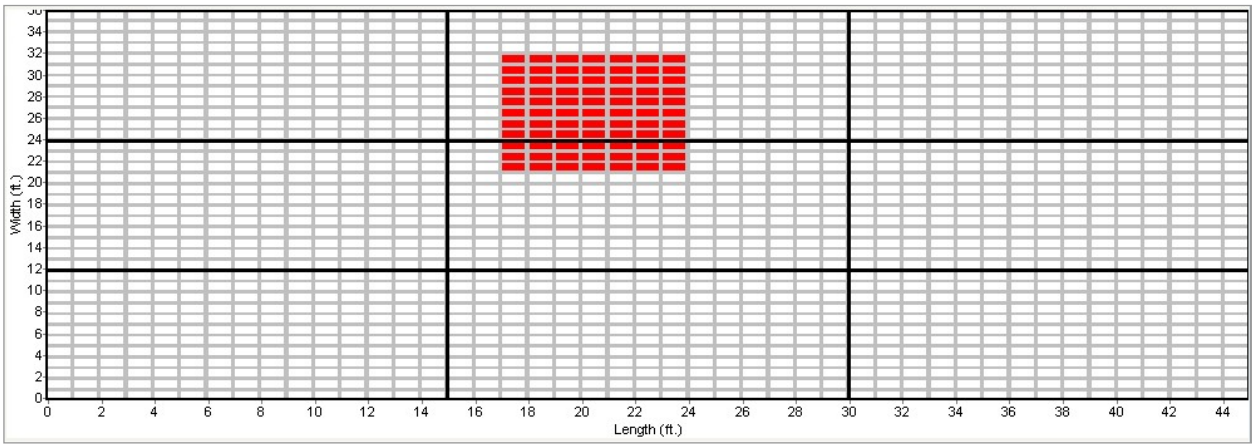

Figure 6.5: Definition of irregularity region.

6.8 Meshing

Isoparametric finite element formulation in NYSLAB permits for the modeling of irregular geometries. Rectangular meshing was used for the slab domains. For the area close to the slab edges, finer meshes are generated automatically to predict the responses in slab edges more accurately. Under the tire loads and anomalies, meshes with higher concentration of nodes are used. The same meshes

generated for the top slab layer will be used for other slab layers and the foundation layers. Consequently, the number of elements is equal in all slab layers.

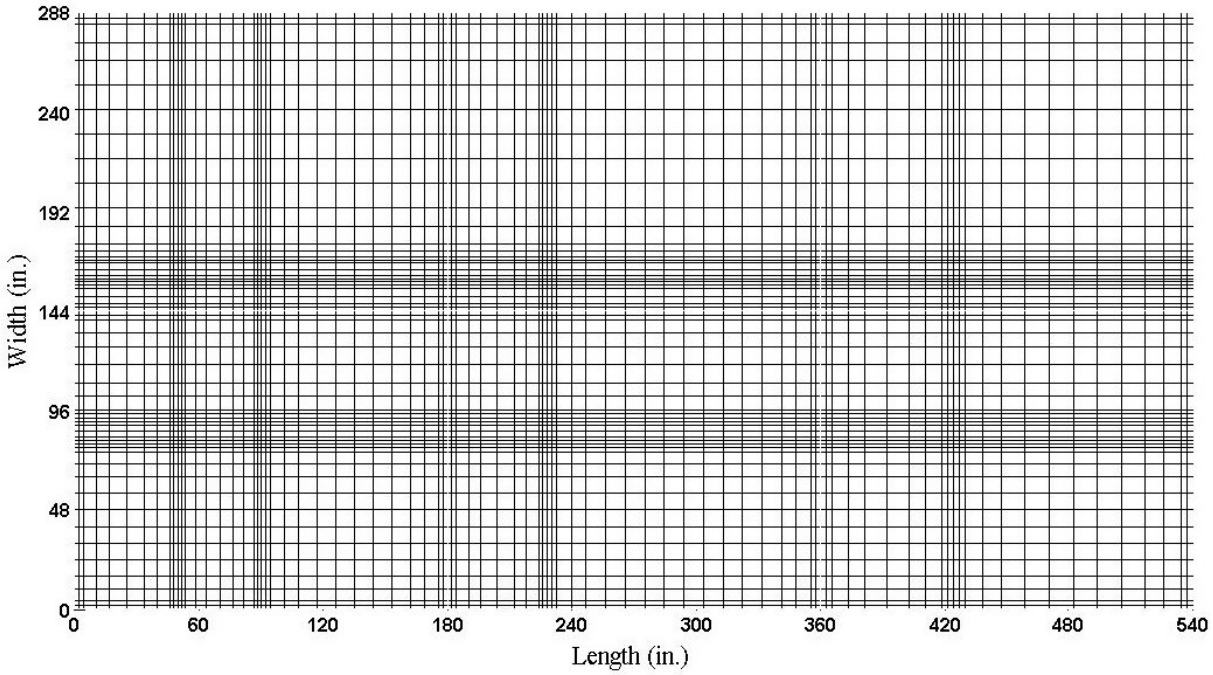

Figure 6.6: Typical mesh in slabs with concentrated grids under the tires.

Chapter 7: Parametric Study

In this chapter, a series of parametric studies were carried out using NYSLAB. One of the goals for performing such studies is to determine whether the governing equations used to idealize the

behavior of jointed concrete pavements in NYSLAB have been accurately selected and implemented in the FE model. The parametric studies in this chapter also attempt to provide a better understanding of the interaction between the most relevant parameters that govern the performance of JPCP. This chapter also aims to conduct several studies on the various aspects of pavement performance by taking advantage of the capabilities of the FE model developed in NYSLAB. This part will involve running the model using an analysis of parameter sensitivity associated with different contact condition between PCC slab and foundation, the effect of base rigidity, nonlinear temperature gradients, etc.

7.1 Effect of Nonlinear Temperature Gradient on Responses of JPCP

Simulating thermal effects with a nonlinear temperature profile allows for a more realistic modeling of temperature variation through the thickness of PCC slabs. In chapter 3 the process of including thermal loads to the finite element formulation of the pavement was described. In this section, results of a series of studies that highlight NYSLAB's capabilities to predict pavement responses under nonlinear temperature gradient are presented.

For this purpose, a two-layer rigid pavement system consisting of six (three by two in longitudinal and transverse direction as shown in Figure 7.1) jointed PCC slabs resting on a Winkler foundation, with the modulus of subgrade reaction of 200 psi/in, was studied. The PCC slabs and the foundation were unbonded in their interface. Each slab was 15 ft long, 14 ft wide and 10 in. thick. The modulus of elasticity of the PCC was set to 4,000 ksi with a Poisson's ratio of 0.15, coefficient of thermal expansion of $6 \times 10^{-6}/°\text{F}$ and a unit weight of 150 pcf. The space between the adjacent slabs was set to 0.25 in. in both directions. The slabs were connected transversely by 1.5-in.-diameter dowels (uniformly spaced at 1 ft intervals) and longitudinally by 1-in.-diameter tie bars (spaced at 2 ft intervals). The coefficient of friction between PCC slabs and foundation was set to 0.3.

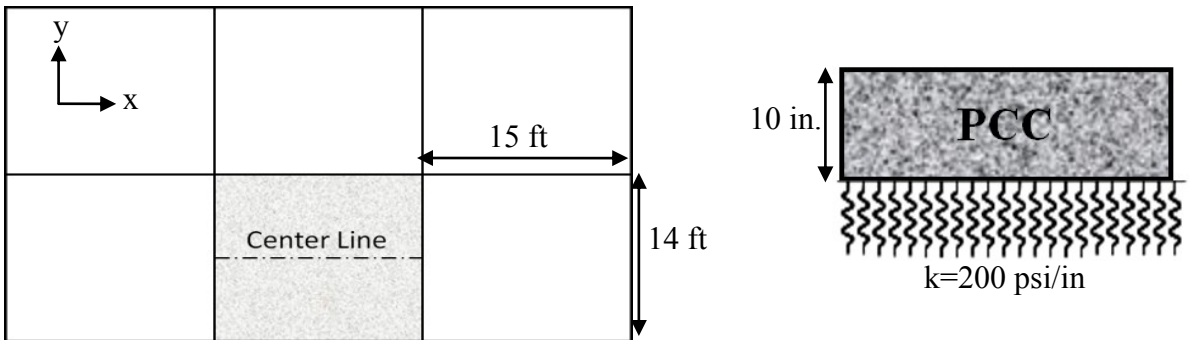

Figure 7.1: Pavement structure and selected slab in the cases studied.

The temperature profile through the thickness of the PCC slab is expressed as a cubic function (Eq. 7-1) that can be fitted by considering the temperature at four different points through the depth. This order of polynomial was selected because it is common for temperature to be measured at four points across the thickness of slabs at pavement test sites (Yu et *al*., 1998). Assuming the origin at the mid-plane of the slab, the temperature gradient is defined as:

$$\Delta T = a_0 + a_1 z + a_2 z^2 + a_3 z^3 \tag{7-1}$$

The constant term a_0 produces expansion and contraction within the PCC slabs. The linear term a_1 produces pure bending in the PCC slab, due to the temperature difference between its top and bottom. The higher-order terms (a_2 and a_3) of temperature profile in Eq. 7-1 produce internal stresses in the PCC slab regardless of its external constraints (Ioannides and Khazanovich, 1998).

The effect of nonlinear temperature profiles was studied by evaluating the stresses and displacements along a longitudinal section that passes through the center of the middle slab, as shown in Figure 7.1 (center line). Two sets of temperature gradients (TG), corresponding to night-time (or negative TG) and day-time (or positive TG), were selected (Figure 7.2 and 7.3). N0 and P0 in those sets represent a linear thermal gradient that the mid-plane of the slabs has zero change in temperature and the difference between temperature at the top and bottom of the slab is -15°F and 15°F, respectively. In the both night-time and day-time state, changing the temperature gradient from N1 to N4 or from P1 to P4 demonstrates the level of deviation from the linear temperature profile. In the night-time state from N1 to N4, the temperatures at the top and bottom of slabs were maintained at 45°F and 60°F, respectively,

while the set temperature was 70°F. This means that thermal contraction occurred throughout the depth of the PCC slab while the decrease in temperature at the top was greater than that at the bottom of the slab. Also, in the day-time state from P1 to P4, the temperatures at the top and bottom of slabs were maintained at 95°F and 80°F, respectively, while the set temperature was 70°F. This is an indication of thermal expansion throughout the depth of the PCC slab while the increase in temperature at the top was greater than that at the bottom of the slab. The coefficients a_i (Eq. 7-1) for all the case studies are shown in Table 7.1 and 7.2.

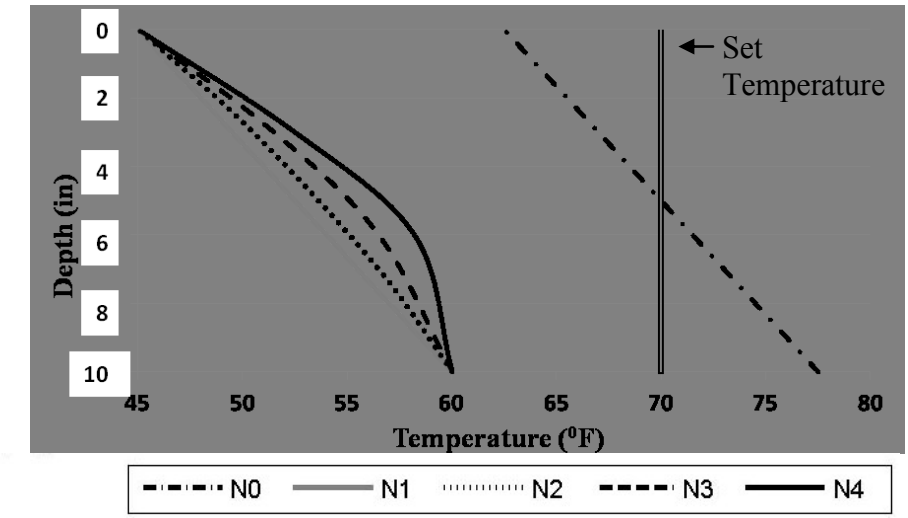

Figure 7.2: Temperature-change profile for the five negative temperature gradients.

Table 7.1: Coefficients of negative temperature-variation profiles.

Case	a_0	a_1	a_2	a_3
N0	0.0	-1.5	0.0	0.0
N1	-17.5	-1.5	0.0	0.0
N2	-16.3	-1.5	-0.0476	0.0
N3	-15.0	-1.572	-0.1008	0.003
N4	-13.5	-1.821	-0.175	0.010

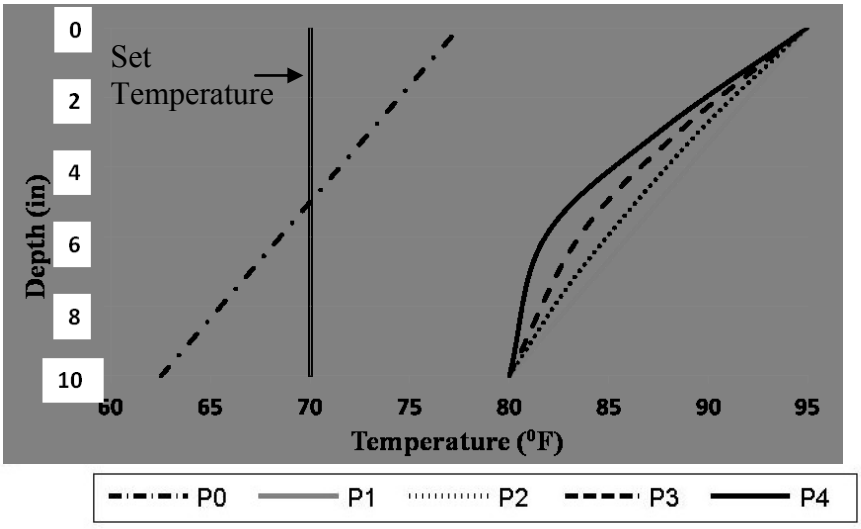

Figure7.3: Temperature-change profile for the five positive temperature gradients.

Table 7.2: Coefficients for positive temperature-variation profiles.

Case	a_0	a_1	a_2	a_3
P0	0.0	1.5	0.0	0.0
P1	17.5	1.5	0.0	0.0
P2	16.3	1.5	0.0476	0.0
P3	15.0	1.572	0.1008	-0.003
P4	13.5	1.821	0.175	-0.010

Figure 7.4 shows the bending stresses in the longitudinal direction (σ_{xx}) at the top and bottom of the PCC slab along the centerline, as described above, due to the negative TG. With a linear temperature profile (N1), the stresses at the top and bottom of the slab are fairly equal in magnitude (top in tension and bottom in compression). The small difference between stresses at the top and bottom of the PCC slab in this case is due to the effect of friction between the PCC slab and the foundation. As the temperature profile becomes more nonlinear (form N1 to N4), the stresses both at the top and bottom shift in the positive (tensile) value about 100 psi and 60 psi, respectively. These results indicate that even though in all four cases the temperature-change at the top and bottom of the slabs are the same, the

nonlinear thermal terms produce significant additional stresses. This translates into internal stresses in the PCC slabs due to nonlinear temperature gradient.

In the cases of N1 to N4, the uniform negative temperature change (a_0) produces additional stresses in the PCC slabs because of the presence of friction. When the PCC slabs contract, the frictional resistance of the foundation layer produces a uniform tensile traction on the PCC slabs. In this case, the moments induced by the frictional resistance reduces the tensile stresses at the top and compressive stresses at the bottom of the PCC slabs. In case N0, the horizontal displacement at the mid-depth of slabs is zero; however, the horizontal displacements at the bottom surface of PCC slabs, as a consequence of curling, can produce frictional tractions. As the bottom surface of the slabs expand, the compressive frictional tractions produce an additional positive moment in the PCC slabs, which can increase the compressive stress at the bottom and tensile stress at the top of the PCC slabs (Figure 7.4). It is worth mentioning that if there was no friction assumed between the PCC slabs and foundation, the stresses in both case N0 and case N1 would be identical.

The bending stresses for the positive TG are shown is Figure 7.5. In this state, as the temperature profile becomes more nonlinear (form P1 to P4), the stresses both at the top and bottom shift in the negative (compressive) value about 100 psi and 50 psi, respectively. In those cases, the frictional resistance of the foundation layer produces a uniform compressive traction on the PCC slabs and the moments induced by the frictional resistance reduces the tensile stresses at the bottom and compressive stresses at the top of the PCC slabs. In the case P0, the bottom surface of the slabs contract, thus the tensile frictional tractions produce an additional negative moment in the PCC slabs, which can increase the compressive stress at the top and tensile stress at the bottom of the PCC slabs.

Figure 7.6 and 7.7 show the longitudinal displacement at the mid-plane of the PCC slab. As expected, longitudinal contraction occurs in the negative TG cases (N1 to N4) and longitudinal expansion occurs in the positive TG cases (P1 to P4), as a consequence of changes in temperature in each case from the set temperature. However, for all the temperature profiles, as the nonlinearity increases the average temperature-change decreases, leading to a decrease in the thermal contraction or expansion of the slab mid-plane. It is important to note that a general conclusion cannot be drawn about

the thermal contraction or expansion pattern since it greatly depends on the shape of the temperature profile. In the cases N0 and P0, the longitudinal displacements at the mid-plane of PCC slab are zero since there is no temperature change at that point.

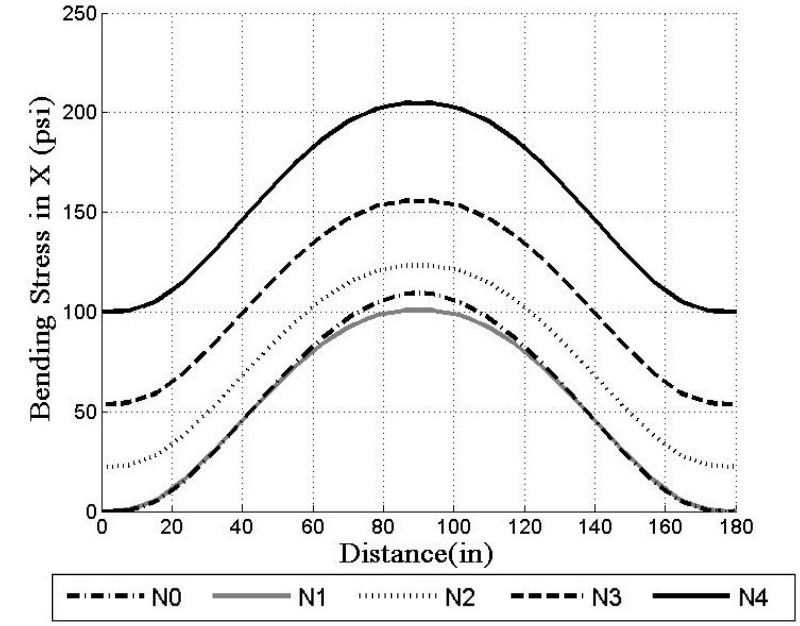

a) Top of PCC slab

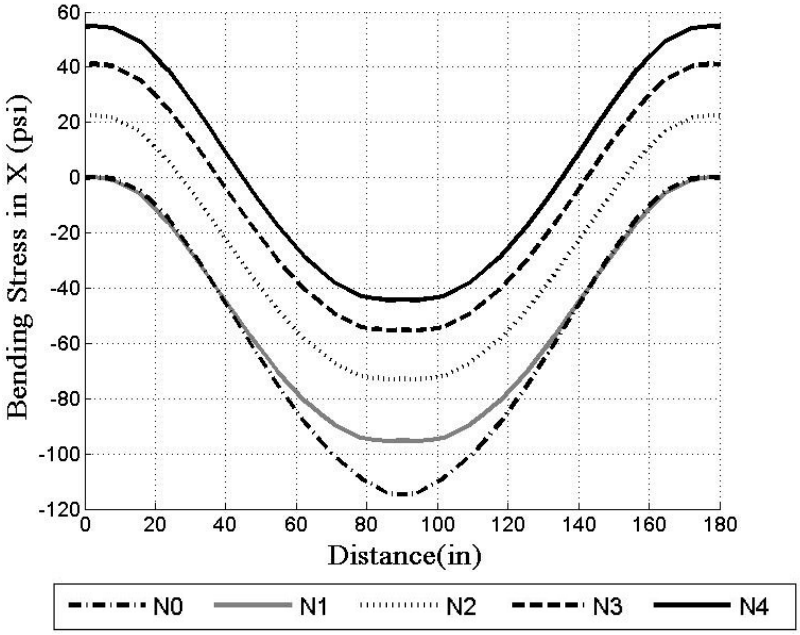

a) Bottom of PCC slab

Figure 7.4: Longitudinal bending stress (σ_{xx}) at the top and bottom of the selected PCC slab through the center line for various negative temperature gradients.

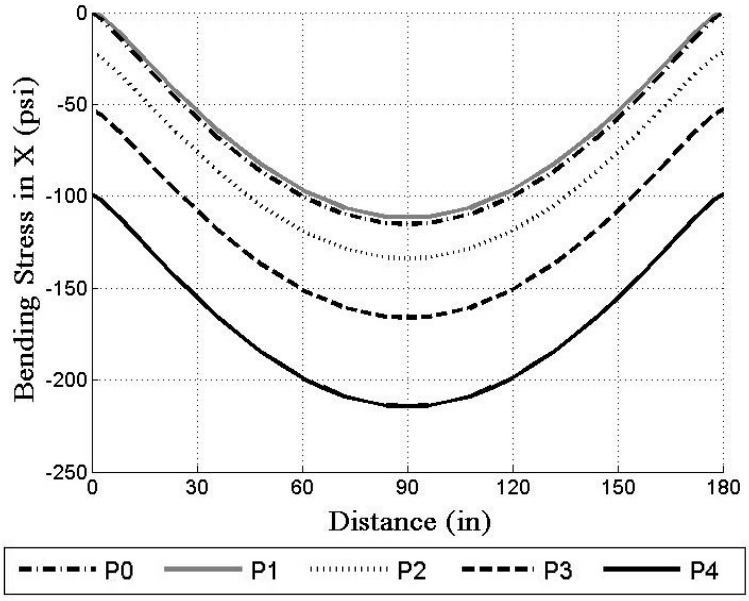

a) Top of PCC slab

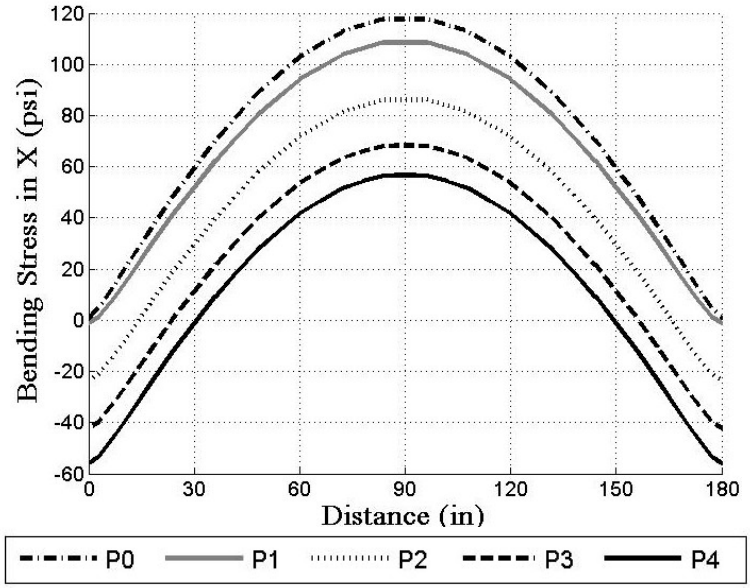

b) Bottom of PCC slab

Figure 7.5: Longitudinal bending stress (σ_{xx}) at the top and bottom of the selected PCC slab through the Center line for various positive temperature gradients.

(Note: Tension is positive and Compression is negative)

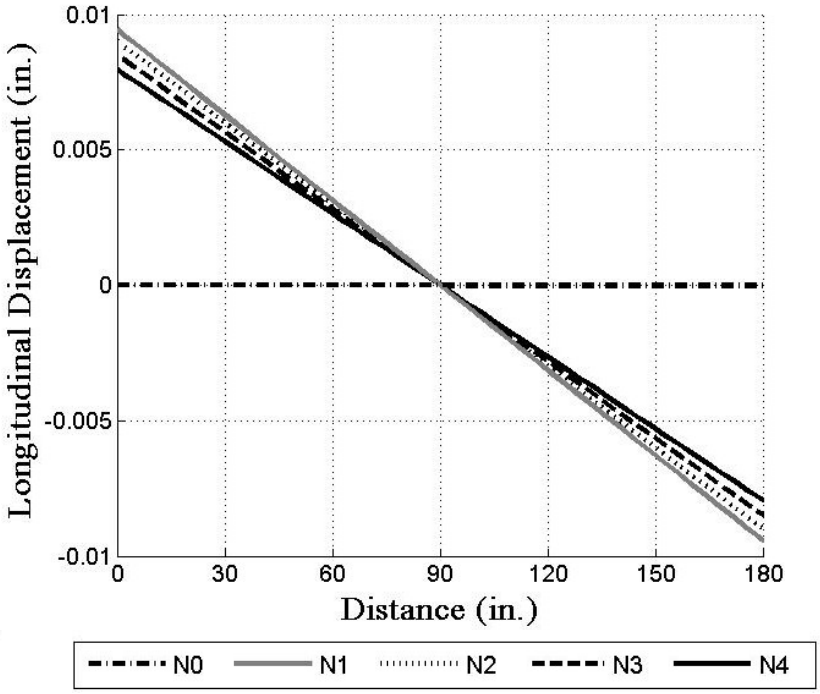

Figure 7.6: Longitudinal displacement of mid-depth of the PCC slab due to negative temperature gradients.

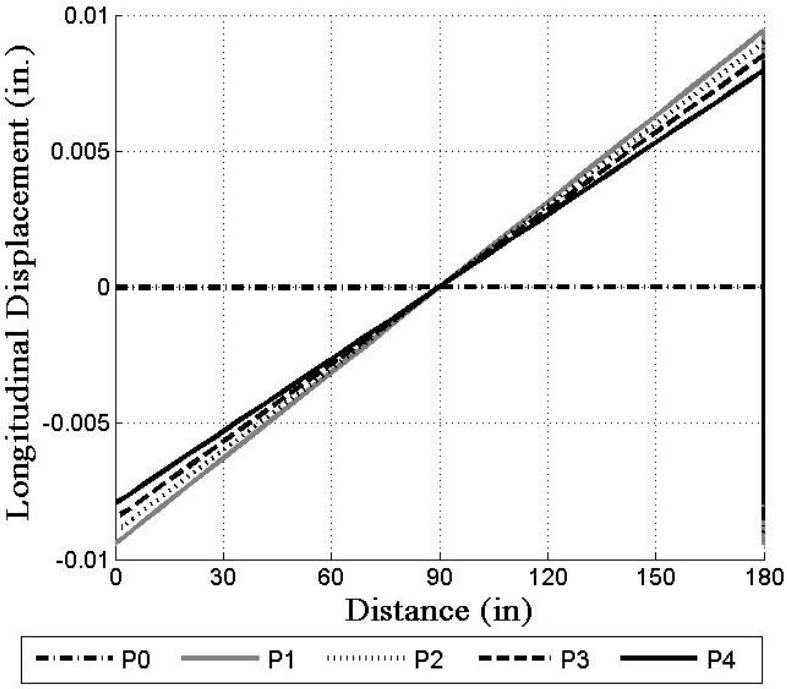

Figure7.7: Longitudinal displacement of mid-depth of the PCC slab due to positive temperature gradients.

To investigate the impact of nonlinearity in temperature gradient, the vertical deflection of the PCC slab was also estimated for different temperature gradients and different contact condition, as shown in Figures 7.8 to 7.11. Due to all the negative temperature gradients, the PCC slab curled upwards while the maximum deflection was higher in the most nonlinear TG case (N4). This is because N4 has the greatest linear term (a_1) that contributes to producing thermal moment. Even though the temperature gradients N0 to N3 have different quadratic terms (a_2 and a_3), the vertical deflections that they produce are slightly different (less than 8%). This is the expected behavior since the thermal moment produced by a quadratic thermal gradient profile is zero. The small difference between the deflections in those temperature gradients is due to the effect of friction at slab-foundation interface. Different constant terms (a_0) in those temperature gradients result in different frictional moments, which in turn produce different curling in the PCC slab. The results for the frictionless case, shown in figure 7.9, demonstrate similar PCC slab vertical deflection for the temperature gradients N0 to N3.

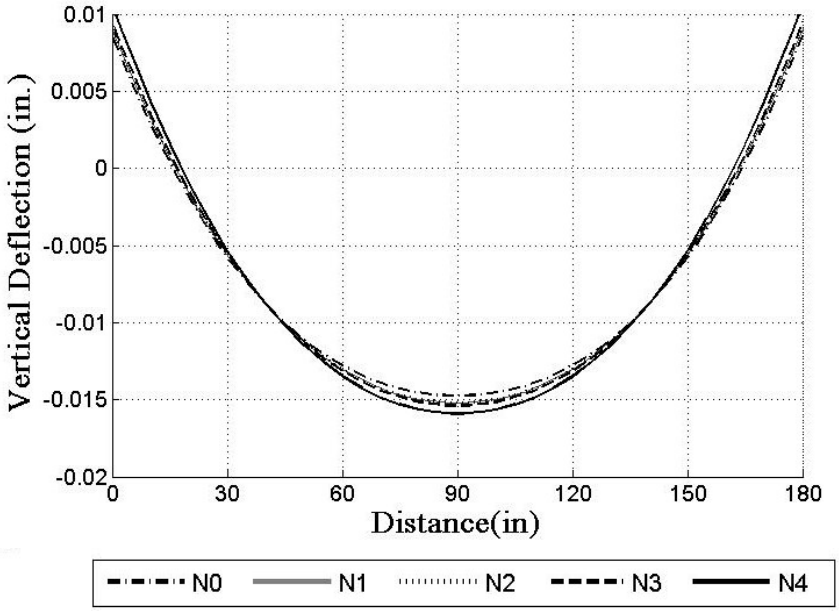

Figure 7.8: Vertical deflection of the PCC slab due to negative temperature gradients.

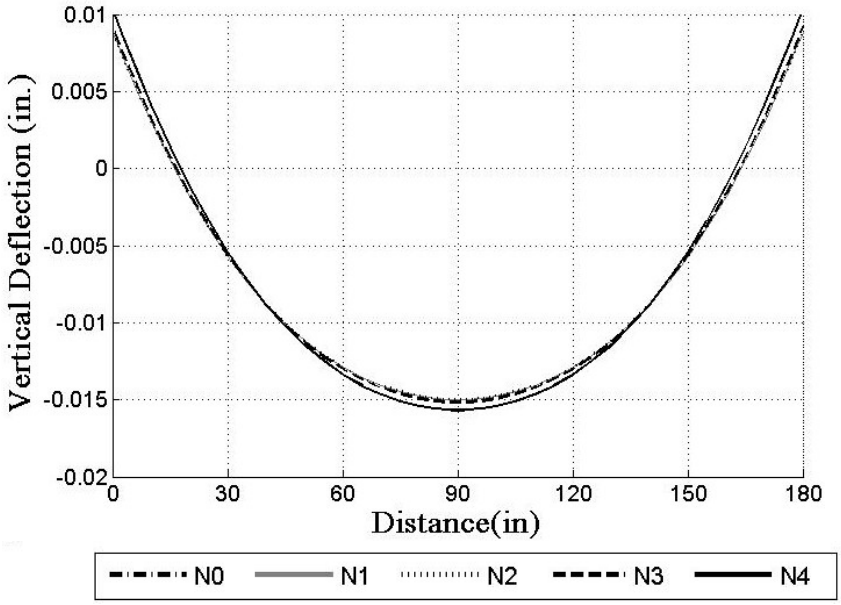

Figure 7.9: Vertical deflection of the PCC slab due to negative temperature gradients (No friction).

Figure 7.10 shows the downward curling of the PCC slab due to the positive temperature gradients. A similar trend from the negative gradient P4 produces the greatest uplifting in the center of PCC slab, because of its higher temperature profile term a_1. In the frictionless case, the similar uplifting for the cases P0 to P2 can be observed (Figure 7.11).

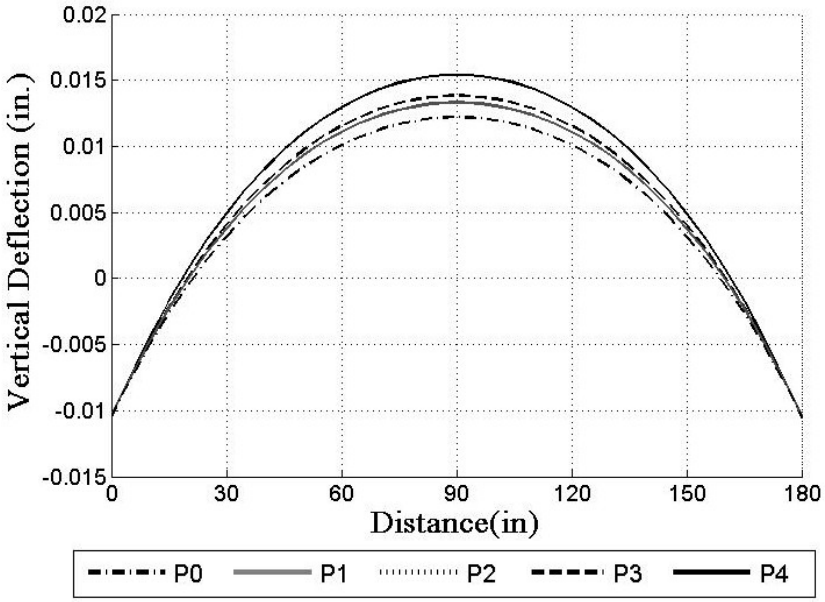

Figure 7.10: Vertical deflection of the PCC slab due to positive temperature gradients.

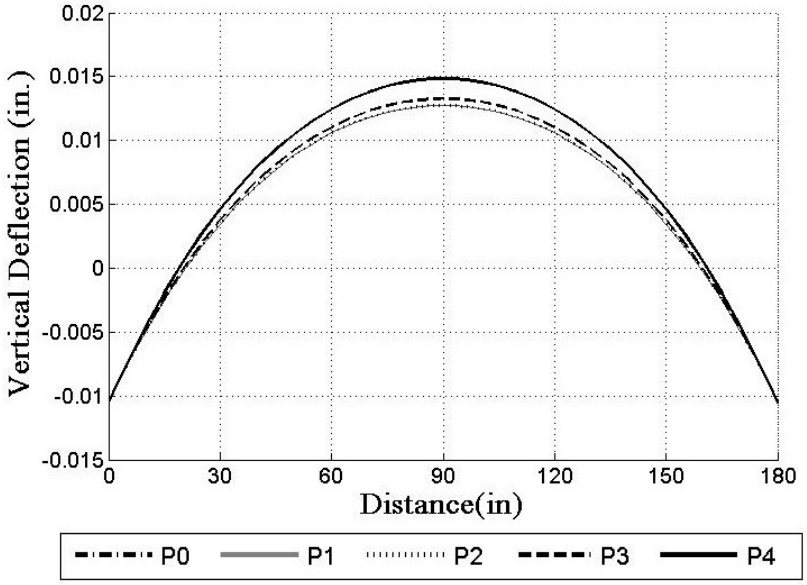

Figure 7.11: Vertical deflection of the PCC slab due to positive temperature gradients (No friction).

7.2 Effect of Slab-Foundation Friction on Responses of JPCP

In JPCP, the contact conditions along the slab-foundation interface significantly impact the mechanical behavior of pavements. Temperature induced curling significantly impacts slab-foundation contact conditions, while interface friction further complicates JPCP analysis—because it introduces some nonlinearity to the problem. The process of modeling frictional contact in the finite element analysis of jointed concrete pavements in NYSLAB was described in chapter 5.

To demonstrate the effect of slab-foundation contact friction on PCC slab stresses and deformations, a series of simulations were performed using the pavement structure described in Figure 7.1. The pavement was subjected to negative and positive temperature gradients (shown in figures 7.2 and 7.3. Interface elements were used to model the frictional contact between the PCC slabs and foundation. The penalty parameters, k_1 and k_2, used in the interface constitutive equation in the normal direction, are selected as 10^{-9} times the minimum of the diagonal of the global stiffness matrix, and 10^3 times the maximum of the diagonal of the global stiffness matrix, respectively. The penalty parameters, k_3 and k_4, used in the interface constitutive equation in the tangential direction, are assumed to be equal to k_2 and k_1, respectively. The coefficient of friction was varied between zero for the case with no

friction to 3. Numerical results of the effect of friction in the slab/foundation interface on PCC slab responses, due to various temperature gradients, are described in the following sections.

Linear Negative Thermal Gradient with Mid-Plane Contraction

Case N1 includes a uniform temperature change of -10°F that tends to produce a contraction of the mid-plane of the PCC slabs and, in fact, causes the entire cross section of the slabs to contract. The longitudinal bending stresses are compared with the frictionless case in Figure 7.12. As expected, the linear temperature profile in Case N1 produces tensile stresses at the top and compressive stresses at the bottom of the PCC slabs. However, the uniform negative temperature change produces additional stresses in the PCC slabs because of the presence of friction. When the PCC slabs contract, the frictional resistance of the foundation layer produces a uniform tensile traction on the PCC slabs. In this case, the moments induced by the frictional resistance reduces the tensile stresses at the top and compressive stresses at the bottom of the PCC slabs. As is apparent in Figure 7.12, increasing the coefficient of friction caused a decrease in the magnitude of the longitudinal stresses, especially in the central area of each slab, by as much as 47% for a coefficient of frictions of 3. This is occurs because, due to the negative temperature gradient curling, only the central areas of slabs maintain contact with the foundation while the areas close to the edges lose their contact and thus the frictional resistance has no impact on those areas. It is important to note that the effects of these frictional tractions are larger at the bottom of the slabs because of their constraining effect and lead to a non-symmetric longitudinal bending stress profile about the mid-plane of the slabs.

Figure 7.13 shows the effect of the frictional tractions on the vertical deflection of PCC slabs. By increasing the coefficient of friction from zero to 3, the vertical deflection increases about 20%, because of the resulting negative moment produced by the frictional tractions at the bottom of the PCC slabs.

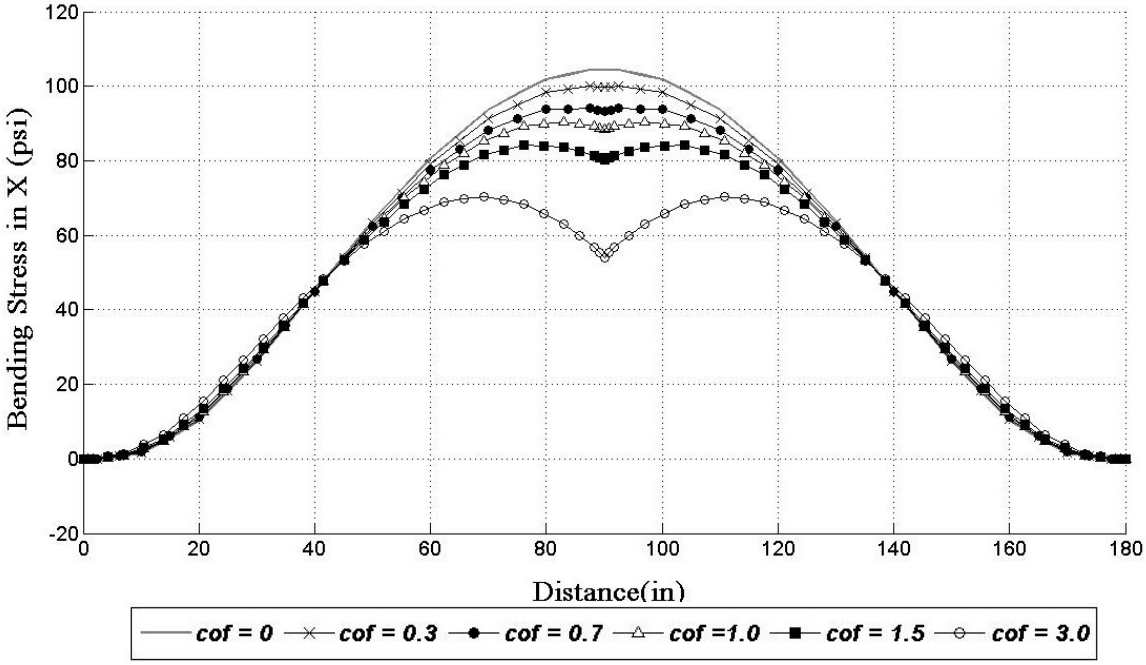

a) Top of PCC slab

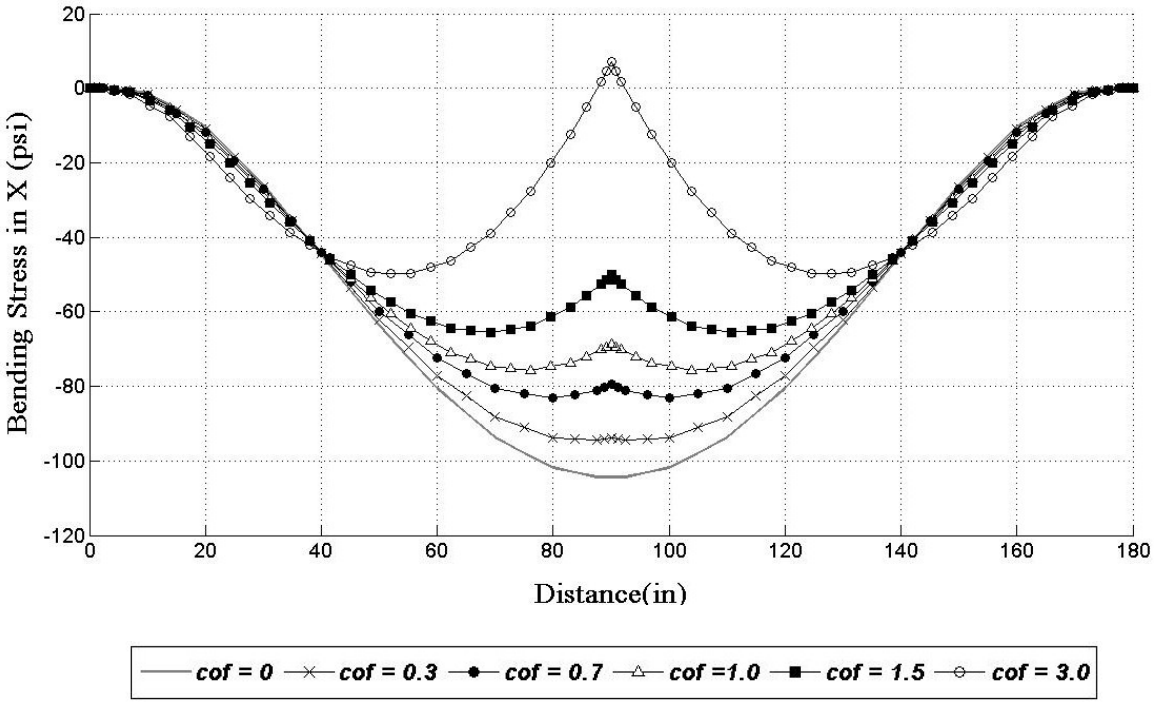

b) Top of PCC slab

Figure 7.12: Bending stress at the top and bottom of PCC slab in longitudinal direction (σxx) through the center line for different coefficients of friction due to temperature gradient N1.

(NOTE: Tension is positive and Compression is negative)

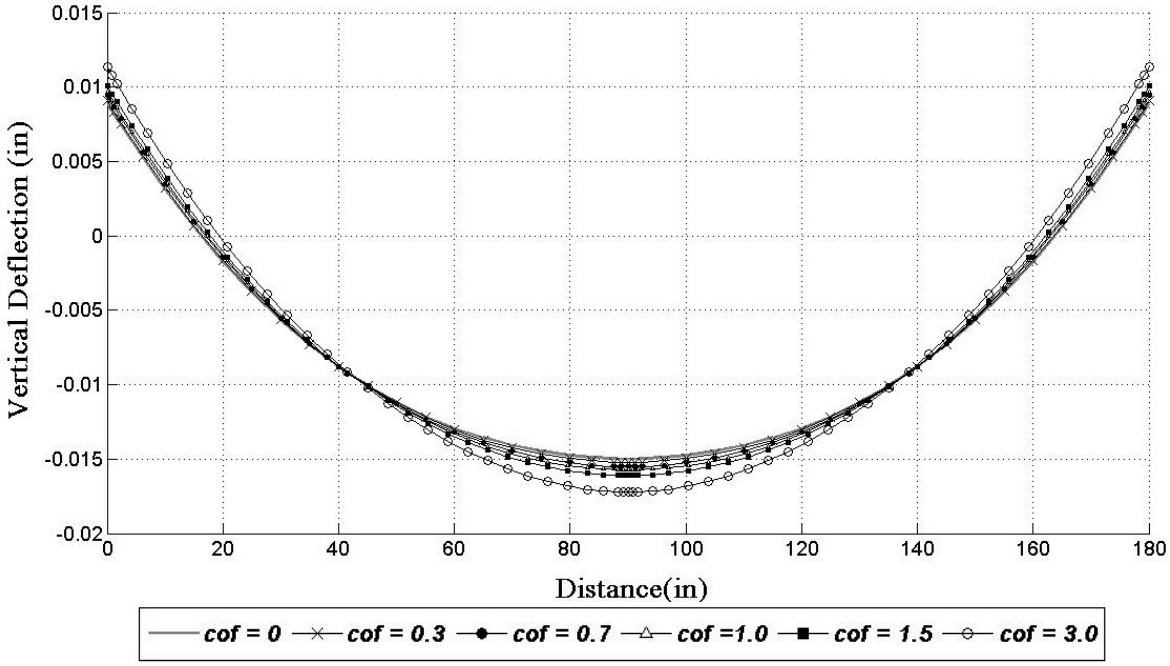

Figure 7.13: Vertical deflections of PCC slab through center line for different coefficients of friction due to linear temperature gradient N1.

Nonlinear Negative Thermal Gradient with Mid-Plane Contraction

In the nonlinear negative temperature gradient N4, the temperature-change at the mid-plane of PCC slab differs from that of the linear temperature gradient N1. However, the temperature-change at the bottom of slab (where the slab is in contact with the foundation) is the same in both the linear and nonlinear temperature gradients. Similar external restrains, due to friction at the slab-foundation interface in case N4, will result in the same frictional tractions as case N1. Therefore, tensile stress at the top and compressive stress at the bottom of the PCC slabs, in the case of nonlinear temperature gradient N4, decrease with the same rate as the stresses decrease due to the linear temperature gradient N1, when the coefficient of friction increases (Figure 7.14).

The impact of friction on vertical deflection is also shown in Figure 7.15. Increasing the coefficient of friction from 0 to 3, results in greater vertical deflection in the PCC slab.

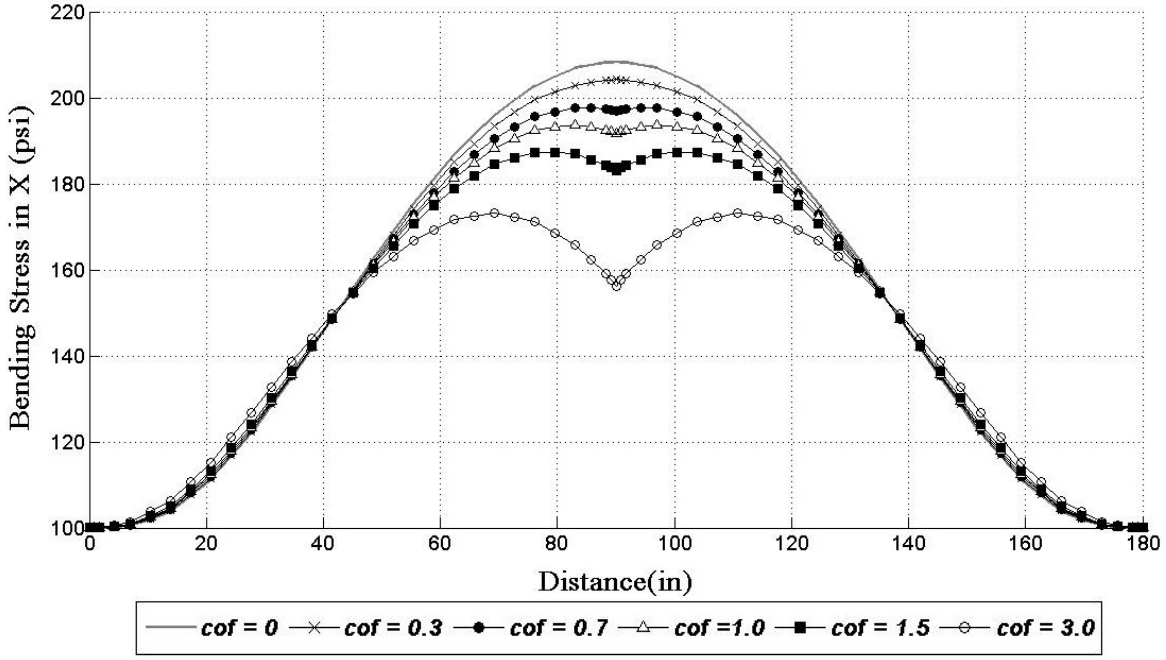

a) Top of PCC slab

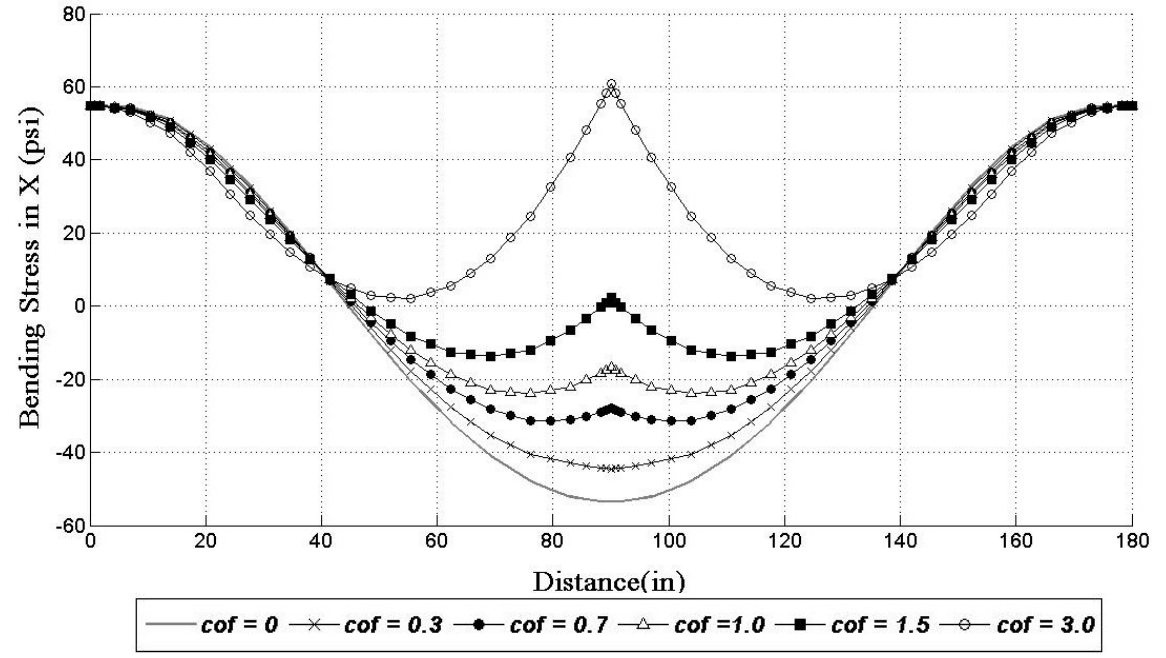

b) Top of PCC slab

Figure 7.14: Bending stress at the top and bottom of PCC slab in longitudinal direction (σ_{xx}) through the center line for different coefficients of friction due to nonlinear temperature gradient N4.

(NOTE: Tension is positive and Compression is negative)

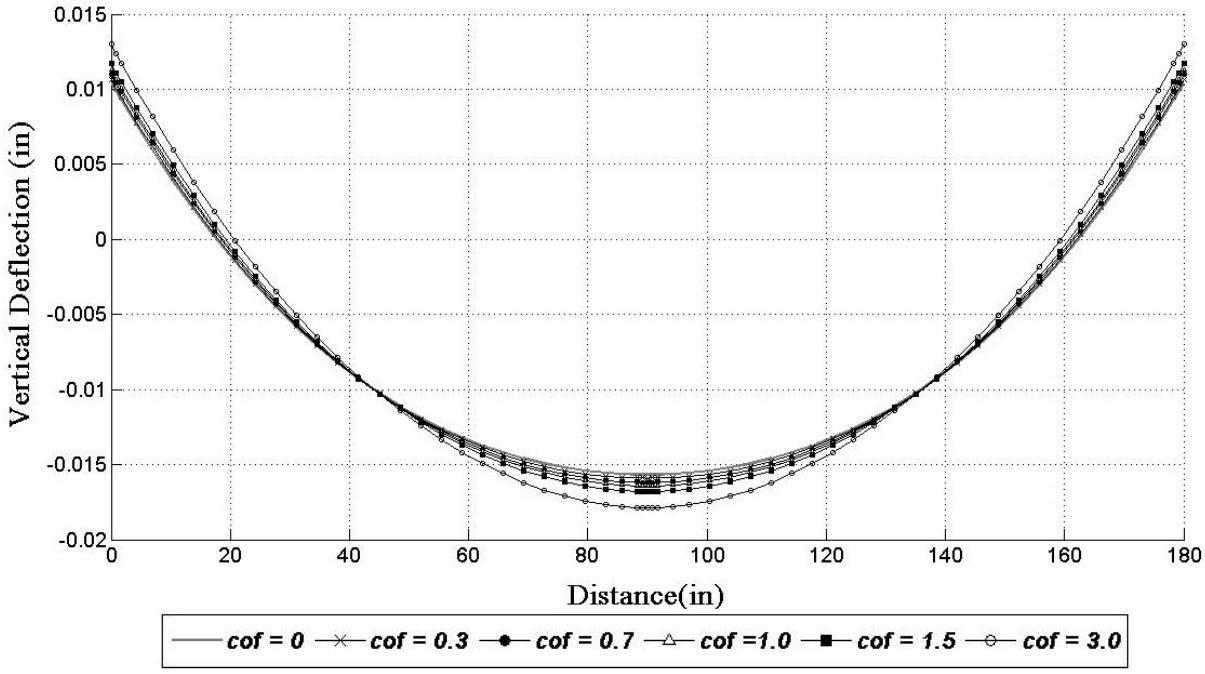

Figure 7.15: Vertical deflections of PCC slab through center line for different coefficients of friction due to nonlinear temperature gradient N4.

Linear Negative Thermal Gradient without Mid-Plane Contraction

In this case study the effect of friction between PCC slabs and foundation was examined when the linear thermal gradient is such that the mid-plane of the slabs has zero change in temperature. The negative temperature gradient N0 causes the bottom of the slabs to expand. Therefore, although the horizontal displacements at the mid-depth of slabs are zero, the horizontal displacements at the bottom surface of PCC slabs can produce frictional tractions. Figure 7.16 shows the longitudinal stress at the top and bottom of PCC slab for different coefficients of friction. As expected, a negative temperature gradient produces tensile stresses at the top and compressive stress at the bottom of PCC slabs. As the bottom surface of slabs expand, the compressive frictional tractions produce an additional positive moment in the PCC slabs. By increasing the coefficient of friction and consequently the frictional tractions, the additional moment produces additional tensile (50%) and compressive stresses (100%) at the top and the bottom of PCC slab for a coefficient of friction of 3. These results are the opposite of those obtained in the case study (case due to N1) described before—where the top and bottom stresses actually decreased in magnitude. This is due to the fact that, while both case studies imposed a negative thermal gradient, in

the first case study the bottom of the slabs is contracting while in the present case it is expanding. This translates into frictional tractions that actually have opposite senses and thus lead to opposing effects on the longitudinal bending stresses.

Moreover, the vertical deflection in this case decreases as the coefficient of friction increases (see Figure 7.17). This is because the moments caused by the frictional tractions reduce the curling effect of the negative thermal gradient and consequently decrease the vertical deflections.

Linear Positive Thermal Gradient with Mid-Plane Expansion

Temperature gradient P1 includes a uniform temperature change of 10°F that causes the entire cross section of the slabs to expand. A positive temperature gradient is expected to produce compressive stress at the top and tensile stress at the bottom of the PCC slab (Figure 7.18). When the concrete slab expands, uniform compressive stresses are produced on the slab due to the frictional resistance of the foundation layer. In this case, the moment induced by the frictional resistance slightly reduces the compressive stress at the top and produces additional compressive stress at the bottom of PCC slab. By increasing the coefficient of friction from 0 to 3, the compressive stress at the top of slab increases about 20% and the tensile stress at the bottom of slab decreases about 45%. In the case of positive temperature gradient, the frictional resistance of the foundation causes the slab to lose its contact in a wide area in the center of the slab from the foundation. In this case the effect of frictional tractions are larger at the bottom of the slabs as well because of their constraining effect which leads to a non-symmetric longitudinal bending stress profile about the mid-plane of the slabs.

Figure 7.19 shows the effect of friction on the vertical deflection of PCC slabs. The frictional resistance of the foundation helps the slab lift up from the foundation in a wide area in the center of the slab. By increasing the coefficient of friction, the vertical deflection increases slightly because of the resulting positive moment produced by the frictional tractions at the bottom of the PCC slabs.

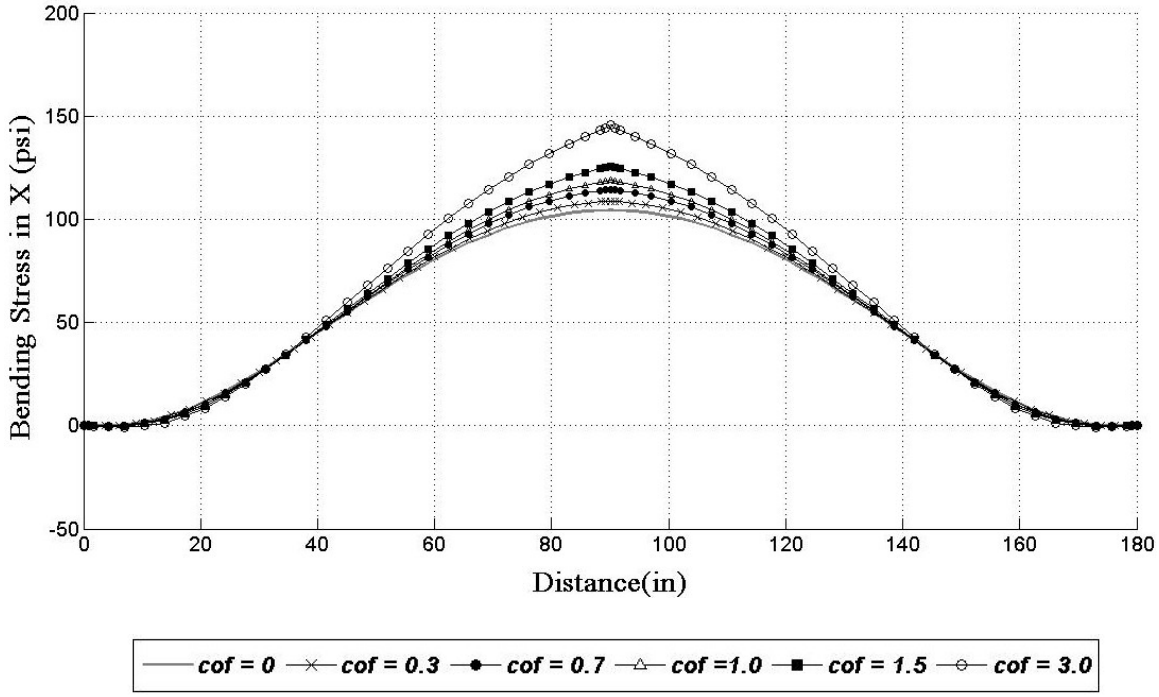

a) Top of PCC slab

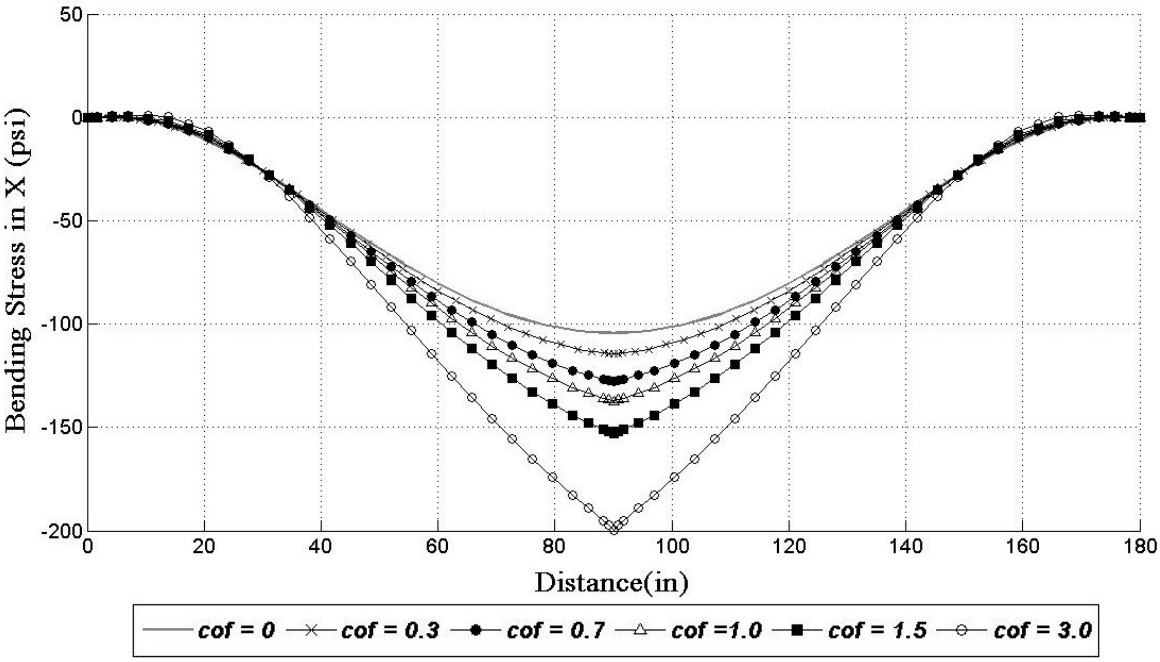

b) Bottom of PCC slab

Figure 7.16: Bending stress at the top and bottom of PCC slabs in longitudinal direction (σ_{xx}) through center line for different coefficients of friction due to temperature gradient N0.

(NOTE: Tension is positive and Compression is negative)

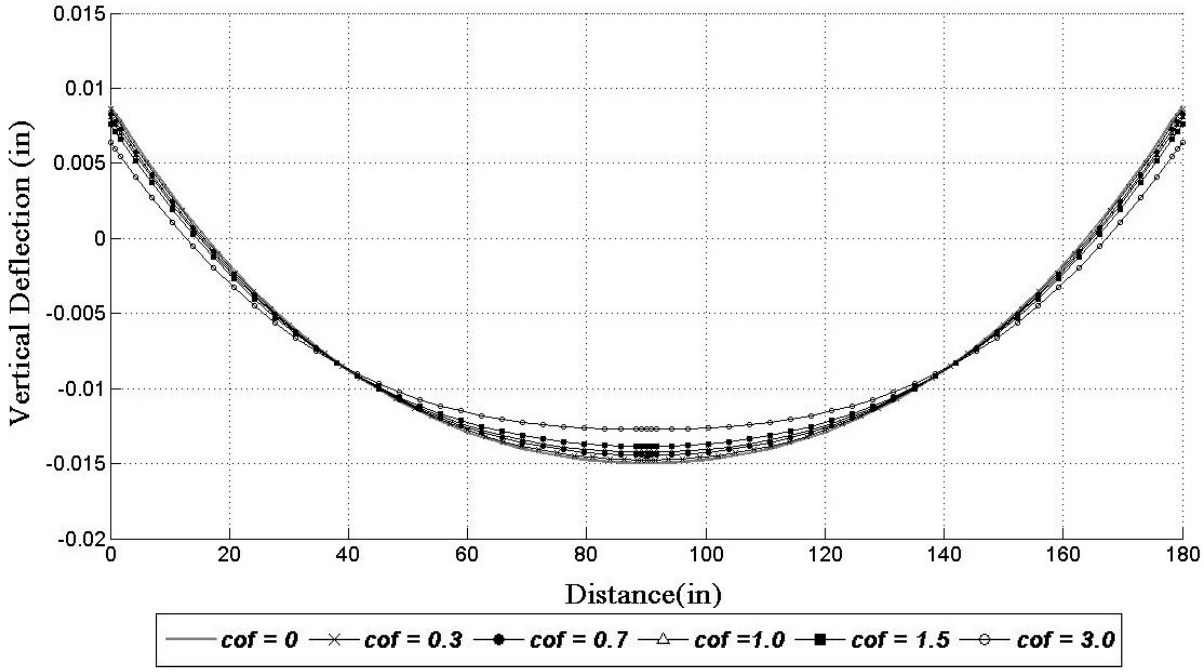

Figure 7.17: Vertical deflections of PCC slab through center line for different coefficients of friction due to temperature gradient N0.

Linear Positive Thermal Gradient without Mid-Plane Expansion

In this case study the effect of friction between PCC slabs and foundation was examined when the positive linear thermal gradient is such that the mid-plane of the slabs has zero change in temperature. The positive temperature gradient P0 causes the bottom of slabs to contract and lose contact in their center area. Figure 7.20 shows the longitudinal stress at the top and bottom of PCC slabs for different coefficients of friction. As expected, a positive temperature gradient produces compressive stresses at the top and tensile stresses at the bottom of PCC slabs. As the bottom surface of slab contract, the tensile frictional tractions produce an additional negative moment in the PCC slabs. By increasing the coefficient of friction and consequently the frictional tractions, the additional moment produces additional compressive (20%) and tensile stresses (45%) at the top and the bottom of PCC slab for a coefficient of friction of 3.

Figure 7.21 shows the changes in PCC slab vertical deflection with the variation of coefficient of friction. Increasing the friction in this case will result in smaller uplifting in the slab center.

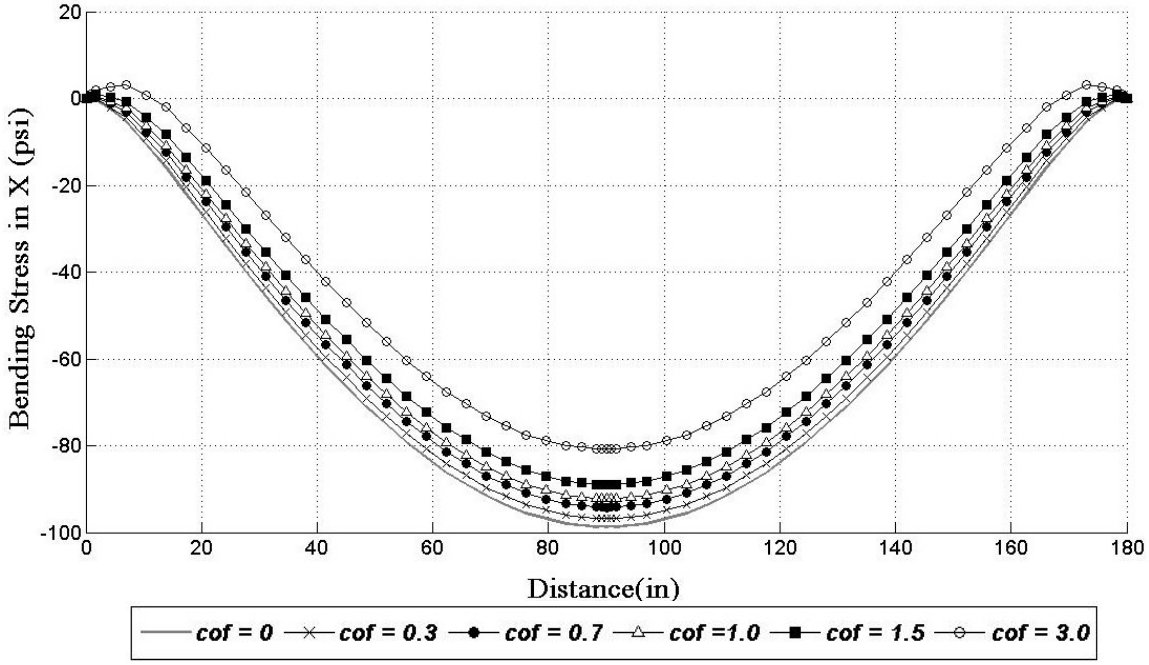

a) Top of PCC slab

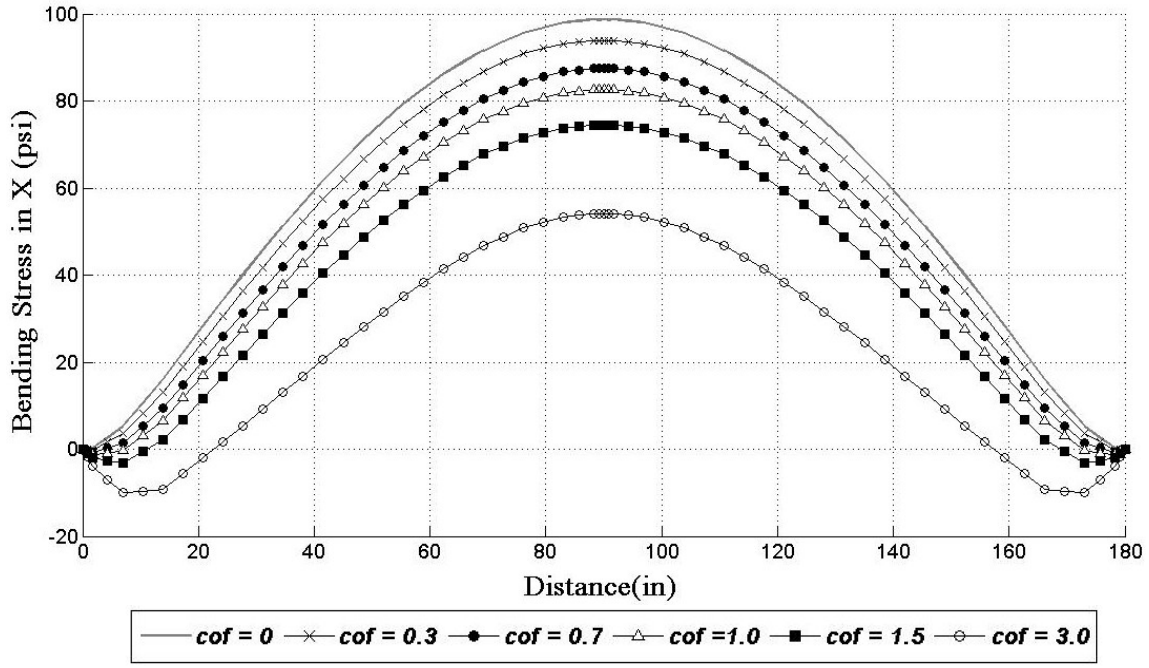

b) Bottom of PCC slab

Figure 7.18 Bending stress at the top and bottom of PCC slab in longitudinal direction (σ_{xx}) through the center line for different coefficients of friction due to temperature gradient P1.

(NOTE: Tension is positive and Compression is negative)

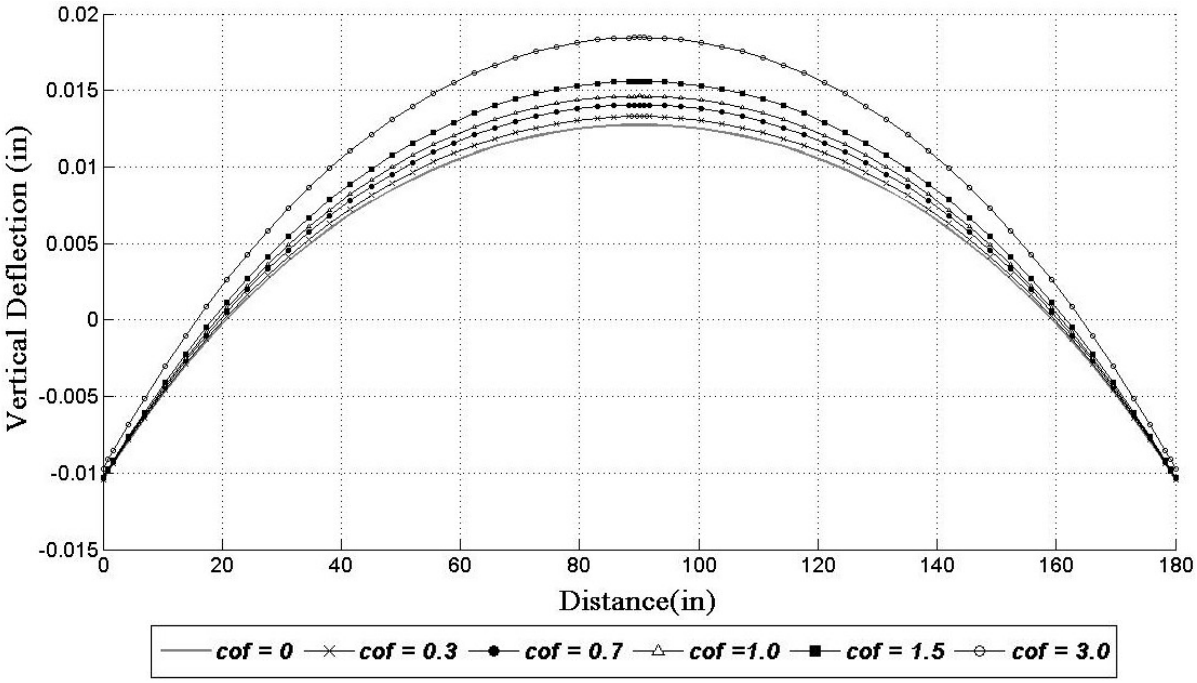

Figure 7.19 Vertical deflections of PCC slab through center line for different coefficients of friction due to temperature gradient P1.

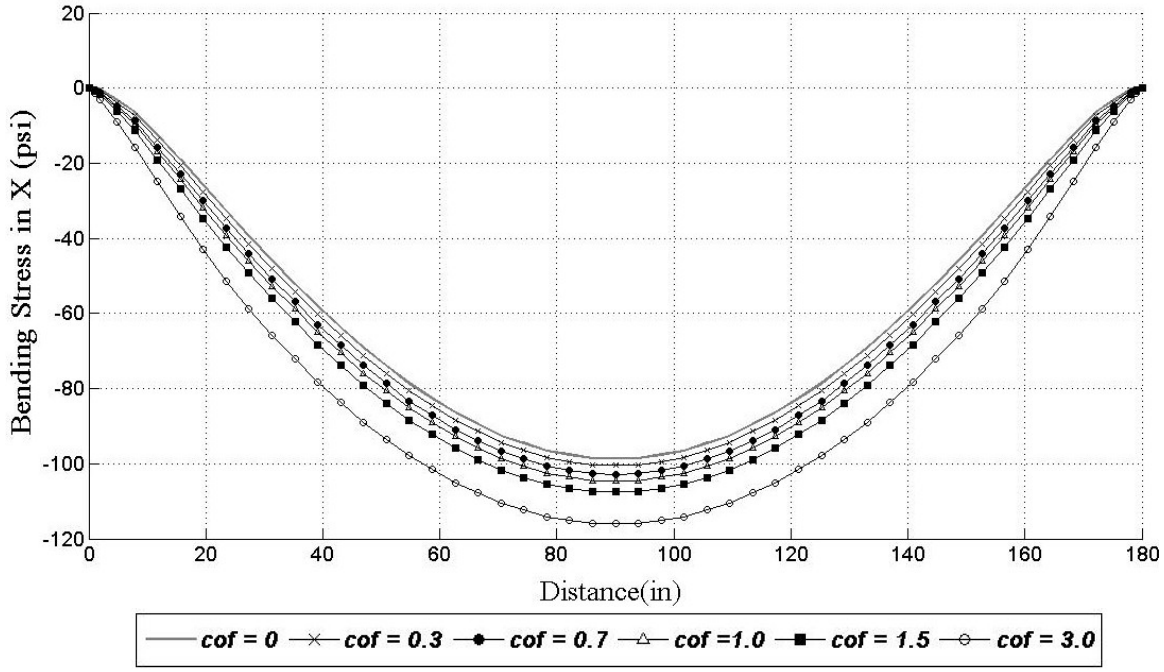

a) Top of PCC slab

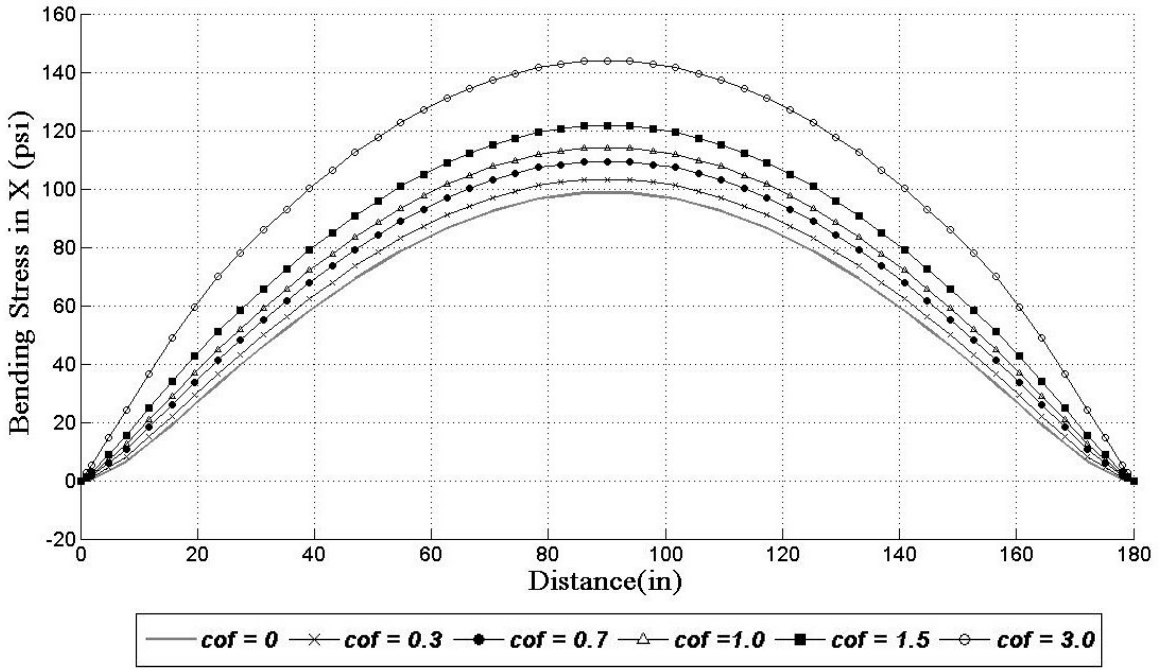

b) Bottom of PCC slab

Figure 7.20 Bending stress at the top and bottom of PCC slab in longitudinal direction (σ_{xx}) through the center line for different coefficients of friction due to temperature gradient P0.

(NOTE: Tension is positive and Compression is negative)

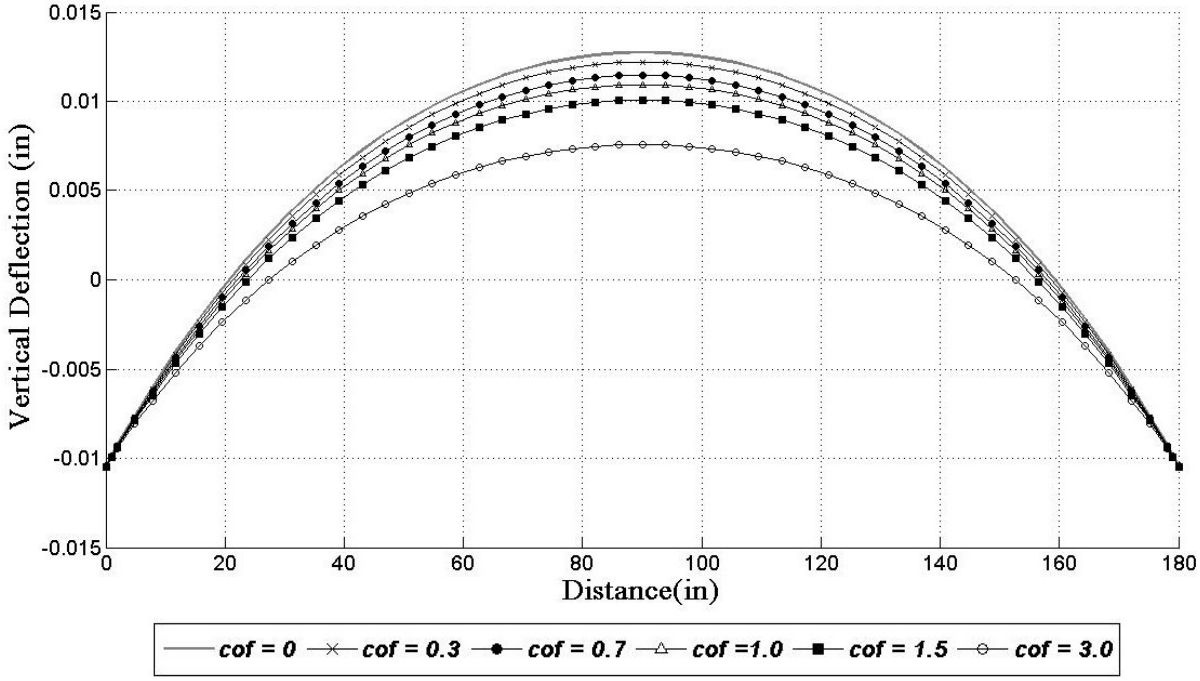

Figure 7.21 Vertical deflections of PCC slab through center line for different coefficients of friction due to temperature gradient P0.

7.3 Impact of Different Approaches to Modeling Rigid Pavement Base Layer on Slab Curling Stresses

The magnitude of stresses induced in jointed concrete slabs due to thermal loads is influenced by the stiffness of underlying foundation layers (base, subbase and subgrade). The layer that most significantly affects the PCC slab responses is the base. Field observations have demonstrated the increases in reflecting cracking of PCC slabs placed over relatively stiff base layers (Darter et *al*., 1995; Hall et al., 2005; Gary, 2009; Lederle et *al*., 2001). To predict thermo-mechanical responses of jointed PCC slabs accurately, appropriate idealization of foundation layers in finite element analysis is required. Several modeling methods have been proposed to idealize the effect of the base layer. These methods differ on the structural contribution assigned to the base layer in the pavement concrete system. Three approaches for modeling the base layer in finite element analysis of jointed concrete pavements are presented in this chapter. The first approach involves modeling the base as a plate, separate from the other foundation layer(s). In the second and third approach, the base layer is modeled as part of a Winkler or Vlasov foundation, respectively. A series of parametric studies are carried out to evaluate the

capability and feasibility of each modeling approach proposed in this study in reflecting the effect of the base course rigidity on the PCC slab responses under thermal and vehicular loads.

7.3.1 Modeling of the Foundation System in Different Design Guide

In a rigid pavement system, the PCC slab layer is the most important structural element that provides major bearing capacity against the applied loads. The foundation layers (base, sub-base and subgrade) that provide support to the PCC slab can also significantly impact the performance of the pavement. The magnitude of stress and deformation responses induced by traffic and environmental loads in the PCC slab is controlled by the stiffness of the underlying foundation. Two-dimensional FE based rigid pavements analysis tools such as ILLI-SLAB, JSLAB, ILSL2, and ISLAB are on the basis of a medium-thick plate placed over an elastic foundation (e.g, Winkler, Vlasov, and solid elastic).

An important concern in using the Winkler foundation model is the determination of the magnitude of the modulus of subgrade reaction or k-value. The methods for determining the value of k (e.g. correlation methods, backcalculation methods, and plate testing methods) and their accuracy have been reported in chapter 2 and 4. The 1986 and 1993 AASHTO pavement design guide recommended the concept of composite k-value, which includes all the foundation layers under the PCC slab in the estimation of *k* (Darter et *al*., 1995). This concept is called "top-of-the-base" k-value. In this approach, the effect of the base layer in the analysis of concrete pavements resulted in an increased/decreased composite k-value. In a similar approach, the Portland Cement Association used the results of plate load tests on top of the base layer to estimate the composite k-value (Hall et *al.*, 2005). Darter et *al*. (1995) concluded that the actual performance of a base layer depends more on its bending stiffness rather than its compressibility that was reflected in the calculation of composite k-value. They indicated that the composite k-value was unrealistic and was not able to reflect the effects of the base layers on the PCC slab responses. The Federal Aviation Administration (FAA) design guide incorporated the effect of stabilized base layers in thickness design for airport pavements to accommodate heavy aircrafts (Gary, 2009). In the FAA design procedure, the PCC layer thickness was determined solely based on the stresses created by wheel loads. The effects of temperature and moisture variation were incorporated indirectly through the damage analysis and joint design. The contributions of stabilized bases in the

FAA design procedure were reflected in the assumption of higher modulus of subgrade reaction. In their studies, higher foundation modulus tended to decrease the surface deflection and the bending stresses imposed by the wheel loads (Gary, 2009). However, higher stiffness bases tended to increase stresses generated by thermal loads.

The Mechanistic-Empirical Pavement Design Guide (2004) recommended the pavement structure to be modeled as an equivalent two-layered plate system, consisting of a slab and a base, with an effective single k-value representing the compressibility of all sub-base layers underneath the base layer. MEPDG also recommended that any type of base layer (unbound or stabilized) should be modeled as a separate layer, with the interface between the slab and base considered either bonded or unbonded. The fully-bonded base and slab are combined into a composite plate in 2D models that idealize the pavement structure as a slab placed on grade. The recommendations of the MEPDG (2004) in this case are to assign the same Poisson's ratio and coefficient of thermal expansion to the base and PCC slab and to set a constant temperature variation throughout the base layer. In the procedure of mechanistic design of jointed plain concrete pavements, Darter and Khazanovich (2001) stated that at least one base layer should be modeled as a medium-thick plate. The underlying unbound layers should be included as part of the foundation when the pavement system utilizes one stabilized base. When more than one stabilized base layer is considered, the composite layer, consisting of bonded stabilized base layers, should be modeled separately from the foundation. In the 2008 AASHTO MEPDG, however, only the bound bases were considered as separate plate layers from the rest of the foundation layers. It was recommended that the effective k-value be determined for all unbound bases, subbase, and subgrade layers.

7.3.2 Modeling of the Base Layer in FE Analysis Tools

Most rigid pavement analysis tools are capable of modeling at least a two-layer slab on top of a foundation. FE programs such as ILLI-SLAB and JSLAB usually convert the two plate layers to an equivalent single-layer system in both bonded and unbonded state. Full strain compatibility is assumed between layers for fully-bonded PCC/base contact state. In turn, shear stresses at the interface are assumed negligible for unbonded contact state (Heinrichs et *al*., 1989; Ioannides et *al*., 1992). This type of model does not capture the separation or sliding between unbonded layers as a consequence of

thermal loads. To model the independent behavior of the PCC and base layers, FE programs ILSL2 and ISLAB2000 incorporate the Totsky model, which idealizes those layers as a series of springs and plates. In the Totsky model, the stiffness associated with the degrees of freedom of the base and foundation layers is added to the stiffness matrix of the top PCC slab layer. For this reason, modeling thermal curling is not possible when the continuous foundation models (e.g. Vlasov and Boussinesq) are used. The Totsky model (Khazanovich and Ioannides, 1994) allows for modeling vertical separation between the slab and the foundation (only the Winkler foundation), but cannot model the horizontal in-plane interaction of those layers. The 3D FE program EverFE models bases as continuous layers with linear elastic material behavior. For unbonded PCC slab/base interface, EverFE allows for modeling separation and also capturing shear transfer in the interface via a bilinear constitutive relation (Davids and Wang, 2003).

7.3.3 Modeling of the Base Layer in NYSLAB

NYSLAB has the ability to model the base layer either as a separate slab layer or as part of the foundation. When the base is modeled as a separate slab layer that is fully-bonded to the PCC slab, both layers, with different material properties and thickness, are modeled as a single composite laminate. In the case of unbonded contact, the PCC slab and base layer are connected through interface elements. The use of interface elements allows for independent actions of those layers. As such, modeling of the loss of contact (separation), due to thermal curling, and sliding, due to thermal expansion and contraction, between the PCC slab and the base layer is achievable. The frictional stresses at the slab-base interface can also be determined by using the interface elements and incorporating a Mohr-Coulomb friction law (see chapter 5). When the base is to be modeled as part of the foundation, the elastic properties and thickness of the base layer are incorporated to determine foundation parameters. In this case, the pavement system is represented as a plate (PCC slab) on top of a composite foundation (base+subgrade). The composite foundation can be represented either as an equivalent single layer (Winkler) model or a two-layered (Vlasov) model. In the case of Winkler foundations, the foundation domain is modeled as a series of independent spring elements. The foundation layer below each jointed slab is modeled as disconnected segments to allow for the independence of Winkler springs across the

joints. In the case of Vlasov foundations, shear interaction between the spring elements are considered by connecting them with a shear layer. The foundation layers in the Vlasov model is extended beyond the slab edges to better capture the stiffness of the surrounding foundation. The foundation elements are connected across the joints with stiff springs (soil continuity elements) to account for the continuous nature of the Vlasov model. NYSLAB allows for the curling analysis of jointed concrete slab systems (not limited to only one slab) on top of the Vlasov foundation, with no need to convert it to the Kerr foundation.

7.3.3 Pavement System Properties for Parametric Study

To investigate the effect of base rigidity on the PCC slab bending stresses induced by thermal loads, a series of parametric studies were carried out. A three-layer rigid pavement system consisting of six (three by two as shown in Figure 7.22) jointed PCC slabs resting on top of a base course and subgrade was studied. The PCC slabs and the base layer were unbonded in their interface. Each slab was 15 ft long, 15 ft wide and 10 in. thick. The modulus of elasticity of the PCC was set to 4,000 ksi with a Poisson's ratio of 0.15, coefficient of thermal expansion of $5.5 \times 10^{-6}/°\text{F}$ and a unit weight of 150 pcf. The slabs were connected transversely by 1.5-in.-diameter dowels (uniformly spaced at 1 ft intervals) and longitudinally by 1-in.-diameter tie bars (spaced at 2 ft intervals). Six different base material properties, from very rigid (lean concrete) to soft (crushed gravel), were considered. Two different subgrades (soft and stiff) were also considered. The material properties and thickness of each layer are shown in Table 7.3 and 7.4 and Figure 7.22.

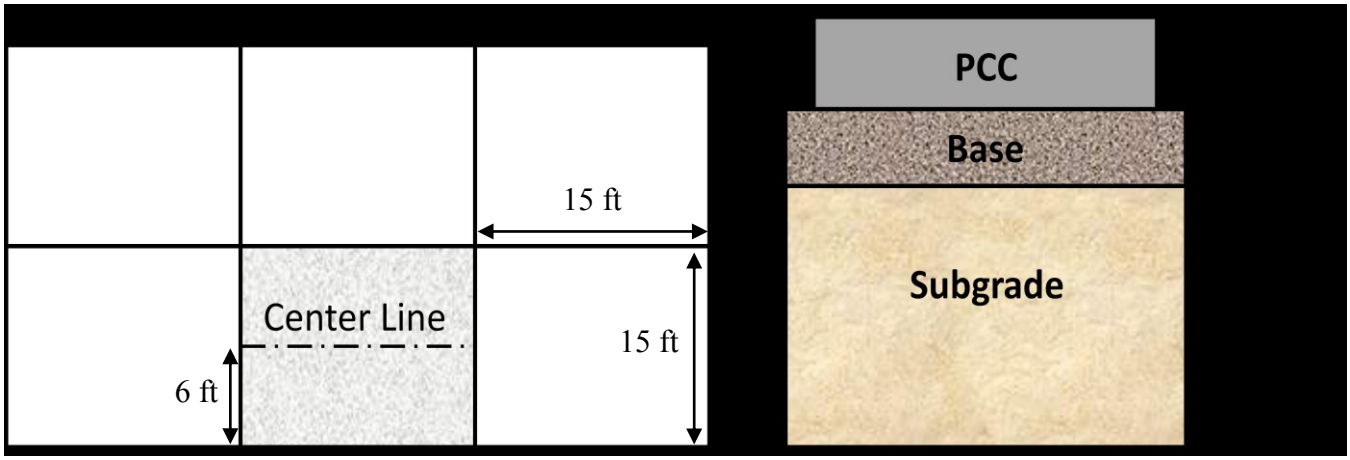

Figure 7.22: Pavement structure.

Table 7.3: Designation of two different subgrades

Subgrade Designation	*E (ksi)*	*v*
Soft	9	0.35
Stiff	16	0.35

Table 7.4: Designation of six different bases

Base Designation	Type	*E (ksi)*	*v*	*γ (pcf)*
LCB	Lean Concrete	2000	0.17	150
CTGB	Cement Treated Granular	1000	0.17	150
CTPB	Cement Treated Permeable	750	0.2	150
ATPB	Asphalt Treated Permeable	300	0.26	140
CSB	Crushed Stone	50	0.35	120
CGB	Crushed Gravel	20	0.35	120

The following four approaches were used for the modeling of the pavement system:

1. **Modeling Base as a Plate**. In this scenario, the PCC slabs and the base layer were modeled as unbonded plates. The mathematical model is shown in Figure 7.23. "Interface elements" as described in the previous section were implemented at the interface of the PCC slab and the base, and between the base and the subgrade, to simulate the separation and sliding between layers. The penalty parameters for the contact constitutive relations, for both the normal and tangential directions, were assigned similar to those used in the previous parametric study (section 7.2). The contact constitutive relation in normal (vertical) direction, corresponding to the vertical stiffness of interface elements, was defined based on the impenetrability of two plate elements. The subgrade was modeled as a Winkler foundation model. The modulus of subgrade reaction or k-value is the only parameter needed to characterize the Winkler springs. Backcalculation procedures (e.g., AREA or Best-fit methods), which require the pavement response from falling weight deflectometer (FWD) deflection testing, are the most appropriate technique to calculate the value of *k* (Hall et *al*., 1997). In the present case study the FWD data is not available, thus it was decided to simulate the FWD test with a 3D finite element model. In that FE model, which incorporated the elastic properties of the PCC slab and the subgrade layer, a 9-ksi-load was applied on the top of the PCC slab and the subgrade layer was extended beyond the slab edges to capture the effect of surrounding soil. The deflection basin at the top of the PCC slab obtained from the 3D analysis, was compared with the deflection profile obtained from the 2D FE analysis of the PCC slab on top of a Winkler foundation. The k-value corresponding to the best-fit of the deflection basin was selected as the Winkler parameter in the analysis, as reported in Table 7.5. Three-dimensional modeling of the subgrade may be incompatible with the Winkler model, because the former idealizes the foundation as a continuous domain while the latter idealizes it as disconnected springs. However, the 3D model is a suitable tool (in absence of FWD data) that can be incorporated for estimating the k-value.

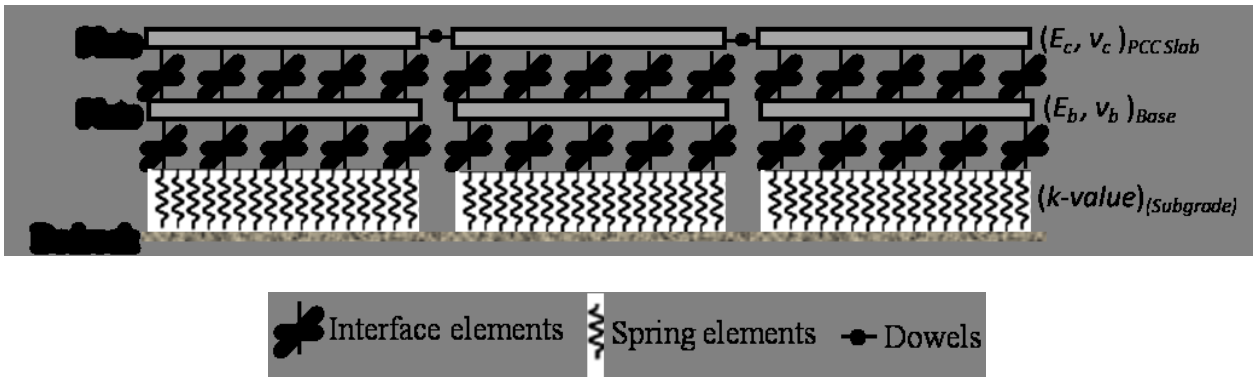

Figure 7.23: Pavement system as modeled in the first modeling approach.

Table 7.5: *k*-value of subgrade

Subgrade type	*k*-value (psi/in.)
Soft	165
Stiff	320

2. **Modeling Base as a Plate, Applying the Totsky Interlayer Stiffness**. In this scenario, the PCC slabs and the base layer were modeled as unbonded plates as well. The vertical stiffness of the interface elements between the first and second plate elements (slab and base layers) were modified based on the interlayer spring stiffness proposed by the Totsky model. The stiffness of interlayer springs is determined by adding the stiffness of two springs, corresponding to the top and the bottom layer, in series, as follow (Khazanovich and Ioannides, 1994):

$$k_{Interface} = \frac{1}{\frac{1}{k_c} + \frac{1}{k_b}} \tag{7-2}$$

where,

$$k_c = \frac{2E_c(1-\nu_c)}{h_c(1-\nu_c-2\nu_c^2)} \qquad k_b = \frac{2E_b(1-\nu_b)}{h_b(1-\nu_b-2\nu_b^2)} \tag{7-3}$$

E_c, ν_c and E_b, ν_b are the modulus of elasticity and Poisson's ratio of the PCC and base, respectively, and h_c and h_b are the thickness of the PCC slab and the base layer.

3. **Modeling Base as Part of a Winkler Foundation.** In this scenario, only the PCC slab was modeled as a plate and two-layered foundation system, consisting of the base course and the subgrade, were represented by a single k-value (Figure 7.24). Interface elements were implemented in the slab/foundation interface. The equivalent k-value was calculated with the similar method as the first scenario but for a two-layered foundation system. The calculated k-value for all the combination of base and subgrade studied are presented in Table 7.6. The k-value for each of the two-layer system (base + subgrade) increases from the softest base (CGB) to the most rigid base (LCB), also from soft to stiff subgrade.

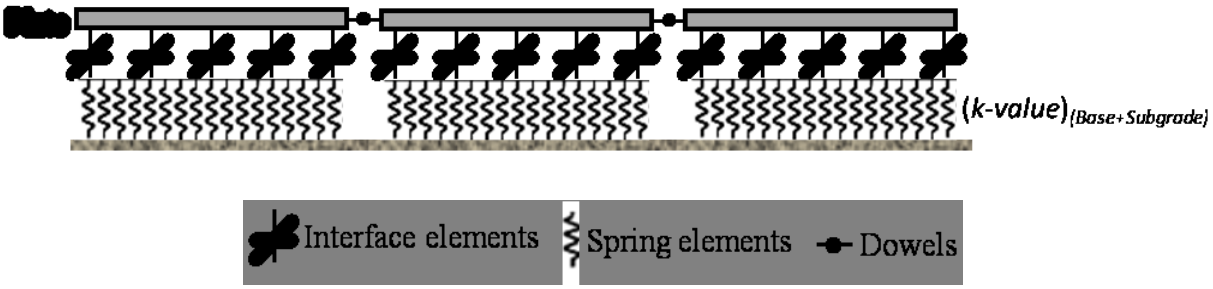

Figure 7.24: Pavement system as modeled in the third modeling approach.

Table 7.6: Equivalent k-value of two-layered foundation (base+subgrade)

Base Designation	k-value (psi/in.)	
	Soft Subgrade	Stiff Subgrade
LCB	300	540
CTGB	240	450
CTPB	225	430
ATPB	195	370
CSB	175	335
CGB	165	310

4. **Modeling Base as Part of a Vlasov Foundation.** In this scenario, the base course and the subgrade were modeled as two separate Vlasov foundation layers (Figure 7.25). This mathematical foundation model cannot be reduced to an equivalent single layer, as is the case in the Winkler model. Each Vlasov layer was characterized with two parameters, the layer normal stiffness (κ) and layer shear stiffness (τ). Vlasov parameters were calculated internally for each layer in NYSLAB, using an iterative process described in Chapter 4. It is worth mentioning that the normal stiffness in this method does not correspond to the modulus of subgrade reaction since it is being calculated for each layer and not the entire foundation structure. The Vlasov parameters for the first layer (base) solely depend on its elastic properties and thickness. The Vlasov parameters for the bottom layer (subgrade) depend on the stiffness of its top layer (base layer) and the loading condition, in addition to the dimensions of the slab and the foundation layers. The calculated Vlasov parameters for the subgrade layer will be shown in the subsequent section, for all combination of the base course and the subgrade type and for different loading scenarios. In the present modeling approach, the PCC slab was connected to the foundation with "interface elements" as well.

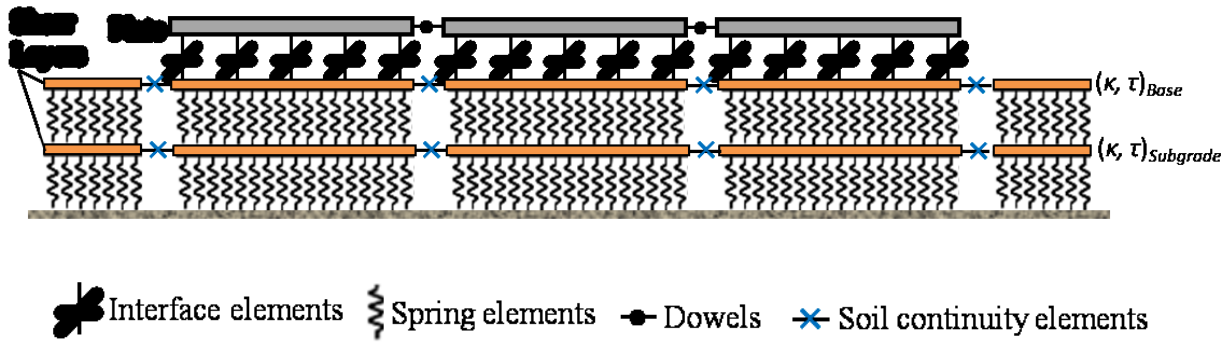

Figure 7.25: Pavement system as modeled in the fourth modeling approach.

7.3.4 Numerical Results

The bending stresses in longitudinal direction (σ_{xx}) at the top of the PCC slab and the vertical deflection of the PCC slab through the center of the slab (highlighted slab in Figure 7.22) were evaluated in this study to examine the effect of different approaches of base modeling on PCC slab responses. Two linear negative temperature gradients (low and high) and two linear positive temperature gradients (low

and high) were applied to the PCC slabs. Negative gradients, where the decrease in temperature at the top of the slab is greater than that at its bottom, varied -1ºF/in. (low) and -1.5 º F/in. (high) throughout the slab thickness and Positive gradients varied +1ºF/in. (low) and +1.5 º F/in. (high) throughout the slab thickness. In another set of parametric studies, the highlighted slab was loaded with a single tire at its center. The magnitude of load was 9000 lb and the tire had dimensions of 8 in. by 6 in.. The Vlaosov parameters for each loading scenario are shown in Table 7.7 and 7.8. The Vlasov parameters for the base layer, which is calculated based on a linear equation (Eq. 4-43), are similar for all the loading scenarios. In the case of thermal loads, the subgrade normal stiffnesses (κ_2) increase while the subgrade shear stiffnesses (τ_2) decrease as the base rigidity decrease (from LCB to CGB). This is attributed to the increase in nonlinearity of the vertical deflection profile in the subgrade layer (γ increases in Eq. 4-46) as the base layer becomes softer, which results in higher normal stiffness and lower shear stiffness in the subgrade. In case of the wheel load, since the impact of the load on PCC slab is smaller than the thermal loads, the subgrade layer vertical deflection profile is less nonlinear. Consequently, the changes in the Vlasov parameter of the subgrade layer are less significant than those from the thermal loads, as the base becomes softer.

Table 7.7: Estimated two parameters of Vlasov foundation models for base layers

Base Designation	Base layer normal stiffness (κ_1)* (psi/in.)	Base layer shear stiffness (τ_1) (lb/in.)
LCB	238,860	2,564,120
CTGB	119,430	1,282,100
CTPB	92,593	937,500
ATPB	40,785	357,140
CSB	8916	55,556
CGB	4458	22,222

Table 7.8: Estimated two parameters of Vlasov foundation models for subgrade layers

a) High negative temperature gradient (-1.5 º F/in.)

Base Designation	Subgrade normal stiffness (κ_2) * (psi/in.)		Subgrade shear stiffness (τ_2) (lb/in.)	
	Soft Subgrade	Stiff Subgrade	Soft Subgrade	Stiff Subgrade
LCB	144	257	110,480	190,140
CTGB	144	257	109,400	187,090
CTPB	144	257	108,680	185,890
ATPB	145	258	105,140	179,490
CSB	146	261	100,570	175,590
CGB	147	263	98,098	173,960

b) Low negative temperature gradient (-1.0 º F/in.)

Base Designation	Subgrade normal stiffness (κ_2) * (psi/in.)		Subgrade shear stiffness (τ_2) (lb/in.)	
	Soft Subgrade	Stiff Subgrade	Soft Subgrade	Stiff Subgrade
LCB	144	257	110,460	194,790
CTGB	144	257	109,350	191,590
CTPB	144	257	108,570	189,900
ATPB	145	258	105,610	184,680
CSB	147	262	98,758	174,100
CGB	148	264	95,999	170,050

c) High positive temperature gradient (+1.5 º F/in.)

Base Designation	Subgrade normal stiffness (κ_2) * (psi/in.)		Subgrade shear stiffness (τ_2) (lb/in.)	
	Soft Subgrade	Stiff Subgrade	Soft Subgrade	Stiff Subgrade
LCB	144	257	110,920	196,700
CTGB	144	257	110,550	195,260
CTPB	144	257	110,200	194,080
ATPB	145	258	107,940	187,210
CSB	149	277	94,956	152,630
CGB	154	287	87,426	143,590

d) Low positive temperature gradient (+1.0 º F/in.)

Base Designation	Subgrade normal stiffness (κ_2) * (psi/in.)		Subgrade shear stiffness (τ_2) (lb/in.)	
	Soft Subgrade	Stiff Subgrade	Soft Subgrade	Stiff Subgrade
LCB	144	257	110,950	196,810
CTGB	144	257	110,620	195,830
CTPB	144	257	110,420	195,130
ATPB	145	258	109,100	191,660
CSB	146	266	100,470	166,300
CGB	150	270	93,556	160,890

e) Wheel load

Base Designation	Subgrade normal stiffness (κ_2) * (psi/in.)		Subgrade shear stiffness (τ_2) (lb/in.)	
	Soft Subgrade	Stiff Subgrade	Soft Subgrade	Stiff Subgrade
LCB	144	257	110,720	195,890
CTGB	144	257	110,040	193,900
CTPB	144	257	109,560	192,840
ATPB	144	258	107,740	189,640
CSB	145	258	104,730	185,960
CGB	145	258	104,680	185,280

Longitudinal Bending Stress Due to Negative Temperature Gradient

By modeling the base as a plate (the first modeling approach described above), the bending stresses on top of the PCC slab for different pavement systems, with six different base rigidities on top of either soft or stiff subgrade, are shown in Figure 7.26. As expected, the tensile stress at the top of the PCC slab, due to the high negative temperature gradient (-1.5ºF/in.), increases as the base becomes stiffer (from CGB, the softest to LCB, the stiffest). These stresses increase by about 8% in the case of the stiff subgrade and by 13% in the case of the soft subgrade. In the case of lower temperature gradient (-1ºF/in.), the increase in tensile stress from the CGB to LCB is about 5% for the stiff subgrade and 8% for the soft subgrade. In that case, except for the most rigid base, the maximum PCC tensile stresses are not significantly affected by the change in base rigidity. This can be justified by the fact that modeling the base as a plate does not allow the PCC slab to "sink" into the base layer. This pattern occurs because the mathematical model of the plate elements only considers their flexural and shear stiffness, and does not consider their vertical or compressive stiffness. Therefore, modeling base as a plate may lead to an under-estimation of the stresses. In the case of stiffer subgrade, the base deformation decreases, which in turn reduces the effect of bending stiffness of the base layer on the PCC slab. For both thermal gradients and all bases considered, the PCC slab tensile stresses increase as the subgrade becomes stiffer. This indicates that in this modeling approach the impact of subgrade rigidity is more important than the base rigidity in the magnitude of PCC slab stresses.

Figure 7.27 illustrates the PCC slab stresses when the base layer is modeled with a plate element and the vertical stiffness of interface elements is modified based upon the Totsky model. As the base rigidity increases, the PCC slab stresses increase by about 13% (stiff subgrade) and by 18% (soft subgrade), due to high temperature gradient, and increase about 7% (stiff subgrade) and 12% (soft subgrade), due to low temperature gradient.

Figure 7.28 shows the PCC slab stresses when the base layer is modeled as part of a Winkler foundation in the third modeling approach. For the high temperature gradient, the PCC slab tensile stress increases about 13% (stiff subgrade) and 20% (soft subgrade) as the base rigidity increases from CGB to LCB, and for the low temperature gradients, the PCC slab tensile stress increases about 14.5% (stiff subgrade) and 24% (soft subgrade). As in the case where the base is modeled as a plate, the PCC slab tensile stresses in this modeling approach for all bases increase as the subgrade becomes stiffer.

The bending stresses at the top of the PCC slabs are shown in Figure 7.29 when the base and subgrade layer are modeled as part of a Vlasov foundation (fourth approach). The effect of base course rigidity on the PCC slab curling stresses is more pronounced in this modeling approach. The PCC slab stresses increase by about 43% (stiff subgrade) and 63% (soft subgrade), for the high temperature gradient, and increase by about 30% (stiff subgrade) and 51% (soft subgrade), for the low temperature gradient, as the base rigidity increases. In this modeling approach, the maximum PCC stresses for the rigid bases (LCB and CTGB) remain unchanged as the rigidity of the subgrade changes. This demonstrates the significance of the effect of rigid bases on the PCC slab curling stress, regardless of the rigidity of the subgrade. Modeling the base as part of the foundation allows the PCC slab to “sink” into the underlying base layer and thus capture the extended area of support from the base away from the center of the slab. Thus, softer bases result in smaller curling stresses because of this additional support.

By comparing the slab stresses estimated from different modeling approaches, for different temperature gradients and base and subgrade stiffness, the following observations can also be made:
The stresses calculated using the second method (base as a plate and applying the Totsky stiffness) is fairly similar to those from the first method (base as a plate). Only the PCC stresses resting on top of the softer bases (CSB and CGB) are slightly lower (less than 5%) than those from the first modeling

approach. The smaller stiffness of the Totsky interlayer springs for the softer bases provide a softer support and causes the PCC slab to sink more to that layer. This results in lower curling stress in the PCC slab. In both the high and low temperature gradient, modeling the base as a Winkler foundation, for all the bases, predicts slightly higher stresses (less that 5%) than the first and second approach (base as plate). From Figures 7.26 through 7.29, the maximum PCC slab stresses predicted from the fourth modeling approach (base as part of a Vlasov foundation) are relatively higher (40% for LCB and 10% for CGB for the stiff subgrade) than those obtained from the other modeling approach. The differences in stresses are more pronounced for the stiffer bases and in the case of higher temperature gradient.

Vertical Deflection Due to Negative Temperature Gradient

Figure 7.30 and 7.31 show the PCC slab vertical deflections calculated with the four approaches, due to the high negative temperature gradient, for both the stiff and soft subgrade. The vertical deflections of the PCC slab, when the base is modeled as a plate, do not change appreciably as the base rigidity changes. The PCC slab vertical deflection for the softer bases (CSB and CGB) is slightly increased (less than 10%) when the Totsky stiffness is applied in the second modeling approach. For the cases where the base is modeled as a Winkler or Vlasov layer, the impact of the base course rigidity on the PCC slab vertical deflections is more pronounced. As the base becomes stiffer from CGB to LCB, the PCC slab vertical deflection decreases about 31% (stiff subgrade) and 32% (soft subgrade), in case of a Winkler base model, and decreases about 77% (stiff subgrade) and 80% (soft subgrade) when modeled using a Vlasov layer. The maximum PCC slab vertical deflections at the center of the slab, when the base is modeled as a plate, seem to be greater than those for the Winkler and Vlasov models. However, the uplifting of the PCC slab edges shows the opposite trend; where uplifting is lower for the case where the base is modeled as a plate. This is attributed to the effect of the vertical or compressive stiffness offered by the Winkler or Vlasov layers, which is absent when the base is modeled as a plate.

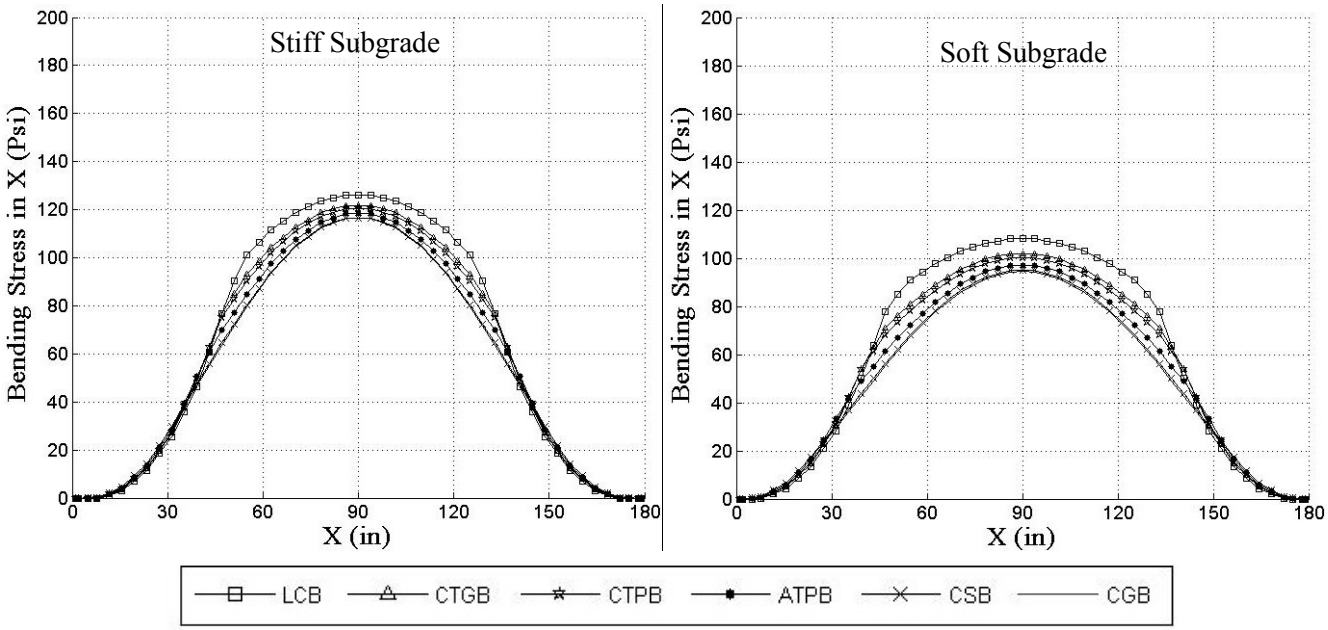

a) High temperature gradient

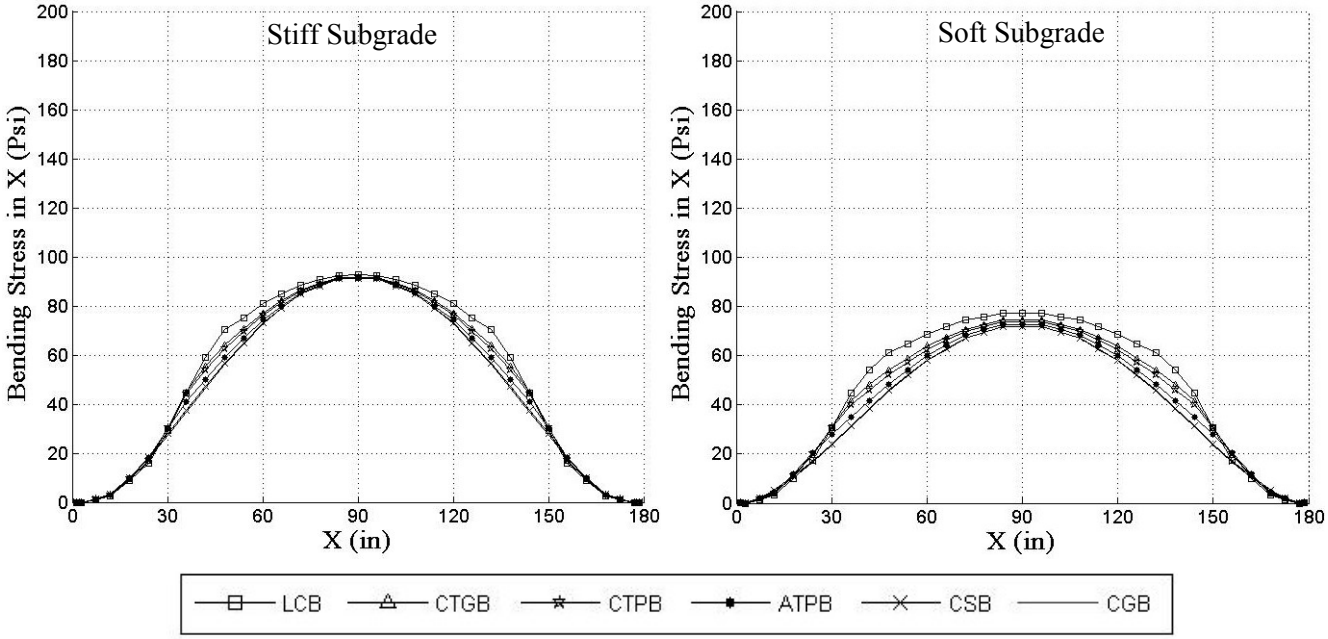

b) Low temperature gradient

Figure 7.26: Bending stresses (σ_{xx}) at the top of PCC slab through centerline for different base course and subgrade rigidity due to thermal loads when the base is modeled as a plate.

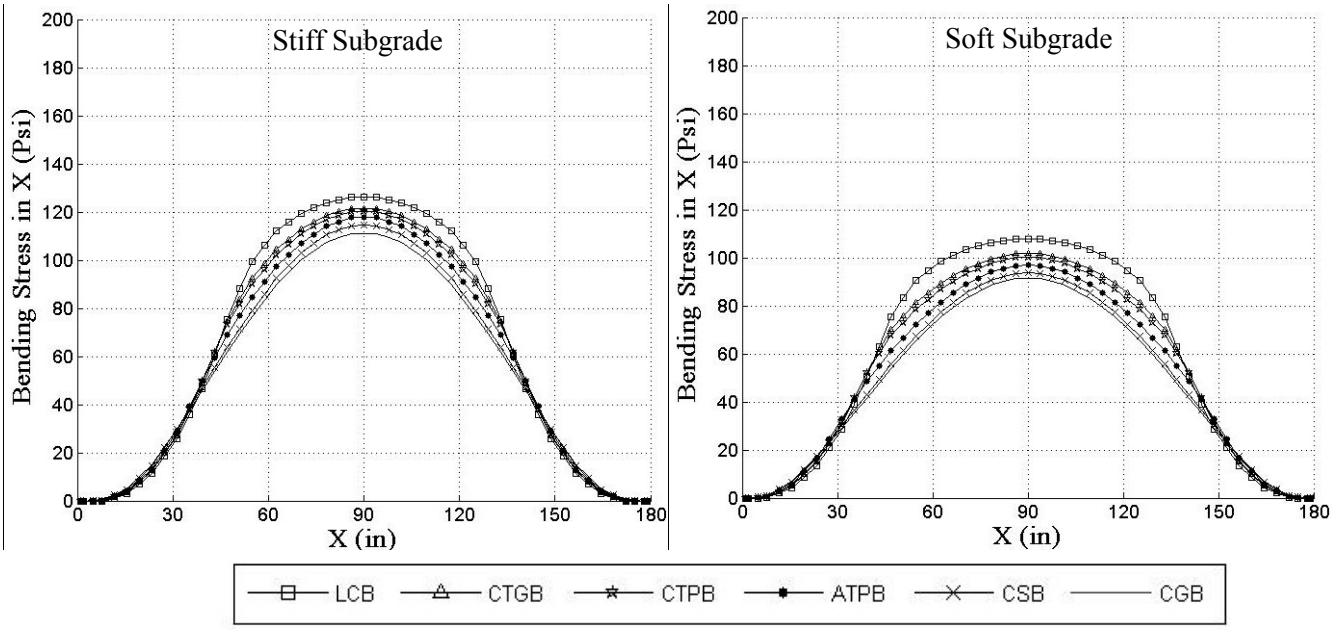

a) High temperature gradient

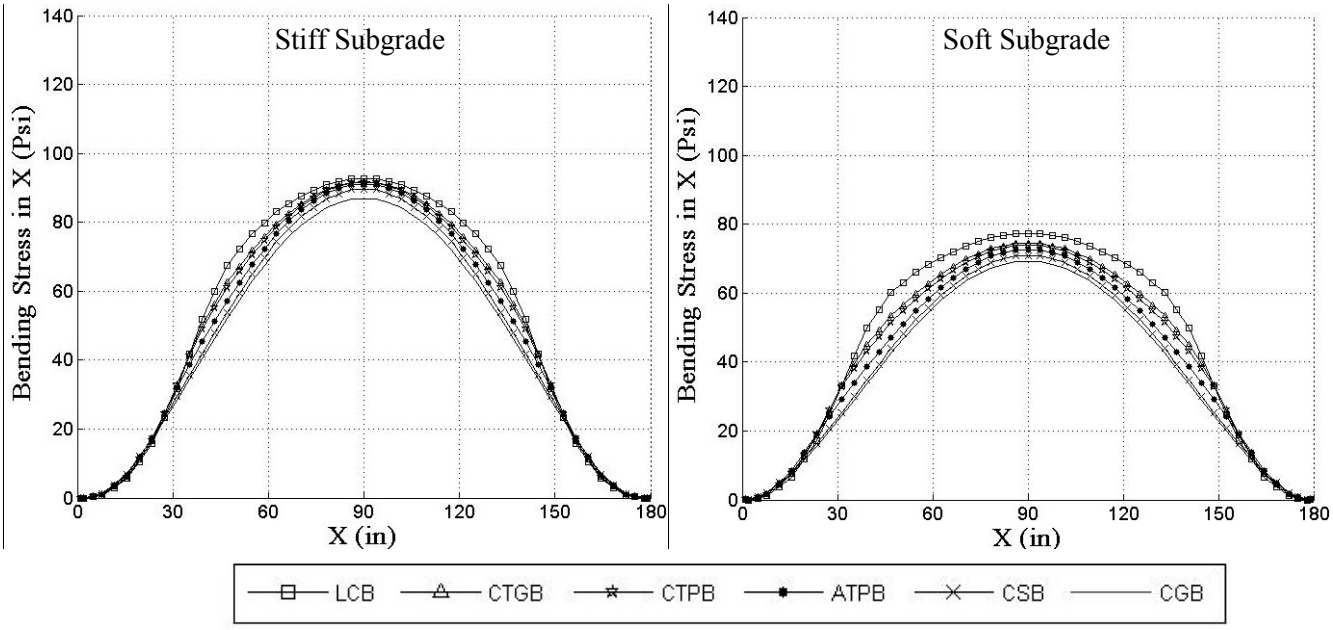

b) Low temperature gradient

Figure 7.27: Bending stresses (σ_{xx}) at the top of PCC slab through centerline for different base course and subgrade rigidity due to thermal loads when the base is modeled as a plate and using Totsky model.

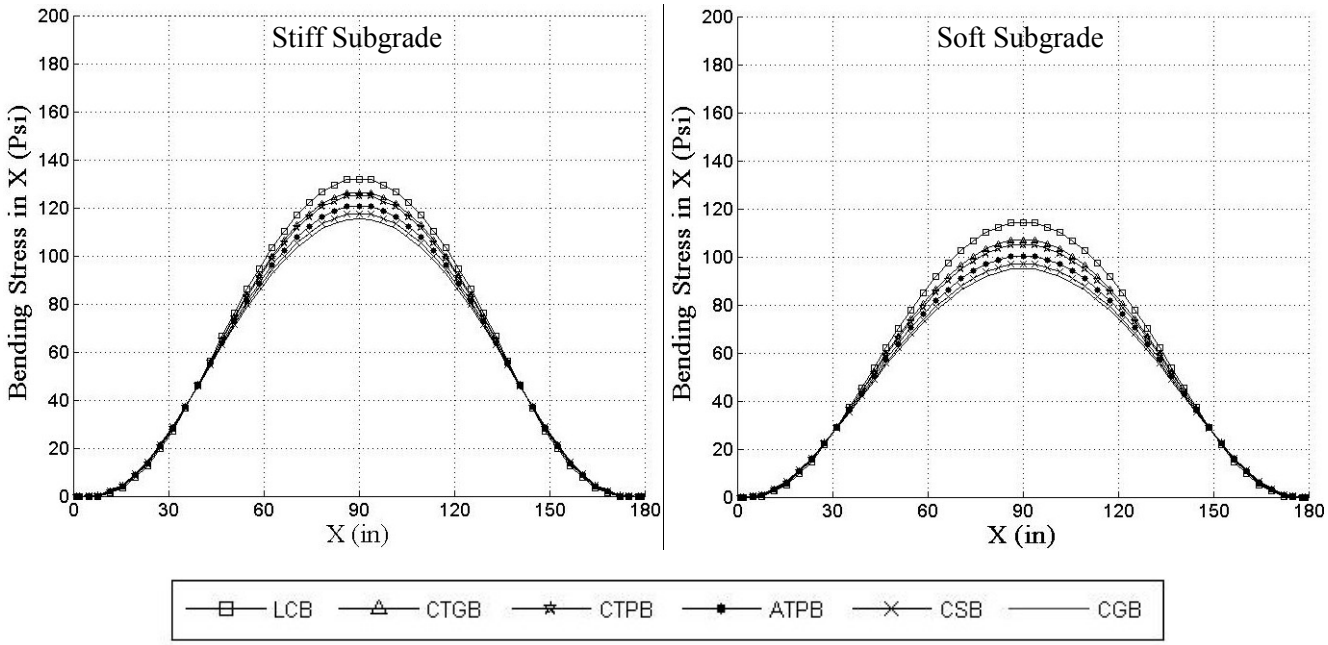

a) High temperature gradient

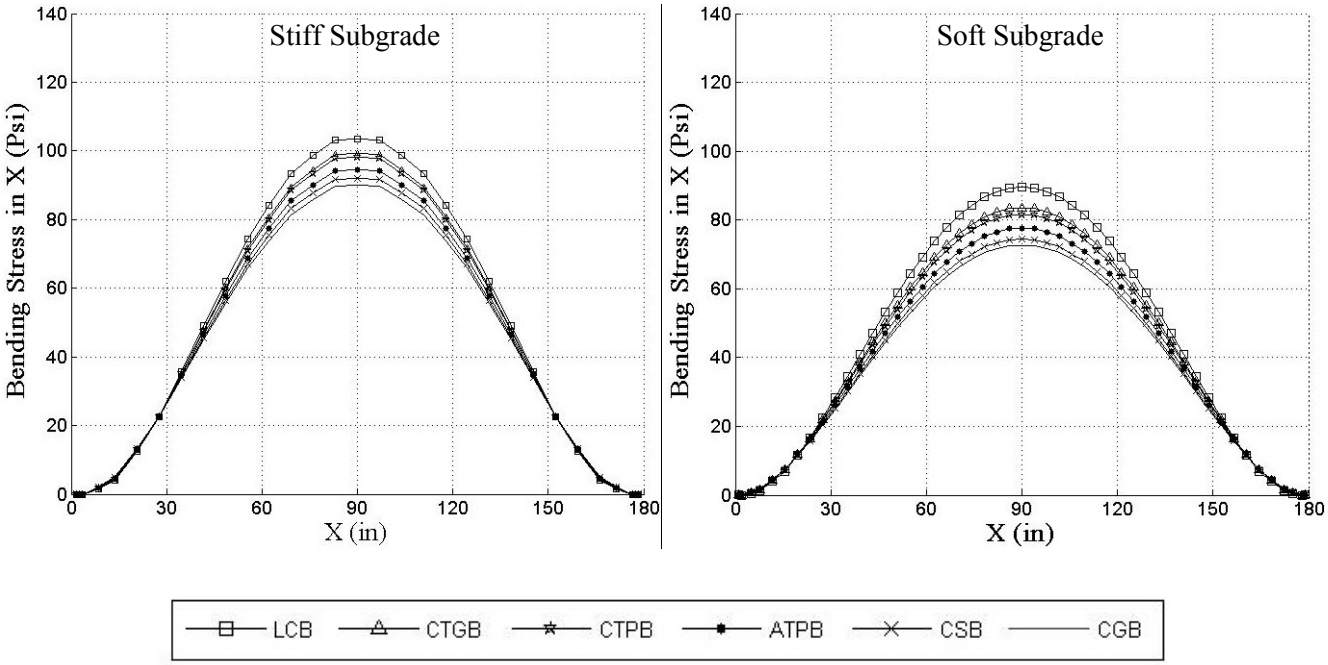

b) Low temperature gradient

Figure 7.28: Bending stresses (σ_{xx}) at the top of PCC slab through centerline for different base course and subgrade rigidity due to thermal loads when the base is modeled as part of a Winkler foundation.

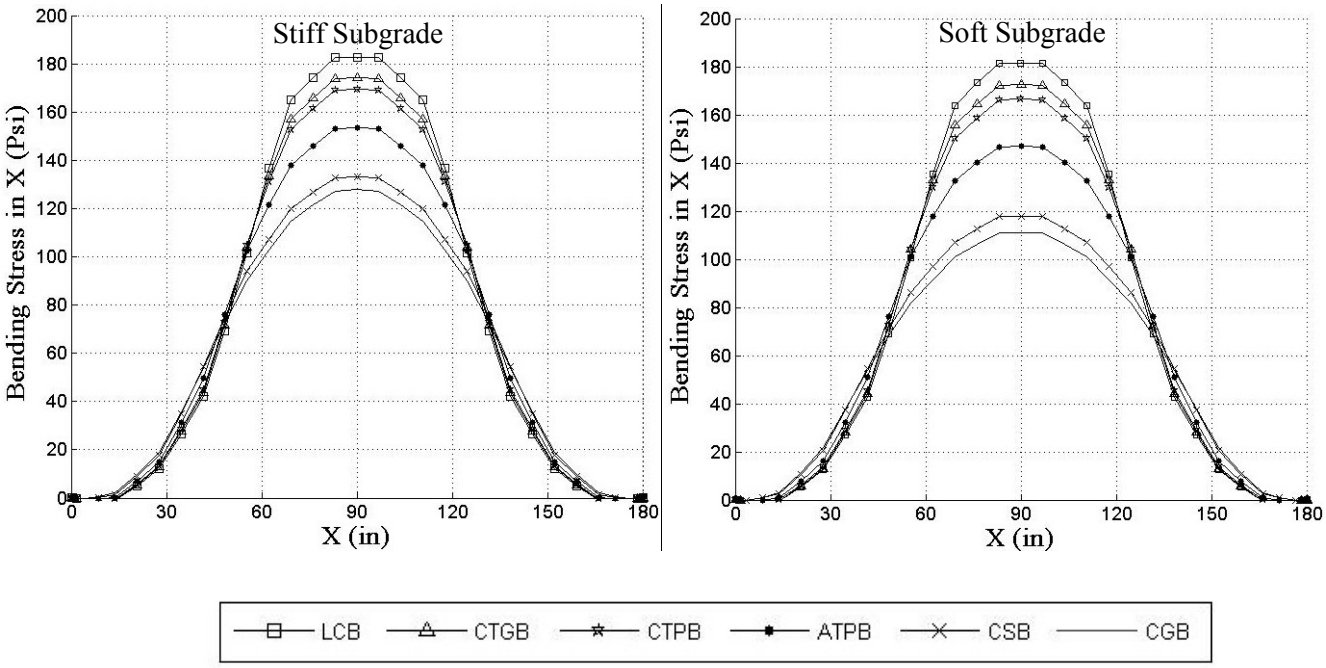

a) High temperature gradient

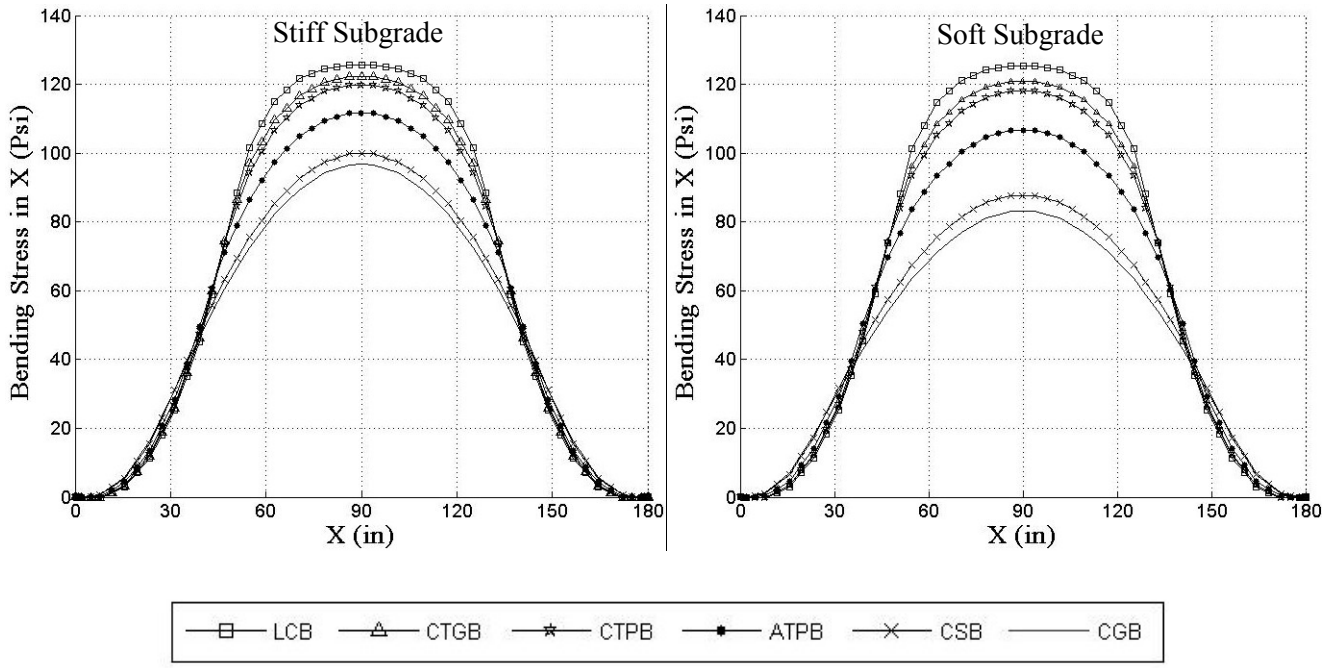

b) Low temperature gradient

Figure 7.29: Bending stresses (σxx) at the top of PCC slab through centerline for different base course and subgrade rigidity due to thermal loads when the base is modeled as part of a Vlasov foundation.

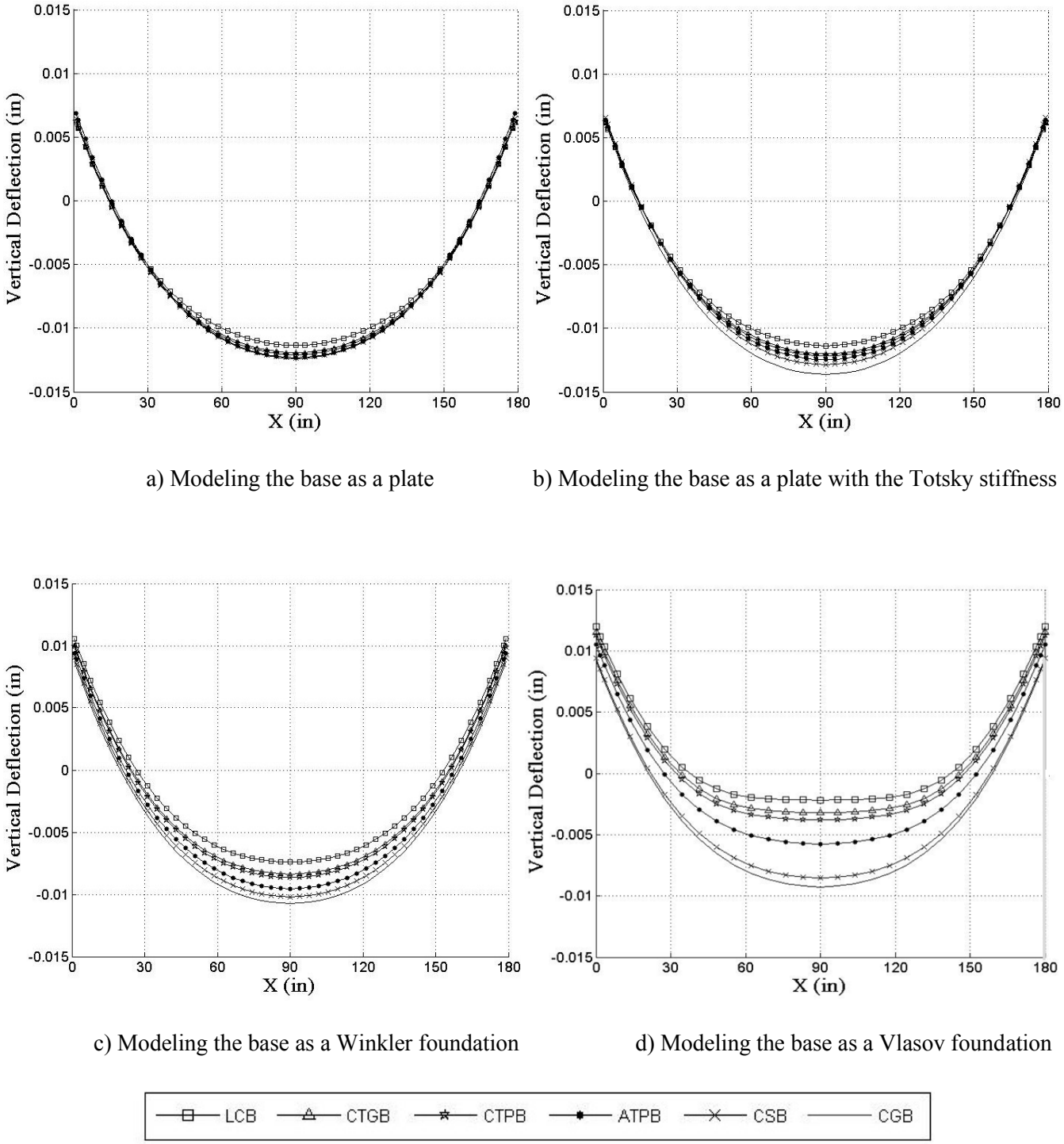

a) Modeling the base as a plate

b) Modeling the base as a plate with the Totsky stiffness

c) Modeling the base as a Winkler foundation

d) Modeling the base as a Vlasov foundation

Figure 7.30: Vertical deflection of PCC slab through centerline for different base course on the stiff subgrade due to high negative temperature gradient.

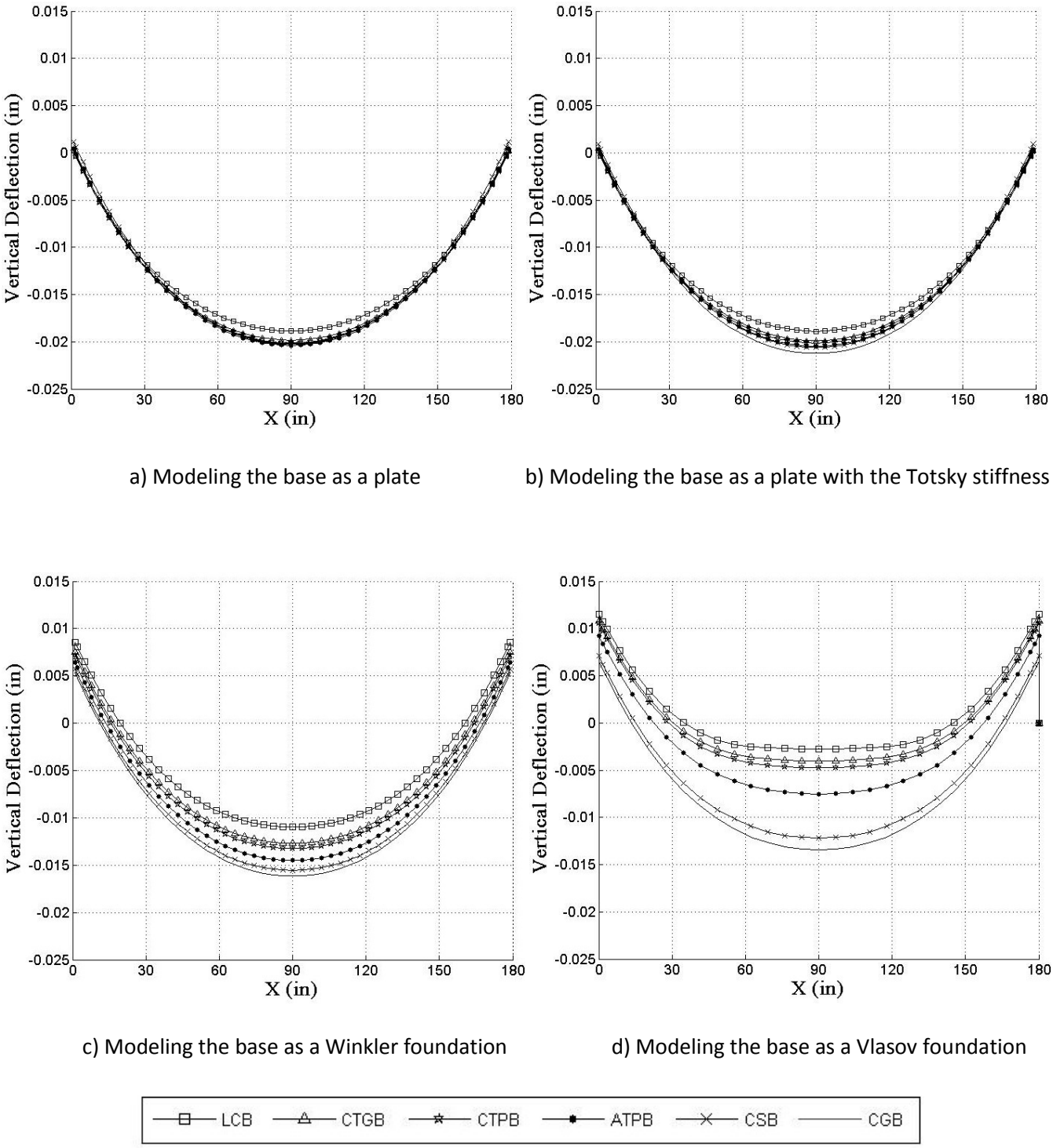

a) Modeling the base as a plate

b) Modeling the base as a plate with the Totsky stiffness

c) Modeling the base as a Winkler foundation

d) Modeling the base as a Vlasov foundation

Figure 7.31: Vertical deflection of PCC slab through centerline for different base course on the soft subgrade due to high negative temperature gradient.

Longitudinal Bending Stress Due to Positive Temperature Gradient

By modeling the base as a plate (the first modeling approach described above), the bending stresses on top of the PCC slab for different pavement systems, with six different base rigidities on top of either soft or stiff subgrade, are shown in Figure 7.32. As expected, the compressive stress (in absolute value) at the top of the PCC slab, due to high positive temperature gradient (+1.5ºF/in.), increases as the base becomes stiffer (from CGB, the softest to LCB, the stiffest). These stresses increase by about 14% in the case of the stiff subgrade and by 24% in the case of the soft subgrade. In case of lower temperature gradient (1ºF/in.), the increase in compressive stress from the CGB to LCB are about 17% (stiff subgrade) and 12% (soft subgrade). For both positive thermal gradients and all bases considered, the PCC slab compressive stresses increase as the subgrade becomes stiffer. The stress responses show quite similar trend when the Totsky stiffness is applied (Figure 7.33). The impact of Totsky model is more pronounced in the case of softer bases, when it results in lower compressive stresses as compared to the first modeling approach.

Figure 7.34 shows the PCC slab stresses when the base layer is modeled as part of a Winkler foundation in the third modeling approach. The PCC slab compressive stress increases about 8% (stiff subgrade) and 12% (soft subgrade), due to positive temperature gradient +1.5ºF/in., and about 10% (stiff subgrade) and 17% (soft subgrade), due to positive temperature gradient +1.0ºF/in., as the base rigidity increases from CGB to LCB. As in the case where the base is modeled as a plate, the PCC slab compressive stresses in this modeling approach for all bases increase as the subgrade becomes stiffer.

The bending stresses at the top of the PCC slabs are shown in Figure 7.35, when the base and subgrade layer are modeled as part of a Vlasov foundation (fourth approach). This approach predicts higher PCC slab stresses than the other approaches. The PCC slab stresses increase by about 13% (stiff subgrade) and 15% (soft subgrade) for the high temperature gradient, and increase by about 7% (stiff subgrade) and 9% (soft subgrade) for the low temperature gradient as the base rigidity increases. In this modeling approach, the maximum PCC stresses for the rigid bases (LCB, CTGB, CTPB and ATPB) remain unchanged as the rigidity of subgrade changes. This demonstrates the significance of the effect of rigid bases on the PCC slab curling stress regardless of the rigidity of the subgrade.

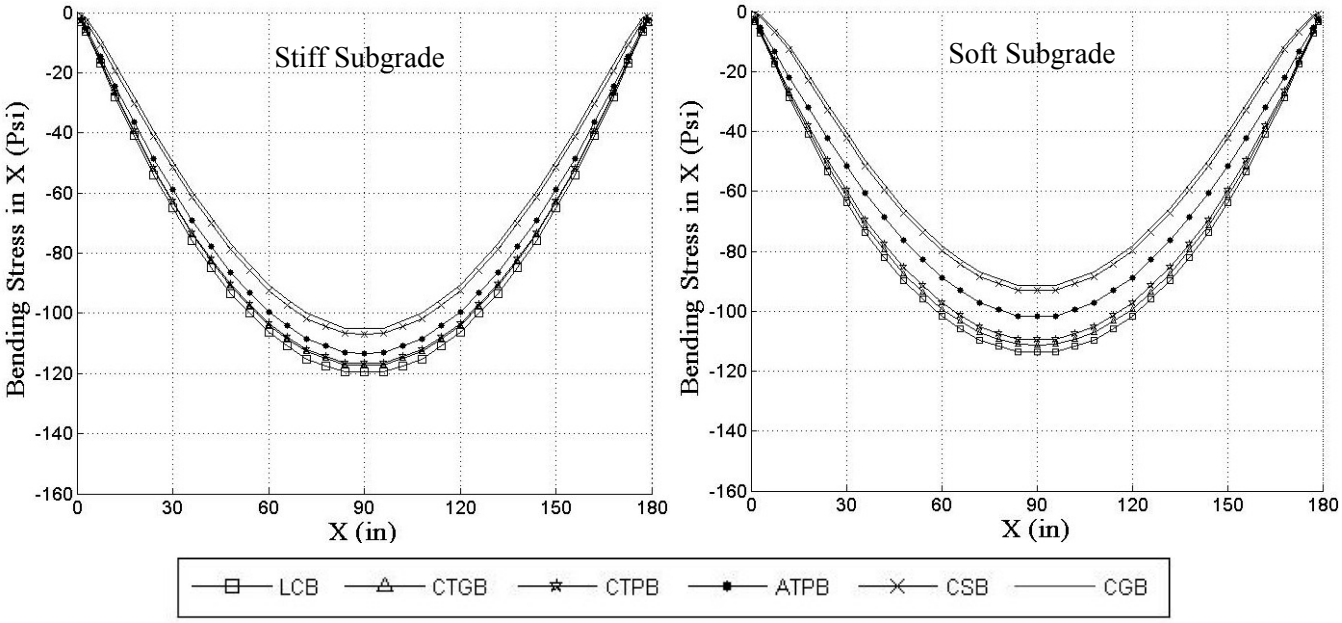

a) High temperature gradient

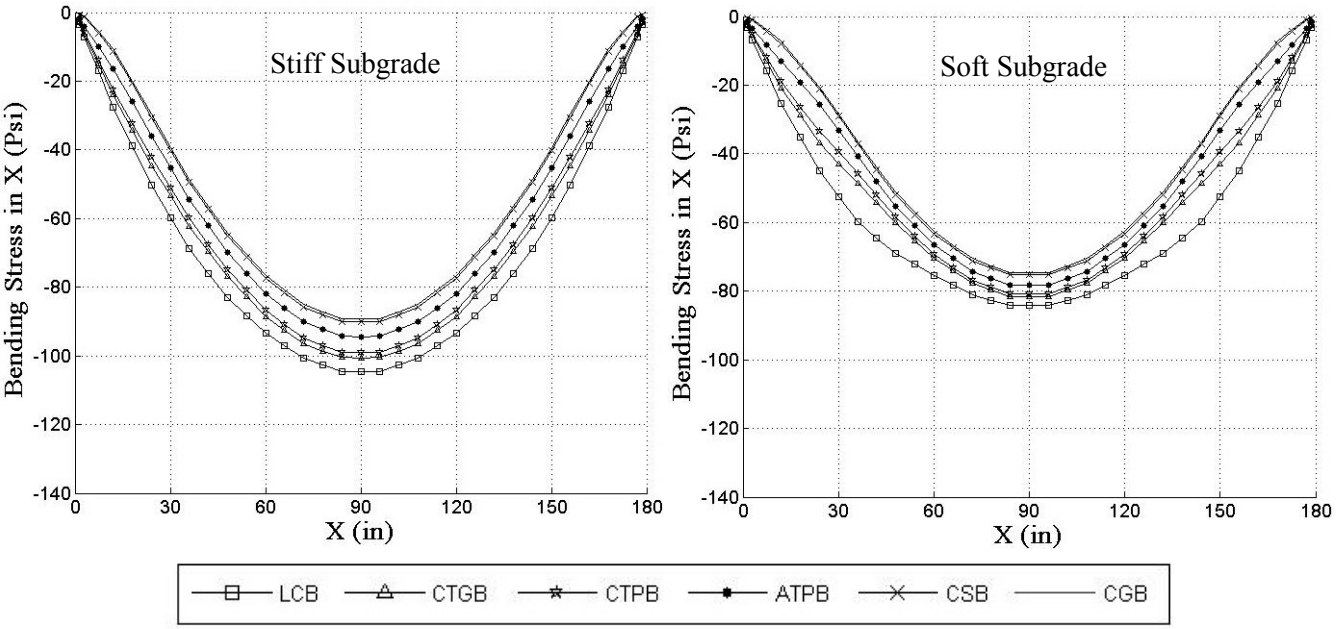

b) Low temperature gradient

Figure 7.32: Bending stresses (σ_{xx}) at the top of PCC slab through centerline for different base and subgrade rigidity due to positive temperature gradient when the base is modeled as a plate.

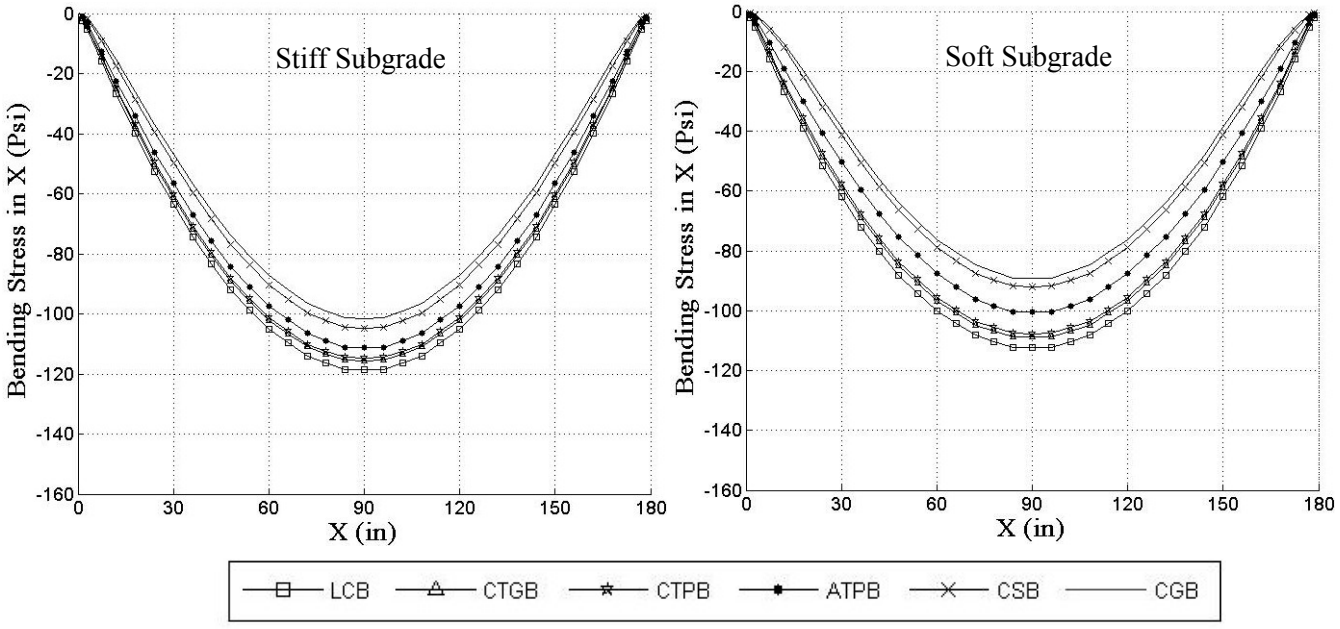

a) High temperature Gradient

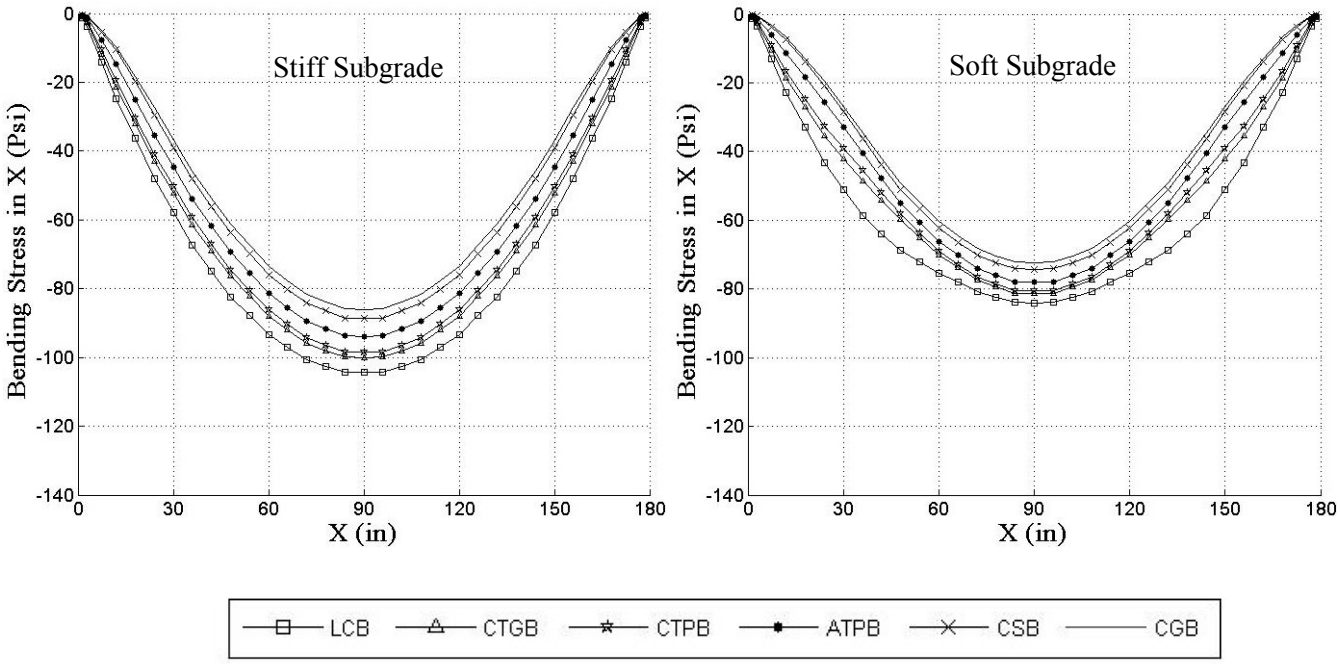

b) High temperature Gradient

Figure 7.33: Bending stresses (σ_{xx}) at the top of PCC slab through centerline for different base and subgrade rigidity due to positive temperature gradient when the base is modeled as a plate and using Totsky model.

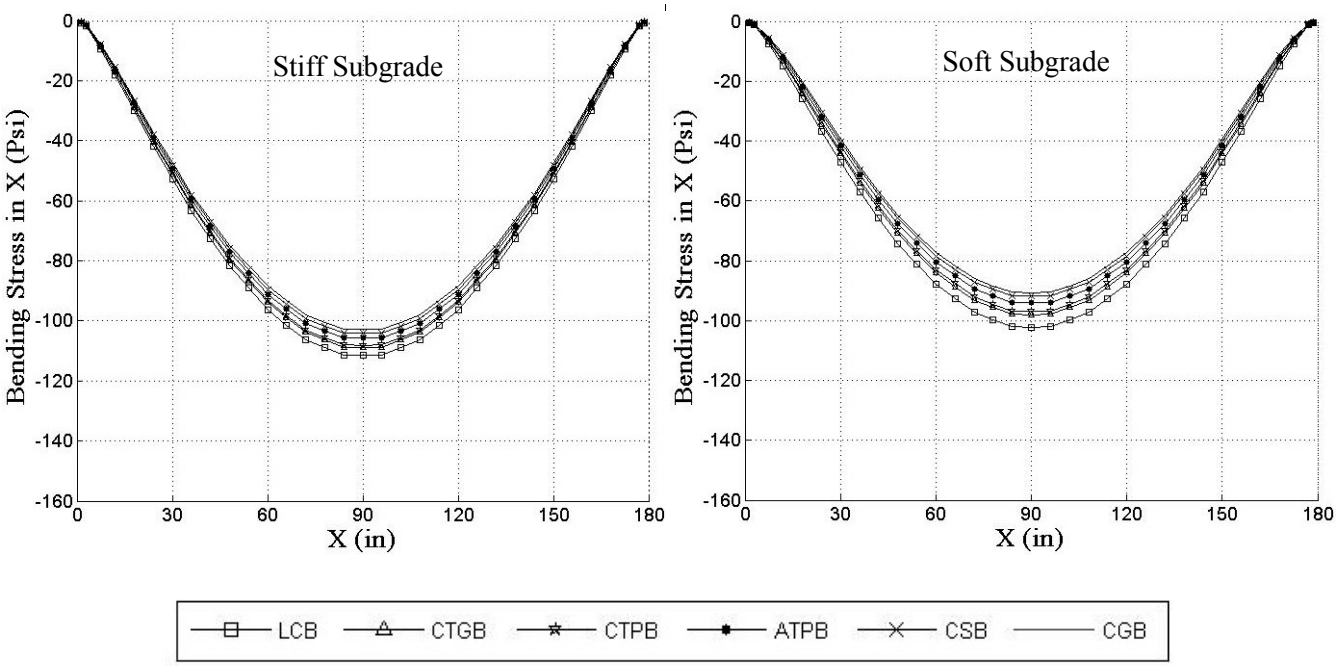

a) High temperature gradient

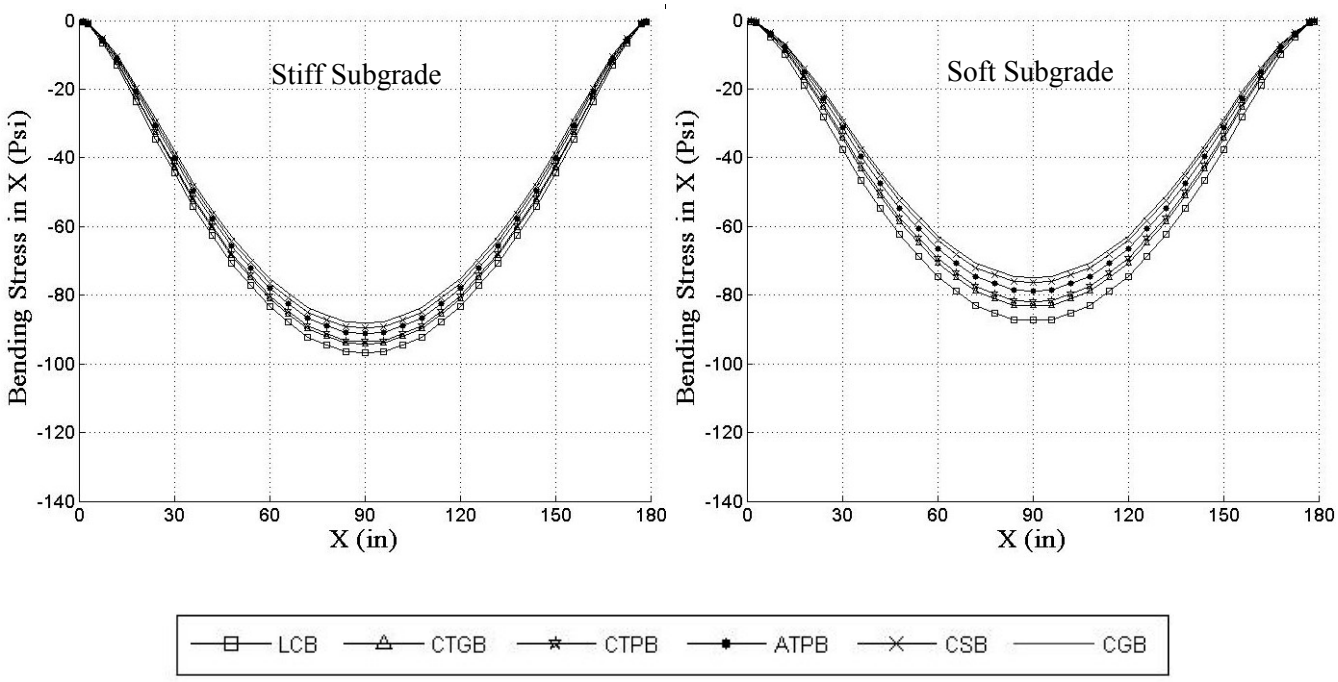

b) Low temperature gradient

Figure 7.34: Bending stresses (σ_{xx}) at the top of PCC slab through centerline for different base and subgrade rigidity due to positive temperature gradient when the base is modeled as part of a Winkler foundation.

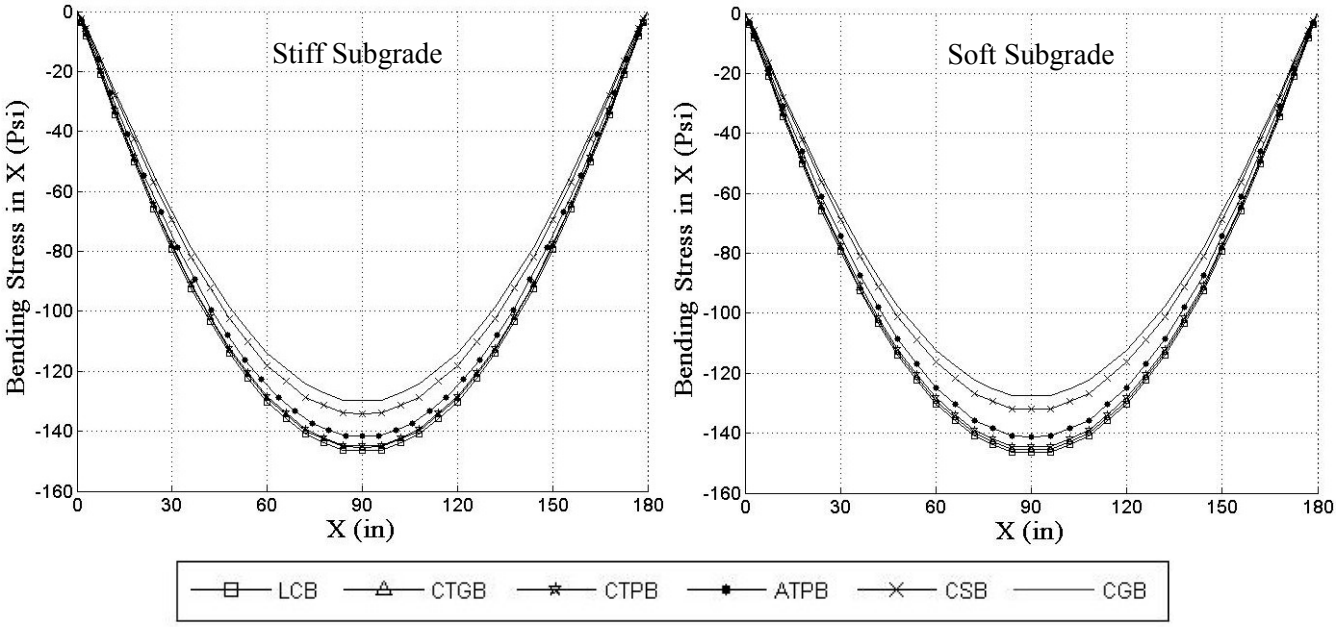

a) High temperature gradient

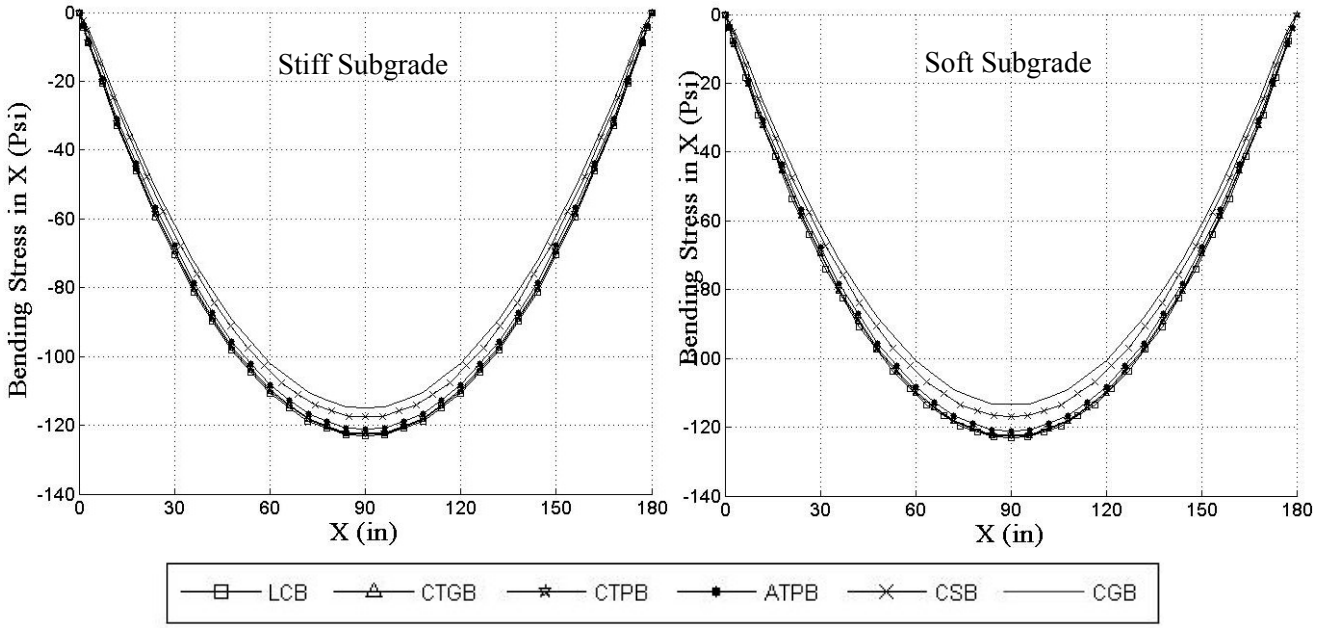

b) Low temperature gradient

Figure 7.35: Bending stresses (σ_{xx}) at the top of PCC slab through centerline for different base and subgrade rigidity due to positive temperature gradient when the base is modeled as part of a Vlasov foundation.

Bending Stress Due to Single Wheel Load at Slab Center

In this section, the effect of base modeling is evaluated for a pavement slab subjected to a single wheel load at the slab center (Figure 7.36). The dimension of wheel is 8 x 6 in. and the magnitude of load is 9000 lb. In case of wheel load, stiffer bases should result in lower PCC slab bending stresses. As is apparent from Figure 7.37, the impact of base rigidity on PCC slab bending stress is better pronounced when the base is modeled as a plate (decrease by 34% from LCB to CGB) and when it is modeled as a Vlasov foundation (decrease by 90% from LCB to CGB). The slab bending stresses do not change appreciably as the base rigidity changes when the base is modeled as part of a Winkler foundation. The modified interlayer vertical stiffness offered by the Totsky model results in higher stresses when the base is modeled as a plate (Figure 7.37 (a) and (b)). Moreover, the PCC bending stress under the applied load increases as the subgrdae becomes softer. However, in the case when the base is modeled as a Vlasov foundation, the bending stress does not change appreciably as the subgrade become softer, for the rigid bases (LCB, CTGB and CTPB).

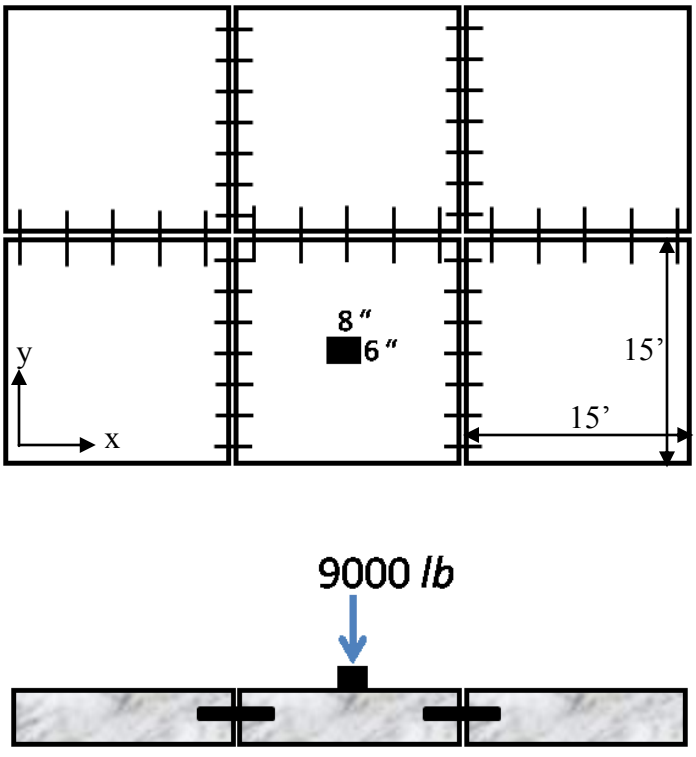

Figure 7.36: Pavement structure with center load.

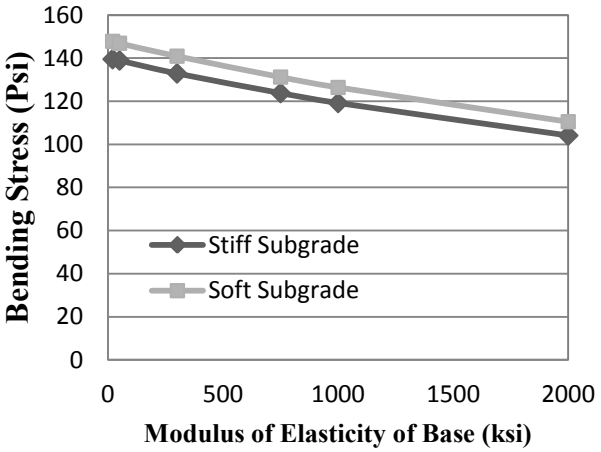

a) Modeling the base as a plate

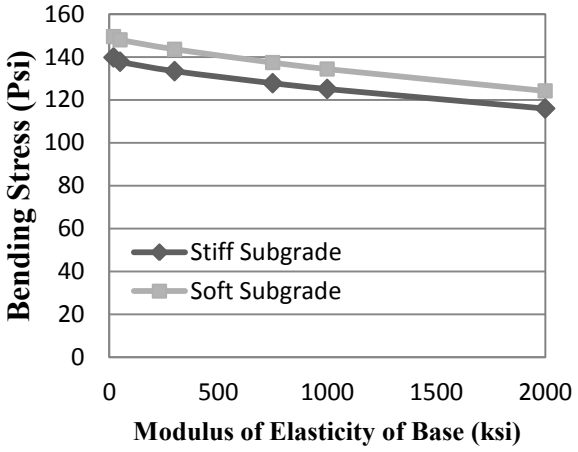

b) Modeling the base as a plate with the Totsky stiffness

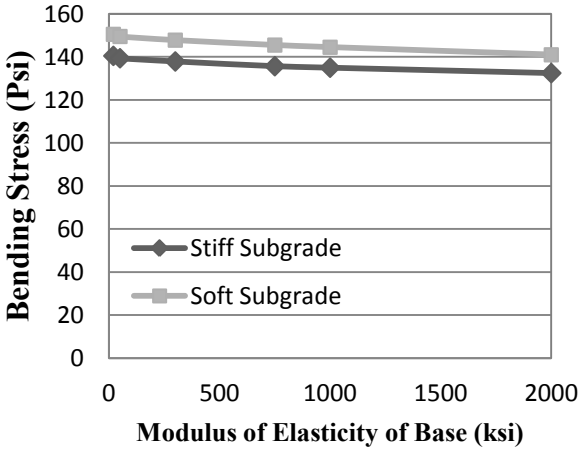

c) Modeling the base as a Winkler foundation

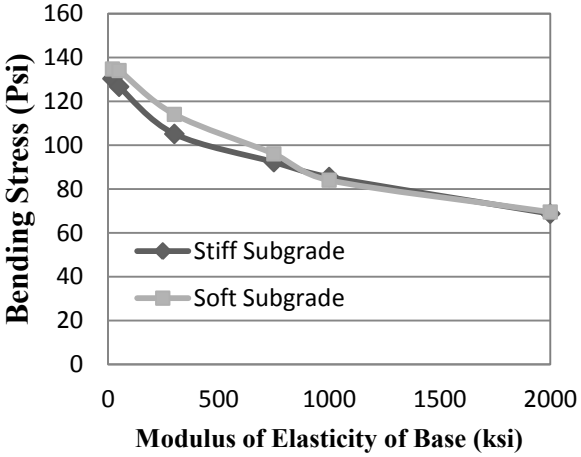

d) Modeling the base as a Vlasov foundation

Figure 7.37: Bending stresses (σ_{xx}) at the bottom of PCC slab under the tire load for different base and subgrade rigidity.

Bending Stress Due to Single Wheel Load at Slab Corner

In this section, the effect of base modeling is evaluated for a pavement slab subjected to a single wheel load at the slab corner (Figure 7.38). The dimensions of wheel are 6 x 6 in. and the magnitude of load is 9000 lb. The maximum PCC slab bending stress in longitudinal (σ_{xx}) and transverse (σ_{yy}) direction, due to a corner load, are shown in Figure 7.39 and 7.40 using the investigated modeling approaches. It is expected for bending stress to have lower value in the longitudinal direction since the load transfer elements (dowels) are stiffer in that direction as compared to those in the transverse direction (tie bars). The bending stress at the bottom of slab decreases as the base rigidity increases (about 15% and 22% in the longitudinal and transverse directions, respectively), when the base is modeled as a plate. In this case, while the stresses in longitudinal direction are not impacted by subgrade rigidity, the stress in transverse direction decreases as the subgrade become stiffer. In the case when the base is modeled as a Winkler foundation, the longitudinal bending stress does not change appreciably as the base or subgrade become stiffer. The transverse bending stress slightly decreases as the base rigidity increases and subgrade becomes stiffer. This indicates that the Winkler foundation is not an appropriate model to account for the edge or corner stresses. In the case when the base is modeled as a Vlasov foundation, the bending stresses in the longitudinal and transverse directions decrease about 22% and 24%, respectively, as the base rigidity increase. In this model, the impact of subgrade rigidity was only reflected for the bases with low rigidity.

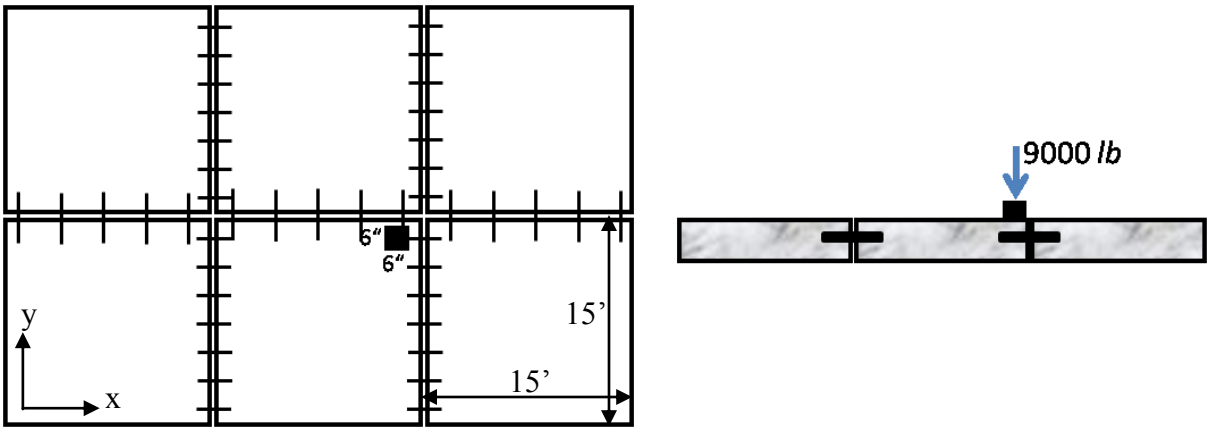

Figure 7.38: Pavement structure with corner load.

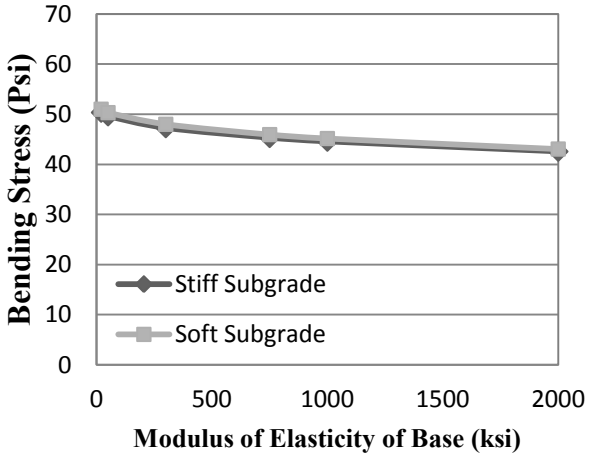

a) Modeling the base as a plate

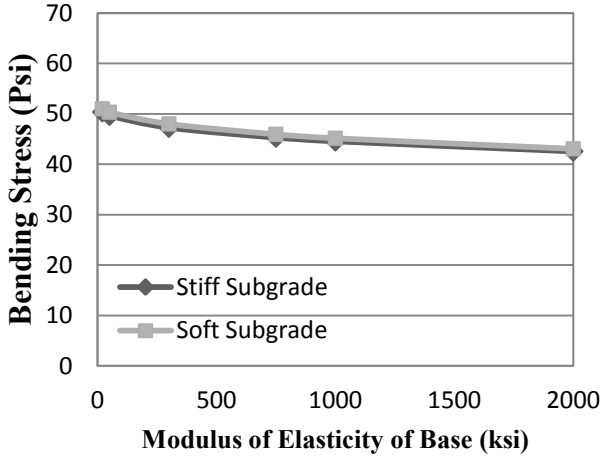

b) Modeling the base as a plate with the Totsky stiffness

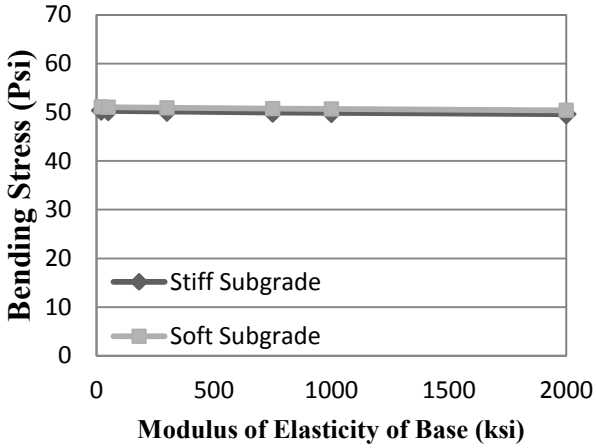

c) Modeling the base as a Winkler foundation

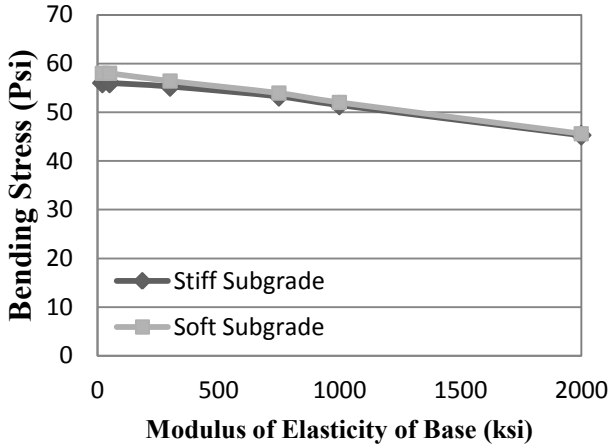

d) Modeling the base as a Vlasov foundation

Figure 7.39: Maximum longitudinal bending stress (σ_{xx}) at the bottom of PCC slab under the corner load for different base and subgrade rigidity.

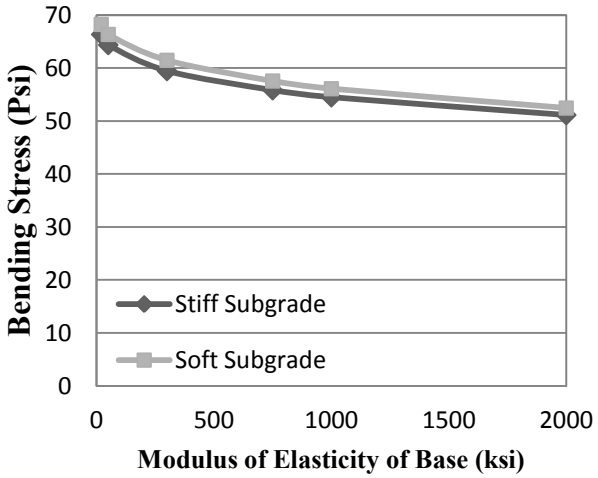

a) Modeling the base as a plate

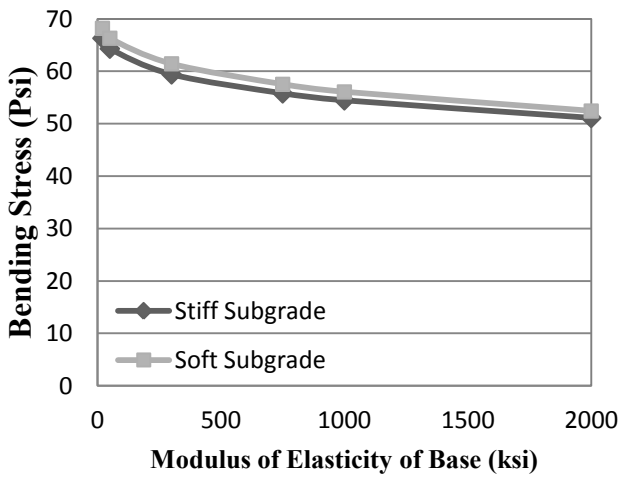

b) Modeling the base as a plate with the Totsky stiffness

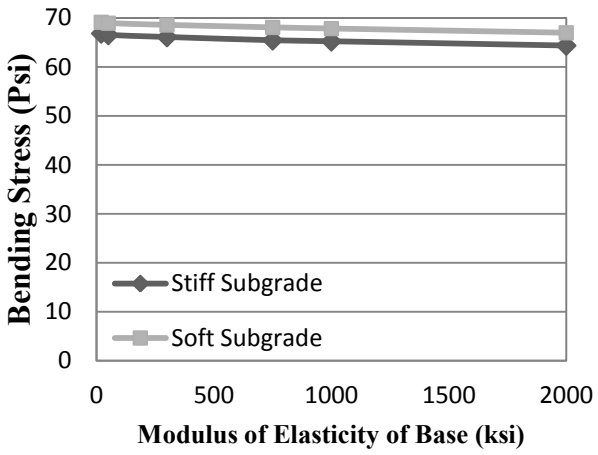

c) Modeling the base as a Winkler foundation

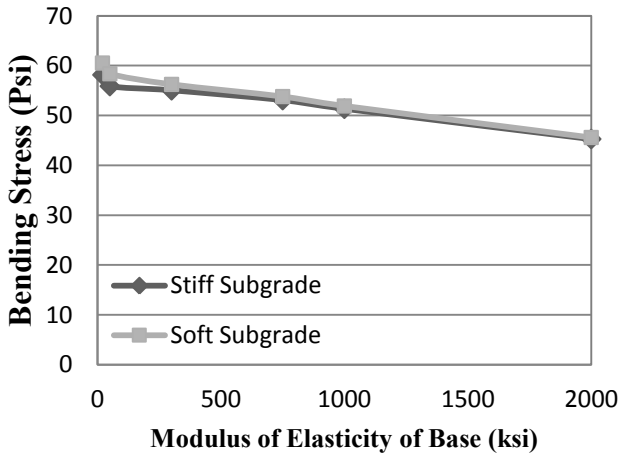

d) Modeling the base as a Vlasov foundation

Figure 7.40: Maximum transverse bending stress (σ_{yy}) at the bottom of PCC slab under the corner load for different base and subgrade rigidity.

7.4 Effect of Loss of Support Due to Built-In Curling on PCC Slab Stresses

As discussed in chapter 2, the effective built-in curling from hot weather construction and high relative humidity add an extra negative temperature gradient that results in the production of permanent upward curling in PCC slabs. This condition increases the loss of slab support when a high negative temperature gradient is applied to the slab. Also, the built-in curling may prevent the slab corners coming in contact with the underlying base layer in case of positive temperature gradients during daily temperature change.

The loss of slab support can be a major factor producing fatigue cracking in the pavement slabs. If only the truck loads are considered, the common bottom-up cracking failure mode in this case can shift to the top-down fatigue cracking in case of severe loss of support. In this case, the location of maximum stress shifts toward the center of slab. In case when pavement slabs are exposed to negative temperature gradients, the maximum tensile stress at the center of slabs will be increased due to the effect of loss of support, which in turn increases the risk of developing fatigue cracking.

Hansen et *al.* (2002) conducted several studies to determine the effect of loss of support and the simultaneous action of truck loads and temperature gradient on the creation of top-down cracking in PCC slabs. They concluded that the slab stress, due to the combined effect of built-in and daily temperature changes and multi-axle loading at joints, is below the stress necessary to initiate fatigue failure (below 45% of the flexure strength) (Hansen et *al*., 2006). They also indicated that the additional slab uplift due to moisture warping is a factor for inducing top-down cracking. In their study, the results of the finite element analysis of a rigid pavement system exposed to a negative temperature gradient and truck loads were compared to the field observation of the same pavement system subjected to the same loads. The results from the finite element modeling using ISLAB2000 appeared to underestimate the real stresses. This was attributed to the limitation of the employed finite element model in considering the effect of loss of support in the analysis.

The fact remains that modeling the deformed slab due to permanent curling is a complex physical behavior. The applicability of plate theories in modeling pavement slabs is limited to flat slabs with no in-plane curvatures. A curved slab is more likely to behave as a shell element. However, the curvatures developed in the pavement slabs due to permanent curling are rather small and modeling

them with plate elements would not make significant errors. Therefore, the solution strategy in modeling curved slabs could be still using the same plate theory together with accounting the impact of uplifting from the base layer or their loss of support in the analysis. To investigate the effect of loss of support due to built-in curling on PCC slab stresses, the following procedure was designed in NYSLAB to analyze the pavement system (as illustrated in Figure 7.41):

1. Run the pavement model in NYSLAB with a temperature gradient corresponding to the built-in temperature gradient and calculate the amount of uplifting of each node of the PCC slab from the underlying base layer.
2. Assign the amount of uplifting in each node of the PCC slab finite element mesh as initial gap to those nodes.
3. Remove the built-in temperature gradient and analyze the pavement system with the desired temperature gradient or truck loads. In each interface element, the initial gap should be defined in each nodal point based on the results in step 2 to calculate the interface element stiffness matrix (G in Eq. 5-16).

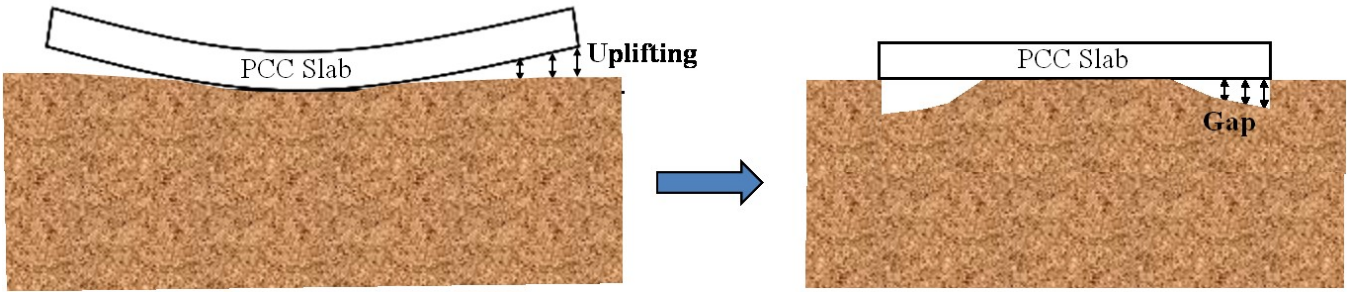

Figure 7.41: Modeling the loss of support due to Built-in curling.

7.4.1 Results of Parametric Study

A series of parametric studies were carried out in this section to investigate the effect of loss of support on the magnitude and location of the maximum PCC slab stresses. A two-layer rigid pavement system consisting of six (three by two as shown in Figure 7.42) jointed PCC slabs resting on top of a Winkler foundation was studied. Two different subgrade (soft and stiff) with the modulus of subgrade

reaction of 180 psi/in. and 350 psi/in. were considered. The modulus of elasticity of the PCC was set to 4,000 ksi with a Poisson's ratio of 0.15, coefficient of thermal expansion of $6 \times 10^{-6}/°F$ and a unit weight of 150 pcf. The joint connection elements have the same properties as those in the previous case studies. Two equivalent built-in temperature gradients (TG_B), -1ºF/in. and -2ºF/in., were considered in the analysis. These gradients can cover the range of built-in temperature gradients suggested by several researchers and the AASHTO design guide.

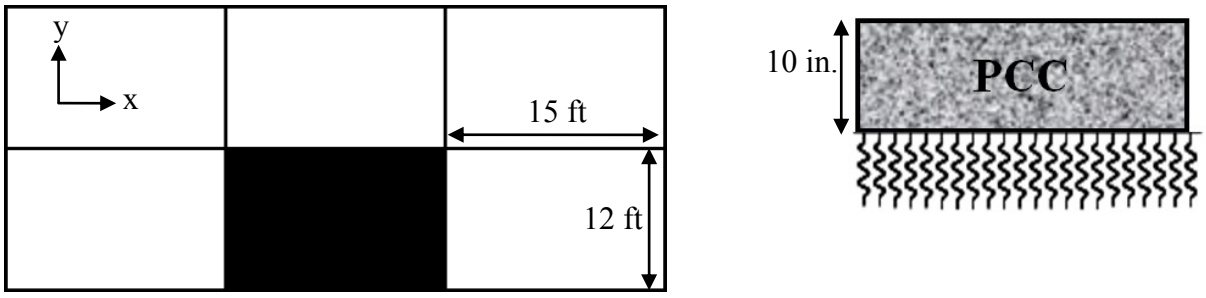

Figure 7.42: Pavement structure in the cases studied.

Figure 7.43 and 7.44 show the uplifting of slabs obtained from running the finite element program with two built-in temperature gradients. These uplifts are considered as loss of supports in the PCC slabs and will be used as initial gaps between the PCC slabs and subgrade. As expected, the magnitude of uplifting and the number of nodes lifting off from the subgrade increase, as the subgrade become stiffer and the built-in temperature gradient increases.

To examine the effect of loss of support due to built-in curling on PCC slab stresses, the pavement system was loaded with an 11- axle truck as shown in Figure 7.45. Each tire had dimensions of 8 in. by 6 in., with a contact pressure of 90 psi. The steering axle and the axle group 2 were placed outside of the three by two slab system. When applicable a negative linear temperature gradient (-1ºF/in.) is also applied to the pavement slabs. The simultaneous action of the axle configuration shown in Figure 7.45 and the negative temperature gradient is the critical loading scenario that produces top-down cracking in PCC slabs according to the 2004 AASHTO design guide.

Four different scenarios were selected to compare the stresses produced in the PCC slabs:

Scenario 1: Only truck load, with no loss of support.

Scenario 2: Only truck load, with loss of support due to two built-in temperature gradients.

Scenario 3: (Truck + thermal) load with no loss of support.

Scenario 4: (Truck + thermal) load with loss of support due to two built-in temperature gradients.

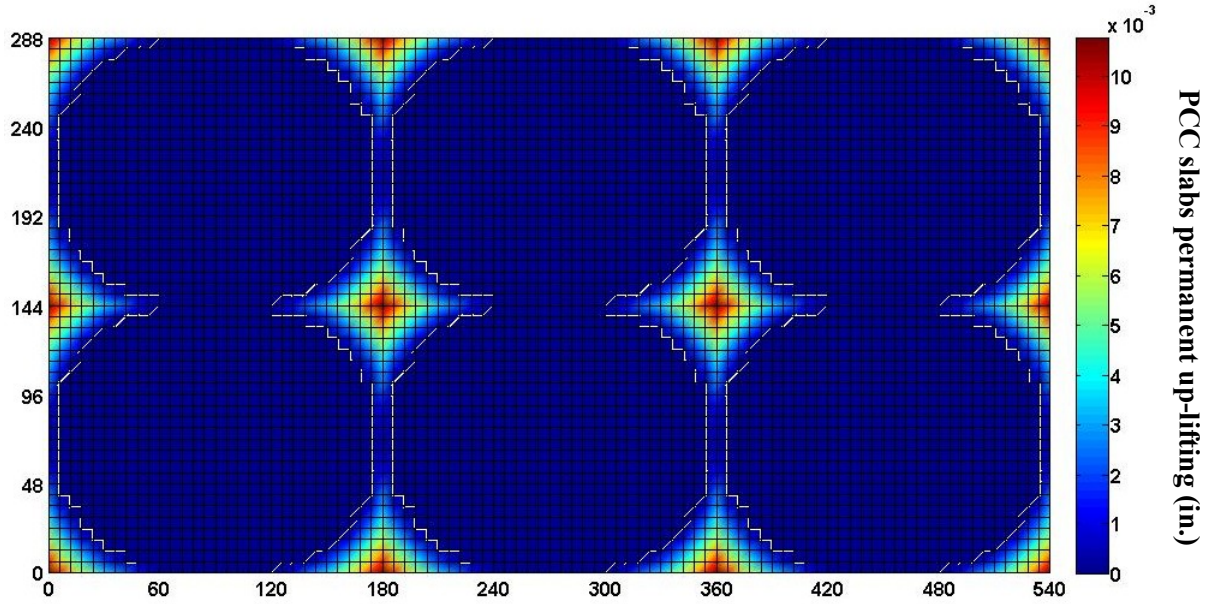

a) Soft Subgrade (k=180 psi/in.)

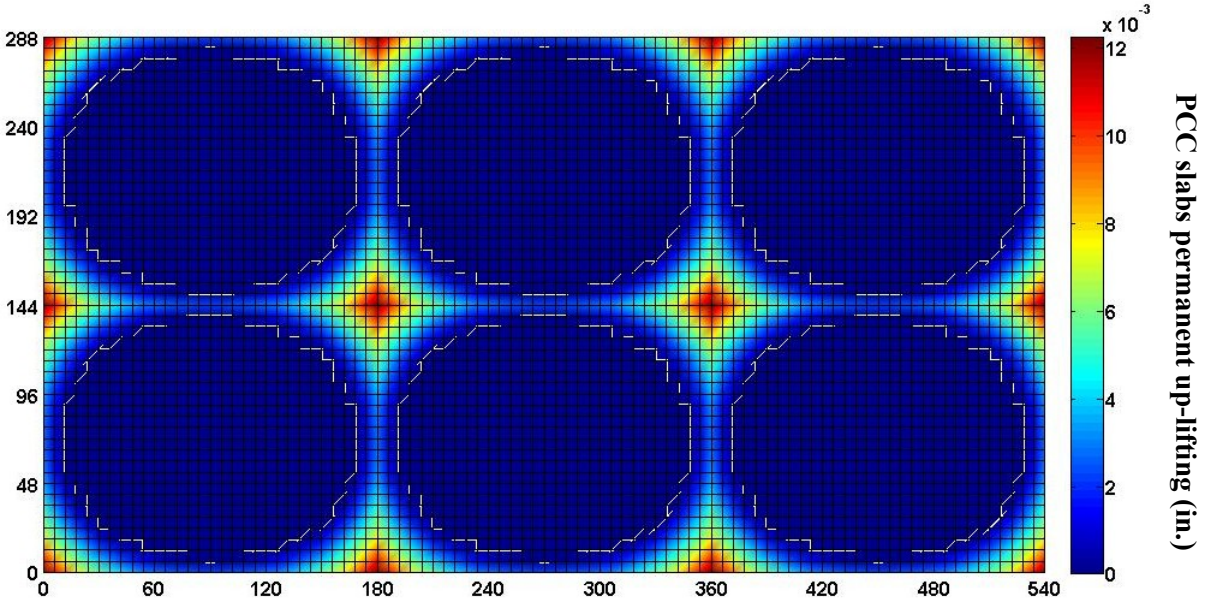

b) Stiff subgrade (k=350 psi/in.)

Figure 7.43: PCC slabs uplifting due to built-in temperature gradient (TG_B = -1ºF/in.).

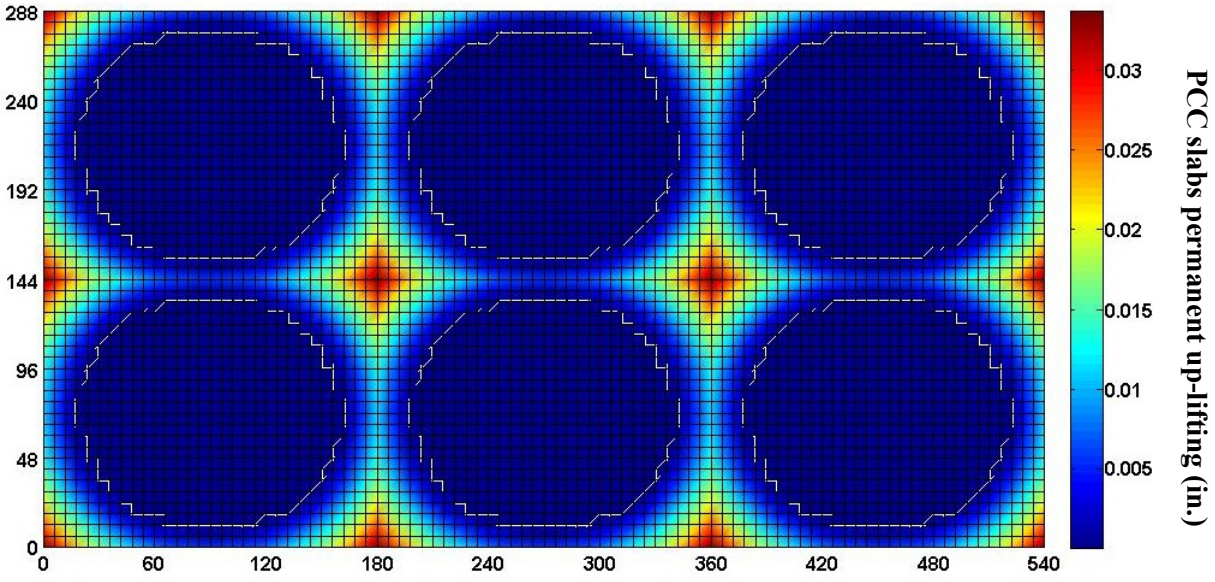

a) Soft Subgrade (k=180 psi/in.)

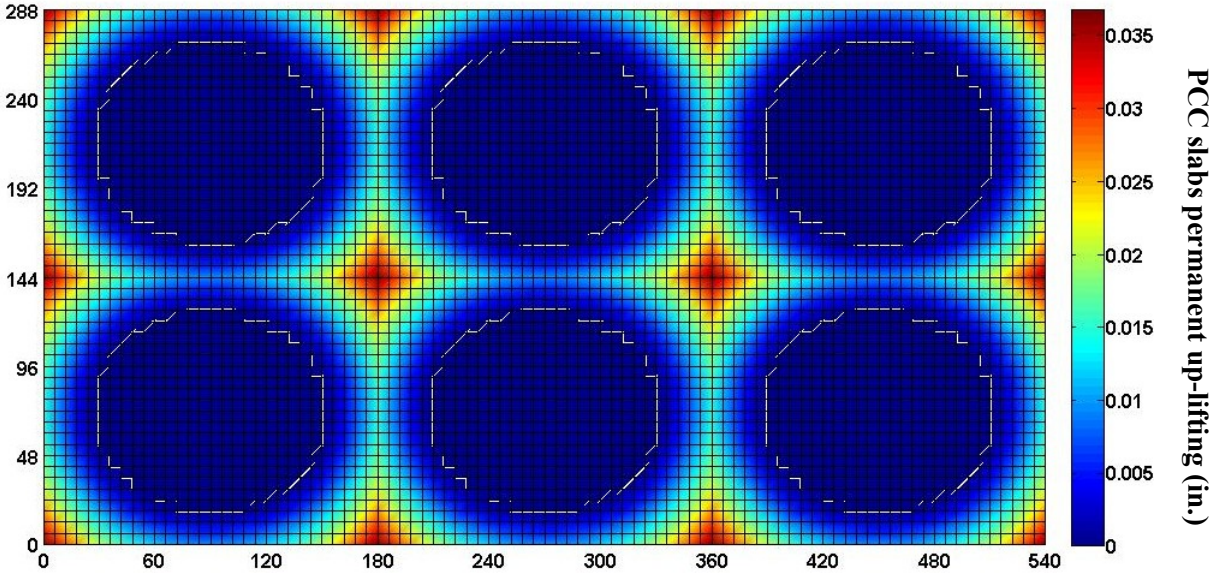

b) Stiff subgrade (k=350 psi/in.)

Figure 7.44: PCC slabs uplifting due to built-in temperature gradient (TG_B = -2ºF/in.).

Figure 7.45: Placement of 11- axle truck load.

The bending stresses through the stress line (see Figure 7.45), where the maximum tensile stresses occur, for the four scenarios described above are shown in Figures 7.46 to 7.47 for different subgrade rigidity and built-in curling. In case of the PCC slabs placed over the softer subgrade (k=180 psi/in.), the maximum PCC slab tensile stress increases by as much as 13% when the loss of support equal to -1ºF/in. was built into the slabs for the pavement solely subjected to the truck load. The simultaneous action of truck and negative temperature gradient can increase the maximum tensile stress at the center of PCC slabs to up to 30% with and without accounting the effect of loss of support.

Figure 7.47 shows the PCC slab bending stress through the stress line for the same slab system with the same built-in temperature gradient, but placed over stiffer subgrade (k=350 psi/in.). Stiffer subgrade causes greater loss of support due to built-in temperature gradient, which in turn increases the maximum tensile stress about 28%. Moreover, the tensile stress due to the combined effect of truck and thermal load increases about 73% at the middle part of the slab close to the longitudinal edge.

Figure 7.48 and 7.49 show the bending stresses through the stress line for the four scenarios, where the loss of support is due to the built-in temperature gradient equal to -2 ºF/in.. In these cases, due to the high amount of loss of support, the tensile stresses can increase up to 86% (soft subgrade) and 100% (stiff subgrade). This can lead to producing significant top-down fatigue cracking in the PCC slabs.

To clarify the stresses produced in the four scenarios, Figure 7.50 demonstrates the PCC slab bending stress contour in longitudinal direction (σ_{xx}) when the PCC slabs is placed over stiffer subgrade (k=350 psi/in.) and a temperature gradient equal to -2ºF/in. was built into the slabs.

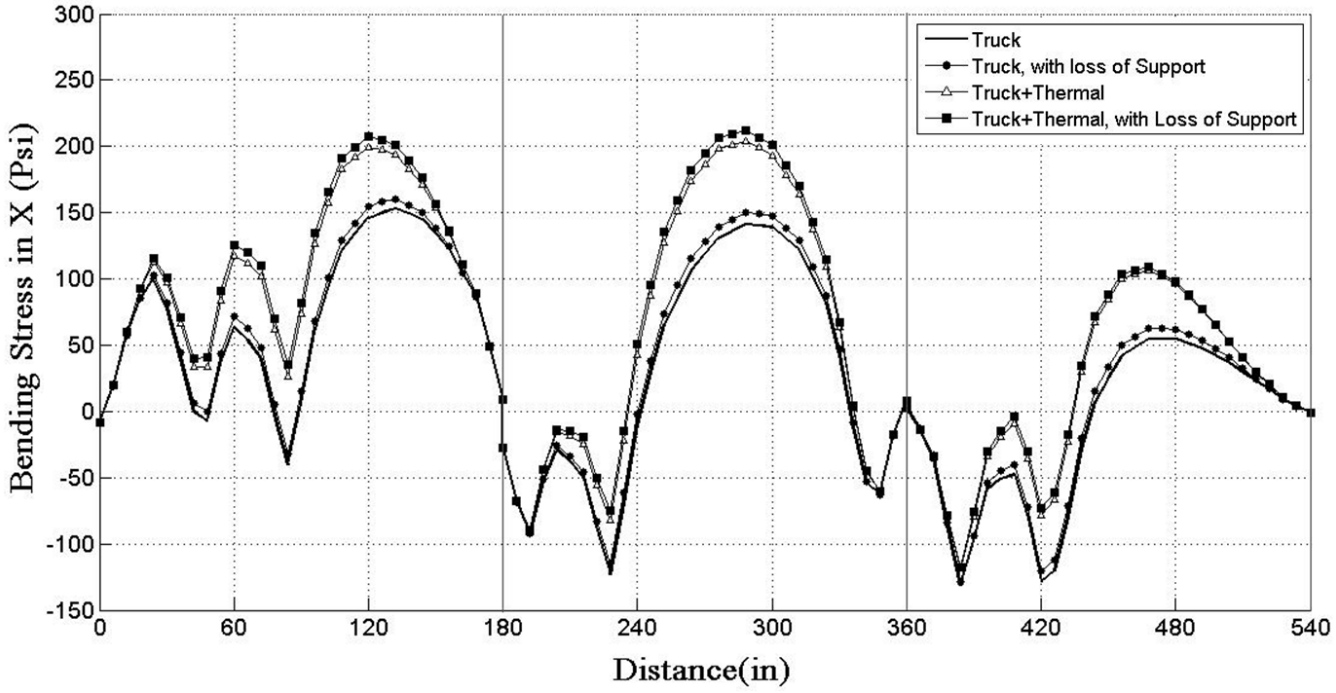

Figure 7.46: PCC slabs bending stress (σ_{xx}) through stress line when $k_{subgrade}$=180 psi/in. and TG_B = -1ºF/in.

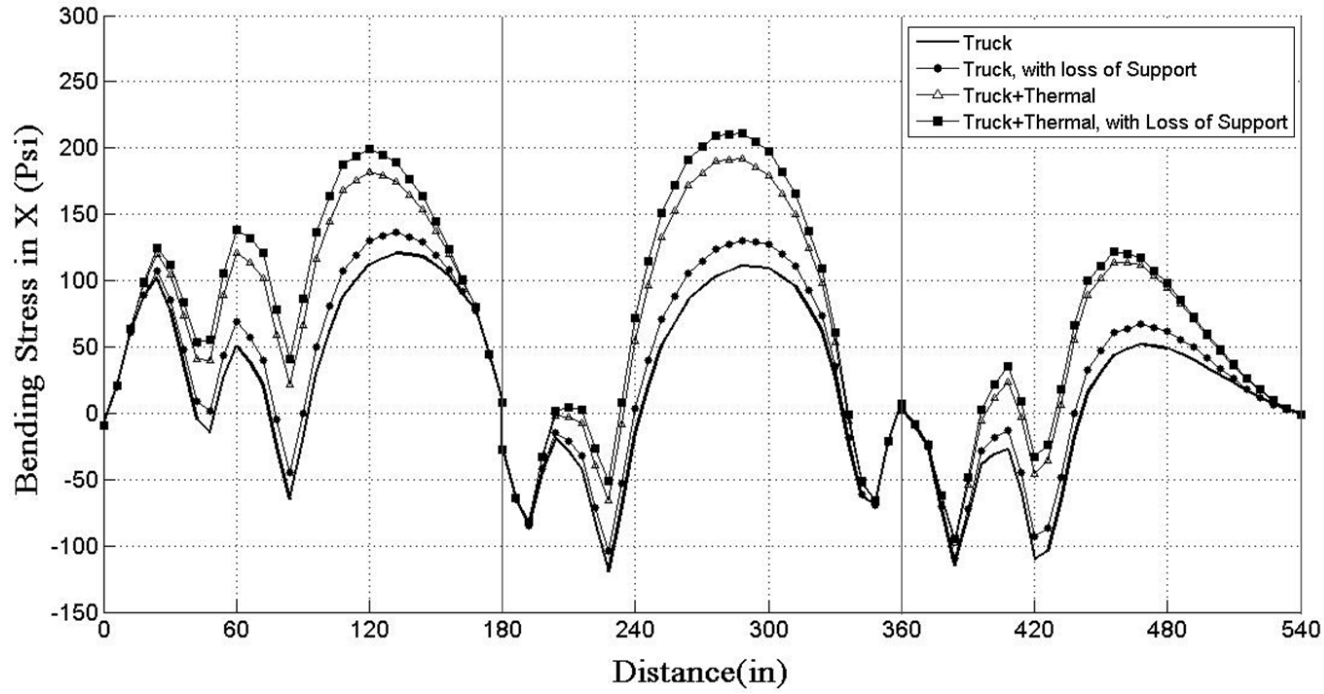

Figure 7.47: PCC slabs bending stress (σ_{xx}) through stress line when $k_{subgrade}$=350 psi/in. and TG_B = -1ºF/in.

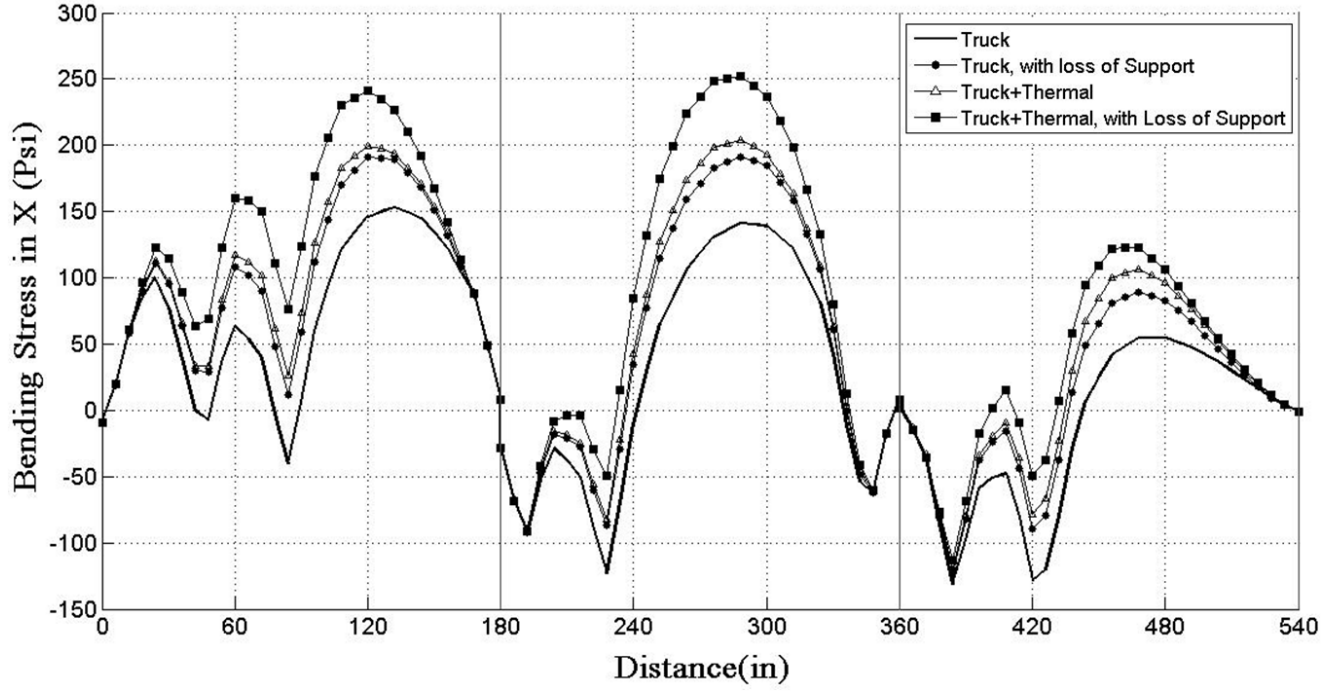

Figure 7.48: PCC slabs bending stress (σ_{xx}) through stress line when $k_{subgrade}$=180 psi/in. and TG_B = -2ºF/in.

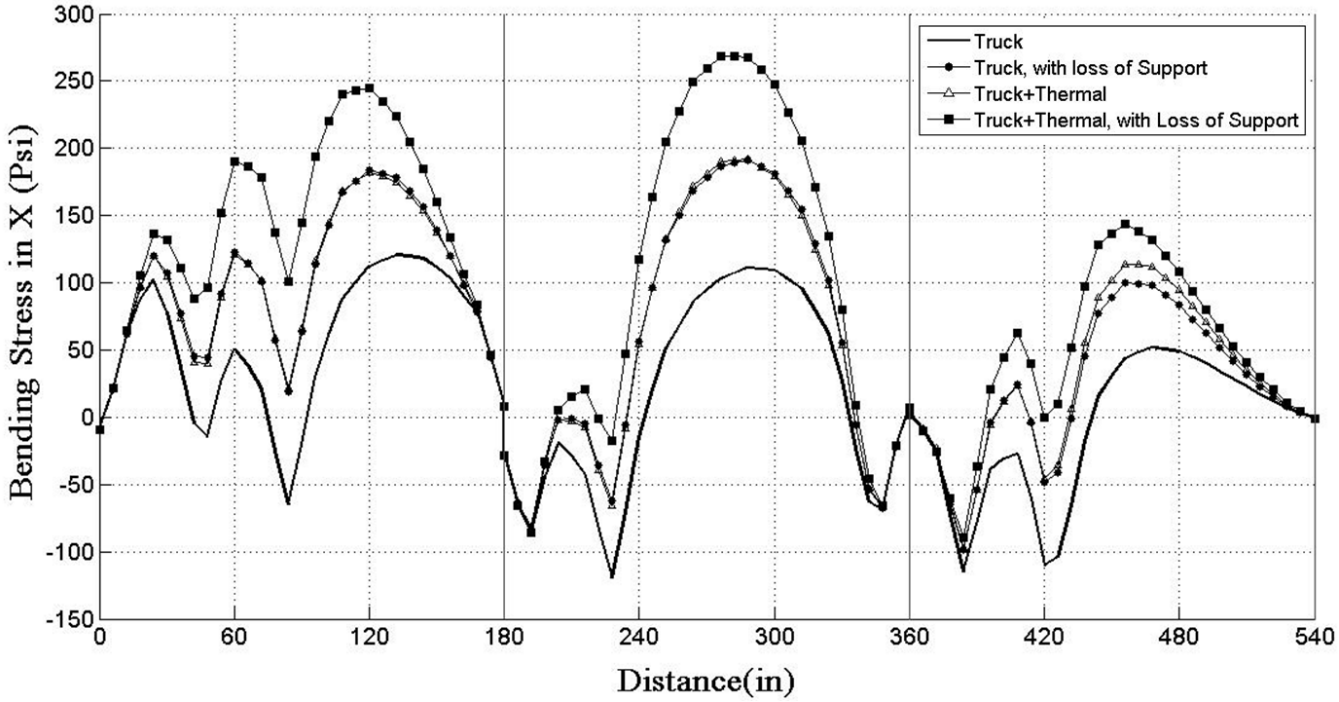

Figure 7.49: PCC slabs bending stress (σ_{xx}) through stress line when $k_{subgrade}$=350 psi/in. and TG_B = -2ºF/in.

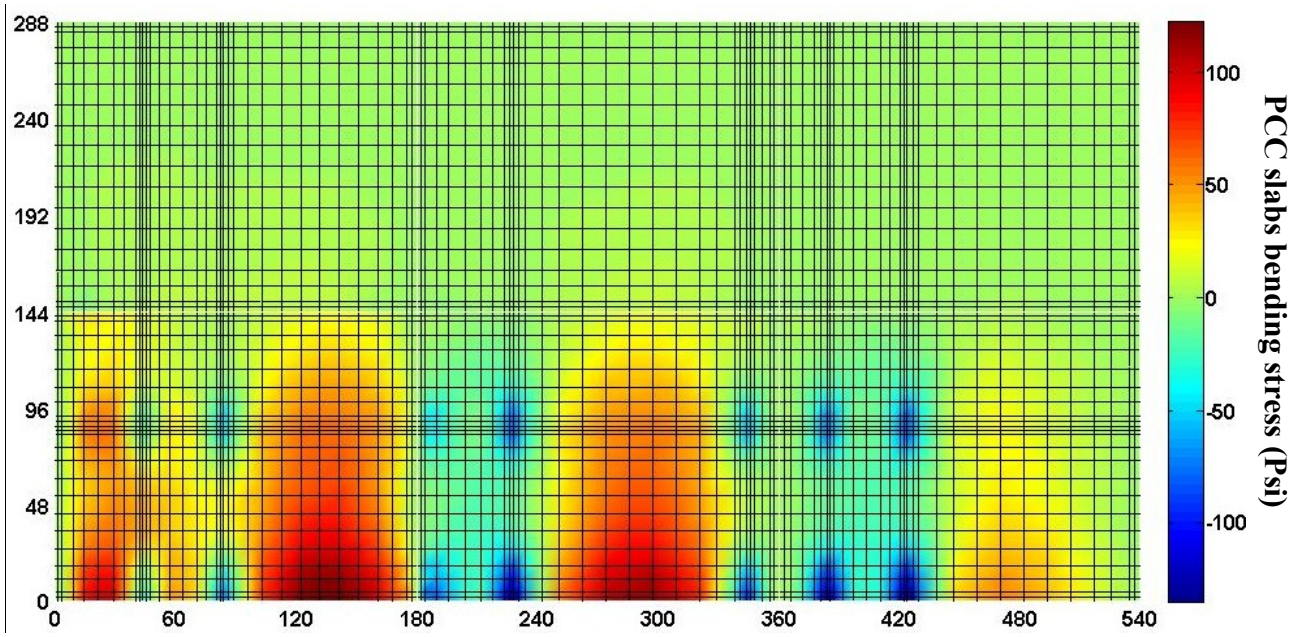

a) Truck load

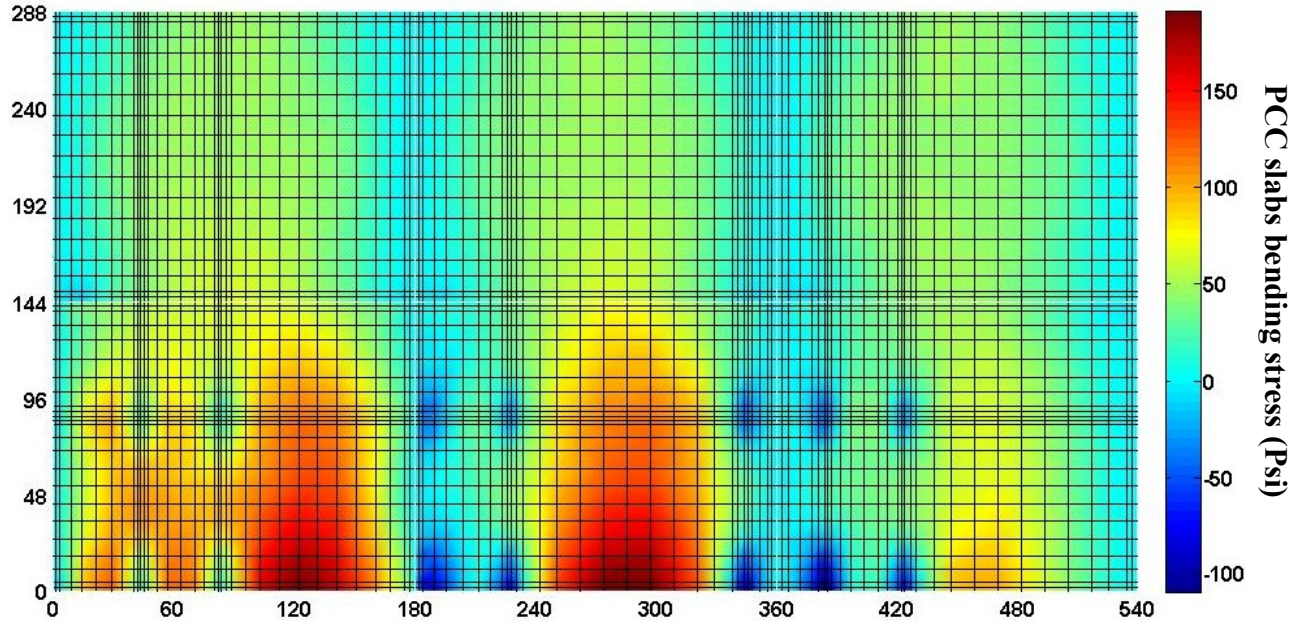

b) Truck load, with loss of support

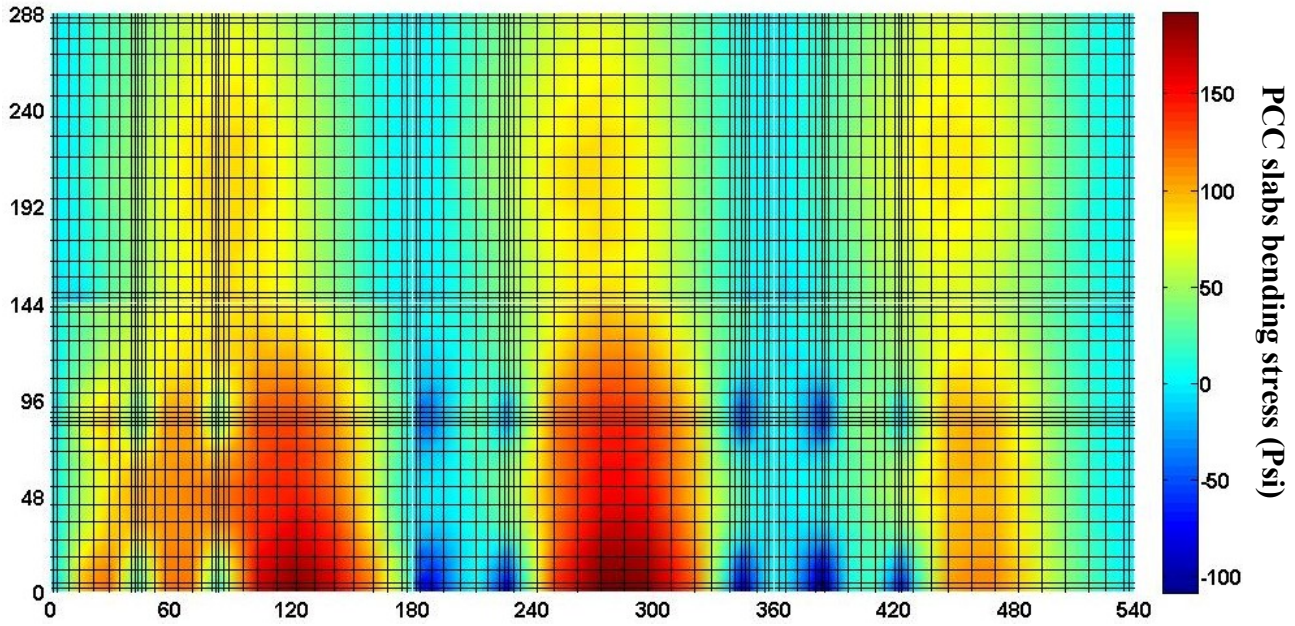

c) Truck Load + negative temperature gradient

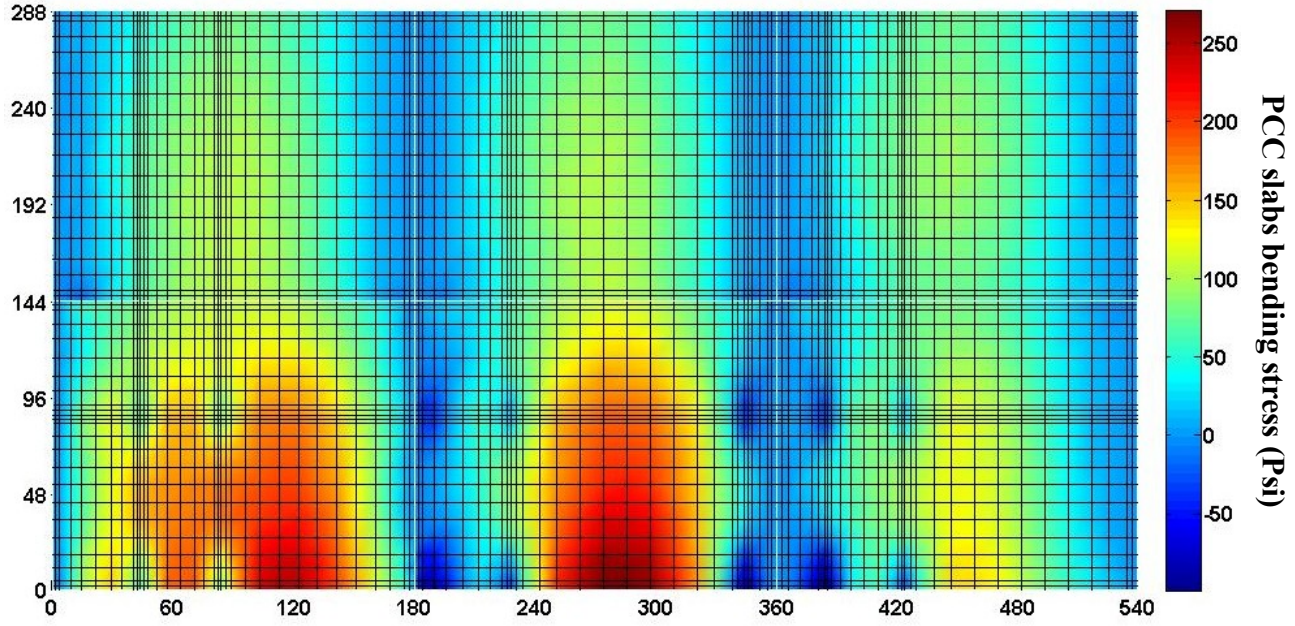

d) Truck Load + negative temperature gradient, with loss of support

Figure 7.50: Bending stress (σ_{xx}) contour in PCC slabs placed over stiff subgrade with TG_B = -2ºF/in. and exposed to different loading condition.

Chapter 8: Summary and Conclusion

In jointed concrete pavements, nonlinear temperature gradients through the depth of PCC slabs during daily temperature change can produce stresses in the slabs because of their external and internal restrains. Bending stresses are produced in slabs as a consequence of thermal curling and because of interactions of supporting foundation, slab self-weight and contact with adjacent slabs. Additional tensile or compressive stresses occur in PCC slabs as a consequence of thermal expansion and contraction and because of slab-foundation friction. In addition to the stiffness of PCC slabs, the stiffness of supporting foundation layers, the contact condition between pavement layers and the stiffness of load transfer elements have significant impacts on the magnitude of stresses developed in the PCC slabs.

In order to predict the responses of jointed concrete pavements, subjected to vehicular loads and environmental conditions, several analysis tools have been developed over the last four decades. Finite element methods have been established as the most promising tool to idealize the behavior of pavement sections and predict their thermo-mechanical responses. This study aimed to investigate the capabilities, potentialities and limitations of current rigid pavement analysis tools and develop a new tool to appreciably enhance their efficiency and applicability. The new finite element based tool was named NYSLAB. It improved the capabilities of current analytical and numerical models in predicting the thermo-mechanical behavior of jointed concrete pavements. The structural and geotechnical theories employed in NYSLAB, and the procedure of implementation of the finite element model of jointed concrete pavements, were examined in this dissertation.

8.1 Summary

An extensive review on the characterization of elements of jointed concrete pavements and the methods for their idealization was conducted to develop an improved model with the ability to predict the thermo-mechanical responses of jointed concrete pavements.

Using nine-node quadrilateral isoparametric plate finite elements and incorporating the “first order shear deformation laminated plate theory”, a mathematical model to idealize the behavior of pavement slabs was developed in NYSLAB. This allowed for modeling composite pavement systems

that are bonded in their interface. This finite element model did not suffer from shear locking and showed appropriate performance, without any instabilities and numerical problems, in modeling relatively thick slabs. Five degrees of freedom considered for each plate element nodal point (two in-plane displacements, one vertical displacement, and two rotations) permitted for capturing the flexural and shear strains of concrete slabs as well as their membrane strains.

Load transfer elements (dowels, tie bars, aggregate interlock and key connection) were utilized at slab joints to simulate the load transfer mechanism. Linkage elements were employed to account for the horizontal interaction between jointed slabs during extensive thermal expansions. The process of implementation of truck loads and nonlinear temperature gradients in the load vector was also included.

To idealize the behavior of supports under pavement slabs, the mathematical model of several foundation types (Winkler, Vlasov, Kerr, and Boussinesq) were implemented in NYSLAB. Winkler foundation parameter or k-value can be calculated internally in NYSLAB for any number of foundation using backcalculation methods. An iterative procedure was also developed to determine the Vlasov parameters as a function of soil elastic properties and layer thickness for up to two foundation layers.

To model the contact between pavement slabs and between the bottom slab and the foundation, interface finite elements were implemented with the ability to capture the separation and sliding between contacting layers. An isoparametric Mohr-Coulomb friction law was employed to calculate the shear or frictional stress at the slab-slab or slab-foundation interface. An iterative procedure in the finite element analysis was developed to solve the nonlinear system of algebraic equations obtained from the equilibrium equations of layers in contact.

Finally, a series of parametric studies were carried out to determine whether the governing equations used to idealize the behavior of jointed concrete pavements in NYSLAB have been accurately selected and implemented in the FE model. Those studies focused specifically on the ability of NYSLAB in the following subjects:

Modeling nonlinear temperature gradient. A two-layer rigid pavement system consisting of six (three by two in longitudinal and transverse direction) jointed PCC slabs resting on a Winkler foundation and

subjected to two sets of nonlinear temperature gradient (negative and positive) was studied. The temperature profile through the thickness of the PCC slab was expressed as a cubic function.

Modeling the friction between pavement layers. The same two-layer pavement system as the first study, subjected to negative and positive temperature gradients, was considered. The coefficient of friction between PCC slab and foundation was varied between zero for the case with no friction to 3.

Modeling the base layer with different finite elements. The effects of base course rigidity on the PCC slab responses due to thermal loads and wheel loads were studied by examining four alternative approaches in NYSLAB for modeling a pavement system consisting of jointed PCC slabs on top of a base and subgrade. Four modeling approaches that were used in that parametric study were: 1) modeling the base as a plate, 2) modeling the base as a plate and applying the Totsky stiffness, 3) modeling the base as part of a Winkler foundation and 4) modeling the base as part of a Vlasov foundation. Six different base stiffness and two subgrade stiffness for the analysis of the PCC slabs, subjected to high and low temperature gradients, were considered. In different cases the PCC slab was loaded with a single tire load at the center and the corner.

Modeling the effect of loss of support due to built-in curling. The same two-layer pavement section as the first study was considered. Two different subgrade (soft and stiff) and two equivalent built-in temperature gradients were considered in the analyses. Four different scenarios were selected to compare the stresses produced in the PCC slabs: 1) Only truck load, with no loss of support, 2) Only truck load, with loss of support due to built-in temperature gradients, 3) Truck + thermal load with no loss of support, 4) Truck + thermal load with loss of support due to built-in temperature gradients. For truck load, an 11- axle truck and for the thermal load, a negative linear temperature gradient was applied.

8.2 Conclusion

Based on the numerical results obtained from analyzing a typical JPCP system, subjected to different nonlinear temperature gradient, the following conclusions can be made:

1) The nonlinear terms in the temperature gradient can produce additional internal stresses at the top and bottom of PCC slabs. This demonstrates that assuming a linear temperature

gradient tends to under-estimate the stresses within the pavement slabs and may lead to their significant under-design.

2) Increasing the level of deviation from the linear temperature gradient results in a significant increase in tensile stress in the night-time (negative) temperature-change state and decrease in tensile stress in the day-time (positive) temperature-change state.
3) For all the temperature profiles studied, the average temperature-change decreases as the non-linearity increases. This leads to a decrease in the thermal contraction (in the case of negative temperature gradient) or thermal expansion (in the case of positive temperature gradient) of the slab mid-plane. This is, however, not a general conclusion about the effect of nonlinear negative or positive temperature gradient on thermal contraction or expansion pattern of the slab mid-plane since it greatly depends on the shape of the temperature profile. This case study was intended to demonstrate the ability of the finite element model in NYSLAB in predicting the in-plane or horizontal displacements of a slab subjected to nonlinear temperature gradients.
4) Vertical deflections of the PCC slabs mostly depend on the linear term (a_1) of nonlinear temperature gradient since that term contributes to producing thermal moments. The thermal moment produced, due to quadratic (a_2, a_3) terms in the temperature gradient profile, is zero. The uniform term (a_0) can also impacts the slab vertical deflection because it can produce frictional moments.

Based on the numerical results obtained from analyzing a typical JPCP system, with different coefficient of friction at slab/foundation interface, the following can be concluded:

1) Friction between pavement layers significantly affects the bending stresses in PCC slabs, and should be included in their analysis. The effect of friction is especially significant when the PCC slabs are subjected to thermal loads. The magnitude of stresses due to friction in the PCC slabs depends on the relative movements of the bottom surface of the slab and the top surface of the underlying foundation layer during thermal expansions and contractions. This

translates into frictional tractions that act in the opposite direction of the relative displacement of the bottom of the slab and produces tensile or compressive stresses.

2) Due to a negative linear temperature gradient, thermal contraction at the bottom of slab produces additional stresses in the PCC slabs because of the presence of friction. The frictional resistance of the foundation layer produces uniform tensile tractions and negative moments in the PCC slabs. By increasing the coefficient of friction from zero (frictionless) to 3, the frictional tractions and frictional moments reduces the tensile stresses at the top and compressive stresses at the bottom of the PCC slabs. By increasing the coefficient of friction, the vertical deflection slightly increases because of the resulting negative moment produced by the frictional tractions at the bottom of the PCC slabs.
3) In case of negative temperature gradients, the impact of friction between the slab and the foundation on PCC slab stresses is better pronounced in the central area of the slab. This is because, due to the negative temperature gradient curling, only the central areas of the slabs maintain contact with the foundation—while the areas close to the edges lose their contact and thus the frictional resistance has no impact on those areas.
4) Due to a positive linear temperature gradient, the bottom of the PCC slab expands and uniform compressive frictional tractions and positive frictional moments are produced. By increasing the coefficient of friction from 0 to 3, the compressive stress at the top of slab and the tensile stress at the bottom of slab decrease. By increasing the coefficient of friction, the vertical deflection slightly increases because of the resulting positive moment produced by the frictional tractions at the bottom of the PCC slabs.
5) The effects of frictional tractions are more pronounced at the bottom of the slabs because of their constraining effect. This leads to a non-symmetric longitudinal bending stress profile about the mid-plane of the slabs.
6) In cases when truck loads are considered, the stresses due to frictional tractions between the PCC slabs and foundation may not be as significant as the stresses with the thermal loads.

Based on the numerical results obtained from analyzing a three-layer pavement system subjected to thermal loads and truck loads by using four modeling approaches for idealizing the base layer, the following can be concluded:

1) Modeling the base as a plate does not allow the PCC slab to sink into the base layer because plate elements do not consider vertical or compressive stiffness. For this reason, this modeling approach does not accurately capture the support provided by the deformed base. In this case, it is the subgrade that provides this vertical support to the base and the PCC slabs and explains the significant dependence of PCC bending stresses on the stiffness of the subgrade when thermal loads are applied. Furthermore, as expected, the PCC slab bending stresses decrease as the thermal gradient decreases. But their variation as the base stiffness increases is significantly smaller. In this modeling approach, as the subgrade becomes stiffer, the PCC slab stresses increase approximately with the same magnitude for all the base stiffnesses. Another feature of this modeling approach is that the effect of base rigidity on the vertical deflections is minimal.
2) The major difference between the first and second modeling approach is the vertical stiffness offered by the Totsky model for the interlayer springs between the PCC slab and the base. This interlayer vertical stiffness in the Totsky model is implemented to account for the vertical stiffness of the base layer, which is absent in plate elements. For the rigid bases, the stress and deformation responses predicted by this model are similar with the first model, where the Totsky model is not applied. For the soft bases, the stiffness of the interlayer springs is relatively small (as compared to the rigid bases). This allows the PCC slab to sink into the base layer, which in turn results in lower stresses in comparison to the first modeling approach.
3) Modeling the base as a plate implies that the base can sustain large tensile stresses. However, in much of the base courses used in rigid pavement systems, especially bases with unbound materials, these tensile stresses are not achievable. Moreover, care should be taken to model

the base as a semi-infinite layer with appropriate boundary conditions. Otherwise, the PCC slab edge stresses can be significantly inaccurate.

4) Modeling the base as a Winkler foundation does allow the PCC slab to sink into the foundation, more accurately modeling the support provided by the deformed base. In this method, the stiffness of both the base and subgrade, which are combined into an equivalent *k*-value, contribute to the PCC slab bending stresses. For this modeling approach the base rigidity tends to have a higher impact on the vertical deflections when compared to the case where the base is modeled as a plate.
5) Modeling the base as part of a Vlasov foundation also allows the PCC slab to sink into the base layer just like in the case of the Winkler foundation. The impact of base rigidity on the PCC slab stresses are more pronounced in this approach than the other three modeling approaches. Unlike the other two approaches, when modeling the foundation as two Vlasov layers for the stiff bases (LCB, CTGB, and CTPB), the magnitude of PCC slab stresses remains unchanged as the subgrade rigidity changes. This may be a more reasonable response that indicates that, in the case of rigid bases, the PCC slab curling stresses are not influenced by the stiffness of the subgrade. The vertical deflections show the same trend as the bending stresses where the effect of changes in subgrade rigidity is only significant for low stiffness bases.
6) In summary, modeling the base as part of a Vlasov foundation system seems to outperform other investigated methods to capture the effects of the base and subgrade rigidity. However, the high values of curling stresses computed from the Vlasov method reveal the need for through re-evaluation in the accuracy of the Vlasov parameters. The applicability and accuracy of each of the investigated modeling approaches in predicting PCC slab responses can only be confirmed by performing a comprehensive comparison study with data obtained from actual field testing.
7) In the case of a single tire load, the impact of base rigidity on PCC slab bending stress is better pronounced when the base is modeled as a plate and as a Vlasov foundation. The slab

bending stresses do not change appreciably as the base rigidity changes when the base is modeled as part of a Winkler foundation.

Based on the numerical results obtained from analyzing a two-layer pavement system subjected to truck and thermal loads, and by considering loss of support due to built-curling, the following conclusions can be drawn:

1) Stiffer foundations and higher built-in temperature gradients result in slabs with higher amounts of uplifting or loss of support.
2) Considering the loss of support in the finite element analysis results in higher stresses in the PCC slabs subjected to thermal loads and truck loads and the simultaneous action of truck and thermal loads.

8.3 Contribution of Study

The major contribution of this research is an enhanced finite element analysis tool for modeling the thermo-mechanical responses of jointed concrete pavements under vehicular and environmental loads. The stress and strain responses can be employed to predict the type and location of distresses that may occur in concrete slabs. The significant highlights of capabilities of the new analysis tool (NYSLAB) developed in this study are:

- No limitation in the number of jointed slabs and pavement layers.
- Using isoparametric finite element formulations to model irregular geometries.
- Modeling bonded slabs as a composite laminate. Using laminated plate theories allow for modeling the slab layers with different material property and thickness more accurately as compared to plate theories. Modeling multiple bonded slabs with one layer can reduce the required memory and computation time.
- Using the First-Order Shear Deformation Laminated Plate theory that accounts for out-of-plane shear strains to model thick slabs.
- Using a nine-node quadrilateral plate element for discretizing the pavement slabs. This element does not suffer from numerical instability and shear locking.

- Modeling the in-plane deformations in concrete slabs by considering five degrees of freedom per plate finite element node.
- Modeling horizontal or frictional contact as well as vertical contact between unbonded slabs and between the bottom slab and the foundation surface.
- Incorporating a nine-node interface element to capture the relative displacements of surfaces in contact in the normal and two tangential directions and define the state of contact at each element node.
- Extending foundation layers beyond the slab edges, in case of continuous foundation models (Vlasov and Boussinesq), to account for rigidity of surrounding soil and to accurately model the slab edge deflections and stresses.
- Performing thermal analysis for multiple jointed slabs on continuous foundations.
- Calculating the Winkler and Vlasov foundation parameters internally in NYSLAB.
- Modeling of nonlinear temperature gradient applied to any number of PCC layers.
- Modeling the loss of slab support due to built-in curling.

8.3 Recommendation for Future Work

Based on the investigations on the available mathematical models of the components of jointed concrete pavements and based on the finite element model developed in this study and the numerical analyses carried out, the following recommendations for future work are proposed to improve the applicability and accuracy of methods for the design and analysis of rigid pavements:

1) Since the soil (foundation) elements were assumed infinitely rigid in the horizontal directions, the analysis of contact between PCC slabs and foundations was reduced to sliding a plate on a rigid body with no horizontal movements. In reality, the top surface of foundation can move with the bottom surface of the slab because of friction created when the slab is subjected to thermal loads. Considering this factor produces different relative horizontal displacements between the nodes of two surfaces in contact, which in turn lead to different frictional tractions. More investigations are recommended on the behavior of foundations to improve their mathematical model and account for the in-plane stiffness.

2) In the case of some stabilized bases, the cohesion between the base layer and PCC slabs would tend to change the frictional characteristics as compared to unstabilized bases. Thus, shear tractions cannot be correlated linearly to normal tractions. An extensive study is needed to propose a constitutive model by considering the effect of cohesion.
3) In modeling the dowels (or tie bars), the dowel looseness and dowel misalignment may have significant impact on their mechanistic behavior. The amount of dowel looseness will change their effective free length, which results in different flexural or shear stiffnesses. Further study on the modeling of dowel elements by considering their effective length can improve the accuracy of the idealization of load transfer mechanism.
4) No test method has been proposed to determine the Vlasov foundation parameters. Appropriate back calculation methods for calculating the normal and shear parameters of Vlasov model can help improve and validate the numerical model of determining the Vlasov parameters explained in chapter 4. This would be a great contribution that leads to utilizing the Vlasov model with more confident, largely because the only drawback with this foundation model is the reliability of its parameters.
5) The representativeness of numerical models in NYSLAB can be verified from the results obtained through several experimental tests on different rigid pavement systems subjected to different thermal and truck loads.

References

Airport Pavement Design and Evaluation. 2009: Federal Aviation Administration, 150/5320-6E.

Concrete Pavement Rehabilitation, Guide for Load Transfer Restoration, FHWA-SA-97-103.

Guide for Mechanistic-Empirical Design of New and Rehabilitated Pavement Structures, Appendix QQ: Structural Responses Models for Rigid Pavements. 2003. National Cooperative Highway Research Program, Transportation Research Board, I-37A.

Guide for Mechanistic-Empirical Design of New and Rehabilitated Pavement Structures. 2004: National Cooperative Highway Research Program, Transportation Research Board, I-37A.

Mechanistic-Empirical Pavement Design Guide: A Manual of Practice, AASHTO, 2008.

Alfano, G., F. Auricchio, L. Rosati, and E. Sacco. 2001. MITC Finite Elements for Laminated Composite Plates. International Journal for Numerical Methods in Engineering, 50(3):707-738.

Barbero, E. J., R. Luciano, and E. Sacco. 1995. Three-Dimensional Plate and contact/friction Elements for Laminated Composite Joints. Computers & Structures, 54 (4): 689-703.

Bathe, K. J., F. Brezzi, and S. W. Cho. 1989. The MITC7 and MITC9 Plate Bending Elements. Computers & Structures, 32 (3): 797-814.

Bathe, K. J. and E. N. Dvorkin. 1985. A four-node Plate Bending Element Based on Mindlin/Reissner Plate Theory and a Mixed Interpolation. International Journal for Numerical Methods in Engineering, 21 (2): 367-383.

Beckemeyer, C. A., L. Khazanovich, and H. Thomas Yu. 2002. Determining Amount of Built-in Curling in Jointed Plain Concrete Pavement: Case Study of Pennsylvania 1-80. Transportation Research Record: Journal of the Transportation Research Board, 1809 (1): 85-92.

Beer, G. 1985. An Isoparametric Joint/Interface Element for Finite Element Analysis. International Journal for Numerical Methods in Engineering, 21 (4): 585-600.

Bhatti, M. A. 2006. Advanced Topics in Finite Element Analysis of Structures: with Mathematica and MATLAB Computations John Wiley.

Bordelon, A., J. Roesler, and J. Hiller. 2009. Mechanistic-Empirical Design Concepts for Jointed Plain Concrete Pavements in Illinois. Report: FHWA-ICT-09-052.

Boukari, D. and A. Fiacco. 1995. Survey of Penalty, Exact-Penalty and Multiplier Methods from 1968 to 1993." Optimization 32 (4): 301-334.

Bradbury, Royall Douglas. 1938. Reinforced Concrete Pavements.

Buch, N., D. Gilliland, K. Vongchusiri, and T. J. Van Dam. 2004. A Preliminary Mechanistic Evaluation of PCC Cross-Sections using ISLAB2000–A Parametric Study.

Buczkowski, R. and W. Torbacki. 2001. Finite Element Modeling of Thick Plates on two-parameter Elastic Foundation." International Journal for Numerical and Analytical Methods in Geomechanics, 25 (14): 1409-1427.

Byrum, C. R. 2011. Joint Load Transfer in Concrete Airfield Pavement : Summary Report. IPRF-01- G-002-05-2.

Campos, L., J. Oden, and N. Kikuchi. 1982. A Numerical Analysis of a Class of Contact Problems with Friction in Elastostatics. Computer Methods in Applied Mechanics and Engineering, 34 (1): 821-845.

Carol, I. and E. Alonso. 1983. A New Joint Element, for the Analysis of Fractured Rock. Presented at the 5th ISRM Congress.

Carrasco, C., M. Limouee, C. Tirado, S. Nazarian, and J. Bendaña. 2011. Development of NYSLAB, Improved Analysis Tool for Jointed Pavements. Transportation Research Record: Journal of the Transportation Research Board 2227 (1): 107-115.

Çelik, M. and A. Saygun. 1999. A Method for the Analysis of Plates on a Two-Parameter Foundation. International Journal of Solids and Structures, 36 (19): 2891-2915.

Ceylan, H., E. Tutumluer, and E. J. Barenberg. 1999. Artificial Neural Networks for Analyzing Concrete Airfield Pavements Serving the Boeing B-777 Aircraft. Transportation Research Record: Journal of the Transportation Research Board, 1684 (1): 110-117.

Chandrasekaran, N., W. Haisler, and R. Goforth. 1987. A Finite Element Solution Method for Contact Problems with Friction. International Journal for Numerical Methods in Engineering, 24 (3): 477-495.

Channakeshava, C., F. Barzegar, and G. Z. Voyiadjis. 1993. Nonlinear FE Analysis of Plain Concrete Pavements with Doweled Joints. Journal of Transportation Engineering, 119 (5): 763-781.

Cheung, Y. and O. Zinkiewicz. 1965. Plates and Tanks on Elastic foundations - an Application of Finite Element Method. International Journal of Solids and Structures, 1 (4): 451-461.

Chilton, D. S. and J. W. Wekezer. 1990. Plates on Elastic Foundation. Journal of Structural Engineering, 116 (11): 3236-3241.

Choi, S. and M. C. Won. 2009. Design of Tie Bars in Portland Cement Concrete Pavement Considering Nonlinear Temperature Variations. Transportation Research Record: Journal of the Transportation Research Board, 2095 (1): 24-33.

Choubane, B. and M. Tia. 1992. Nonlinear Temperature Gradient Effect on Maximum Warping Stresses in Rigid Pavements. Transportation Research Record, 1370: 11-19.

Christopher, B., C. Schwartz, and R. Boudreau. 2006. Geotechnical Aspects of Pavements. Federal Highway Administration, Report Number FHWA NHI-05-037.

Daniel, I. M. and O. Ishai. 1994. Engineering Mechanics of Composite Materials. Vol. 3 Oxford University press, New York.

Darter, M., L. Khazanovich, M. Snyder, S. Rao, and J. Hallin. 2001. Development and Calibration of a Mechanistic Design Procedure for Jointed Plain Concrete Pavements. Presented at the Seventh International Conference on Concrete Pavements. The use of Concrete in Developing Long-Lasting Pavement Solutions for the 21st Century.

Darter, M., K. T. Hall, and C. Kuo. 1995. Support Under Portland Cement Concrete Pavements. NCHRP, report 372. National Academy Press, Washington, D.C.

Davids, Bill. 2003. EverFE Theory Manual.

Davids, W. G. 2000. Effect of Dowel Looseness on Response of Jointed Concrete Pavements. Journal of Transportation Engineering, 126 (1): 50-57.

Davids, W. G., G. M. Turkiyyah, and J. P. Mahoney. 1998. EverFE: Rigid Pavement Three-Dimensional Finite Element Analysis Tool. Transportation Research Record: Journal of the Transportation Research Board, 1629 (1): 41-49.

Davids, W. G., Z. Wang, G. Turkiyyah, J. P. Mahoney, and D. Bush. 2003. Three-Dimensional Finite Element Analysis of Jointed Plain Concrete Pavement with EverFE2.2. Transportation Research Record: Journal of the Transportation Research Board, 1853 (1): 92-99.

Day, R. and D. Potts. 1994. Zero Thickness Interface elements—Numerical Stability and Application. International Journal for Numerical and Analytical Methods in Geomechanics, 18 (10): 689-708.

Desai, C. S., M. M. Zaman, J. G. Lightner, and H. J. Siriwardane. 1984. Thin-layer Element for Interfaces and Joints. International Journal for Numerical and Analytical Methods in Geomechanics, 8 (1): 19-43.

Dutta, S. C. and R. Roy. 2002. A Critical Review on Idealization and Modeling for Interaction among soil–foundation–structure System. Computers & Structures, 80 (20): 1579-1594.

Fang, Y. 2001. Environmental Influences on Warping and Curling of PCC Pavement. Presented at the Seventh International Conference on Concrete Pavements. the use of Concrete in Developing Long-Lasting Pavement Solutions for the 21st Century.

Feng, Y and D. Owen. 1996. Iterative Solution of Coupled FE/BE Discretizations for plate–foundation Interaction Problems. International Journal for Numerical Methods in Engineering, 39 (11): 1889-1901.

Filonenko-Borodich, M. M. 1940. Some Approximate Theories of the Elastic Foundation. Uchenyie Zapiski Moskovskogo Gosudarstvennogo Universiteta Mechanica, Vol. 46 (1940), pp. 3–18.

Francavilla, A. and O. Zienkiewicz. 1975. A Note on Numerical Computation of Elastic Contact Problems. International Journal for Numerical Methods in Engineering, 9 (4): 913-924.

Fredriksson, B., G. Rydholm, and P. Sjoblom. 1977. Variational Inequalities in Structural Mechanics with Emphasis on Contact Problems. Finite Elements in Nonlinear Mechanics, 2: 863-884.

Gens, A., I. Carol, and E. E. Alonso. 1990. A Constitutive Model for Rock Joints Formulation and Numerical Implementation. Computers and Geotechnics, 9 (1): 3-20.

Gens, A., I. Carol, and E. E. Alonso. 1989. "An Interface Element Formulation for the Analysis of Soil-Reinforcement Interaction." Computers and Geotechnics, 7 (1): 133-151.

Ghaboussi, J., E. L. Wilson, and J. Isenberg. 1973. Finite Element for Rock Joints and Interfaces. Journal of the Soil Mechanics and Foundations Division, 99 (10): 849-862.

Girija Vallabhan, C. and Y. C. Das. 1991. Modified Vlasov Model for Beams on Elastic Foundations. Journal of Geotechnical Engineering, 117 (6): 956-966.

Giroud, J. 1968. Settlement of an Embankment Resting on a Semi-Infinite Elastic Soil. Highway Research Record.

Goodman, R. E., R. L. Taylor, and T. L. Brekke. 1968. A Model for the Mechanics of Jointed Rock. Journal of Soil Mechanics & Foundations Div.

Goswami, S. 2006. A C^0 Plate Bending Element with Refined Shear Deformation Theory for Composite Structures. Composite Structures, 72 (3): 375-382.

Guo, H., R. M. Larson, and M. B. Snyder. 1993. A Nonlinear Mechanistic Model for Dowel Looseness in PCC Pavements. Presented at the Fifth International Conference on Concrete Pavement Design and Rehabilitation.

Haider, S. W. and R. S. Harichandran. 2007. Relating Axle Load Spectra to Truck Gross Vehicle Weights and Volumes. Journal of Transportation Engineering 133 (12): 696-705.

Hall, J. W. 2005. Stabilized and Drainable Base for Rigid Pavement: A Design and Construction Guide Programs Management Office. Innovative Pavement Research Foundation Report IPRF-01-G-002-021(G), Applied Research Associates, Skokie, IL

Hall, K. T., M. I. Darter, T. E. Hoerner, and L. Khazanovich. 1997. LTPP Data Analysis.Phase I: Validation of Guidelines for K-Value Selection and Concrete Pavement Performance Prediction.

Hall, K. T. 1992. Backcalculation Solutions for Concrete Pavements. A Paper Prepared for Long-Term Pavement Performance Data Analysis.

Hammons, M. I. and A. M. Ioannides. 1997. Advanced Pavement Design: Finite Element Modeling for Rigid Pavement Joints. Report 1: Background Investigation.

Hammons, M. I. and J. B. Metcalf. 1999. Effect of Transverse Shear on Edge Stresses in Rigid Pavements. Journal of Transportation Engineering, 125 (2): 93-100.

Hammons, M. I., D. W. Pittman, and D. D. Mathews. 1995. Effectiveness of Load Transfer Devices.

Hansen, W., Y. Wei, D. L. Smiley, Y. Peng, and E. A. Jensen. 2006. Effects of Paving Conditions on Built-in Curling and Pavement Performance. International Journal of Pavement Engineering, 7 (4): 291-296.

Hansen, W., D. L. Smiley, Y. Peng, and E. A. Jensen. 2002. Validating Top-Down Premature Transverse Slab Cracking in Jointed Plain Concrete Pavement. Transportation Research Record: Journal of the Transportation Research Board, 1809 (1): 52-59.

Harik, I. E, P. Jianping, H. Southgate, and D. Allen. 1994. Temperature Effects on Rigid Pavements. Journal of Transportation Engineering, 120 (1): 127-143.

Heinrichs, K. W., M. J. Liu, M. I. Darter, S. H. Carpenter, and A. M. Ioannides. 1989. Rigid Pavement Analysis and Design. Final Report. Phase l. Report Number : FHWA-RD-88-068.

Heyliger, P. R. and J. N. Reddy. 1987. A Mixed Computational Algorithm for Plane Elastic Contact problems—Formulation. Computers & Structures, 26 (4): 621-634.

Hu, J. and Z. Shi. 2009. Analysis for Quadrilateral MITC Elements for the Reissner-Mindlin Plate Problem. Mathematics of Computation, 78 (266): 673-711.

Huang, Y. H. 1993. Pavement Analysis and Design. Prentice Hall, Englewood Cliffs, N. J.

Hughes, T. J. and T. Tezduyar. 1981. Finite Elements Based upon Mindlin Plate Theory with Particular Reference to the Four-Node Bilinear Isoparametric Element. Journal of Applied Mechanics, 48: 587.

Ioannides, A. M, L. Khazanovich, and J. Becque. 1992. Structural Evaluation of Base Layers in Concrete Pavement Systems. Transportation Research Record: Journal of the Transportation Research Board, 1370 (1): 20-28.

Ioannides, A. M, M. Thompson, and E. Barenberg. 1985. Finite Element Analysis of Slabs-on-Grade using a Variety of Support Models. Third International Conference on Concrete Pavement Design and Rehabilitation.

Ioannides, A. M. 2006. Concrete Pavement Analysis: The First Eighty Years. International Journal of Pavement Engineering, 7 (4): 233-249.

Ioannides, A. M. 1990. Dimensional Analysis in NDT Rigid Pavement Evaluation. Journal of Transportation Engineering, 116 (1): 23-36.

Ioannides, A. M. and L. Khazanovich. 1998. Nonlinear Temperature Effects on Multilayered Concrete Pavements. Journal of Transportation Engineering, 124 (2): 128-136.

Ioannides, A. M. and G. T. Korovesis. 1990. Aggregate Interlock: A Pure-Shear Load Transfer Mechanism. Transportation Research Record: Journal of the Transportation Research Board, 1286 (1): 14-24.

Ioannides, A. M. and G. T. Korovesis. 1992. Analysis and Design of Doweled Slab-on-Grade Pavement Systems. Journal of Transportation Engineering, 118 (6): 745-768.

Ioannides, A. M., J. Donnelly, M. Thompson, and E. Barenberg. 1984. Analysis of Slabs-on-Grade for a Variety of Loading and Support Conditions. Annual Report, 1. University of Illinois at Urbana-Champaign.

Janssen, D. J. 1987. Moisture in Portland Cement Concrete. Transportation Research Record: Journal of the Transportation Research Board, 1121 (1): 40-44.

Janssen, D. J. and M. B. Snyder. 2000. Temperature-Moment Concept for Evaluating Pavement Temperature Data. Journal of Infrastructure Systems, 6 (2): 81-83.

Jeong, J. and D. G. Zollinger. 2004. Early-Age Curling and Warping Behavior: Insights from a Fully Instrumented Test-Slab System. Transportation Research Record: Journal of the Transportation Research Board, 1896 (1): 66-74.

Jones, R. and J. Xenophontos. 1976. On the Vlasov and Kerr Foundation Models. Acta Mechanica, 25 (1-2): 45-49.

Jones, R. and J. Xenophontos. 1977. The Vlasov Foundation Model. International Journal of Mechanical Sciences, 19 (6): 317-323.

Jones, R. M. 1975. Mechanics of Composite Materials. Vol. 2, Taylor & Francis London.

Kerr, A. D. 1964. Elastic and Viscoelastic Foundation Models. Journal of Applied Mechanics, 31: 491.

Khazanovich, L. 2003. Finite Element Analysis of Curling of Slabs on Pasternak Foundation. 16th ASCE Engineering Mechanics Conference, Seattle, WA.

Khazanovich, L. and A. M. Ioannides. 1994. Structural Analysis of Unbonded Concrete Overlays under Wheel and Environmental Loads. Transportation Research Record: Journal of the Transportation Research Board, 1449 (1): 174-181.

Khazanovich, L., H. Yu, S. Rao, K. Galasova, E. Shats, and R. Jones. 2000. ISLAB2000-Finite Element Analysis Program for Rigid and Composite Pavements. User's Guide. Champaign, IL: ERES Consultants.

Khazanovich, L. 1994. Structural Analysis of Multi-Layered Concrete Pavement Systems. PhD Dissertation. University of Illinois at Urbana-Champaign.

Khazanovich, L. and A. M. Ioannides. 1993. Finite Element Analysis of Slabs-on-Grade using Higher Order Subgrade Soil Models. Proceeding of the Airport Pavement Innovations Conference. Theory to Practice, Vicksburg, Mississippi, USA.

Khazanovich, L., S. D. Tayabji, and M. I. Darter. 2001. Backcalculation of Layer Parameters for LTPP Test Sections, Volume 1: Slab on Elastic Solid and Slab on Dense-Liquid Foundation Analysis of Rigid Pavements.

Kolár, V. and I. Nemec. 2012. Modelling of Soil-Structure Interaction. Elsevier.

Lederle, R. E., R. W. Lothschutz, and J. E. Hiller. 2011. Field Evaluation of Built-in Curling Levels in Rigid Pavements. Report Number: MN/RC 2011-16.

Lee, P. and H. Sin. 1994. Mindlin Plate Finite Elements by a Modified Transverse Displacement. KSME Journal, 8 (1): 19-27.

Li, J., L. M. Pierce, M. E. Hallenbeck, and J. Uhlmeyer. 2009. Sensitivity of Axle Load Spectra in the Mechanistic-Empirical Pavement Design Guide for Washington State. Transportation Research Record: Journal of the Transportation Research Board, 2093 (1): 50-56.

Lim, S., J. Jeong, and D. G. Zollinger. 2004. Moisture Profiles and Shrinkage in Early-Age Concrete. In Proceeding of the 83th Annual Meeting, Transportation Research Board.

Limouee, Maryam. 2009. Verification of NYSLAB a Software for the Analysis of Jointed Pavements. Thesis, University of Texas at El Paso.

Maitra, S. R., K. Reddy, and L. Ramachandra. 2009. Load Transfer Characteristics of Dowel Bar System in Jointed Concrete Pavement. Journal of Transportation Engineering, 135 (11): 813-821.

Mallela, J. and A. Gotlif. 2009. A Mechanistic-Empirical Tie Bar Design Approach for Concrete Pavements. American Concrete Pavement Association.

Mohamed, A. R. and W. Hansen. 1996. Prediction of Stresses in Concrete Pavements Subjected to Non-Linear Gradients. Cement and Concrete Composites, 18 (6): 381-387.

Motamarri, S. 2003. Dowel-Concrete Contact Characteristics. Thesis, West Virginia University.

Nishizawa, T., T. Fukuda, and S. Matsuno. 1989. A Refined Model of Doweled Joints for Concrete Pavement using FEM Analysis. Presented at the 4th International Conference on Concrete Pavement Design and Rehabilitation, West Lafayette, USA.

Ochoa, O. O. and J. N. Reddy. 1992. Finite Element Analysis of Composite Laminates. Vol. 7, Springer.

Oden, J. and N. Kikuchi. 1982. Finite Element Methods for Constrained Problems in Elasticity. International Journal for Numerical Methods in Engineering, 18 (5): 701-725.

Oden, J. and E. Pires. 1984. Algorithms and Numerical Results for Finite Element Approximations of Contact Problems with Non-Classical Friction Laws. Computers & Structures, 19 (1): 137-147.

Oden, J. and E. Pires. 1983. Numerical Analysis of Certain Contact Problems in Elasticity with Non-Classical Friction Laws. Computers & Structures, 16 (1): 481-485.

Okamoto, N. and M. Nakazawa. 1979. Finite Element Incremental Contact Analysis with various Frictional Conditions. International Journal for Numerical Methods in Engineering, 14 (3): 337-357.

Ozgan, K. and A. T. Daloglu. 2008. Effect of Transverse Shear Strains on Plates Resting on Elastic Foundation using Modified Vlasov Model. Thin-Walled Structures, 46 (11): 1236-1250.

Pande, G. and K. Sharma. 1979. On joint/interface Elements and Associated Problems of Numerical ill-conditioning. International Journal for Numerical and Analytical Methods in Geomechanics, 3 (3): 293-300.

Pane, I., W. Hansen, and A. R. Mohamed. 1998. Three-Dimensional Finite Element Study on Effects of Nonlinear Temperature Gradients in Concrete Pavements. Transportation Research Record: Journal of the Transportation Research Board, 1629 (1): 58-66.

Pantano, A. and R. C. Averill. 2002. A Penalty-Based Finite Element Interface Technology. Computers & Structures, 80 (22): 1725-1748.

Pasternak, P.. 1954. On a New Method of Analysis of an Elastic Foundation by Means of Two Foundation Constants. Gosudarstvennoe Izdatel'stvo Litearturi Po Stroitel'stvu i Arkhitekture, Moscow, USSR (in Russian).

Perić, D. and D. R. J. Owen. 1992. Computational Model for 3-D Contact Problems with Friction Based on the Penalty Method. International Journal for Numerical Methods in Engineering, 35 (6): 1289-1309.

Pervez, T., A. C. Seibi, and F. Al-Jahwari. 2005. Analysis of Thick Orthotropic Laminated Composite Plates Based on Higher Order Shear Deformation Theory. Composite Structures 71 (3): 414-422.

Pickett, G. and G. K. Ray. 1951. Influence Charts for Rigid Pavements. American Society of Civil Engineers Transactions.

Rao, S. and J. R. Roesler. 2005. Characterization of Effective Built-in Curling and Concrete Pavement Cracking on the Palmdale Test Sections. Institute of Transportation Studies Pavement research Center, University of California Berkeley.

Reddy, J. N. 2004. Mechanics of Laminated Composite Plates and Shells: Theory and Analysis. CRC press.

Reddy, J. N. 2007. Theory and Analysis of Elastic Plates and Shells. CRC press.

Richardson, J. M. and J. M. Armaghani. 1987. Stress Caused by Temperature Gradient in Portland Cement Concrete Pavements. Transportation Research Record: Journal of the Transportation Research Board, 1121 (1): 7-13.

Rolfes, R. and K. Rohwer. 1997. Improved Transverse Shear Stresses in Composite Finite Elements Based on First Order Shear Deformation Theory. International Journal for Numerical Methods in Engineering, 40 (1): 51-60.

Sachdeva, T. and C. Ramakrishnan. 1981. A Finite Element Solution for the two-dimensional Elastic Contact Problems with Friction. International Journal for Numerical Methods in Engineering, 17 (8): 1257-1271.

Shahin, M. Y. 2005. Pavement Management for Airports, Roads, and Parking Lots. Springer.

Shoukry, S. N., G. W. William, and M. Riad. 2003. Nonlinear Temperature Gradient Effects in Dowel Jointed Concrete Slabs. International Journal of Pavement Engineering, 4 (3): 131-142.

Shyu, S., T. Chang, and A. Saleeb. 1989. Friction-Contact Analysis using a Mixed Finite Element Method. Computers & Structures, 32 (1): 223-242.

Simo, J. C., P. Wriggers, and R. L. Taylor. 1985. A Perturbed Lagrangian Formulation for the Finite Element Solution of Contact Problems. Computer Methods in Applied Mechanics and Engineering, 50 (2): 163-180.

Simons, J. and P. Bergan. 1986. A Finite Element Formulation of Three-Dimensional Contact Problems with Slip and Friction. Computational Mechanics, 1 (2): 153-164.

Snyder, M. B. 2011. Guide to Dowel Load Transfer Systems for Jointed Concrete Roadway Pavements. Institute for Transportation, Iowa State University.

Straughan, W. Th. 1990. Analysis of Plates on Elastic Foundations. PhD Dissertation, Texas Tech University.

Tabatabaie, A. M., E. J. Barenberg, and R. Smith. 1979. Longitudinal Joint Systems in Slip-Formed Rigid Pavements. Volume II. Analysis of Load Transfer Systems for Concrete Pavements. Report Number: FAA-RD-79-4-2.

Tabatabaie, A. M. and E. J. Barenberg. 1980. Structural Analysis of Concrete Pavement Systems." Transportation Engineering Journal, 106 (5): 493-506.

Tabatabaie, A. M. and E. J. Barenberg. 1978. Finite-Element Analysis of Jointed or Cracked Concrete Pavements. Transportation Research Record: Journal of the Transportation Research Board, 671 (1): 11-19.

Tayabji, S. D. and B. E. Colley. 1986. Analysis of Jointed Concrete Pavements.

Tayabji, S. D. and B. E. Colley. 1983. Improved Rigid Pavement Joints. Transportation Research Record: Journal of the Transportation Research Board, 930 (1): 69-78.

Teller, L. W. and E. C. Sutherland. 1935. The Structural Design of Concrete Pavements. Part 2: Observed Effects of Variations in Temperature and Moisture on the Size, Shape and Stress Resistance of Concrete Pavement Slabs. 15 (9): 169-197.

Terzaghi, K. 1955. Evalution of Conefficients of Subgrade Reaction. Geotechnique, 5 (4): 297-326.

Thomlinson, J. 1940. Temperature Variations and Consequent Stresses Produced by Daily and Seasonal Temperature Cycles in Concrete Slabs. Concrete Constructional Engineering, 36 (6): 298-307.

Timoshenko, S., S. Woinowsky-Krieger, and S. Woinowsky. 1959. Theory of Plates and Shells. Vol. 2, McGraw-hill, New York.

Tirado, C., C. Carrasco, J. M. Mares, N. Gharaibeh, S. Nazarian, and J. Bendaña. 2010. Process to Estimate Permit Costs for Movement of Heavy Trucks on Flexible Pavements. Transportation Research Record: Journal of the Transportation Research Board, 2154 (1): 187-196.

Torstenfelt, B. 1983. Contact Problems with Friction in General Purpose Finite Element Computer Programs. Computers & Structures, 16 (1): 487-493.

Turhan, A. 2012. A Consistent Vlasov Model for Analysis of Plates on Elastic Foundations using the Finite Element Method. Texas Tech University.

Urzua, J. L., D. A. Pecknold, L. A. Lopez, and W. H. Munse. 1977. Analysis Procedure for Frictional Contact Problem using Interface Finite Elements. PhD Dissertation. University of Illinois at Urbana-Champaign.

Vallabhan, C. G. and A. T. Daloglu. 1999. Consistent FEM-Vlasov Model for Plates on Layered Soil. Journal of Structural Engineering, 125 (1): 108-113.

Vallabhan, C. G. and Y. Das. 1988. Parametric Study of Beams on Elastic Foundations. Journal of Engineering Mechanics, 114 (12): 2072-2082.

Vesic, A. 1961. Bending of Beams Resting on Isotropic Elastic Solid. Journal of Soil Mechanics and Foundation Engineering, ASCE 87 (2): 35-53.

Vlasov, V. Z. and Leont'ev, N. N. 1966. Beams, Plates and Shells on Elastic Foundations. Israel Program for Scientific Translations, Jerusalem.

Wesevich, J. W., B. F. McCullough, and N. H. Burns. 1987. Stabilized Subbase Friction Study for Concrete Pavements. Center for Transportation Research, University of Texas at Austin.

Westergaard, H. M. 1927. Analysis of Stresses in Concrete Pavements due to Variations of Temperature. Presented at the proceeding of Highway Research Board.

Westergaard, H. M. 1926. Stresses in Concrete Pavements Computed by Theoretical Analysis. Public Roads.

Yu, H. T., L. Khazanovich, and M. Darter. 2004. Consideration of JPCP Curling and Warping in the 2002 Design Guide. presented at the proceeding of the 83rd Annual Meeting of the Transportation Research Board, Washington, DC.

Yu, H. T., L. Khazanovich, M. Darter, and A. Ardani. 1998. Analysis of Concrete Pavement Responses to Temperature and Wheel Loads Measured from Intrumented Slabs. Transportation Research Record: Journal of the Transportation Research Board, 1639 (1): 94-101.

Yu, H. T, K. Smith, M. Darter, J. Jiang, and L. Khazanovich. 1998. Performance of Concrete Pavements.Volume III: Improving Concrete Pavement Performance. Report Number: FHWA-RD-95-111.

Zienkiewicz, O. C. 1977. Finite Element Method. McGraw Hill.

Zokaei Ashtiani, M. A., C. Carrasco, and S. Nazarian. 2013. Effect of Nonlinear Temperature Gradient on Responses of Jointed Concrete Pavements. In proceeding of the Ninth International Conference on the Bearing Capacity of Roads, Railways and Airfields, Trondheim, Norway.

Zokaei Ashtiani, M. A., C. Carrasco, C. Tirado, S. Nazarian, and Julian Bendana. 2013. Modeling of Slab-Foundation Friction in Jointed Concrete Pavements under Nonlinear Thermal Gradient or Traffic Loads. Transportation Research Record: Journal of the Transportation Research Board, 2367 (1): 123-131.

Zokaei Ashtiani, M. A., C. Carrasco, and S. Nazarian. 2014. Finite Element Modeling of Slab-Foundation Interaction on Rigid Pavement Applications. Accepted for publication in Computers and Geotechnics.

VitaMohammad-Ali Zokaei-Ashtiani was born in Tehran, Iran in a highly educated family. He received his B.Sc. degree in Civil Engineering in 2003 from Sharif University of Technology (SUT), which is widely known as the best technical university in the country and also well known internationally. To maintain contact with academic areas, he worked at the Earthquake Engineering Research Center at SUT as a researcher for two years after his under graduate study. He began his graduate study in Structural Engineering at Khaje-Nasir-Toosi University of Technology, one of the most competitive Structural and Earthquake Engineering program in Iran. His M.Sc. thesis was titled "Determination of Demand Parameters in MDOF systems by Multi-Mode Pushover Analysis". After completing his master's studies in 2008, he began working as a retrofitting project manager at one of the well-known consulting company across Iran. In January 2010, he entered the PhD program of the Civil Engineering department at the University of Texas at El Paso (UTEP). He received the Eisenhower Hispanic Serving Institutions (HSI) Fellowships in 2011 and 2012, Cotton Trust Presidential Scholarship in 2012, Graduate School travel Grant in 2013, and Graduate School Dodson Research Grand in 2014. He also received the certificate of Teaching Seminar for Graduate Student Instructors in 2011. He has been working in the Center for Transportation Infrastructure Systems (CTIS) at UTEP since 2010. He has been the lead graduate research assistant in NYPAS project funded by the Federal Highway Administration and Ney York Department of Transportation. He developed a finite element based analysis tool for modeling jointed concrete pavement responses that is a state-of-the-art tool that can be used by different agencies for pavement analysis and design. He published a paper in Transportation Research Record and a paper in the proceeding of BCRRA conference in Norway. He submitted two papers to Computers and Geotechnics journal and the Journal of Transportation Engineering (ASCE) for peer review. He has presented at several national and international conferences.

Permanent address: 6105 Maiden Ln., Bethesda, MD, 20817

Emails: mzokaeiashtiani@miners.utep.edu, ali.zokaei@gmail.com

This dissertation was typed by Mohammad Ali Zokaei Ashtiani.